

ENTERIC COATED MUCOADHESIVE MICROPELLETS IN ROTARY AGGLOMERATION PROCESS FOR WET SPHERONIZATION

Dissertation zur Erlangung des Grades
„Doktor der Naturwissenschaften“

am Fachbereich Chemie und Pharmazie und Geowissenschaften
der Johannes Gutenberg-Universität
Mainz

Marcus Hans Knöll
geb. in Frankfurt / Main

Mainz 2006

D 77

Tag der mündlichen Prüfung: 8. Dezember 2006

To

ACKNOWLEDGEMENTS

TABLE OF CONTENTS

DEDICATION	I
ACKNOWLEDGEMENTS	III
TABLE OF CONTENTS	V
LIST OF TABLES	IX
LIST OF FIGURES	XI
ABBREVIATIONS	XV
INTRODUCTION	1
AIMS	1
CHAPTER I BACKGROUND.....	3
I.1. Basis for Drug Delivery to the Gastrointestinal Tract.....	3
I.1.1. Anatomy and Physiology of the Gastrointestinal Tract.....	3
I.1.2. Secretions of the Mucosa of the Gastrointestinal Tract.....	5
I.2. Transit of Dosage Forms.....	6
I.2.1. Oesophageal Transit.....	6
I.2.2. Gastric Emptying of Liquid Dosage Forms	6
I.2.3. Gastric Emptying of Non-Digestible Solids (Solid Dosage Forms and Drug Particles)	7
I.2.4. Small Intestinal Transit.....	7
I.2.5. Large Intestinal Transit	8
I.2.6. Prolongation of Gastrointestinal Transit Time.....	8
I.3. Mucoadhesion.....	9
I.3.1. Mechanisms of Mucoadhesion	10
I.3.2. Mucoadhesive Polymer Types.....	11
I.3.3. Challenges to the Concept of Mucoadhesion	15
I.4. Mucoadhesive Polymers.....	16
I.4.1. Natural Polymers.....	16
I.4.2. Semi-Synthetic Polymers.....	19
I.4.3. Synthetic Polymers	21
I.5. Granulation Processes.....	28
I.5.1. Binding Forces of Granules	28
I.5.2. Growth Mechanisms of the Particles	29
I.5.3. Fluidized Bed Technology.....	30
I.5.4. Rotary Processor	34
CHAPTER II MATERIALS AND EQUIPMENT.....	40
II.1. Materials	40
II.2. Equipment / Software.....	41
CHAPTER III METHODS.....	43
III.1. Manufacturing of Pellets Using the GPCG1 Rotary Processor.....	43
III.1.1. Na-CMC Micropellets Production.....	43
III.1.2. Na-Alginate Micropellets Production.....	48
III.1.3. Chitosan Micropellets Production	50
III.1.4. Carbopol® Micropellets Production	53
III.1.5. Noveon Micropellets Production	53
III.2. Characterization of Micropellets.....	54
III.2.1. Particle Size Distribution	54

III.2.2.	Tapped Density	55
III.2.3.	Friability Testing	55
III.2.4.	Water Content at the End of the Spraying Period.....	55
III.2.5.	Drying Kinetics of the Micropellets.....	55
III.2.6.	Scanning Electron Microscopy (SEM)	55
III.2.7.	True Density.....	55
III.2.8.	Estimation of the Surface Area with the Modified Blaine Method.....	56
III.2.9.	NMR for Acetic Acid Content in the Chitosan Micropellets.....	57
III.2.10.	Content Uniformity of Theophyllin within Micropellets by HPLC.....	57
III.2.11.	Statistical Analysis	58
III.3.	Enteric Coating of the Micropellets	58
III.3.1.	Terminology	58
III.3.2.	Formulation of the Spraying Suspension.....	58
III.3.3.	Enteric Coating using the Mini-Glatt	60
III.3.4.	Enteric Coating using the Hüttlin Mycrolab®	63
III.4.	Dissolution Testing.....	66
III.4.1.	Screening of Dissolution Methods for Mucoadhesive Micropellets	66
III.4.2.	Dissolution of the Developed and Manufactured Micropellets using App. 2 and App. 4... ..	69
III.4.3.	Dynamic Hydration Properties of Excipients for Mucoadhesive Micropellets.....	71
III.4.4.	Electron Dispersive X-Ray Method for Proving the Separation of an Enteric Coating Layer from a Mucoadhesive Matrix Layer.....	73
III.4.5.	Improving the Solubility of Lipophilic Drugs by Adjusting the Hydrophilic Lipophilic Balance (HLB Value) of the Drug Carrier System	76
CHAPTER IV RESULTS		79
IV.1.	Production of Na-CMC Micropellets in the GPCG1 Rotary Processor	79
IV.1.1.	Screening of Process Parameters	79
IV.1.2.	Development of Process Parameters for Na-CMC Micropellets	81
IV.2.	Na-Alginate Micropellets Production in the GPCG1 Rotary Processor	90
IV.2.1.	Screening of Process Parameters	90
IV.2.2.	Development of Process Parameters for Na-Alginate Micropellets.....	93
IV.3.	Production of Chitosan Micropellets in the GPCG1 Rotary Processor.....	96
IV.3.1.	Screening of Process Parameters	96
IV.3.2.	Development of Process Parameters for Chitosan Micropellets	97
IV.4.	Carbopol® Micropellet Production in the GPCG1 Rotary Processor.....	101
IV.5.	Noveon® AA1 Micropellet Production in the GPCG1 Rotary Processor.....	103
IV.6.	Comparison between Rotating Cylinder and the Bolatec Friabimat for Friability Measurements	104
IV.7.	Rotor Torque Measurement for Monitoring the Pelletization Process as In Process Control	105
IV.8.	Measurements of Air Humidity.....	107
IV.8.1.	Differences between Inlet and Outlet Air Humidity in Relationship to Product Temperature	107
IV.8.2.	Dependence of Outlet Air Humidity on Rotor Speed	108
IV.8.3.	Water Content of Outlet Air.....	109
IV.8.4.	Total Water Added at Different Inlet Air Humidities	110
IV.9.	Drying Kinetics of the Na-CMC Micropellets.....	110
IV.10.	True Density and Estimation of Surface Area of the Micropellets	111
IV.11.	Content Uniformity of the Batches	111
IV.12.	Dynamic Hydration Properties of Excipients used for the Manufacture of Mucoadhesive Micropellets	113
IV.13.	Enteric Coating of Mucoadhesive Micropellets	116
IV.13.1.	Coating of Na-CMC Micropellets with EUDRAGIT® L 30 D-55 using the Mini-Glatt	116
IV.13.2.	Enteric Coating using the Hüttlin Mycrolab®	117
IV.14.	Results of the Dissolution Tests.....	122
IV.14.1.	Comparison of the Different Dissolution Apparatus.....	122
IV.14.2.	Dissolution of the Final Batches and Comparison of Different Agitation Rates using the Paddle Apparatus and Flow-Through Cell.....	131
IV.14.3.	Summary of the Dissolution Results.....	138
IV.15.	Evaluation of the Separation of an Enteric Coating Layer from a Mucoadhesive Matrix Layer by Electron Dispersive X-Ray	139
IV.15.1.	Method X1, Evaluation of the Separation of Poured Films.....	139

IV.15.2.	Method X2, Evaluation of Separation of Multifunctional Polymers using Coated Micropellets	142
IV.15.3.	Summary on Separation of an Enteric Layer from the Mucoadhesive Polymer	146
IV.16.	Improving the Solubility of Lipophilic Drugs in Lipid Matrices	146
IV.16.1.	Correlation Between HLB and logP	146
IV.16.2.	Estimation of the HLB Value of Different Lipid Matrices and of Spironolactone.....	151
IV.16.3.	Determination of the Solubility of Spironolactone in Different Single Lipid Matrices	151
IV.16.4.	Solubility of Spironolactone in Mixtures of Lipid Matrices with Adjusted HLB	161
CHAPTER V. DISCUSSION.....		169
V.1.	The Granulation Process	169
V.1.1.	Process Variables Influencing the Morphology and Topographical Quality of Micropellets ..	170
V.1.2.	Process Variables Influencing Particle Size	170
V.1.3.	Process Variables Influencing the Span	171
V.1.4.	Process Variables Influencing Tapped Density	171
V.1.5.	Process Variables Influencing Friability	172
V.1.6.	Impact of Inlet Air Conditions and Drying Conditions on the Total Yield	173
V.1.7.	Influence of Acetic Acid Concentration on the Formation of Chitosan Micropellets	174
V.1.8.	Differences Between Mucoadhesive Polymers	174
V.1.9.	Statistical Analysis	174
V.2.	Friability and Tapped Density	174
V.3.	Torque Measurements	175
V.4.	Enteric Coating Process.....	176
V.4.1.	Amount of Enteric Coating	176
V.4.2.	Comparison between the Mini-Glatt and the Hüttlin Mycrolab®	176
V.5.	Dissolution and EDX	177
V.5.1.	Influence of the Dissolution Method.....	177
V.5.2.	Dissolution of the Micropellets using App.2 and 4	177
V.6.	Perspectives of the Mucoadhesive Micropellets	179
V.7.	Improving the Solubility of Spironolactone by Adjusting the HLB Value.....	179
CHAPTER VI. SUMMARY		181
CHAPTER VII. APPENDIX.....		183
CHAPTER VIII. REFERENCES		207
CURRICULUM VITAE.....		221

LIST OF TABLES

Table I.1	Intestinal enzyme population – luminal pancreatic enzymes.....	4
Table I.2	pH-values in the human gastrointestinal tract.....	4
Table I.3	Bacterial microflora and exo-enzymes.....	5
Table I.4	Representative gastric residence times (expressed as half-lives of gastric emptying) for several types of dosage forms (Macheras, 1995) ^a	6
Table I.5	Ranking of mucoadhesive properties (Bernkop-Schnurch, 2001b).....	13
Table I.6	Multifunctional polymers that display a permeation enhancing effect (Bernkop-Schnurch, 2001b).....	14
Table I.7	Polyacrylic polymers (Noveon).....	25
Table III.1	Screening of the process parameters for Na-CMC micropellets containing 20% MCC.....	44
Table III.2	Screening of the process parameters for Na-CMC micropellets containing 30% MCC.....	44
Table III.3	Process parameters for the development of Na-CMC micropellets.....	46
Table III.3 continued	Process parameters for the development of Na-CMC micropellets.....	47
Table III.4	Characteristic process parameters and batches for the development of Na-CMC micropellets.....	48
Table III.5	Screening of the process parameters for Na-alginate micropellets.....	49
Table III.6	Process parameters for the development of Na-alginate micropellets.....	50
Table III.7	Screening of the process parameters of chitosan micropellets.....	52
Table III.8	Process parameters for the development of chitosan micropellets.....	52
Table III.9	Process parameters for the development of Carbopol [®] micropellets.....	53
Table III.10	Components of the powder masses.....	53
Table III.11	Process parameters for the development of Noveon AA1 micropellets.....	54
Table III.12	Spraying rates for batch 15658/51.....	63
Table III.13	Spraying rates for batch 15658/52.....	64
Table III.14	Spraying rates for batch 15658/54.....	64
Table III.15	Spraying rates for batch 15658/56.....	65
Table III.16	Spraying rates for batch 15658/57.....	65
Table III.17	Spraying rates for batch 15658/58.....	65
Table III.18	Spraying rates for batch 15658/59.....	66
Table III.19	Timing for the change of the rows of the reciprocating cylinder.....	68
Table III.19	Summary of the micropellet batches tested and dissolution methods employed.....	71
Table IV.1	Properties of micropellets formulated with 20% MCC.....	79
Table IV.2	Properties of micropellets formulated with 30% MCC.....	80
Table IV.3.	Properties of micropellets formulated with 30% MCC during the development phase.....	82
Table IV.3. continued	Properties of micropellets formulated with 30% MCC during the development phase.....	83
Table IV.3. continued	Properties of micropellets formulated with 30% MCC during the development phase.....	84
Table IV.4	Effect of the average spraying rate of liquid binder on particle size, tapped density and friability.....	85
Table IV.5	Influence of the inlet air humidity on friability and tapped density of micropellets and impact of the inlet air humidity in combination with the drying air temperature on the yield.....	89
Table IV.5	Reproducibility of the Na-CMC micropellets manufacturing process.....	89
Table IV.6.	Properties of Na-alginate micropellets. Screening of process parameters with 20% MCC.....	91
Table IV.7	Properties of Na-alginate micropellets. Screening of process parameters with 30% and 44% MCC, respectively.....	91
Table IV.8	Properties of Na-alginate micropellets produced during development of the process parameters.....	94
Table IV.9	Influence of the average spraying rate on the quality of the micropellets.....	95
Table IV.10	Influence of the Liquid Binder Amount on the quality of the micropellets.....	95
Table IV.11	Influence of the rotor speed on the quality of the micropellets.....	95
Table IV.12	Properties of chitosan micropellets.....	97
Table IV.13	Development of process parameters for chitosan micropellets. Properties of micropellets.....	98

Table IV.14	Influence of the rotor speed and average spraying rate on properties of chitosan micropellets.....	99
Table IV.15	Influence of the type of rotor disc on properties of chitosan micropellets.	99
Table IV.16	Influence of the amount of liquid binder on properties of chitosan micropellets.....	99
Table IV.17	Influence of the acetic acid concentration of the liquid binder on properties of chitosan micropellet.....	100
Table IV.18	Properties of Carbopol® micropellets.....	102
Table IV.19	Noveon® AA1 micropellet properties.....	103
Table IV.20	Comparison of friabilities between the rotating cylinder and the Bolatec Friabimat.	104
Table IV.21	True density of the mucoadhesive micropellets measured using the pycnometer method.	111
Table IV.22	Surface area of the mucoadhesive micropellets measured by a modified Blaine method.	111
Table IV.23	Content uniformity of Theophyllin of coated and uncoated mucoadhesive micropellets.....	112
Table IV.24	Comparison between the theoretical ratio of the content between coated and uncoated microparticles and the determined ratio.	112
Table IV.25	Screening of process parameters for enteric coating.....	117
Table IV.26	Main manufacturing parameters of the final enteric coating formulation of mucoadhesive micropellets. ...	120
Table IV.27	HLB values and LogPs of different emulsifiers.	147
Table IV.28	HLB Values of Different Lipid Matrices.....	151
Table V.1	Process Parameters Affecting the Properties of Micropellets.	169
Table V.1 continued	Process Parameters Affecting the Properties of Micropellets.	170

LIST OF FIGURES

Figure I.1	Structure of chitosan.....	17
Figure I.2	Structure of cellulose.....	18
Figure I.3	Structure of sodium carboxymethylcellulose.....	19
Figure I.4	Carbopol general structure.....	21
Figure I.5	Crosslinked polycarbophil.....	23
Figure I.6	Liquid distribution in a dispersive solid system (Schubert, 1973).....	29
Figure I.7	Analogy between a liquid and a fluidized bed (Beranek, 1975).....	31
Figure I.8	Different states of the fluidized bed (Beranek, 1975).....	31
Figure I.9	Relationship between air flow and loss of pressure.....	32
Figure I.10	Fluidized bed equipments.....	33
Figure I.11	Ventilus Technology.....	33
Figure I.12	Product movement in a rotary processor.....	34
Figure I.13	Depiction of rotor plates with different designs of surface (Gu, 2004).....	36
Figure III.1	Variation in spraying rate patterns.....	45
Figure III.2	Apparatus for estimation of the surface area.....	57
Figure III.3	Vessel with sieve inlay.....	68
Figure III.4	Modified Enslin apparatus.....	72
Figure III.5	Three layer film model.....	74
Figure IV.1	Morphology and topographical quality of micropellets formulated with 20% MCC.....	80
Figure IV.2	Morphology and topographical quality of micropellets formulated with 30% MCC.....	81
Figure IV.3	Pareto diagram of the standardized variables. Response variable was the particle size.....	85
Figure IV.4	Pareto diagram of the standardized variables. Response variable was the span.....	86
Figure IV.5	Pareto diagram of the standardized variables. Response variable was the friability.....	87
Figure IV.6	Pareto diagram of the standardized variables. Response variable was the tapped density.....	88
Figure IV.7	Morphology and topographical quality of selected batches of Na-CMC micropellets.....	90
Figure IV.8	Morphology and topographical quality as a result of screening of the process parameters of Na-alginate micropellets with 20% Na-CMC.....	92
Figure IV.9	Morphology and topographical quality as a result of screening of the process parameters of Na-alginate micropellets with 30% Na-CMC.....	92
Figure IV.10	Morphology and topographical quality of Na-alginate micropellets.....	96
Figure IV.11	Morphology and topographical quality as a result of screening of the process parameters of chitosan micropellets.....	97
Figure IV.12	Morphology and topographical quality of the chitosan micropellets.....	101
Figure IV.13	Size comparison of the attempts to form micropellets with Carbopol®.....	102
Figure IV.14	Size comparison of the attempts to form micropellets with Noveon® AA1.....	104
Figure IV.15	Rotor torque measurement during the production of Na-CMC micropellets.....	105
Figure IV.16	Relationship between water content at the end of the spraying period and maximum torque during Na-CMC micropellet production.....	106
Figure IV.17	Torque measurement of the rotor for chitosan micropellets.....	107
Figure IV.18	Differences between air humidities in inlet and outlet.....	108
Figure IV.19	Dependence of outlet air humidity on rotor speed of the GPCG1.....	109
Figure IV.20	Relative humidity of the outlet air at 23°C during an entire production process.....	109
Figure IV.21	Impact of the inlet air humidity onto the product water content.....	110
Figure IV.22	Drying kinetics of Na-CMC micropellets using a drying balance.....	111
Figure IV.23	Dynamic hydration properties of mucoadhesive polymers (described as method H1).....	113
Figure IV.24	Dynamic hydration properties of mucoadhesive polymers (described as method H2).....	114
Figure IV.25	Dynamic hydration properties of mucoadhesive polymers (described as method H2).....	114

Figure IV.26	Dynamic hydration properties of mucoadhesive polymers (described as method H2).....	115
Figure IV.27	Dynamic hydration properties of Carbopol at different pH (described as method H2).	115
Figure IV.28	Na-CMC micropellets coated with a 30% coating layer (batch 15658/46a).	116
Figure IV.29	Na-CMC micropellets coated with a 30% coating layer (batch 15658/46b).	116
Figure IV.30	Dissolution test for gastric resistance of the mucoadhesive theophyllin micropellets in 1000ml of 0.1N HCl.	118
Figure IV.31	Na-CMC micropellets coated with EUDRAGIT® L 30D-55 (batch 15658/51).....	119
Figure IV.32	Na-CMC micropellets coated with EUDRAGIT® L 30D-55 (batch 15658/56).....	120
Figure IV.33	Na-alginate micropellets coated with EUDRAGIT® L 30D-55 (batch 15658/57).	121
Figure IV.34	Chitosan micropellets coated with EUDRAGIT® L 30D-55 (batch 15658/58).	121
Figure IV.35	Na-CMC micropellets coated with EUDRAGIT® FS 30D (batch 15658/59).	122
Figure IV.36	Dissolution profile of theophyllin containing Na-CMC micropellets using APP.2 at 100rpm, described as D1 (n=6).	123
Figure IV.37	Dissolution profile of theophyllin containing Na-CMC micropellets using APP.2 modified with a 250µm sieve inlay at 100rpm, described as D2 (n=6).....	124
Figure IV.38	Dissolution profile of theophyllin containing Na-CMC micropellets between 400µm and 500µm using APP.2, modified with a 250µm sieve inlay at 100rpm, described as D3 (n=6).	125
Figure IV.39	Dissolution profile of theophyllin containing Na-CMC micropellets between 400µm and 500µm using APP.2, modified with a 360µm sieve inlay at 100rpm, described as D4 (n=6).	126
Figure IV.40	Dissolution profile of theophyllin containing Na-CMC micropellets using APP.1 at 100rpm, described as D5 (n=6).	126
Figure IV.41	Dissolution profile of theophyllin containing Na-CMC micropellets using APP.1 at 25 dips per minute, described as D6 (n=6).....	127
Figure IV.42	Dissolution of theophyllin containing Na-CMC micropellets in the reciprocating cylinder apparatus.	128
Figure IV.43	Dissolution profile of theophyllin containing Na-CMC micropellets using APP.4 at a flow rate of 10g/min.	128
Figure IV.44	Dissolution profile of 0.5g theophyllin containing Na-CMC micropellets using APP.4 at a flow rate of 10ml/min, described as D8 (n=5).....	129
Figure IV.45	Dissolution profile of 0.5g theophyllin containing Na-CMC micropellets using APP.4 at a flow rate of 20ml/min, described as D9 (n=5).....	130
Figure IV.46	Dissolution profile of 0.5g theophyllin containing Na-CMC micropellets using APP.4 at a flow rate of 10ml/min, described as D10 (n=5).....	130
Figure IV.47	Dissolution profile of batch 15658/56: theophyllin containing Na-CMC micropellets coated with EUDRAGIT L 30D-55 using App.2 and applying different agitation rates (D13).	132
Figure IV.48	Dissolution profile of Na-CMC uncoated and EUDRAGIT® L 30D-55 coated theophyllin containing micropellets using App.4 (D15 and D 17).	132
Figure IV.49	Dissolution profile of Na-CMC uncoated and EUDRAGIT® FS 30D coated theophyllin containing micropellets using APP.2 (D12 and D14).	133
Figure IV.50	Dissolution profile of Na-CMC uncoated and EUDRAGIT® FS 30D coated theophyllin containing micropellets using APP.4 (D16 and D18).	134
Figure IV.51	Dissolution profile of theophyllin containing uncoated Na-alginate micropellets (batch 15658/60) using App.2 and applying different agitation rates (D11).	135
Figure IV.52	Dissolution profile of batch 15658/57 theophyllin containing Na-alginate micropellets coated with EUDRAGIT L 30D-55 using App.2 and applying different agitation rates (D13).	135
Figure IV.53	Dissolution profile of Na-alginate uncoated and EUDRAGIT® L 30D 55 coated theophyllin containing micropellets using APP.4 (D15 and D17).	136
Figure IV.54	Dissolution profile of theophyllin containing chitosan micropellets (batch 15658/32) using App.2 and applying different agitation rates (D11).....	137
Figure IV.55	Dissolution profile of theophyllin containing chitosan micropellets (batch 15658/59) coated with EUDRAGIT L 30D-55 using App.2 and applying different agitation rates (D13).	137
Figure IV.56	Dissolution profile of chitosan uncoated and EUDRAGIT® L 30D 55 coated theophyllin containing micropellets using APP.4 (D15 abd D17).	138
Figure IV.57	EDX of poured EUDRAGIT® L 30D-55 over chitosan film before and following dissolution.	140

Figure IV.58	EDX of poured EUDRAGIT® L 30D-55 over Na-alginate film before and following dissolution.	141
Figure IV.59	EDX of poured EUDRAGIT® FS 30D over Na-CMC film before and following dissolution.	142
Figure IV.60	EDX of Na-CMC micropellets coated with EUDRAGIT® L 30D-55 before and following dissolution.	143
Figure IV.61/1	SEM of Chitosan micropellets coated with EUDRAGIT® L 30D-55 before and following dissolution.	144
Figure IV.61/2	SEM of Chitosan micropellets coated with EUDRAGIT® L 30D-55 before and following dissolution.	145
Figure IV.62	SEM of Na-alginate micropellets coated with EUDRAGIT® L 30D-55 before and following dissolution.	145
Figure IV.63	Relationship between HLB value and Moriguchi logP of the different emulsifiers presented in Table IV.28. ...	148
Figure IV.64	Relationship between HLB value and S+logP of the different emulsifiers presented in Table IV.28.	148
Figure IV.65	Relationship between HLB Value and ALOGPs of the different emulsifiers presented in Table IV.28.	149
Figure IV.66	Relationship between HLB value and CLOGP of the different emulsifiers presented in Table IV.28.	149
Figure IV.67	Relationship between HLB value and Kowwin LogP of the different emulsifiers presented in Table IV.28.	150
Figure IV.68	Relationship between HLB value and XLOGP of the different emulsifiers presented in Table IV.28.	150
Figure IV.69	DSC curve of pure spironolactone.	152
Figure IV.70	DSC curve of Softisan 138.	152
Figure IV.71	DSC curve of blended Softisan 138 and spironolactone (95:5).	153
Figure IV.72	DSC curve of blended Softisan 138 and spironolactone (90:10).	153
Figure IV.73	DSC curve of blended Softisan 138 and spironolactone (70:30).	153
Figure IV.74	DSC curve of blended Softisan 138 and spironolactone (60:40).	154
Figure IV.75	DSC Curve of blended Softisan 138 and Spironolactone (50:50).	154
Figure IV.76	DSC curve of Softisan 154.	155
Figure IV.77	DSC curve of blended Softisan 154 and spironolactone (95:05).	155
Figure IV.78	DSC curve of blended Softisan 154 and spironolactone (90:10).	156
Figure IV.79	DSC curve of blended Softisan 154 and spironolactone (80:20).	156
Figure IV.80	DSC curve of blended Softisan 154 and spironolactone (70:30).	156
Figure IV.81	DSC curve of blended Softisan 154 and spironolactone (60:40).	157
Figure IV.82	DSC curve of blended Softisan 154 and spironolactone (50:50).	157
Figure IV.83	DSC curve of vitamin E TPGS.	158
Figure IV.84	DSC curve of blended vitamin E TPGS and spironolactone (95:05).	158
Figure IV.85	DSC curve of blended vitamin E TPGS and spironolactone (90:10).	159
Figure IV.86	DSC curve of blended vitamin E TPGS and spironolactone (80:20).	159
Figure IV.87	DSC curve of blended vitamin E TPGS and spironolactone (70:30).	159
Figure IV.88	DSC curve of blended vitamin E TPGS and spironolactone (60:40).	160
Figure IV.90	DSC curve of blended vitamin E TPGS and spironolactone (50:50).	160
Figure IV.90	DSC curve of blended Softisan 138 and vitamin E TPGS (71.55:28.45).	161
Figure IV.91	DSC curve of blended Softisan 138 and vitamin E TPGS (71.55:28.45) containing 5% spironolactone.	161
Figure IV.92	DSC curve of blended Softisan 138 and vitamin E TPGS (71.55:28.45) containing 10% spironolactone.	162
Figure IV.93	DSC curve of blended Softisan 138 and vitamin E TPGS (71.55:28.45) containing 15% spironolactone.	162
Figure IV.94	DSC curve of blended Softisan 138 and vitamin E TPGS (71.55:28.45) containing 20% spironolactone.	162
Figure IV.95	DSC curve of blended Softisan 138 and vitamin E TPGS (71.55:28.45) containing 25% spironolactone.	163
Figure IV.96	DSC curve of blended Softisan 138 and vitamin E TPGS (71.55:28.45) containing 30% spironolactone.	163
Figure IV.97	DSC curve of blended Softisan 138 and vitamin E TPGS (71.55:28.45) containing 40% spironolactone.	163
Figure IV.98	DSC curve of blended Softisan 138 and vitamin E TPGS (71.55:28.45) containing 50% spironolactone.	164
Figure IV.99	DSC curve of blended Softisan 154 and vitamin E TPGS (67.20:32.80).	164
Figure IV.100	DSC curve of blended Softisan 154 and vitamin E TPGS (67.20:32.80) containing 5% spironolactone.	165
Figure IV.101	DSC curve of blended Softisan 154 and vitamin E TPGS (67.20:32.80) containing 10% spironolactone.	165
Figure IV.102	DSC curve of blended Softisan 154 and vitamin E TPGS (67.20:32.80) containing 15% spironolactone.	166
Figure IV.103	DSC curve of blended Softisan 154 and vitamin E TPGS (67.20:32.80) containing 20% spironolactone.	166
Figure IV.104	DSC curve of blended Softisan 154 and vitamin E TPGS (67.20:32.80) containing 25% spironolactone.	166
Figure IV.105	DSC curve of blended Softisan 154 and vitamin E TPGS (67.20:32.80) containing 30% spironolactone.	167
Figure IV.106	DSC curve of blended Softisan 154 and vitamin E TPGS (67.20:32.80) containing 40% spironolactone.	167
Figure IV.107	DSC curve of blended Softisan 154 and vitamin E TPGS (67.20:32.80) containing 50% spironolactone.	167

Figure IV.108	Two subsequent DSC scans of Imwitor 312.	168
Figure V.1	Relationship between water content at the end of the spraying period and tapped density.	172
Figure V.2	Relationship between micropellet water content at the end of the spraying period and pellet friability.	173
Figure V.3	Scheme of a Wurster inlet in comparison to the diskjet bottom by Hüttlin®.	176

ABBREVIATIONS

AA	Acidic acid
API	Active Pharmaceutical Ingredient
APP.1	The USP Basket Apparatus
APP.2	The USP Paddle Apparatus
APP.3	The USP Reciprocating Cylinder
APP.4	The USP Flow Through Cell
BF	Bolatec Friabimat
BP	British Pharmacopeia
Ca ²⁺	Calcium ion
conc.	concentrated
cPs	centi Pascal
Da	Dalton
D ₂ O	Deuterium
DDS	Drug Delivery System
DSC	Differential Scanning Calorimetry
EDTA	Ethylene Diamine Tetraacidic Acid
e.g.	for example
FDA	Food and Drug Administration
GI	Gastro intestinal
GMS	Glycerolmonostearate
GRAS	Generally Recognized As Safe
h	hour
HA	Hyaluronic acid
HCl	Hydrochloric acid
HLB	Hydrophilic Lipophilic Balance
HPMC	Hydroxypropylmethylcellulose
INN	International Non-proprietary Name
IMMC	interdigestive migrating motor complex
JP	Japanese Pharmacopeia
LogP	logarithm partition coefficient
MA	Methylacrylate
MCC	Microcrystalline cellulose
min	Minute
ml	milliliter
mm	millimeter
Mw	Molecular weight
μJ	Micro Joule
Na	Sodium
Na-CMC	Sodium Carboxymethylcellulose
n.d.	not determined
NF	National Formulary
pH	pH
Pharm.Eur.	European Pharmacopeia
pKa	logarithm ionization constant
Poly-EA/MMA	Poly- Ethacrylate / methylmethacrylate
RA	Rotary agglomeration
RC	Rotating cylinder

RS	Rotor speed
SR	Spraying rate
Temp	Temperature
TMC	N,N,N-trimethylchitosan chloride
US	United States
USP	United States Pharmacopeia
w/v	Weight by volume
w/w	Weight by mass
wt. %	weight in %

INTRODUCTION

Mucoadhesive dosage forms represent an interesting strategy to deliver active pharmaceutical ingredients (APIs) of poor oral bioavailability, such as substances belonging to the biopharmaceutical classification system classes 3 and 4. They can also be valuable for targeting APIs to specific absorption sites in the GI-tract, e.g. as it is reported for furosemide (Staib, 1989). Improving bioavailability by prolonging and/or intensifying the contact between controlled release dosage forms and the stomach or gut mucosa on one hand, but also by possibly inhibiting the proteolytic enzymes and influencing the permeability of mucosal epithelia (Lehr, 1994b) may also be achieved. Regarding colonic delivery, mucoadhesion may lead to a longer residence times in the proximal and transversal colon where higher water content and lower faeces viscosity may result in an increase in uptake of a drug as compared to the distal colon.

Bioadhesive microparticles combine the advantage of multiparticulate dosage forms with bioadhesion. They are characterized to show a higher dispersibility within the intestine and show less variability in gastrointestinal transit time as compared to single unit dosage forms (Follonier, 1992) which even develop weaker mucoadhesive bonds (Peppas, 1985). Bioadhesive microspheres in general provide a high surface to volume ratio and are able to cover a larger surface of the mucosa.

AIMS

The purpose of this work was the development of bioadhesive micropellets consisting of sodium carboxymethylcellulose (Na-CMC), sodium-alginate, chitosan, polycarbophil and polycarbopol using wet spherization by rotary agglomeration (RA). These polymers are well known for their mucoadhesive properties. They are approved for use in oral dosage forms by the authorities. In an additional step the particles should be enteric coated with polymethacrylates to target the dosage forms to the small intestine or to the colon. In the current thesis micropellets are defined as spheric particles with a diameter less than 700 μ m. Uncoated micropellets of 250 μ m were selected for the following reason: The microparticles are designed to be as small as possible yet sufficiently large to be used for enteric coating by conventional air suspension processes. Since the surface area of particles is growing exponentially by a reduction of their diameter, the amount of polymer needed for the enteric coating grows accordingly. Therefore, particles smaller than 250 μ m would require non-tolerable amounts of polymers. Particles as large as 600 μ m were defined as upper limit for coating purposes to reach a final coated particle size of 700 μ m.

Until today, methods for manufacturing mucoadhesive pellets of the designated size range without the use of crosslinking agents such as calcium or magnesium ions for alginate microbeads (Shilpa, 2003) or tripolyphosphate for chitosan microbeads (Ko, 2002) do not exist. Other manufacturing processes like extrusion/spherization result in comparatively large particles of 700 μ m to 2000 μ m in size (Chatchawalsaisin, 2004; Santos, 2002; Steckel, 2004) or too small particles, for example by solvent evaporation or spray drying (Vasir, 2003).

RA was selected because it is an efficient multistage, single-pot spheroid production method for dense spheroids of a narrow size distribution in the desired particle size range [from 250 μm to 600 μm]. The process has been characterized as a critical process that demands a high level of control of process parameters (Vertommen, 1997b). The use of mucoadhesive polymers in RA poses multiple technical hurdles due to their tendency to building gels, their high swelling capacity and their high tackiness. These properties of the polymers are responsible for the creation of diffusion barriers around dry powder cores causing lumps. To overcome these problems the addition of electrolytes to the wet masses, such as calcium chloride or potassium chloride has been advocated, which are salting out the polymers, and thus reduce their gel-forming-tendency, and tackiness, and decrease the interaction between carboxylate groups (Neau, 2000; Qudan, 2002). The back draft of these methods is a decrease in bioadhesion of the resulting spheres (Neau, 2000).

In this dissertation, particles with suitable friability, tapped density, particle size and yield were manufactured to be used in the subsequent coating process. Initial efforts focused on the development of bioadhesive Na-CMC pellets, including a rigorous evaluation of factors influencing the process parameters of interest. For the characterization of the dissolution behaviour of the prepared micropellets different dissolution methods and conditions were developed and evaluated.

CHAPTER I BACKGROUND

1.1. Basis for Drug Delivery to the Gastrointestinal Tract

1.1.1. Anatomy and Physiology of the Gastrointestinal Tract

Each part of the gastrointestinal tract (GI-tract) has been anatomically designed to accomplish specific goals. In general, the **oesophagus** serves simply as a conduit between the mouth and the stomach. The environment and anatomical conditions of the stomach result in the reduction in bacterial count of ingested material, liquefaction of solid food and for many solid dosage forms that are conducive to disintegration and drug dissolution. The small intestine represents the primary area for digestion, absorption of food constituents and uptake of drugs. Although absorption may take place in the large intestine, the physiologically important events are the exchange (uptake or secretion) of minerals and water. The anatomical characteristics important to drug absorption are presented next.

For oral dosage forms the **stomach** may be considered as a reception area. Although the gastric mucosa is folded into rugae, which increase the epithelial surface area to a limited extent, the stomach is not the principal region for uptake because the total mucosal area is small, the epithelium is dominated by surface mucosal cells rather than absorptive cells and the gastric residence time is limited. In fact, the time required for drug release may exceed the residence time, in which case there will be little or no opportunity for gastric uptake of a drug.

The **small intestine** can be divided into three areas: the duodenum, the jejunum and the ileum. Like the stomach and most of the large intestine, it is covered by a membrane tissue, the mesentery, which contains arteries, veins, nerves and lymphatics. Due to the huge amplification of surface area, the duodenum and jejunum are the main regions for the drug uptake. The large surface area results from folds, villi and microvilli. The villi of the distal duodenum and proximal jejunum are leaf- or finger- shaped and range from 0.5 to 0.8mm in height, whereas those in the ileum are smaller. The villi and their crypts are covered by a single layer of epithelial cells. The apical border of the villous absorptive cells is tightly packed with microvilli of approximately 0.5 to 1.5 μ m in length and 0.1 μ m in width with a membrane about 10nm thick, leading to an enlargement of the absorptive surface by a factor of about 25 (Madara, 1987) (Alberts, 1995). Enzymes, which are present in the microvillus membrane (brush border enzymes) are aminopeptidase A/N, aminooligopeptidase, carboxypeptidase, dipeptidylaminopeptidase IV, glycosidase, lactase, maltase/ isomaltase and sucrase. Enzymes summarized in Table I.1 are present in the lumen of the intestine (Crane, 1975; Kim, 1974). These are primarily engaged in the digestion of nutrients, but may also degrade ingested drugs.

Table I.1 Intestinal enzyme population – luminal pancreatic enzymes.

Carbohydrate Digestion	α -Amylase
Protein Digestion	Endopeptidases: Trypsin α -Chymotrypsin Elastase Exopeptidases: Carboxypeptidases
Fat Digestion	Lipase Phospholipase Esterase

The intestine is further characterized by a distinctive pH profile (Table I.2) starting with very low pH values in the stomach which increase by moving distally along the intestine. There is a slight elevation in the pH at the ileocaecal junction. Depending on the age (Christiansen, 1968; Ogata, 1984) the health status (Fallingborg, 1993), and pre-prandial versus post-prandial conditions (Malagelada, 1976), the pH values may vary greatly between individuals.

Table I.2 pH-values in the human gastrointestinal tract.

Intestinal Segment		Fasted State	Fed State
Stomach		1.4-2.1	4.3-5.4
Small intestine	Duodenum	4.9-6.4	4.2-6.1
	Jejunum	4.4-6.4	5.2-6.2
	Ileum	6.5-7.4	6.8-7.5
Large intestine	Caecum	6.4	
	Colon (upper)	6.0	
	Colon (lower)	7.5	

Values from Uch and Dressman 1996 (Uch, 1996)

Bile and pancreatic fluids are secreted via the common bile duct and the greater pancreatic duct, which enter the duodenum approximately 9-10cm distal to the pylorus.

The large intestine is morphologically divided into three parts. The caecum with the appendix is located just distal to the ileum, followed by the colon, which is further divided anatomically into the ascending (~15cm), transverse (~50cm), descending (~20-25cm) and the sigmoid colon (~40cm). The rectum is the most distal part of the intestine and is contiguous with the anus. The walls of caecum and ascending colon are usually folded into sacs, the so called haustra. Haustra are not fixed structures but are formed by contraction of circular muscle. The main absorptive process of the large intestine is the active uptake of Na⁺ and water. As the chyme moves along the colon, water is reabsorbed and the intestinal content becomes more viscous. Orally administered drugs may be absorbed from the large intestine, with the proximal colon being the most efficient site. The absorption rate is usually slower in the colon than in the small intestine, partly because of a reduction in effective surface area due the lack of villi, and possibly due to the increased viscosity of the colonic contents. Another potential limitation to colonic drug uptake is the biotransformation of the drug by the bacterial flora. The presence of abundant microorganisms is another characteristic of the large intestine, mainly in the proximal part and the caecum. It is suggested that about 400 different bacterial species exist in the large bowel, including bacteroides, coccis, bifidobacteria, eubacteria and lactobacilli, with a total count of about 10¹² bacteria/g gut content (Macfarlane, 1991). These microbial microflora produce bacterial exo-enzymes (Table I.3) and maintain anaerobe

fermentation conditions. Carbohydrates not digested in the small intestine are converted into short chain fatty acids (SCFA), that lower the pH value of the luminal contents by up to 3 pH units compared to the pH value in the ileum, before being absorbed by the large intestine (Bugaut, 1987).

Table I.3 Bacterial microflora and exo-enzymes.
Adopted from Uch 1999 (Uch, 1999).

Species	Enzymes	
	Reductive	Hydrolytic
Bacteroides	Nitroreductase	No enzymes known
Clostridia	Azoreductase Hydrogenases	Glucosidase Sulfatase
Enterobacteria	Nitroreductase N-oxid-reductase Sulfoxid-reductase	Esterase Amidase Glucuronidase Sulfatase
Lactobacilli	Azoreductase Hydrogenase	No enzymes known

1.1.2. Secretions of the Mucosa of the Gastrointestinal Tract

Mucus is secreted throughout the entire GI-tract. It is a viscous, aqueous fluid which covers the mucosa and consists mainly (up to 95%) of an aqueous electrolyte solution. Approximately 5% consists of a complex mixture of glycoproteins which impart viscosity to the mucus. The remainder consists of microorganisms, intracellular organelles, and plasma components. The ability of mucus to protect the sensitive epithelial cells is attributed to the glycoproteins, which are usually called mucins. Although structure, size and contents of mucins vary with the region of the GI lumen, a common feature is their high carbohydrate content (more than 50% w/w) which imparts viscoelastic properties. The type, molecular weight and concentration of polysaccharides determine the ability of mucus to protect the epithelial cells. Intestinal mucins consist of glycoproteins which vary in size (from 2.5×10^5 to 2×10^6 Da) and in structure of the carbohydrate. The most common amino acids are threonine, serine, proline, glycine and glutaminic acid. The most common carbohydrates are fucose (an aldose-pentose), galactose and N-acetylglucosamine. Unlike other gastrointestinal secretions, mucus adheres to the mucosal epithelial surfaces as a water insoluble gel until degradation and erosion takes place (Allen, 1981) leaving a mucin solution or slough on the lumen side of the gel. Functions of the mucus layer include:

- Coating of particles present in the GI lumen (bacteria, destroyed cells, inert non-digestible particles, food residues, etc.), so that they can move along the GI-tract without injuring the membrane of the epithelial cells. The hydrophilic properties and the viscoelasticity of the mucin make it an efficient biological lubricant;
- Protection of the gastric mucosa from the destructive effects of acids, alcohol, and other ingested irritants, and of the small intestinal mucosa from proteolytic pancreatic enzymes;
- Protection of the GI epithelium from invasion by microorganisms which may be ingested with food or which colonize the lower part of the GI-tract;
- Maintaining the mucosa in a hydrated condition via the ability of the mucins to pertain water and ions.

Apart from mucus, **secretions of the gastric mucosa** are pepsinogen, hydrochloric acid and ions (mainly Na⁺ and K⁺). Urease and lipase are also secreted but their participation in digestion is of limited significance. Gastric secretion is stimulated by the presence of food, but even in the fasted state a basal secretion of approximately 20 ml per hour exists in the stomach. A physiological important constituent of gastric chyme is hydrochloric acid because it acts as an antiseptic to the gastric contents and controls activation of pepsin.

Duodenal secretions include mucus, enzymes and isotonic fluid. The amount of mucin that is secreted by the duodenum represents only about 0.5% of the secretions of the glands and crypts the remaining fraction consist of enzymes and aqueous fraction. The aqueous part of the secretions contains Na⁺, Cl⁻, K⁺ and mainly of HCO₃⁻. Enterokinase, which is necessary for the activation of peptidase, is one of the most important enzyme secreted from the duodenal mucosa.

The **secretions of the large intestine** consist mainly of mucus and alkaline solutions which contain HCO₃⁻, Na⁺ and K⁺. Lysozyme, a hydrolase responsible for balancing the bacterial content of the colonic flora, is also secreted.

1.2. Transit of Dosage Forms

Transit along the GI lumen is a complex process which is affected by both the anatomy and the motility characteristics of the various segments of the GI tract.

1.2.1. Oesophageal Transit

Liquids pass along the oesophagus faster than solids. The transit time of a volume of 10ml in a healthy adult in the supine position takes about 20s - even less when the subject is in supine position. In adults with normal oesophageal function, the transit of solids is usually completed in less than 2min regardless of the motility pattern. In contrast to the oesophageal transit where both longitudinal and circular muscles are involved in propagation, gastric emptying is governed entirely by the contractions of the circular muscle. Gastric emptying is controlled by the two motility patterns. Table I.4 gives an idea of the variability of the gastric residence times as a function of the type of dosage form and the motility state.

Table I.4 Representative gastric residence times (expressed as half-lives of gastric emptying) for several types of dosage forms (Macheras, 1995)^a.

Dosage form	Fasted state or after light meal (min)	Fed State (min)
Aqueous solution	8, 18 (4)	40 (14)
Suspension (microspheres)	48 (32-87)	58 (34 – 75)
Pellets (<2 mm)	99 (7), 70 (60-150)	285 (45), 119 (15)
Tablets (indigestible)	45 (15-120)	180-780
Monolithic dosage form	183(77)	>550

^a These representative data have been collected from studies done in the 1980s. The variability is shown in parentheses as standard error of the mean or as range.

1.2.2. Gastric Emptying of Liquid Dosage Forms

The emptying process of liquids with a volume of less than 50ml is controlled by the interdigestive migrating motor complex (IMMC). During phase I gastric emptying is negligible, whereas it reaches a maximum during phase III. With higher volumes gastric emptying is less dependent on the IMMC. Lower pH and hyper-osmolarity lead to slower rates of liquid emptying. Nutrient liquids with volumes more than 200ml empty slower than non-nutrient liquids of identical volume. Kinetics are

approximately zero order. The energy content of the liquid appears to be the most important determinate for the rate of emptying.

1.2.3. Gastric Emptying of Non-Digestible Solids (Solid Dosage Forms and Drug Particles)

Applied in the **fasted state**, solid dosage forms are initially emptied in the fundus of the stomach. If administration is accompanied by less than 50ml of water, both the water and the dosage form leave the stomach in a manner that depends on the phase of the IMMC. Substantial transport to the duodenum occurs only during phase III. If administration is accompanied by more than 50ml of water, gastric emptying will depend on the physical characteristics of the solids. When gelatin capsules or immediate release tablets are administered, drug particles or granules may disperse over the intragastric area. Particles measuring less than 0,5mm in diameter may become trapped in the mucus and in that case will empty only when mucus discharge occurs in conjunction with phase III contractions. Particles with less than 1mm size and a density of 1g/ml will empty the stomach together with the administered water. Gastric emptying of the remaining particles and granules will be dependent on the phase of the IMMC. In general, 2-6mm particles will empty primarily during phase III. Gastric emptying of non-disintegrating dosage forms with a diameter greater than 6mm (monolithic dosage forms) occurs only during phase III contractions, which may be any time from a few minutes up to several hours following administration. Depending on the shape and the flexibility of the dosage form its gastric emptying may be delayed up to 24 h.

The gastric emptying of non-digestible solids in the **fed state** is controlled by intragastric hydrodynamics. Important variables to consider include the size and the density of the solids, as well as the viscosity and emptying rate of the liquid fraction of the gastric contents. In general, particles with a diameter of less than 1mm empty with the liquid fraction of the meal. Larger particles show a lag time prior to the onset of emptying. Particles with diameters from 2 to 5mm and a density of approximately 1g/ml enter the duodenum at a rate inversely proportional to their size according to a pattern similar to that followed by the liquid fraction of the meal. If the size is above 5mm, particles remain in the stomach until the digestive motility pattern is replaced with the fasting pattern and phase III contractions occur.

Apart from food, GI motility is affected by additional factors such as gender, age, emotional status, certain diseases, and administration of other drugs which can therefore indirectly affect the gastric emptying of solids.

1.2.4. Small Intestinal Transit

Small intestinal transit does not differ much between solids and liquids and is independent of meal intake (provided that viscosity is not altered significantly). Also, pathological situations such as those which affect gastric emptying or large intestine pathophysiology such as diarrhea, constipation or ulcerative colitis do not significantly affect transit through the small intestine. For solids, specifically, transit time is independent of density (for densities lower than 3 g/ml) and size (for size smaller than 25 x 9mm). The different transit behaviour between the stomach and small intestine may be attributed, apart from physiological differences, to some key anatomical differences between these two parts of the GI tract, such as:

- the stomach is more fixed in position than the small intestine, which is suspended in the abdominal area by the mesentery;

- in the stomach, the pylorus is located above the stomach curvature, which makes emptying from that region difficult. In contrast, the small intestine lacks variation in its internal diameter;
- the internal diameter of the small intestine is much smaller and the effects of the contraction in the mixing and velocity of the chyme are more significant.

Generally, the time between administration and arrival at the ileo-caecal valve under normal conditions is approximately 4 to 8h in the fasted state and 8 to 12h in the fed state. This difference may be attributed almost entirely to differences in gastric emptying and not in small intestinal transit. Under most conditions small intestinal transit duration is 3 to 4 h (range: 1 to 6 h).

1.2.5. Large Intestinal Transit

The time for arrival of a drug in the colon may range in extreme situations from 4 to 20h. In contrast to the small intestine, dispersion of the drug in the large intestine may occur and colonic transit may vary considerably. In general, particles larger than 6mm (e.g. monolithic dosage forms) pass through the large intestine faster than solutions or small particles. Dosage forms which have approximately the size of a capsule or a tablet pass through the colon in 15 to 30h (range: 1 to 60h) regardless of their density. In contrast, solutions and small particles remain in the colon for 25 to 40h (range: 6 to 50h). Colonic transit varies with gender (1.5 times slower in women than in men) and certain pathological conditions (for example the transit time is significantly faster in the presence of diarrhea whereas in Crohn's disease it is increased). In contrast, inflammatory bowel disease and irritable bowel syndrome have little effect on transit times.

1.2.6. Prolongation of Gastrointestinal Transit Time

Since the small intestine represents the most favourable area for drug absorption, the objective in the majority of cases is to increase the residence of the dosage form, and/or of the drug molecules in regions above the ileo-caecal valve. However, the small intestinal transit is limited to 3 to 4h and difficult to manipulate. In case of colitis ulcerosa the prolongation of the residence time in the colon might be useful.

1.2.6.1. Methods for Increasing Gastrointestinal Residence Time

The strategies for delaying drug transit through the gastrointestinal tract fall into one of three categories. A pharmacological approach involves the co-administration of a drug which delays gastrointestinal transit. Examples include smooth muscle relaxing antimuscarinics, e.g. propantheline (Beermann, 1976; Manninen, 1973) or opiate analgesics or their derivatives such as iperamide (Minami, 1984) which change the motility pattern. However, the potential side effects that may arise from such concomittant treatments on a routine basis would not be acceptable for regulatory approval of a combination drug product. A more physiological approach is given by the use of natural materials or fat derivatives such as triethanolamine myristate, which stimulates the duodenal or jejunal receptors to slow gastric emptying (Gröning, 1984; Gröning, 1989). The use of large amounts of a "volume filling" such as polycarbophil can also cause a decrease in gastrointestinal transit time (Harris, 1990a; Harris, 1990b). Pharmacological and physiological

approaches thus set out to delay gastrointestinal transit by a modification of the rate of gastric emptying using “passage-delaying agents”. Pharmaceutical strategies on the other hand attempt to achieve the same objective by retaining the dosage form at or upstream of its absorption site for as long as possible. This is achieved by particular physical or physicochemical characteristics, for example:

- Swelling balloon hydrogel: If large enough, the formulation will not be expelled from the fasted stomach even when the pyloric sphincter is in its non-contracted state. The size-related retention of a dosage form in the stomach has been studied with various systems for example with swelling balloon hydrogels (Park, 1987). These have though never passed beyond the experimental stage and therefore these gastric retention devices may not be safe. Another approach uses dosage forms of moderately high density, based on the premise that high density formulations remain in the stomach for longer periods than conventional formulations. The effectiveness of this approach has not been confirmed on a broad basis and the evidence thus remains controversial (Moes, 1993).
- Buoyant density/flotation approach: This approach uses buoyant dosage forms which float on the gastric contents as a result of their relatively low density. Moes has attempted to clarify the conflicting views on the gastric retention capabilities of floating system resulting from a number of *in vivo* trials by different authors (Kaus, 1987; Lippold, 1991; Moes, 1993; Muller-Lissner, 1981; Sangekar, 1987; Timmermanns, 1991; Timmermanns, 1990).
- Polymer mucoadhesion: This approach involves attachment or encapsulation of the drug with a polymer which interacts with either the mucosal epithelial/glycocalyx cell lining of the gastrointestinal tract (“direct” mucoadhesion) or the mucus surfaces (the gel and sloughed mucus in the lumen) of mucosal epithelial/glycocalyx cell lining of the gastrointestinal tract, hence providing a macromolecular “break” to the movement of the drug.

1.3. Mucoadhesion

In cases when a polymeric carrier can interact directly with the surface mucosal epithelium or glycocalyx, not only the residence time may be prolonged, but also the decrease in diffusional pathway from the oral DDS (drug delivery system) to the absorbing biological membrane might be an additional advantage for improving drug absorption. This close contact between membrane and DDS minimizes the dilution and possible degradation in the luminal fluids (Hayton, 1980). The DDS may be optimized by addition of penetration enhancers to enable alteration of membrane permeability. Also, the inclusion of specific enzyme inhibitors can provide further protection for instable drugs and consequently, the bioavailability may be increased (Junginger, 1992; Wearley, 1991). The interaction with the mucosal surface/gel lining (thickness 40-450µm) of the gastrointestinal tract provides the most likely strategy, because the epithelium may not be accessible and covered by the gel lining.

The effect of bioadhesion has been studied for over a decade, mainly by *in vitro* or *ex vivo* tests with few *in situ* or *in vivo* studies and even fewer trials in man. Despite the fact that bioadhesion, or more specifically mucoadhesion, has led to some success in drug delivery for ocular, buccal, nasal, vaginal and cervical applications (Bouckaert, 1994; Duchêne, 1988; Graeves, 1993; Nagai, 1986; Nagai, 1984; Schor, 1983; Smart, 1993), gastrointestinal mucoadhesive drug delivery

systems have yet to be successfully established (Fiebrig, 1996; Helliwell, 1993). In the process of mucoadhesion large amounts of water are involved, or more vividly, it could be seen as “adhesion to water in a semisolid form” where mucin plays a key role in maintaining the gel-like properties of the substrate for a potential drug delivery platform.

1.3.1. Mechanisms of Mucoadhesion

The water insoluble mucus gel lining of the mucosa of the gastrointestinal tract is the most relevant target phase for the concept of mucoadhesion. This mucus layer is characterized by a variable thickness of 50– 450 μm in man, about half of that in the rat, with regional differences. For example, mucus thickness in the rat stomach is variable where a layer of 100-150 μm thickness forms a firm layer of adherent gel and another 100 μm of viscous mobile mucus is present on its top. In the colon, the adherent gel has a mean thickness of approx. 65 μm covered with another approx. 700 μm mobile viscous mucus layer on top that can be removed by suction. In both cases the adherent gel barrier is continuous.

The present knowledge about the mechanism and the structural requirements of mucoadhesive hydrogels is still very limited, and no generally accepted theory has been found yet to explain this phenomenon. Most scientists working in the field of mucoadhesion recognized at least two basic steps in the process of adhesion. In step I, the contact stage, an intimate contact between the mucoadhesive polymer and the mucus gel layer is formed. In step II, the consolidation stage, the adhesive bond is strengthened and consolidated, providing a prolonged adhesion. In this second step, chemical and physical interactions are involved. Chemical interactions include:

- hydrogen bonding, which is based on hydrophilic functional groups such as hydroxylic groups, carboxylic groups, amino groups, and sulfate groups;
- ionic interactions such as the interaction of the cationic polymer chitosan with anionic sialic acid moieties of the mucus (Hassan, 1990);
- van der Waals forces, which are based on various dipole-dipole interactions;
- covalent bonds which are much stronger in opposite to secondary bonds, and are not influenced by parameters such as ionic strength and pH: Thiol groups are typically the functional groups that are able to form covalent bonds with the mucus layer. Thiolated polymers are able to mimic the naturally occurring mechanism by which lumenally secreted mucus glycoproteins are immobilized in the mucus by formation of interchain disulfide bonds (Bernkop-Schnurch, 2001b).

The physical interaction is an interpenetration of the mucoadhesive polymer with the mucus gel layer, followed by entanglement of the polymer chains (Iman, 2003). Further factors influencing the mucoadhesion are the cohesive properties and the swelling behaviour. Mucoadhesive DDSs with insufficient cohesive properties will not remain on the mucosa, even if the polymer strongly adheres to the mucus gel layer. This is caused by the circumstances that mucoadhesive bonds will fail within the mucoadhesive polymer itself (Bernkop-Schnurch, 2001b). On one hand, faster swelling polymers are able to achieve greater interpenetration, but on the other hand, intense swelling of the polymers may lead to the risk of loss of gel cohesion and shorter duration of adhesion (Bernkop-Schnurch, 2001b). The swelling behaviour of

ionizable polymers will depend upon the local pH and ionic strength of the liquid adhering to the mucosa. The swelling of the polymers is caused by the occurrence of repulsion forces within the polymer structure resulting from the ionization of the polymers.

Although it has been previously suggested that preferentially highly charged carboxylated polyanions represent good mucoadhesive properties (Gu, 1988; Leung, 1988; Leung, 1990; Park, 1985; Peppas, 1985), the reported mucoadhesive properties of chitosan (Hassan, 1990; Lehr, 1992a) as well as some preliminary data with experimental copolymers of poly(acrylamide) and poly(dimethyl-aminoethyl-methacrylate), show that polycations can be used as well, and their mucoadhesive performance may be even better at neutral pH (Park, 1989). Today, most researchers in the field would probably agree that a high molecular weight, a large – but not unlimited – aqueous swelling capacity, as well as the ability to form hydrogen bonds are features that favour mucoadhesion of polymeric hydrogels (Lehr, 1994b).

1.3.2. Mucoadhesive Polymer Types

1.3.2.1. Non-Covalent Binding Polymers

Anionic mucoadhesive polymers that are used for oral DDS exhibit carboxylic acid groups. These carboxylic acid moieties are believed to form hydrogen bonds with hydroxyl groups of the oligosaccharide sidechains on mucus glycoproteins. The most important anionic mucoadhesive polymers for the DDS are alginate and salts thereof, polyacrylic acid (crosslinked with allylsucrose or divinylglycol), chitosan-EDTA (optionally crosslinked with EDTA), and sodium carboxymethylcellulose. In this group one can find the most adhesive non-covalent binding polymers such as polyacrylates and sodium carboxymethyl-cellulose (Smart, 1984; Toby, 1996). The high charge density of these polymers leads to their high buffer capacity that might be further beneficial for various reasons as discussed in the same Chapter. As mentioned above, the swelling behaviour of anionic polymers strongly depends on the pH level. A lower pH leads to a lower swelling behaviour, which can lead to quite insufficient adhesion. On the other hand, a too rapid swelling of such polymers at higher pH levels can lead to “overswelling”, which may cause a strong decrease in the cohesive and subsequent mucoadhesive properties of the polymer.

Cationic mucoadhesive polymers used for peptide-delivery systems are mainly chitosans and derivatives thereof (Bernkop-Schnurch, 2000b). A possible explanation of the mucoadhesive properties of these polymers is the interaction with anionic substructures such as sialic acid moieties of the mucus gel layer. Because of their mucoadhesive properties and their permeation enhancing effect, and also due to their very safe toxicity profile (Arai, 1968), chitosans are widely used as pharmaceutical excipients (Illum, 1998). The most commonly used chitosans are chitosan and trimethylated chitosan. Backdrafts of chitosan are the rapid hydration in gastric fluids leading to a strong reduction of their cohesive properties and their non ability to swell at pH levels above 6.5 thus preventing mucoadhesion. On the other hand the bioavailability of buserelin, insulin and calcitonin was strongly improved by administration using a chitosan formulation (Lu, 1996; Luessen, 1996a; Luessen, 1991; Takeuchi, 1999; Takeuchi, 1996).

Non-ionic mucoadhesive polymers are less dependent on the pH level and electrolyte concentration of the surrounding fluid than the ionic polymers. Non-ionic

polymers are, in most cases, less adhesive than ionic mucoadhesive polymers, and thus play only a minor role in oral DDSs.

1.3.2.2. Covalent-Binding Polymers

Recently, the bridging structure most commonly encountered in biological systems - the disulfide bond - was also found to be present in the covalent adhesion of polymers to the mucus gel layer. Thiolated polymers, or so-called thiomers, are mucoadhesive basis polymers that display thiol-bearing side chains. These polymers are able to form disulfide bonds between themselves and cysteine-rich subdomains of mucus glycoproteins. These reactions are based on thiol/disulfide exchange reactions and/or simple oxidation processes. These thiomers mimic the natural mechanism of secreted mucus glycoproteins, which are also covalently anchored in the mucus layer by the formation of disulfide bonds. The covalent attachment of cysteine to polycarbophil strongly improved the adhesive properties of the polymers. For example the unmodified basis polymer displays a total work of adhesion (TWA) of $104 \pm 21 \mu\text{J}$, whereas it was $280 \pm 67 \mu\text{J}$ for a corresponding polymer-cysteine conjugate (Bernkop-Schnurch, 1999b). In another study, the mucoadhesive properties of chitosan were improved 4-fold by the covalent attachment of thioglycolic acid to the polymer (Kast, 2001). These improved mucoadhesive properties were shown for various other thiolated polymers (Bernkop-Schnurch, 2001a; Bernkop-Schnurch, 2000c). Further important advantages of the thiomers are the strongly improved cohesive properties which lead to an improvement of adhesion. For example, tablets consisting of polycarbophil disintegrate within 2 hours, whereas tablets based on the corresponding thiolated polymer remain stable even for days in the disintegration apparatus according to Pharmacopoea Europea (Bernkop-Schnurch, 2000d). The thiomers combine the rapid hydration together with the ability to form highly cohesive and viscoelastic gels due to the formation of additional disulfide bonds. Chitosan-cysteine, chitosan-thioglycolic acid, sodium carboxymethylcellulose-cysteine, poly-carbophil-cysteamine, polycarbophil-cysteine are generated polymers, that display strongly improved mucoadhesive properties compared to the corresponding unmodified polymers. The following table (Table I.5) shows a general overview of the mucoadhesive strengths of various multifunctional polymers, ranked in the laboratory from Bernkop-Schnurch (Bernkop-Schnurch, 2001b).

Table I.5

Ranking of mucoadhesive properties (Bernkop-Schnurch, 2001b).

Polymer	Mucoadhesive Rating
Alginate	+
Alginate-Cystein	+++
Chitosan	+++
Chitosan-thioglycolic acid	++++
Polyacrylic acid	+++
Polyacrylic acid-chymostatin ¹	+++
Polyacrylic acid-soybean trypsin inhibitor ²	++
Polycarbophil-cysteine	++++
Sodium carboxymethyl-cellulose	++
Sodium carboxymethyl-cellulose-elastinal ³	++

¹Mucoadhesion strength is classified as either (+) very low, (++) low, (+++) strong, (++++) very strong.

²Soybean trypsin inhibitor is a protein with a molecular weight of 20000 g/mol.

³Chymostatin is a protease inhibitor produced by actinomycetes. [(S)-1-Carboxy-2-phenylethyl]-carbamoyl-a-[2-amidohexahydro-4(S)-pyrimidyl]-(-S)-glycyl-[A = Leu; B = Val; or C = Ile]-phenylalaninal, the major form is A. For chemical structure see Bernkop-Schnürch et al. (Bernkop-Schnurch, 2001).

³Elastinal is a peptic inhibitor of elastase-like serine protease produced by actinomycetes. For chemical structure see Bernkop-Schnürch et al. (Bernkop-Schnurch, 2001).

The use of polymers with adhesive properties can increase the residence both in the small intestine and in the colon. An important drawback of the thiomers is their unclear regulatory status as excipients and secondly their insufficient supply. These issues prevent at present their use in a market near DDS development.

The potential of **multifunctional polymer matrices** has been pointed out in recent years by numerous *in vivo* studies that have demonstrated strongly improved bioavailability of the active after oral dosing (Luessen, 1996a; Marschutz, 2000; Thanou, 2000a; Thanou, 2000b). In addition to mucoadhesive properties a multifunctional matrix exhibits at least one of the following properties:

- Enzyme inhibiting polymers
- Permeation enhancing effects
- High buffer capacity
- Delayed release of API

Several researchers have demonstrated that polymers of acrylic acid have the ability to inhibit a broad range of proteolytic enzymes of the GI-tract *in vitro* (**enzyme-inhibiting polymers**) (Luessen, 1996a) (Bai, 1996). The polymers polycarbophil and Carbopol 934P were able to inhibit a large range of luminal proteolytic enzymes as has been demonstrated by studies in the rat (Luessen, 1996d). Enzymes involved are trypsin, α -chymotrypsin, carboxypeptidase A, cytosolic leucine aminopeptidase, and brush-border peptidase. The main mechanism for the enzyme inhibitory effect is the ability of these acrylic-acid polymers to bind Ca^{2+} and Zn^{2+} ions. It is believed that calcium chelation of the results in a sufficient conformational change in the protein structure (Luessen, 1995b). Walker et al. further suggested that, in addition, trypsin denaturation may occur by the binding of trypsin to the acrylic acid polymer (Walker, 1999). Thiomers of polyacrylic acid have shown an even greater affinity for zinc ions in comparison to the unmodified polymer. They therefore inhibited the zinc-requiring carboxypeptidases A and B at lower concentrations in comparison to the unconjugated polymer (Bernkop-Schnurch, 2000e).

Chitosan does not exhibit any inhibition activity against peptidases. However, it is possible to conjugate chitosan with complexing agents, like EDTA. These conjugates were shown to inactivate membrane-bound Zn²⁺-dependent peptidase as well as carboxypeptidase A and aminopeptidase N. The inhibitory effect of the chitosan-EDTA conjugates onto carboxypeptidase A and aminopeptidase N was stronger than the inhibitory effect of acrylic acid polymers (Bernkop-Schnurch, 1998a). It is also possible to conjugate the polymers with specific enzyme inhibitors such as chymotryptic inhibitors chymostatin- and soybean trypsin and thus improve the enzyme inhibition specificity of the polymers (Bernkop-Schnurch, 1997). A number of advantages are attributed to these new enzyme inhibiting polymers and conjugates as compared to well known peptidase inhibitors. They are not absorbed from the intestine and therefore they are not likely to cause significant systemic toxicity. The mucoadhesive properties of the polymers will in addition provide intimate and prolonged contact between the inhibitor and the adsorbing intestinal membrane, and thus the enzyme inhibitory activity of the polymer and the enzymatically labile drug will be co-localized (Bernkop-Schnurch, 2001b).

The responsible mechanisms for the **permeation enhancing** effect of some mucoadhesive polymers are still unresolved. It has been hypothesized that this effect which is exhibited by e.g. some polyacrylates may be based on the depletion of Ca²⁺ ions, because these polymers display a high binding capacity for Ca²⁺ ions. This theory is based on the knowledge that on the one hand many Ca²⁺ complexing agents, for example EDTA, display a permeation enhancing effect (Tomita, 1994), and on the other hand that Ca²⁺ plays an essential role in the gate fence function of the tight junctions, being mainly responsible for their closing. Cationic polymers such as chitosan may interact with the cell membrane and due to their charge result in a structural reorganization of tight junction associated proteins (Schipper, 1997). The permeation enhancing effect of these mucoadhesive polymers can even be significantly improved due to the immobilization of the cysteine residues (Clausen, 2000b; Clausen, 2001). In Table I.6, a list of permeation enhancing polymers is displayed.

Table I.6 Multifunctional polymers that display a permeation enhancing effect (Bernkop-Schnurch, 2001b).

Polymer	Model Drug
Carbomer	Buserelin
Chitosan	Buserelin, 9-desglycinamide-8-L-arginin vasopressin
Chitosan-cysteine	Bacitracin
Sodium carboxymethyl-cellulose	Insulin, bacitracin
Sodium carboxymethyl-cellulose-cysteine	Insulin, bacitracin
Polycarbophil-cysteine	Bacitracin
Polycarbophil-cysteine	Bacitracin
Starch	Insulin
N-trimethylated chitosan	Buserelin

1.3.2.3 Polymers with High Buffer Capacity

A high buffer capacity of the polymeric excipients may be viewed as an additional advantage. Ionic polymers may act as ion exchange resins and therefore are able to maintain a pH level inside their polymeric network over a considerable time period irrespective of the pH of the surrounding medium. For example, neutralized carbomer matrix tablets can maintain the pH within the matrix for hours when immersed in artificial gastric fluid at pH 2 (Bernkop-Schnurch, 2000f). A pH of

about 7 was even maintained in the gastric fluid for several hours with hydrated ionic polymers. This acidic microenvironment may even provide a stabilization of enzymatically labile drugs against enzymatic degradation. Since many enzymes, e.g. luminally secreted pancreatic proteases are inactive below pH 4 the degradation of drugs which are incorporated in these polymers may be strongly reduced.

1.3.3. Challenges to the Concept of Mucoadhesion

Three physiological aspects remain critical for the concept of gastrointestinal mucoadhesion:

- the turnover of the adherent mucus layer;
- interactions of the formulation with soluble non-adherent mucus prior to adhesion;
- the influence of gastrointestinal motility on mucoadhesion, in terms of housekeeper waves which accelerate the transport along the GI tract and deteriorate mucoadhesion (Code, 1975; Grundy, 1985; Leung, 1988).

1.3.3.1. Turnover of the Adherent Mucus Layer

General understanding supports the idea that the maximal residence time of a bioadhesive DDS at the site of adhesion would be limited to the turnover time of the mucus gel layer, that is the time for the mucus to be renewed as determined by the steady state of synthesis, secretion and degradation of the mucins (Allen, 1981). Systems that have the ability to renew their mucoadhesive surface for repeated adhesion to the intestinal mucosa have not yet been described. Studies on the turnover time of the intestinal mucus gel layer in the rat using an *in situ* loop technique (Poelma, 1987) and a chronically isolated intestinal loops technique (Lehr, 1991) have estimated a relatively crude mucus turnover between 47 and 270min. In humans, the turnover time was estimated between 12h and 24h (Allen, 1984; Forstner, 1978).

There is a considerable lack of anatomical and physiological data on mucus production and degradation in the lower GI-tract. From one study it was concluded that the lower gastrointestinal tract (colon and caecum) may represent a more suitable location for mucoadhesion than its upper parts (stomach and jejunum) because the mucus layer is not as thick and the mucus turnover is slower in the lower gastrointestinal regions (Rubinstein, 1994).

1.3.3.2. Interactions with Soluble Mucin in the Gastrointestinal Lumen

Any formulation entering the gastrointestinal tract that interacts with the mucus layer is likely to interact also with soluble mucins of the "slough" or luminal material or, in case of a multiple unit dosage form, with the other units of the dosage form. This may cause complications which will reduce the efficiency of the adhesive system. Therefore, any adhesive system which is targeted for groups on the mucus gel will also be prone to interactions with the soluble mucus or with itself.

I.4. Mucoadhesive Polymers

I.4.1. Natural Polymers

Alginic acid (Acidum Alginicum; E400; Polymannuronic Acid listed in BP, GRAS, Ph. Eur., USP/NF) is a mixture of polyuronic acids composed of residues of β -D-mannuronic and α -L-guluronic acid extracted from algae (Phaeophyceae). It swells in water but does not dissolve and is practically insoluble in alcohol and other organic solvents. It dissolves in solutions of alkali hydroxides. A 3% dispersion in water has a pH of 1.5 to 3.5.

Sodium alginate (listed in BP, GRAS, Ph. Eur., USP/NF) consists mainly of the sodium salt of alginic acid. It is slowly soluble in water, forming a viscous colloidal solution. Alginic acid is precipitating below pH 3. It is practically insoluble in alcohol, chloroform, ether, and in aqueous solutions containing more than 30% alcohol. Incompatibilities have been observed with acridine derivatives, crystal violet, phenylmercuric acetate and nitrate, calcium salts, alcohol in concentrations greater than 5% and also heavy metals. A high concentration of electrolytes causes an increase in viscosity until salting-out occurs in cases where more than 4% of sodium chloride is present.

Alginic acid and sodium alginate are used in pharmaceutical manufacturing as suspending and thickening agents. They may be used as a stabilizer for oil-in-water emulsions and as binding and disintegrating agents in tablets. Alginate is also interesting as an excipient in controlled drug delivery dosage forms because it forms hydrogels. It is non-toxic, biocompatible, biodegradable, less expensive and freely available. The manufacturing of microparticles at mild conditions (room temperature, no organic solvents) has been described (Shilpa, 2003). Different authors reported mucoadhesive properties for alginates (Shilpa, 2003; Smart, 1982). Alginic acid and alginates are also employed as emulsifiers and stabilizers in the food industry. Various grades are usually available commercially for different applications and result in solutions of varying viscosity.

Chitosan (listed as the hydrochloride in BP, Ph. Eur.) is a polysaccharide created by deacetylation of chitin, a by-product of the seafood industry. Chitosan comprises copolymers of glucosamine and N-acetylglucosamine [(1 \rightarrow 4)-2-amino-2-deoxy- β -D-glucan] pictured in figure I.1. Chitosan is available at different molecular weights (2000- 50000 Da), viscosity grades, and degrees of deacetylation (40-98%).

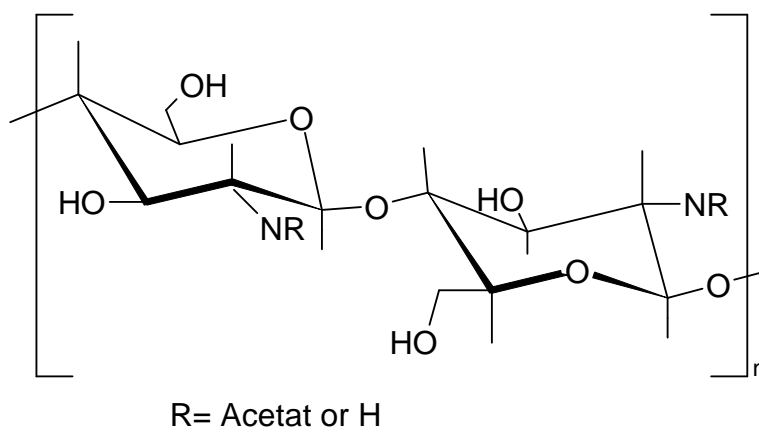


Figure I.1 Structure of chitosan.
A proportion (40% - 98%) of N-acetyl groups is deacetylated.

Chitosan is insoluble at neutral and alkaline pH values, whereas it forms salts with inorganic and organic acids such as glutamic acid, hydrochloric acid, lactic acid and acetic acid. The natural-origin polymer chitosan is generally regarded as biocompatible and slowly biodegradable (Hirano, 1985). In the food industry it is widely used as a food additive and dietary supplement intended to aid in weight loss. The bioadhesive properties of chitosan were described by Lehr et al. (Lehr, 1992a) demonstrating that chitosan in the swollen state is an excellent mucoadhesive at the porcine intestinal mucosa and is also suitable for repeated adhesion. In the same study polycarbophil failed the repeated adhesion test. On the other hand chitosan underwent minimal swelling in artificial intestinal fluids due to its poor aqueous solubility at neutral pH values (Lehr, 1992a). Studies by Artursson et al. demonstrated that chitosan increases the paracellular permeability of [¹⁴C]-mannitol across Caco-2 intestinal epithelial cells (Artursson, 1994) which attributed to chitosan polymers the property of transmucosal absorption enhancement.

The influence of chitosans degree of deacetylation and M_w on the permeability of Caco-2 cell intestinal monolayers was investigated using [¹⁴C]-mannitol at a pH of 5.5. Schipper reported that chitosans with a high degree of deacetylation were effective as permeation enhancers at low and high molecular weight, whereas chitosans of low degree of deacetylation were effective only at high molecular weight and showed low toxicity (Schipper, 1996).

Lueßen et al. studied the *in vivo* absorption enhancement of the peptide analogue busserelin after intraduodenal co-administration with chitosan gels (pH = 6.7) in rats. Chitosan substantially increased the bioavailability of the peptide (5.1%) in comparison to control (no polymer) or Carbopol 934P[®]-containing formulations (Luessen, 1996a). No effect was found for chitosan glutamate solutions at pH = 7.4 in terms of an increase in the paracellular permeability of [¹⁴C]-mannitol and fluorescence labeled dextrane (M_w 4400 Da) *in vitro* using Caco-2 cells (Borchard, 1996), indicating that at neutral pH chitosan is not effective as permeation enhancer. Two chitosan salts (hydrochloride and glutamate) were selected by Kotzé et al. (Kotze, 1998) to study the pH dependency of permeation enhancement. At low pH 6.2, both chitosan salts showed a pronounced effect on the permeability of the marker, leading to 25- (glutamate salt) and 36-fold (hydrochloride salt) enhancement. However, at pH 7.4 both chitosans failed to increase the permeability, due to solubility problems. The authors concluded that there is a need for development of chitosan derivatives, as described in chapter I.4.2, characterized by increased

solubility for use as absorption enhancers in more basic environments such as in the lower intestine (Kotze, 1998). In contrast to this positive result Säkkinen was not able to prove a prolonged gastric transit time with microcrystalline chitosan granules loaded with furosemid investigating blood plasma levels and applying gamma scintigraphy (Sakkinen, 2003b; Sakkinen, 2003).

Chitosan is susceptible to degradation by microbial enzymes in the colon. It is important to protect chitosan as an acid-soluble polymer with an enteric coating (Lorenzo-Lamosa, 1998; Sekigawa, 1993) in formulations where it is used as a coating material for colon-specific drug delivery. Both, the degree of deacetylation and the molecular weight of the polymer can affect the degradation rate. Chitosan is also a suitable polymer material for the manufacture of capsule shells (Tozaki, 1997). Chitosan capsules are commercially available.

Cellulose (listed in BP, GRAS, JP, Ph. Eur., USP/NF) (Figure 1.2) is an unbranched polysaccharide polymer consisting of 1,4- β -linked glucopyranose units. It is the chief constituent of fibrous plant material.

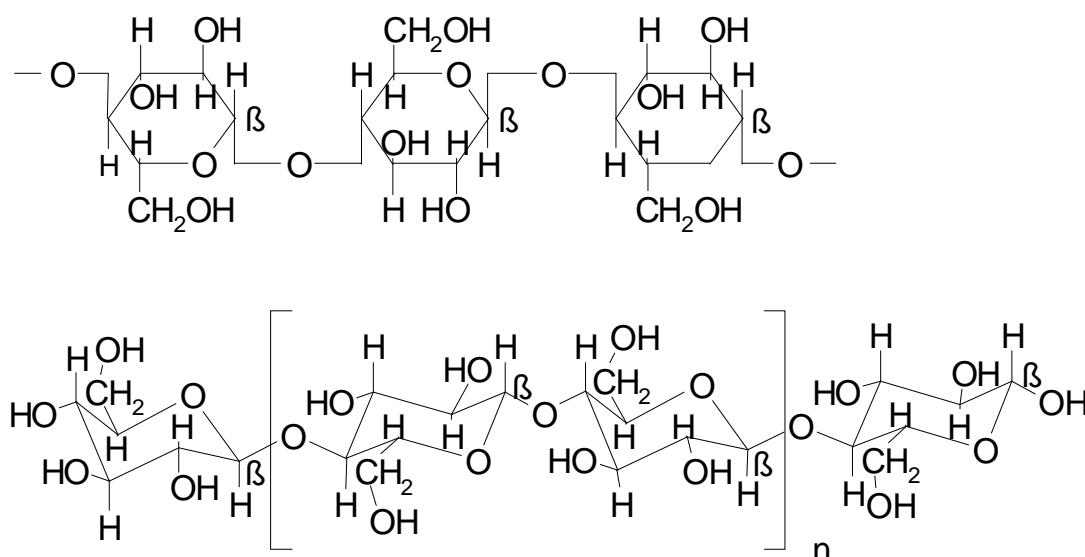


Figure 1.2 Structure of cellulose.

Microcrystalline cellulose (MCC) is a purified partly depolymerized cellulose, prepared by treating alpha-cellulose, obtained as a pulp from fibrous plant materials, with mineral acids. It is a white or almost white, odourless, fine or granular powder which is practically insoluble in water, dilute acids, acetone, dehydrated alcohol, toluene, and most organic solvents and slightly soluble in sodium hydroxide solution (1 part in 20 parts).

Powdered cellulose and microcrystalline cellulose are used in pharmaceutical manufacturing as tablet binders, disintegrates and as capsule and tablet diluents. As a result of its unique properties such as the ability to attribute plasticity to a mass that is sufficient for pellet formation and to act like a water reservoir, MCC is a major component in pelletization processes (Holm, 1996; Sienkiewicz, 1997). Various forms of cellulose have been included in preparations applied in the management of constipation and obesity. Cellulose is also used for adsorbent powder preparations used for skin disorders including hyperhidrosis.

Tragacanth is the dried gum exudation flowing naturally or obtained by incision from the trunk and branches of astragalus gumnifer and some other species

of *Astragalus* (Leguminosae) from western Asia. It is obtained as thin, flattened, more or less curved, ribbon-like, white or pale yellow, translucent, horny odourless strips. It may also appear as a powder. When milled to a powder it forms a mucilaginous gel with about ten times its weight of water. Tragacanth forms viscous solutions or gels with water, depending on its concentration. It is used in pharmaceutical manufacturing as a suspending agent and as an emulsifying agent. In dispensing aqueous preparations of tragacanth, the powdered tragacanth is first dispersed in a wetting agent, such as alcohol, to prevent agglomeration by initial addition of water. Tragacanth is also used for similar purposes in the food industry. Smart and Kellaway reported mucoadhesive properties for tragacanth (Smart, 1982).

1.4.2. Semi-Synthetic Polymers

Three different types of **Carboxymethylcellulose** (CMC, Carmellose (INN)) are available (Figure 1.3):

- Calcium carboxymethylcellulose (listed in BP, JP, Ph. Eur., USP/NF) which is a white to yellowish-white hygroscopic powder. It swells in water to form a suspension and it is practically insoluble in acetone, alcohol, chloroform, ether, and toluene. A 1% suspension in water has a pH of 4.5 to 6.0;
- Sodium carboxymethylcellulose (listed in BP, GRAS, Ph. Eur., USP/NF) is a white to almost white, hygroscopic granular powder. It is easily dispersed in water forming colloidal solutions and is practically insoluble in acetone, dehydrated alcohol, ether, toluene, and most organic solvents. A 1% dispersion in water has a pH of 6.0 to 8.5. Incompatibilities have been reported with strong acidic solutions, with soluble salts of iron and other metals, and with xanthan gum;
- Cross-linked sodium carboxymethylcellulose (cross-carmellose sodium listed in BP, JP, Ph. Eur., USP/NF) is a white or grayish white, free flowing, powder which is partially soluble in water and practically insoluble in acetone, in dehydrated alcohol, in ether, in toluene, and in most other organic solvents. A 1% suspension in water has a pH of 5 to 7.

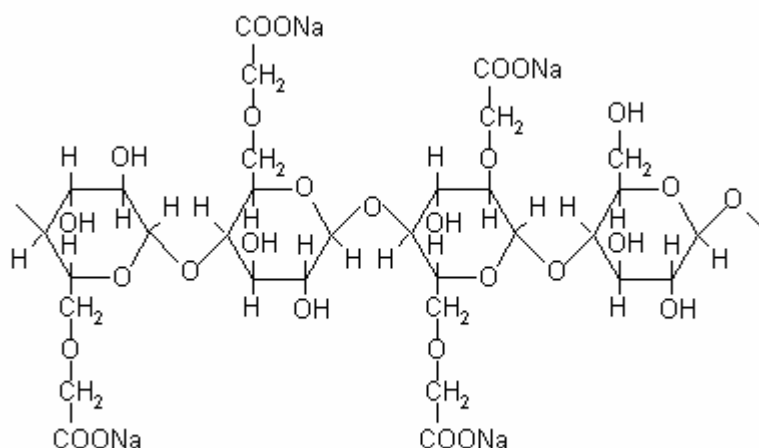


Figure 1.3 Structure of sodium carboxymethylcellulose.

CMC calcium and sodium are useful for several pharmaceutical purposes, including the use as suspending, thickening, and emulsifying agents, and as disintegrants, binders, and coating agents in tablets. Na-CMC is also used as an

emulsifier and stabilizer in the food industry. Cross-carmellose sodium is employed as a tablet disintegrant. It adsorbs water and acts as a bulk-forming agent; the volume of faeces is increased and peristaltics are promoted. The FDA classified Na-CMC as “Gras” substance. Na-CMC is reported by several authors to demonstrate mucoadhesive properties (Lehr, 1992a; Mortazavi, 1995; Prudat-Christiaens, 1996).

Chitosan derivatives (e.g. chitosan salts) lack the advantage of sufficient solubility at neutral pH values. Chitosan precipitates and forms aggregates in solutions at pH values above 6.5, and, under these conditions, is less effective in facilitating the paracellular transport of hydrophilic compounds in contrast to its better soluble derivatives. Thus chitosan can be effective as absorption enhancer only in those intestinal segments in which the pH values are close to the pK_a of chitosan. The pK_a value was reported approximately between 6.1 – 6.7 (Tsai, 2004) Hence, for example, chitosan and its salts will not be suitable for DDS to for instance the jejunum or the ileum. N,N,N-trimethylchitosan chloride (TMC) on the other hand shows much higher aqueous solubility than chitosan in a much broader pH and concentration range (Sieval, 1998). TMC containing formulations exceed the potency of chitosan HCl, and increase the intestinal absorption of a 10mg octreotide dose in the juvenile pig (Thanou, 2000a). This could be attributed to the absorption enhancing action of TMC at neutral pH values, which is related to its enhanced solubility properties but possibly also to the high TMC concentration of the formulation. TMC 10% (w/v) increased remarkably the bioavailability of the peptide from 1.7 to 25% with an absorption enhancement ratio of 14.5, whereas TMC 5% (w/v) resulted in an absolute bioavailability of 13.9% and an absorption enhancement ratio of 7.7 (Thanou, 2000a). The drawback of TMC is its open regulatory status and the lack of an industrial supplier.

Hyaluronic acid (HA) is reported to have bioadhesive potential (Hagerstrom, 2001; Lehr, 1994b). It is a muco-polysaccharide found in the extracellular tissue, synovial fluids, vitreous humour and aqueous humour (Rastrelli, 1990). The physical properties of HA can be altered by controlled esterification with alcohols to produce a variety of dosage forms such as fibres, films, gels, sponges, gauzes and pellets (Benedetti, 1994; Rastrelli, 1990). Microspheres made of esters of HA and produced by spray drying (Kyyrönen, 1992) or solvent evaporation (Benedetti, 1990) have been reported on. Bioadhesive properties of microspheres composed of HA esters were reduced by esterification of HA (Pritchard, 1996). Esterification of HA involves the reaction of the COOH groups with alcohols, and it is the presence of these unionized COOH groups, which promote mucoadhesive properties of HA by formation of hydrogen bonds with components of the biological substrates such as mucus (Leung, 1988). HA is produced by Kiawahako (Osaka, Japan). It is a comparatively expensive product.

Hydroxypropylmethylcellulose (HPMC, Hypromellose) listed in USP/NF, Ph. Eur., JP) is a mixed ether of cellulose containing a variable proportion of methoxy- and 2-hydroxypropoxy- groups. Several grades are available. In the UK they are distinguished by appending a number indicative of the apparent viscosity in millipascal*seconds of a 2% w/w solution at 20°C (e.g. Hypromellose 4500). In the USA they are distinguished by appending a number in which the first 2 digits represent the approximate percentage of the content of methoxy-groups, and the third and fourth digits symbolize the approximate percentage of the hydroxypropoxy-group content (e.g. USP substitution types 2208, 2906 and 2910). Hypromellose is

hygroscopic after drying, it dissolves in cold water, forming a colloidal solution. It is practically insoluble in hot water, dehydrated alcohol, acetone, chloroform, ether, and toluene. A 1% w/w solution in water has a pH of 5.5 to 8.0.

HPMC is used in pharmaceutical manufacturing of film-coated tablets, as a tablet binder, as an extended-release matrix, and as an emulsifier, suspending agent and stabilizer in topical gels and ointments. Hypromellose may also be used as an emulsifier and stabilizer in the food industry. Smart and Kellaway reported mucoadhesive properties for hydroxypropylmethylcellulose (Smart, 1982). The brand name of HPMC is Methocel[®]. It is available in four different chemistries (E, F, J, and K series) based on varying degrees of hydroxypropyl- and methyl- substitution.

Hypromellose phthalate (HPMCP listed in USP/NF, Ph. Eur., JP) is a cellulose derivative in which some of the hydroxyl- groups are present as methyl-ether, others as 2-hydroxypropyl-ether, and again others as phthalyl-ester. The percentage of phthalyl-ester groups ranges from 21 to 35%. On the US market, different product grades are distinguished by appending a number to the product name, in which the first 2 digits represent the approximate percentage of the methoxy-groups content, the next 2 digits the approximate percentage of the hydroxypropoxy-groups content, and the last 2 digits the approximate percentage of the phthalyl-groups content (e.g. USP substitution types 220824, 200731) type. Another system of nomenclature involves appending a number to the product name which indicates the pH value (x 10) at which the polymer dissolves in aqueous buffer solutions (e.g. HPMCP 50, HPMCP 55, HPMCP 55S by ShinEtsu). The USP substitution type 220824 is equal to HPMCP 50 and the USP substitution type 220731 is equal to HPMCP 55 and HPMCP 55S. In addition, letters such as S or F may also be appended to indicate product grades of high molecular-weight polymer or small particle size product, respectively. HPMCP is practically insoluble in water, dehydrated alcohol, and petroleum ether, very slightly soluble in acetone and toluene. It is soluble in a mixture of equal volumes of acetone and methylalcohol, of dehydrated alcohol and acetone, and dichlormethane and methylalcohol. It dissolves in 1N sodium hydroxide.

Hypromellose phthalate is used to provide enteric coating for tablets and granules, for the preparation of sustained-release granules, and as a coating to mask the unpleasant taste of some tablets.

1.4.3. Synthetic Polymers

Carbopol[®] (listed in USP/NF, Pharm. Eur., JP) polymers (Figure 1.4) are flocculated powders of primary particles averaging approximately 0.2 μ m in diameter. The flocculated powders average 2 μ m to 7 μ m, as determined by Coulter counter measurement.

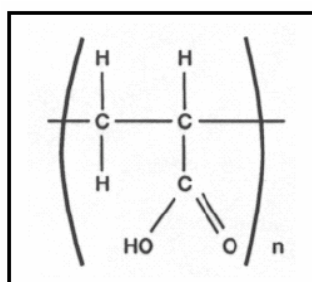


Figure 1.4

Carbopol general structure.

Each primary particle can be viewed as a network structure of polymer chains interconnected by cross-links. Without cross-links, the primary particle is a collection of entangled but not chemically bonded linear polymer chains. The linear structure is represented by linear polymers such as Carbopol 907[®] resin, which is soluble in water (Noveon, 2002). All other Carbopol[®] resins, Permulen[®] and Noveon[®] resins are cross-linked. They swell in water up to 1000 times their original volume (and ten times their original diameter) to form a gel when exposed to a pH above 4.0 to 6.0. Since the pK_a of these polymers is 6.0 ± 0.5 , the carboxylate groups within the polymer ionize, resulting in repulsion between the negative particles, thus adding to the swelling of the polymer. These cross-linked polymers form hydrogels in water; they do not dissolve, instead forming aqueous dispersions (Dittgen, 1997). In the dry state, Carbopol[®] polymers are fluffy, white, mildly acidic, and hygroscopic powders. In the pre-dispersed state, these polymers are tightly coiled, with limited thickening capability. In the hydrated state, the polymer molecule uncoils to a limited extent, and the addition of alkali fully uncoils the polymer, resulting in a gel-like structure. This is due to neutralization of the negatively charged carboxylic acid groups along the backbone of the polymer (Dittgen, 1997).

Carbopol[®] polymers have excellent bioadhesive properties (Dittgen, 1997; Hagerstrom, 2001; Mortazavi, 1995; Singla, 2000) due to their high molecular weight (above 100000), water dispersibility, polymer chain flexibility for chain interpenetration and diffusion with mucin, the presence of a high number of carboxylic groups, and the ability to form hydrogen bonds at pH 4 and 5 (Dittgen, 1997). At pH below 5.0, less than 10% of the Carbopol[®] acid groups will be ionized, resulting in relatively little swelling compared to fully neutralized Carbopol[®] systems. In this environment hydrogen bonding is probably the main mechanism for bioadhesion. When the solution pH exceeds the pK_a of Carbopol[®] (approx. 6.0) the carboxylic groups are ionized to a greater extent and the ability to form hydrogen bonds is reduced. Thereby the mucoadhesion can be reduced. At higher pH the polycarboxylates can interact with cationic (protonated or quaternary) bases and with polyvalent ions of the mucus. Further secondary chemical bonds also occur between the polymer and mucin due to electrostatic interactions, hydrophobic interactions, and van der Waals attraction (Robinson, 1997). The properties described above facilitate the formation of mechanical / physical bonds due to molecular chain entanglement, interdiffusion, and interpenetration with mucin molecules. The polymer hydrates and swells in water and this allows entanglement of the polymer chains with mucin on the tissue surface. For optimal bioadhesion, a high carboxyl group content of the polymer is necessary for both swelling and hydrogen bonding. Carbopol 934 P[®]-coated microspheres (Akiyama, 1995) can increase drug absorption from the gastrointestinal tract. The Carbopol[®]-coated microspheres adhered strongly to the mucosa prepared from the rat stomach and small intestine, followed by prolonged gastrointestinal transit time of the microspheres. Lueßen reported in 1996 a significantly higher intestinal absorption of Buserelin by coadministration with Carbopol 934[®] (Luessen, 1996a). Using the same polymer, low molecular weight Heparin (4500 Da) was better absorbed (Thanou, 2001b). The authors explained these results by a combination of mucoadhesion and tight junctions opening by chelation of Ca^{2+} . Several authors also describe the ability of Carbopol polymers to inhibit degradation by luminal enzymes in the intestine by a temporal acid shield (Bai, 1996) or by depletion of the cofactors Ca^{2+} and Zn^{2+} from the enzymes (Luessen, 1996d). In contrast, the polymers show no or little activity against brush-boarder enzymes (Luessen, 1996b). Carbopol 934P NF[®], Carbopol 971P NF[®], Carbopol

974P NF[®] and Carbopol 71G[®] granules made of Carbopol 971P NF[®] are suitable grades for oral mucoadhesive DDS.

The Table I.7 shows the different Carbopol[®] types and their characteristics (Noveon).

Polycarbophil (listed in USP/NF) (Figure I.5), a homopolymer of acrylic acid cross-linked with divinylglycol, is one of the most potent mucoadhesive polymers in use (Kerec, 2002). The molecular weight of the polymer is high and the pK_a of its functional groups is 6.0 ± 0.5. Polycarbophil does not dissolve in water however it swells up to 1000 times of its original volume to form a gel when exposed to a pH environment above 4.0 to 6.0. Numerous carboxylic groups on the polymer backbone are the main functional groups of polycarbophil and are responsible for the major part of its properties (Noveon, 2002).

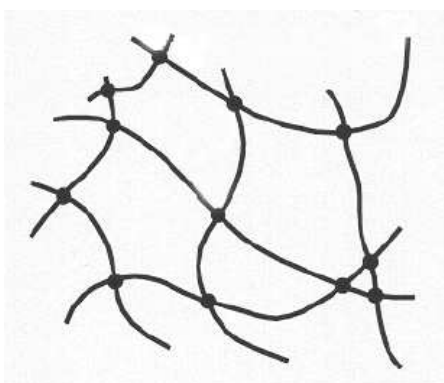


Figure I.5 Crosslinked polycarbophil.

The mucoadhesion of polycarbophil is greatly influenced by the pH of the medium. pH-detachment force profiles have been obtained (Ch'ng, 1985; Park, 1985) and may differ significantly even though they may be obtained using the same mucosal tissue (rabbit stomach). Park reported that at pH values between 2 and 6 the detachment force of polycarbophil decreases with increasing pH, presumably due to increasing repulsion by charged carboxylic groups (Park, 1985). At pH values above 6, the charge repulsion dominates and the detachment force becomes insignificant. Another parameter that may influence the mucoadhesion strength is the swelling property of the polymer. At pH values above the pK_a of polyacrylic acid, polycarbophil adsorbs water up to 100-800 times of its weight, depending on the ionic strength of the aqueous medium. The authors Park et al. concluded that the extent of polycarbophil swelling does not represent a major factor in mucoadhesion. On the contrary, Ch'ng reported that the pH-detachment force increased with increasing pH within a pH range between 2 and 6. Maximum mucoadhesion was observed between pH 5 and 6 (Ch'ng, 1985). At pH 7, mucoadhesion was significantly reduced as a consequence of the increased negative charge repulsion between mucus and polycarbophil. Up to pH 6 the degree of swelling appeared to be one of the factors affecting the mucoadhesion of polycarbophil. Both studies were performed in the same laboratory and described in the paper as identical. Nevertheless the discrepancy between the results was explained by the author based on a change in the experimental technique without any further discussion (Park, 1985).

In addition to the mucoadhesive properties, polycarbophil -similarly to Carbopol- has also the ability to enhance the intestinal absorption of drugs (Lehr, 1992) and to chelate calcium ions (Kriwet, 1996). All effects described about the

inhibition of intestinal enzymatic degradation by Carbopol also apply for Polycarbophil (Bai, 1996; Luessen, 1996b; Luessen, 1996d; Luessen, 1995a; Luessen, 1995b).

The pharmaceutical use of **polymethacrylates** is wide spread resulting from the different combinations of monomers and co-monomers to achieve distinguished properties of the polymers. The performance properties of these polymers thus can be uniquely designed by a combination of a variety of monomers and polymerization techniques. Due to their multifunctional nature -unique properties and good biocompatibility- these polymers are considered to be important excipients in pharmaceutical products. A broad selection of copolymers can be made from acrylic and methacrylic esters or from acrylic acid. Other functional groups can be introduced by using esters as co-monomers. Most of them are sold under the brand name of Eudragit[®].

Table I.7 Polyacrylic polymers (Noveon).

Polymer	Viscosity¹	Properties	Suggested Uses
Carbopol 934 NF Carbopol 2984 Carbopol 5984 EP	30500-39400 45000-80000 25000-45000	Excellent stability at high viscosity. Produces thick formulations, such as medium- to high-viscosity gels, emulsions and suspensions. Short, buttery rheology.	Stable emulsions and suspensions. Water and solvent-based gels.
Carbopol 934P NF Carbopol 974P NF	29400-39400 29400-39400	Carbopol 934P provides drug dependent, near zero-order dissolution kinetics in both simulated gastric fluid (SGF) and simulated intestinal fluid (SIF)	Particularly for oral and mucoadhesive applications, such as controlled release tablets and oral suspensions. Excellent for use in transdermals and topicals
Carbopol 940 NF Carbopol 980 NF Carbopol Ultrez 10	40000-60000 40000-60000 45000-65000	Excellent thickening efficiency at high viscosities with exceptional clarity. Short, buttery rheology. Ultrez 10 is easier to disperse and less susceptible to lumping.	For sparkling clear water or hydroalcoholic topical gels. Efficient solvent thickening with or without neutralizing. Used in water solvent systems.
Carbopol 941 NF Carbopol 981 NF Carbopol ETD 2050	4000-11000 4000-10000 3000-15000	High stable emulsions and suspensions at relatively low viscosities. Good ion tolerance. More efficient than Carbopol polymers 934, 2984, 5984 and 940 at low moderate concentrations (up to 0.1 wt.%). Long rheology. ETD means easy-to-disperse compared to their analogues.	For low viscosity sparkling clear gels, emulsion stabilization of topical lotions. Effective in moderately ionic systems.
Carbopol 971P NF Carbopol 71G NF	4000-11000 4000-11000	Provides drug-dependent near zero-order drug release profiles in SGF/SIF. Rheologic properties are similar to those of Carbopol 941. 71G NF are granules of 971 P NF.	Particularly for oral and mucoadhesive applications, such as controlled-release tablets and oral suspensions. Excellent for use in transdermals and clear, low viscosity topical lotions and gels.
Carbopol 1342 NF Carbopol 1382 Carbopol ETD 2020	9500-26500 ² 25000-45000 ² 32000-77000 ²	Stable thickening in ionic aqueous suspensions. ETD means easy-to-disperse compared to their analogues.	Emulsions stabilization, formulation of pourable products containing suspended incompatible ingredients. Light gallant for water or hydroalcoholic systems.
Permulen TR-1 NF		Primary emulsifier of up to 30% oil.	Formation of low-irritancy lotions and creams. Also of high clarity topical gels.
Noveon AA1-1 USP		Excellent bioadhesive/mucoadhesive	Formation of topical, vaginal, buccal, nasal and ophthalmic bioadhesive gels.
CA-1 USP (coarse) CA-2 USP (fine)		Excellent water absorption	Oral laxative

¹ Brookfield, cPs at 20rpm, 0.5% solution, pH 7.5.

² 1.0 % solution.

1.4.3.1. Chemical Properties of Polymethacrylates

Carboxylic groups in polymethacrylates are easily susceptible to salt formation. During their neutralization in the presence of water, a polycarboxylate anion is formed. The viscosity of aqueous solutions of acrylic and methacrylic acid copolymers increases with pH due to a higher degree of neutralization. This phenomenon is to some extent also dependent on the nature of the salt forming cations. Ca^{2+} , Mg^{2+} salts and those of heavy metals are more or less water-insoluble. Not all copolymers show a very sharp increase in solubility within a small pH range. The dissolution pH of methacrylic acid copolymers occurs as a characteristic value. Their dissolution pH is mainly determined by the carboxylic groups of the polymer. However, the hydrophobicity of the esters co-monomers contributes to this value as well. With increasing pK_a values of the acidic component in the buffer solution the dissolution rate increases. The dissolution rate is very low with sodium salts of chloride ($\text{pK}_a < 1$), medium with acetate ($\text{pK}_a 4.76$) and high with phosphate buffers ($\text{pK}_a 7.20$) (Dittgen, 1997). Similar considerations explain the influence of buffer capacity, so that dissolution rate increases with increasing buffer salt concentrations (Shek, 1978). A further influencing factor is the incorporated drug itself. If the drug is composed of a strong acid and a weak base it will release hydrogen ions in the interface between the core and coating after contact with water. Penetrating hydrogen ions into the film layer will lower the pH and act against the dissolution power of incoming intestinal fluid (Dittgen, 1997). Thus, resistance against gastric fluid is improved, but solubility in intestinal fluid is delayed. On the contrary, when the drug is a salt of weak acid and a strong base, the released hydroxyl ions will cause the opposite effect such that resistance against gastric acid will be decreased and the dissolution in intestinal fluid will be more rapid. Pharmacologically inactive basic or acidic excipients in the core show the same effects. To prevent such effects, it is possible to separate the core with a non-ionic layer from the functional coating layer.

Acrylic polymers containing **tertiary amino groups** in the side chain are used in taste-masking films. At neutral pH conditions which are present in the mouth (pH 5 to 7), these films are insoluble, but they are freely soluble in the acidic environment of the stomach. An acrylic product developed for taste-masking is polydimethyl- aminoethylmethacrylate, -methylmethacrylate, and -butylmethacrylate copolymer (EUDRAGIT[®] E100). Its films dissolve rapidly at a pH below 5.0 and the polymer swells considerably at a pH above 5 and at a neutral pH because of the strong hydrophilicity of the amino groups. Such coatings disintegrate even in case of higher pH values in the stomach caused by a reduced gastric fluid secretion (Dittgen, 1997). The polymer can be used for slow release drug formulations which are made of multilayered units. For example an outer enteric coat may prevent dissolution of an inner amino polymer coat in the stomach. At neutral pH in the intestine, the outer enteric coat dissolves exposing the inner amino polymer coat to the intestinal fluid. In this phase the slow permeation of encapsulated drug across the amino polymeric coating into the intestine occurs (Dittgen, 1997).

Quaternary ammonium groups in side-chains of acrylic polymers are hydrophilic in nature. Polymers contain 1-2 quaternary ammonium groups per 40 monomeric ester units. They form water-insoluble films, despite these films swell in water and their permeability is specifically related to their hydrophilic group content. The swelling of coatings or matrices in digestive fluids controls the rate of drug release by diffusion (Dittgen, 1997). The penetration of water from the surrounding

medium into the core and the diffusion of the dissolved drug molecules from the core into the lumen of the digestive tract occurs preferentially via hydrated hydrophilic pathways (Steward, 1995).

The commercially available ammoniomethacrylate copolymers, NF/USP-types A and B corresponding to EUDRAGIT[®] RL/RS, are miscible by any ratio resulting in intermediate permeability (Lehmann, 1971). A direct correlation exists between the aqueous permeability of these polymers and their ability to slow down drug release. The aqueous permeability is defined as the amount of water steam defined which penetrates with one day through a one square meter large and 25µm thick film layer into blue gel at surrounding conditions of 23°C and 85% relative humidity. The permeability of drugs across polymer films depends on the drugs chemical structure, molecular weight, and solubility. The structural characteristics of drug molecules may influence ionic interactions, hydrogen bonding and hydrophobic interactions (Dittgen, 1997).

The **neutral polymer** poly-EA/MMA (Eugragit[®] NE30D) was first used as a film-forming latex for non-specific coloured film coating. The film itself is very soft and flexible. Sustained-release formulations can be prepared by coating pellets (Ghebre-Sellassie, 1997). Poly-EA/MMA is also added as a softener in the preparation of polymer blends in order to improve film forming conditions and overcome the brittleness of enteric coating on the basis of MA copolymers (Lehmann, 1986).

1.4.3.2. Toxicological Properties

The fully polymerized macromolecular products which are free of residual monomers are regarded to be non-toxic and highly biocompatible (Dittgen, 1997). After oral uptake, acrylic resins are not metabolized in the body and are not absorbed in the digestive tract (Lehmann, 1997). When different types of EUDRAGIT[®] were administered in acute oral tests, it was not possible to determine a LD50 value (Dittgen, 1997) (Eisele, 2003). Even at doses of 8 to 10 g/kg body weight, no animals died. The individual dosage considerations calculated for dry polymer substances were 2mg/kg/day for EUDRAGIT[®] L 30 D-55 and 15mg/kg/day for EUDRAGIT[®] FS 30D. These considerations are based on relevant chronic (6 months) oral toxicity studies with repeated administrations to rats and include a safety factor of about 100 (Eisele, 2003). The usual range of solid polymer material applied with a controlled-release oral drug formulation is in the range of 10 to 250 mg/day, which is equivalent to 0.1 to 4.0 mg/kg body weight in adult humans.

1.4.3.3. Polymethacrylates in Oral Dosage Forms

The following dosage forms contain polymethacrylic acid polymers and copolymers for drug delivery in the gastrointestinal tract (Dittgen, 1997):

- Conventional fast releasing dosage forms designed for drug delivery in the upper part of the gastrointestinal tract;
- Delayed-release dosage forms defined as those that release the drug at any time other than promptly after administration;
- Extended-release dosage forms (also called timed-release dosage forms) defined as those that allow at least a twofold reduction in frequent dosing (e.g. once a day).

Most polymethacrylic polymers take part in the drug delivery process by swelling, interpenetrating or eroding the polymer network, and by dissolution, rupture or melting (Dittgen, 1997).

1.5. Granulation Processes

As a result of granulation processes, agglomerates are formed which consist of larger particles than powders. Granules can be differentiated by their method of manufacturing. Products of wet granulation are being manufactured by fluidized bed, extrusion, and mixing granulation with water or specific binding excipients. Products of dry granulation can be manufactured by hot melt extrusion and roller compaction.

1.5.1. Binding Forces of Granules

In granulation processes, particles aggregate under certain conditions and remain as a collective. Binding forces exist which are directed in opposite to the separation forces of the aggregates, e.g. shearing forces, impulse forces and gravitation force. Aggregation takes place if the sum of the binding forces is higher than the sum of the separating forces. Types of binding forces are as follows (Rumpf, 1958; Rumpf, 1958b; Rumpf, 1974):

- Solid bonds such as binder residues, chemical reactions, sintering, crystallization of dissolved particles during drying, or bonds after melting;
- Adhesion by freely moving fluids with capillary force and boundary surface energy as liquid bonds. Pores of particles may be on one hand partly or completely filled with fluid, or on the other hand the particle coherence occurs via fluid drops;
- Adhesion and cohesion by not freely moving fluids, as high viscosity binders or adsorption layers;
- Adhesion between solid particles as van der Waals attractions, electrostatic attraction;
- Form-locked connections.

The binding forces of fluids -in particular the capillary forces- have particular impact for wet granulation processes. The characteristic value of the liquid fraction of a bulk is the saturation point S. The saturation point S admits the ratio of volume of the liquid VF to the volumes of the pore VH, as is presented by the formula

$$S = V_F / V_H$$

Pietsch (Pietsch, 1967) and Schubert (Schubert, 1979) defined, dependent on the liquid amount, four ranges of the saturation point S (Figure I.6):

- Pendular state (a) $S < 0,3$
- Funicular state (b) $0.3 < S < 0.8$
- Capillary state (c) $0.8 < S < 1$
- Droplet state (d) $S > 1$

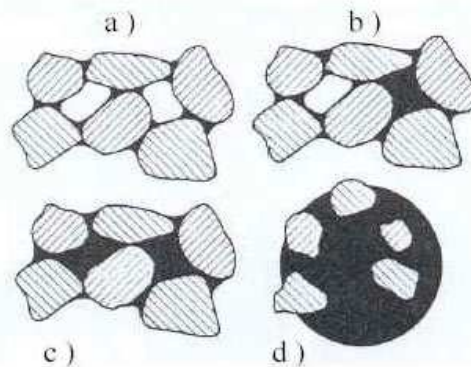


Figure I.6 Liquid distribution in a dispersive solid system (Schubert, 1973). Letters refer to the states as given in the text.

After the first addition of liquids to the powder mass, liquid bonds are formed between particles. In that stage, the cohesion of the particles is mainly driven by capillary forces. This is a function of the surface tension, the wetting angle of contact, the particle size and geometry of liquid bonds (Rumpf, 1972; Sastry, 1973). This first phase is therefore called "pendular state" and is characterized by a low saturation point < 0.3 (Figure I-6. (a)). In the second phase -the so called funicular state- those liquid bonds are still dominating, but they begin to coagulate beyond the pendular state in the ongoing process caused by the high fraction of liquid ($0.3 < S < 0.8$) (Rumpf, 1974; Sastry, 1973). The capillary state (Figure I-6 (c)) is characterized by a high saturation point ($0.8 < S < 1$). In this state all pores are filled with liquid and the liquid creates concave surfaces at the surface pores, thus increases the binding forces between the particles up to 3 times in contrast to the pendular state (Schubert, 1973). Within the capillary state, the agglomerates are characterized by a high plasticity caused by the high fraction of liquid in the pores. With further addition of liquids, the mass becomes over-moistened, the saturation point then being greater than 1. In that stage the agglomerates are held together by the surface tension of the liquid drop. The surface tension of the drops leads to coalescence and a suspension-like mass is created which sticks and leads to an uncontrolled granulation process. Therefore, the droplet state should be avoided. A bulk densification can also lead to higher liquid saturation since the volume of the pores is reduced (Gu, 2004).

1.5.2. Growth Mechanisms of the Particles

The nucleation is to be regarded as preliminary stage of particle enlargement. In this elementary phase of particle growth few primary particles are forming the nucleus. The nucleation is characterized by a change of mass and number of nuclei as a function of time (Ghebre-Sellassie, 1989; Sastry, 1973). The nuclei formed are able to grow among themselves to larger agglomerates by coalescence (Capes, 1967). This process is favoured by a defined amount of surface water, which leads to higher plasticity and thus favours particle growth. The mechanism of coalescence is characterized by the fact that the total mass of the

primary particles remains constant, just their number is reduced (Ghebre-Sellassie, 1989; Sastry, 1973).

After formation of the nuclei the adhesion of fine primary particles of powder onto the nuclei surface is possible. This stage is called layering. This mechanism is characterized by a symmetrical increase of the nucleus size at constant quantity of nuclei (Ghebre-Sellassie, 1989; Sastry, 1973). In practice, a combination of particle enlargement and destruction by breakage or abrasion will always be present. The resulting fine particles aggregate again with larger particles. This is being termed abrasion transfer. During this process the quantity of particles remains constant, on the other hand the particle size constantly varies with time (Sastry, 1973).

Three growth regions in a wet granulation process are described by Sastry and Fuerstenau (Sastry, 1971; Sastry, 1972; Sastry, 1973):

- Nuclei growth region;
- Intermediate transition region;
- Balling growth.

In the nuclei growth region, the particle size is characterized by $D_{50} < 250\mu\text{m}$. The granulation enlargement takes place via a fusion process from primary starting particles. In this region adhesion with liquid bonds prevails, and the saturation point lies between the pendular and funicular state. The further growth of the nuclei takes place by coalescence.

In the intermediate transition region the ratio of the pores filled with binder over empty pores rises. As a result liquid is moved towards the surface and the powder bed starts to fall damp. The agglomerates in this region consist of a liquid and a solid phase, whereby this region is characterized by a movement of the liquid. The agglomerates show more or less plasticity depending on the material. In this region granules grow by abrasion transfer and by breakage and coalescence.

In the balling growth region the particles reach a size, where further growth is only possible by adhesion of smaller particles. The growing of product with small size distribution is rather homogenous, the growing of product with a wide size distribution is only in the first state homogenous, whereas further during the process it may be inhomogeneous and irregular (Linkson, 1973; Sastry, 1970).

1.5.3. Fluidized Bed Technology

The basic principle of a conventional fluidized-bed is an upwards directed air stream passing through a bulk and shifting the bulk into a liquid-like state -the fluidized-bed. In a fluidized-bed, a horizontal surface is formed, the fluidized-bed can overflow and particles with a lower density will float on top of the surface (Figure I.7) (Beranek, 1975). Furthermore, the product would pour out of an opening space, similar to a liquid.

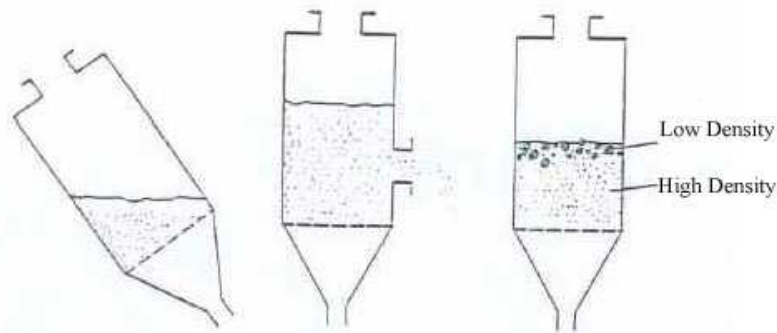


Figure I.7 Analogy between a liquid and a fluidized bed (Beranek, 1975).

Beranek differentiated the fluidized bed states, presented in Figure I.8 below (Beranek, 1975). The homogeneous fluidized bed (a) is an ideal case, which occurs rarely in practice. It is characterized by a symmetrical distribution of the particles within the bed. The particle concentration is constant and therefore independent of time and position. This state offers the best conditions for heat transfer and a homogenous coating process.

A classifying (b) fluidized-bed results from the turbulence of particles of similar density, but different particle size. The smaller particles are mainly in the upper, the larger within the lower range of the bed, respectively. The cooking or bubbling fluidized bed (c) is the most frequently occurring state. Analogies to a liquid are quite obvious. The surface is in motion, and with an increase of the gas flow solid-free bubbles are created. The pushing fluidized bed (d) frequently appears in equipments with small diameter. The bubbles fill the total cross-sectional area and divide the fluidized-bed. The longitudinal interrupted fluidized bed (e) is an unsuccessful experiment of turbulence, since very small particles tend to build up tunnels due to electrostatic loading or moisture of the particles. The sputtering fluidized-bed is a modification of the fluidizing bed (f). Due to the high air speed in the centre of the cross-sectional area the particles are ejected from the bed.

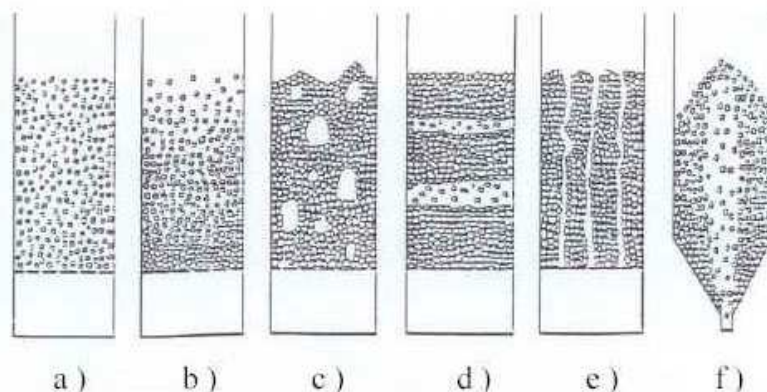


Figure I.8 Different states of the fluidized bed (Beranek, 1975).

The transformation of the particle bed is identifiable by a curve of loss pressure between inlet and outlet pressure (Figure I.9). A rise of the airflow increases the pressure difference due to an increase in the flow resistance. Below the fluidizing point (u_F) the bulk remains in its position and air flows through interparticular spaces.

At the fluidizing point (u_F) transformation occurs from the solid state to the fluidized bed and the airflow is just able to carry the bulk. If the air flow exceeds the sink rate (u_S) of the particles they are ejected from the bed. Consequently, the range of the fluidized bed is between the fluidizing point and the point where the air flow exceeds the sink rate of the particles. In practice, due to a wider particle size distribution, the fluidizing point is more a fluidizing area.

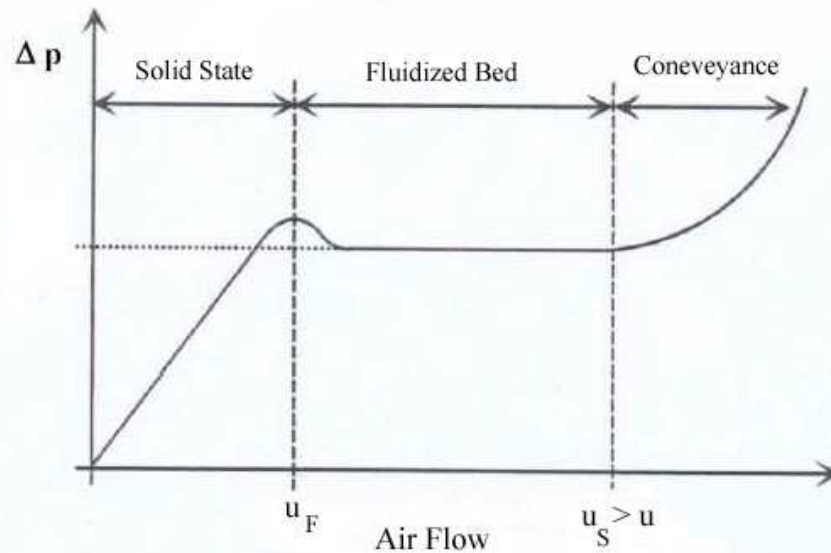


Figure I.9 Relationship between air flow and loss of pressure.
 u_F = fluidising point;
 u_S = airflow exceeding particle sink rate;
 Δp = pressure difference between in- and outlet pressure.

A “fluidized-bed-equipment” can be operated under different technical setups (Figure I.10):

- Top-Spray;
- Bottom-Spray in conjunction with a Wurster module;
- Kugelcoater with Discjet or Rotorjet Booster;
- Rotary fluidized bed;
- Ventilus Technology with Orbiter Booster (Figure I.11).

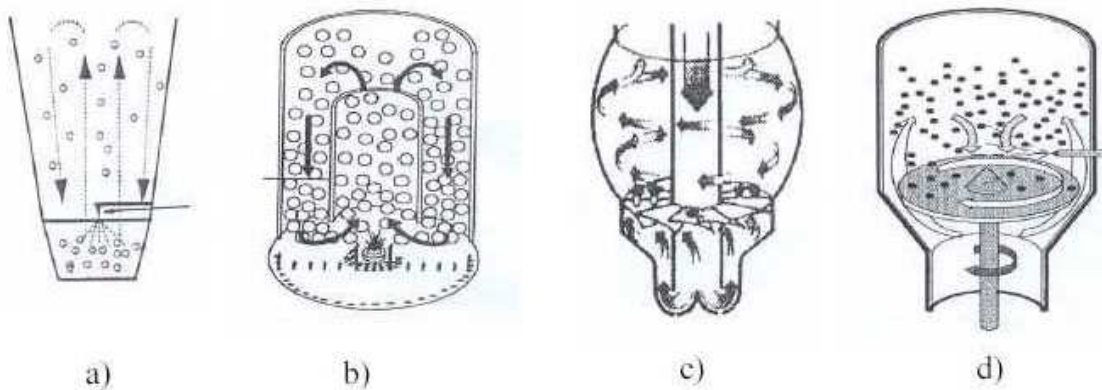


Figure I.10 Fluidized bed equipments.
a = Top-Spray, b = Bottom-Spray with Wurster module, c = Kugelcoater, d = Rotary fluidized bed.



Figure I.11 Ventilus Technology.
The figure was kindly donated from Mr. Holger Hüttlin, Innojet Technologies, Lörrach, Germany.

In the rotary fluidized bed the particles move in a spiral torus-like motion, which is more controlled and more homogenous than the movement generated in conventional fluid-bed equipment (Bauer, 1998). One backdraft is the higher mechanical stress, based on use of the rotor disc, acting upon the product and a second backdraft is the lower air throughput based on the reduced area of the air openings resulting in longer drying times. The Kugelcoater and the Ventilus technology also lead to a more homogenous and controlled movement of the particles, yet they do not have any movable inserts. The more homogenous and controlled particle movements, and the “hovercraft-effect¹” of the booster can lead to faster process times, lower batch to batch variabilities resulting in a more homogenous product when compared to the results of a conventional fluidized-bed-equipment. All of the five different fluidized-bed-equipments are suitable for coating, drying and granulation processes.

¹ This effect is characterized by a contact-free movement of the product on top of the bottom of the equipment.

1.5.4. Rotary Processor

In pharmaceutical technology rotary processing is mainly used for direct pelletization of powders (Chukwumezie, 2004; Holm, 1996; Kristensen, 2000; Vertommen, 1997b; Vertommen, 1998), but it is also used for powder layering processes (Narisawa, 1994; Wang, 2000) and coating of cores (Ghebre-Sellassie, 1989; Neumerkel, 1999; Vecchio, 1998; Wang, 2000). Furthermore, melt granulation (Faham, 2000; Maejima, 1997) and microencapsulation (Georgarakis, 1987) have been reported. Centrifugal granulator, rotary fluidized bed granulator, rotary fluid bed, rotary processor and rotor granulator are some of the common used synonyma of the equipments in use. Particles with enhanced spherical morphology in conjunction with a higher density are the advantages of products manufactured by rotary processing in comparison to a conventional fluidized bed equipment. Kristensen even reported that pellets produced by applying this method have the same quality as pellets produced using the conventional multi-step extrusion/spheronization process (Kristensen, 2000). The reason for these advantages in product properties is the special movement of the product in the equipment in conjunction with higher forces input into the powder mass. Further, a lower airflow is sufficient to generate a fluidized bed and higher product water contents are achieved without the risk of a collapsed bed opposite to a conventional fluidized bed.

1.5.4.1. Equipment and Product Movement

The powder mix is converted into spheroids by spraying a moistening liquid onto the powder mass while it moves in coil-wreath shape or rope-like motion (Figure I.12) (Gu, 2004).

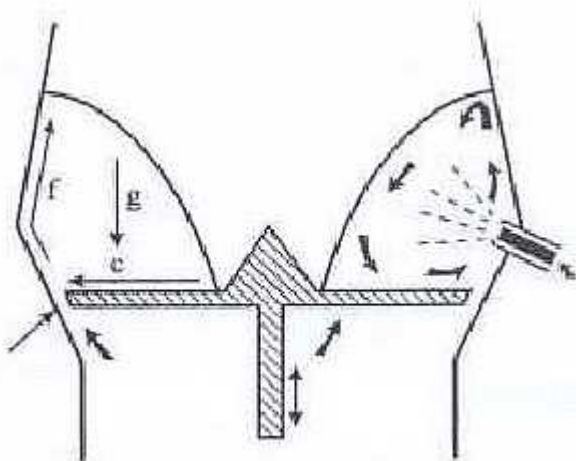


Figure I.12 Product movement in a rotary processor.
c = centrifugal force, g = gravitational force, f = fluidizing force.

Responsible for the motion are three major forces (centrifugal, gravitational and fluidizing), which act on the product from different directions. The revolution of the rotating plate generates the centrifugal forces (Figure I.12c) and tends to push the material towards the wall of the processing chamber at the periphery of the rotating plate (Ghebre-Sellassie, 1995; Jager, 1982). The incoming air from the gap between the rotor disc and the wall accelerates the particles upwards into asymptotic motion (Figure I.12f). As the particle velocity decreases with increasing distance to the gap, caused by reduction of airflow, the material loses its upwards momentum

and cascades downwards and inwards due to the gravitational force (Figure I.12g) (Gu, 2004). The centrifugal force is a function of the rotational speed, the rotor disc diameter and rotor type. The fluidizing force is a function of the gap air velocity, which is itself a function of the air flow and gap distance. In this equipment a tangential spray mode is applied, which means the spray gun is located at the lower portion of the wall such that it is fully immersed in the spheronizing powder mass. The spray droplets travel in a tangential path concurrent to the motion of the material. Dense spheroids of a narrow size distribution can be prepared by rotary spheronization.

The uniqueness of the rotary processor is mainly based on movement of the rotor disc which sets up forces to enable liquid distribution and material mixing during the liquid addition phase at spheroid production (Gu, 2004). Nonpareil seeds and core spheroids are generally characterized by better flow properties than fine powders hence a smooth rotor disc is sufficient for powder layering or coating processes.

Pišek reported that a smooth rotor disc is successful for avoiding material adhesion but it does not supply sufficient shear forces for effective spheronization. For supplying higher shear effectiveness it is suggested to use patterned discs. Different patterned discs are available such as discs with grooved surfaces, also in a cross-hatch pattern or with grooves arranged in radial pattern, well known from conventional extruder-spheronizers. Special types of discs (Figure I.13) are available in which protuberances do not have as angular edges to avoid cutting. In the literature, studs are described in pyramidal shape, square studs with rounded edges or in teardrop shape (Holm, 1996b; Holm, 1996; Liew, 2002; Liew, 2000; Wan, 1994; Wan, 1995).

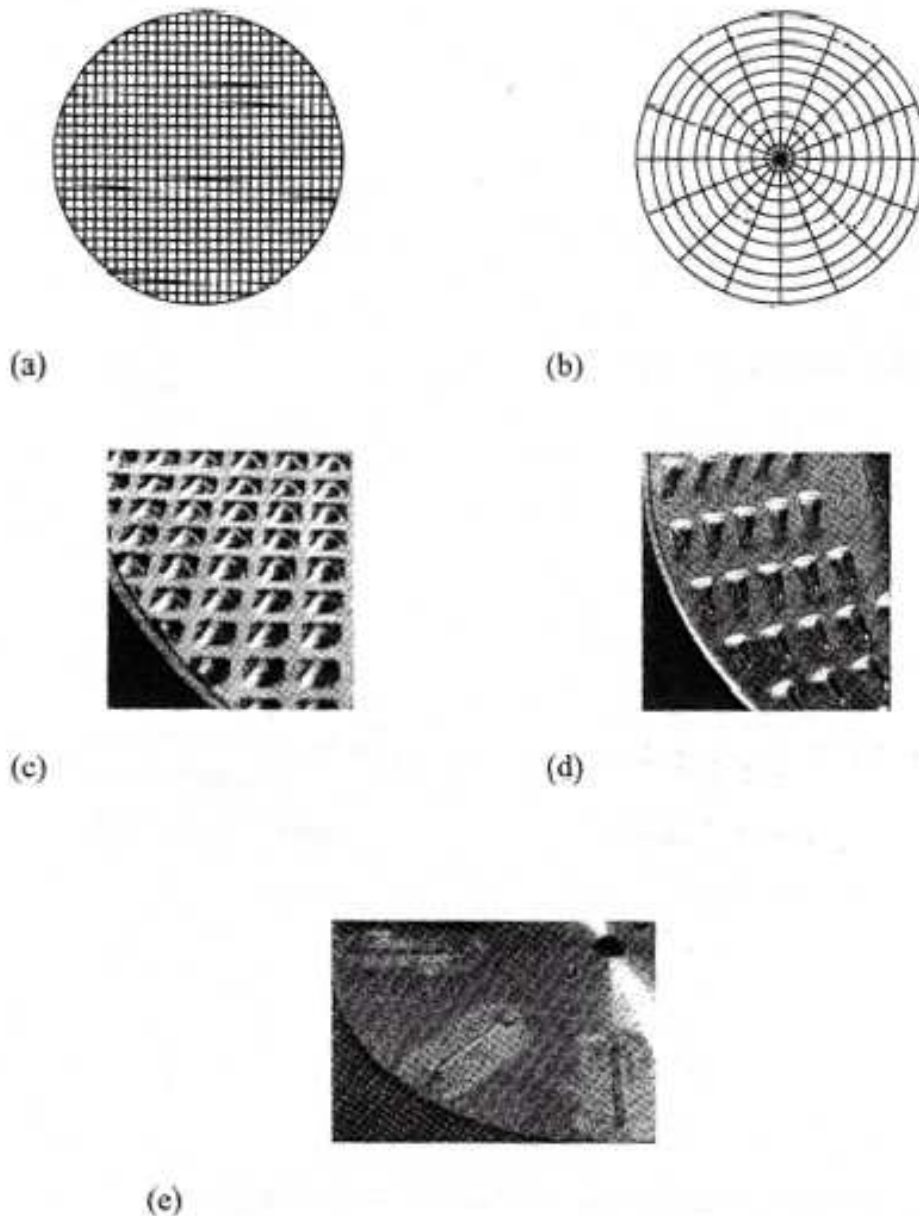


Figure 1.13 Depiction of rotor plates with different designs of surface (Gu, 2004).
 a: Grooves in cross-hatch pattern; b: grooves in radial pattern; c: pyramidally shaped studs in cross-hatch pattern; d: teardrop shaped studs in radial pattern; e: smooth surface plate with wide spaced baffles.

1.5.4.2. Process Parameters Influencing the Final Spheroid Quality

As previously described an increase of the **moisture content at the end of the liquid addition phase** resulting by a lower drying of the liquid or application of a higher liquid amount, increases the liquid saturation of the spheroids. Hence more moisture is available for the formation of bonds between the particles. Furthermore, as described above, the increased moisture content improves the surface plasticity and assists the deformation and coalescence of the particles during collisions. Consequently, the particles agglomerate and consolidate to form spheroids. An improved surface plasticity enhanced deformation and assisted the rounding of spheroids (Ghebre-Sellassie, 1989; Wan, 1994). An increase of the moisture content

at the end of the liquid addition phase is reported with an increase in particle size, wider size distribution and a decrease of friability (Vertommen, 1997b; Vertommen, 1997). Other studies also show the importance of the moisture content at the end of the liquid addition phase in controlling size, size distribution, friability, and other physical characteristics of the spheroids (Chukwumezie, 2002; Chukwumezie, 2004; Heng, 2002; Holm, 1996; Vertommen, 1996; Vertommen, 1997b). Taking all information together, most authors agree that one of the most important critical and influential variables is the moisture content at the end of the liquid addition phase. To ensure the production of spheroids of appropriate size and size distribution, the amount of liquid binder should reach the required level and be controlled within narrow limits. By adding too much liquid binder, a large amount of undesired oversized lumps is produced due to a less controlled agglomeration. Considering the high impact of the moisture content at the end of the liquid addition period all variables which are influencing the moisture content have to be controlled. The known influencing variables are:

- the Amount of liquid binder;
- the Batch size;
- the Airflow;
- the Inlet air temperature;
- the Inlet air humidity;
- the Liquid addition rate (a longer liquid addition period leads to increase of liquid evaporation);
- the Moisture of the product at the start of the process.

The **rotation speed** of the friction plate is an important process variable since it affects the agitation and the shape of the agglomerates. Successful spherization requires a balance between agglomeration of powder particles and breakdown of large oversized agglomerates or lumps. Strong centrifugal forces can supply sufficient energy for the system to lead to particle agglomeration by coalescence. Concurrently these forces contribute to size reduction by attrition or breakage (Gu, 2004). Increasing rotational speed may lead to more dense (Holm, 1996b) (Vertommen, 1998) and smoother agglomerates (Vertommen, 1998), as well as to agglomerates with lower friability (Vertommen, 1997b), reduced pore volume (Vertommen, 1998), higher crushing strength (Robinson, 1991) and also to more spherical agglomerates (Vertommen, 1997). The results of the impact of rotor speed on the particle size and particle size distribution are contrary in the literature. Some studies showed an increase in rotor speed leading to larger particles (Holm, 1996b; Liew, 2002; Liew, 2000) and narrower size distribution (Holm, 1996). Other studies show a decrease of particles size (Korakianiti, 2000) and slightly wider particles size distribution (Vertommen, 1997b) with higher rotor speed. Heng and Liew reported a narrow size distribution and a minimum amount of oversized particles in the total product yield by applying a low-high-low protocol for the rotor speed (Heng, 2002; Liew, 2002; Liew, 2000). A low rotor speed during the spherization period, which is the time after the liquid addition phase and during the drying period, implies the risk of forming lumps because of low centrifugal forces. Furthermore, the low impact on

the mass, may lead to adherence of the material to the rotor disc. The effect of the rotation speed, however, depends on the actual formulation (Holm, 1996b).

As a result of its unique properties, microcrystalline cellulose (MCC) seems to be a key **granulation excipient** in the manufacturing of pellets by wet granulation in a rotary processor (Kristensen, 2000b). The choice of MCC grade seems not to be crucial. It has only a small effect on the pellet characteristics when changing the MCC type (Sienkiewicz, 1997). On the other hand, the amount of MCC in a formulation has been reported to be crucial for the success of the formation of pellets (Vertommen, 1997b) (Sienkiewicz, 1997). Generally, an amount of 15% to 30% (W/W) MCC has been reported being necessary to produce spherical agglomerates with suitable properties (Vecchio, 1994). A decrease in the proportion of MCC resulted in higher deposition and adhesion of moistened material, the formation of large, irregularly shaped lumps, and augmentation of electrostatic charges causing material to stick on the product container (Vecchio, 1994). The actual amount needed seems to depend on other excipients, as well as on the type of rotary processor. A higher amount of MCC resulted in larger agglomerates, a wider size distribution, and less friable and more spherical agglomerates (Holm, 1996b; Holm, 1996; Vertommen, 1997b; Vertommen, 1997). Holm reported a narrower particle size distribution for an increase in the amount of MCC from 10%(W/W) to 30%(W/W). On the opposite, Vertommen reported a wider particle size distribution by increasing the amount of MCC from 30% (W/W) to 35% (W/W) (Holm, 1996b; Vertommen, 1997b). The porosity of the agglomerates was not affected by the content of MCC in the range from 10% to 30% (w/w) (Holm, 1996b). The particle size of both - soluble and insoluble - excipients and has also influences the pellet size distribution where a decreasing particle-size of the starting material results on one hand in pellets of less uniform particle size and on the other hand in an increased amount of oversized pellets coupled with an increased amount of fine portion (Holm, 1996b; Sienkiewicz, 1997).

A considerable influence on the size and size distribution of the **liquid addition rate** was found (Vecchio, 1994; Vertommen, 1997b). The spheroid size increases with an increase in spraying rate (Holm, 1996b; Holm, 1996; Wan, 1994). A higher liquid spraying rate allowed for a larger amount of moistening liquid to be delivered to the powder mix per unit time. This resulted in an increased availability of moisture for wetting of the powder mix. The higher spray rates also reduced the liquid addition period. Consequently, there was a decrease in the total amount of moisture loss due to evaporation during the granulation period. These factors were conducive for the formation of more liquid bonds which facilitated a greater granule growth during the spheroid formation period (Wan, 1994).

To control the process, the moisture content of the mass at the end of the liquid addition period has to be exactly controlled either directly or indirectly (**endpoint monitoring**). In the rotary processor, it has been proposed either to fix all of the parameters affecting the moisture content, or to adjust the amount of water to be added on the basis of calculations of the actual process conditions (Vertommen, 1998b). An alternative approach to end point control might be the use of indirect methods such as measuring the power consumption of the friction plate. These methods are assumed to reflect the consistency of the wet mass, which depends on the moisture content (Kristensen, 2000). Correlations have been found between the granule size of the final product and the power consumption as well as the torque at

the end of the liquid addition, while all other variables influencing the torque, such as batch size, rotor speed, and disc type were kept constant.

The **atomizing air pressure** was found to have only a negligible effect on the agglomerate size. After the end of liquid addition, usually **wet massing** is continued for 5 to 20min in order to obtain further agglomerate growth, a narrow size distribution, and more spherical agglomerates (Chukwumezie, 2004; Heng, 1996; Holm, 1996b; Holm, 1996; Kristensen, 2000; Liew, 2000; Pisek, 2000; Pisek, 2001; Robinson, 1991; Sienkiewicz, 1997; Vecchio, 1994; Vertommen, 1997; Vertommen, 1998; Wan, 1994; Wan, 1995).

CHAPTER II MATERIALS AND EQUIPMENT

II.1. Materials

<u>Compound</u>	<u>Producer / Vendor</u>
Acetic acid 96% pro analysi	Merck (Darmstadt, Germany)
Aerosil 200	Degussa (Frankfurt, Germany)
Caprylic/capric glycerides (Imwitor 742)	Sasol (Witten, Germany)
Carbopol 71G	Noveon (Cleaveland, USA)
Carbopol 71G milled <90µm	Noll (Köln, Germany)
Carbopol 71G milled <70µm	Noll (Köln, Germany)
Cellets [®] (350-500µm)	Synthapharm (Mühlheim-Ruhr, Germany)
Chitosan pharma grade	Synthapharm (Mühlheim-Ruhr, Germany)
EUDRAGIT [®] FS 30 D	Degussa Röhm Pharma Polymere (Darmstadt, Germany)
EUDRAGIT [®] L 30D-55	Degussa Röhm Pharma Polymere (Darmstadt, Germany)
Glyceryl caprylate (Imwitor 308)	Sasol (Witten, Germany)
Glycerol monostearate	Sasol (Witten, Germany)
Glyceryl laurate (Imwitor 312)	Sasol (Witten, Germany)
Hydrogenated Coco-Glycerides (Softisan 138)	Sasol (Witten, Germany)
Hydrogenated Palm Oil (Softisan 154)	Sasol (Witten, Germany)
Microcrystalline cellulose (MCC, Vivapur [®] 101)	JRS (Rosenberg, Germany)
Phosphorous acid (H ₃ PO ₃ 85%)	Merck (Darmstadt, Germany)
Polycarbophyl (Noveon [®] AA1)	Noveon (Cleaveland, USA)
Polyvinylpyrrolidone (Kollidon 25)	BASF (Ludwigshafen, Germany)
Potassium phosphate (KH ₂ PO ₄) pro analysi	Merck (Darmstadt, Germany)
Sodium acetate (NaC ₂ H ₃ O ₂ x 3H ₂ O)	Merck (Darmstadt, Germany)
Sodium-alginate (Na-alginate)	Biomex (Mannheim, Germany)
Sodium-carboxymethylcellulose (Na-CMC)	Hercules (Düsseldorf, Germany)

Sodium-carboxymethylcellulose milled 30-40µm (Na-CMC)	Noll (Köln, Germany)
Sodium chloride (NaCl)	Merck (Darmstadt, Germany)
Sodium hydroxide (NaOH) pro analysi	Merck (Darmstadt, Germany)
Spironolacton	Caelo (Hilden, Germany)
Talcum	Merck (Darmstadt, Germany)
Theophyllin	BASF (Ludwigshafen, Germany)
Titrisol (for 1L 1N HCl)	Merck (Darmstadt, Germany)
Titrisol (for 1L 1N NaOH)	Merck (Darmstadt, Germany)
Triethyl citrate (TEC)	Morflex (Greensboro, USA)
Trisodium phosphate-dodecahydrate (Na ₃ PO ₄ *12H ₂ O) pro analysi	Merck (Darmstadt, Germany)
Tween 80	Merck-Schuchardt Hohenbrunn (Germany)
Vitamine E acetate	Merck (Darmstadt)
Vitamine E TPGS	Eastman (Kingsport, USA)

II.2. Equipment / Software

<u>Equipment</u>	<u>Producer / Vendor</u>
ALOGPS 2.1 program	http://www.vccclab.org
Biocontrol B3 Release Rate Tester	Hansen Research Corporation (Chatsworth, USA)
Centrifuge type 5834R	Eppendorf (Hamburg, Germany)
Differential Scanning Calorimeter Pyris 1 (DSC)	Perkin Elmer (Überlingen, Germany)
Differential Scanning Calorimeter heat flux calorimeter DSC 910	TA-Instruments (New Castle, USA)
Dissotest Type C 610	Sotax AG (Basel, Switzerland)
Dissotest Type CY-6-V (pump)	Sotax AG (Basel, Switzerland)
Drying balance Precisa XM 60	Precisa (Bisingen, Germany)
Drying oven	Binder (Tuttlingen, Germany)
Easysieve Evaluation Software	Retsch (Haan, Germany)
EDX system INCA Energy 200	OXFORD (Wiesbaden, Germany)
Electric pipette Pipetus	Glaswerk (Wertheim, Germany)
Erweka DT6R Dissolutiontester	Erweka (Heusenstamm, Germany)
Erweka DT7R Dissolutiontester	Erweka (Heusenstamm, Germany)

Erweka DT 80 Dissolutiontester	Erweka (Heusenstamm, Germany)
Friabimat	Bolatec (Gladenbach, Germany)
Filter type GF/D (glass micro fiber)	Whatman (Brentford, UK)
Filter 0.45µm RC-45/25 (regenerated cellulose)	Macherey-Nagel (Düren, Germany)
Membrane Filter 0.45µm	Schleicher and & Schuell (Dassel, Germany)
Filter 5µm type FP 30/5.0 CN	Schleicher and & Schuell (Dassel, Germany)
Frit Por 3	Schott (Mainz, Germany)
GPCG1 Rotary Processor	Glatt (Binzen, Germany)
Humidity and Temperature Sensor Type 71315 & 71316	Hygrocontrol (Hanau, Germany)
Mastersizer 2000	Malvern (Worcestershire, UK)
Hüttlin Mycrolab®	Hüttlin (Steinen, Germany)
Mini-Glatt	Glatt (Binzen, Germany)
Motor AR 400	Erweka (Heusenstamm, Germany)
Nucleosil-100 HPLC Column	Machery-Nagel (Düren/Germany)
Powder feeder Scirocco	Malvern (Worcestershire, UK)
PFT-NMR–Spectrometer Varian Unity Inova 400	Varian (Palo Alto, USA)
Poroplast 10µm filter	Erweka (Heusenstamm, Germany)
PT-TD1	Pharma-Test (Hainburg, Germany)
Pycnometer 50ml	Schott, (Mainz, Germany)
QMPRPlus program	Simulation Plus (Lancaster, USA)
Scanning electron Microscope JEOL JSM 840 A type	JEOL (Peabody, USA)
Sieve bottom (250µm & 360µm mesh size)	self made, manufactured by Degussa (Darmstadt, Germany) US Patent 412979
Sieve Retsch VE 1000	Retsch (Haan, Germany)
Statistica	StatSoft (Hamburg, Germany)
Tapping volumeter JEL ST 2	Engelmann (Ludwigshafen, Germany)
Ultra Turrax	Ika (Staufen, Germany)
UV/VIS spectrometer type Lambda 20	Perkin Elmer (Überlingen, Germany)

CHAPTER III METHODS

III.1. Manufacturing of Pellets Using the GPCG1 Rotary Processor

III.1.1. Na-CMC Micropellets Production

All studies were performed using a GPCG1 rotary processor either with a plane or with grooves in a hatch pattern rotor disc. The GPCG1 was specially equipped with a rotor torque measurement system and inlet and outlet air humidity sensors. The torque was read from the frequent converter of the rotor engine. De-ionized water was used as a liquid binder. Theophyllin was incorporated either in the raw powder mass or in the liquid binder as a marker drug for dissolution. In all studies the airflow, the in- and outlet temperature, the product temperature, the liquid binder amount, spraying rate and the rotor speed were recorded. Depending on the study, the torque of the rotor and also the inlet air humidity alone or inlet and outlet air humidity together was measured. The MCC amount of the powder, the batch size, the inlet air temperature, the airflow, the liquid binder amount, the spraying rate, the rotor speed, the rotor type and different inlet air humidities were evaluated as process parameters.

III.1.1.1 Initial Screening of the Process Parameters

Na-CMC pellets with 20% MCC content were manufactured. In Table III.1 the applied process parameters are presented. The batch size for all trials was set to 754g. The powder mass was composed of 600g Na-CMC, 150g MCC and 4g Theophyllin. Initially the rotor speed was set to 400rpm and after addition of 120g of liquid binder it was increased to 1300rpm. Further changes of the rotor speed are presented in Table III.1. In all trials atomizing air pressure at 2bar, an 800 μ m spray nozzle and a plane rotor disc were applied. The trials started with an airflow of 40m³/h. During the trials, the airflow was increased along an individual pattern for each experiment in up to 7 steps. As a comparable parameter, the amount of fluidizing air in the liquid addition period is presented in the Table III.1. In all experiments raw material was first filled into the GPCG1. Thereafter, the run was started with the preheating phase. After wet massing, the process was stopped and the product was transferred into the drying oven at 40°C for 24h.

Na-CMC pellets with 30% MCC content were manufactured. In Table III.2 the process parameters applied are presented. The batch size for all trials was set to 754g. The powder mass was composed of 525g Na-CMC, 225g MCC and 4g Theophyllin. In all trials atomizing air pressure at 2bar, an 800 μ m spray nozzle and a plane rotor disc were applied. The trials started with an airflow of 40m³/h. During the trials the airflow was increased along an individual pattern for each experiment in up to 7 steps. As a comparable parameter the amount of fluidizing air in the liquid addition period is presented in the Table III.2. In all experiments raw material was first filled into the GPCG1. Thereafter, the run was started with the preheating phase. The batches 15176/23, 15176/26 and 15176/28 were dried for 10 minutes inside the GPCG1 according to the parameters listed in Table III.2. At the end of the process, the product was transferred into the drying oven at 40°C for 24h.

Table III.1

Screening of the process parameters for Na-CMC micropellets containing 20% MCC.

Batch	RS [rpm] ¹	RS [rpm] ¹	RS [rpm] ¹	RS [rpm] ¹	RS during the Sphero-nization Period [rpm]	SR ² [g/min]	Amount Liquid [g]	Amount Fluidizing Air in the Liquid Addition Period [m ³]	Sphero-nization Time [min]	Prod. Temp. [°C] ³
15176/30	-	-	-	-	400	21	400	14	10	34
15176/39	-	-	-	-	400	21	650	28	10	35
15176/41	1801 (624)	-	-	-	460	21 29 (590)	650	22	10	38
15176/42	-	-	-	-	1500	29	470	11	10	31
15176/46	-	-	-	-	400	21	800	39	10	31
15176/47	-	-	-	-	400	21	650	29	10	34
15176/48	-	-	-	-	400	21	650	29	10	33
15176/49	-	-	-	-	400	21	650	29	10	30
15176/50	-	-	-	-	400	21	650	28	10	35
15176/51	-	-	-	-	400	21	650	29	10	32
15176/52	-	-	-	-	400	21	650	29	20	35
15176/53	-	-	-	-	400	21	650	29	30	33
15176/54	-	-	-	-	400	21	650	28	10	33
15176/56 ^{4c}	1003 (434)	900 (506)	500 (586)	400 (640)	200	21	700	33	10	33
15176/57	1006 (409)	700 (480)	500 (550)	400 (600)	200	21	650	32	10	33
15176/58	1003 (414)	-	-	500 (500)	200	21	600	29	10	34
15176/59	1000 (418)	-	-	500 (520)	200	21	800	45	10	30

¹ In brackets the amount of liquid when the rotor speed (RS) was set is given.² SR = Spraying Rate.³ Product temperature at the beginning of the spraying period.⁴ The rotor speed was also decreased at 506g liquid to 898 rpm, 540g liquid to 793 rpm, 639g liquid to 403 rpm.

Table III.2

Screening of the process parameters for Na-CMC micropellets containing 30% MCC.

Batch	RS [rpm] ¹	RS [rpm] ¹	RS during the Sphero-nization Period [rpm] ¹	RS in the Drying Period [rpm] ¹	SR [g/min]	Amount Liquid [g]	Amount Fluidizing Air in the Liquid Addition Period [m ³]	Sphero-nization Time [min]	Airflow during Drying Period [m ³ /h]	Prod. Temp. [°C] ²
15176/23	502	n.d.	1305	500	31	403	15	10	42	37
15176/26	1204	n.d.	1800	1150	32	700	21	10	42	37
15176/28	400	1310 (170)	417	170	21	400	13	10	90	32
15176/29	401	1311 (286)	416	n.d.	21	400	15	10	n.d.	35

¹ In brackets the amount of liquid when the rotor speed (RS) was set is given.² Product temperature at the beginning of the spraying period.

III.1.1.2. Development of the Process Parameters for Na-CMC Micropellets

The powder was composed of 70% Na-CMC and 30% MCC. For the start of the process, the powder was directly filled into the preheated GPCG1. After 10 minutes, the spraying was started for mixing and temperature calibration. The binder liquid was composed of 15g Theophyllin in 2500g of de-ionized water. The drug was dissolved in the binder to reach molecular drug dispersity in the micropellets since it was supposed to simulate the presence of a highly active drug. A backdraft of this method was the change of drug loading by applying different binder amounts. Generally this procedure was applied for all trials. The spheronization time was set to 10 minutes. The following process parameters were varied: batch size, amount of binder, airflow, airflow during the spheronization period, airflow during the drying period, rotor speed, type of rotor disc, inlet air temperature in different periods and average spraying rate. In addition, different spraying rate patterns were applied: First a continuous spraying rate and second a non continuous spraying pattern which was characterized by a higher spraying rate at the start of the process and a decrease in the spraying rate afterwards in one or two steps. The rate of the decrease of the spraying rate is given as the parameter "Slope Spraying Rate" (see Figure III.1), which represents the line of best fit over all different spraying rates. The different spraying rates are schematically shown in Figure III.1. The different batches and the applied process parameters are given in Table III.3. In Table III.4 an overview over the main characteristic process parameters and batches of Table III.3 including a statistical analysis is given.

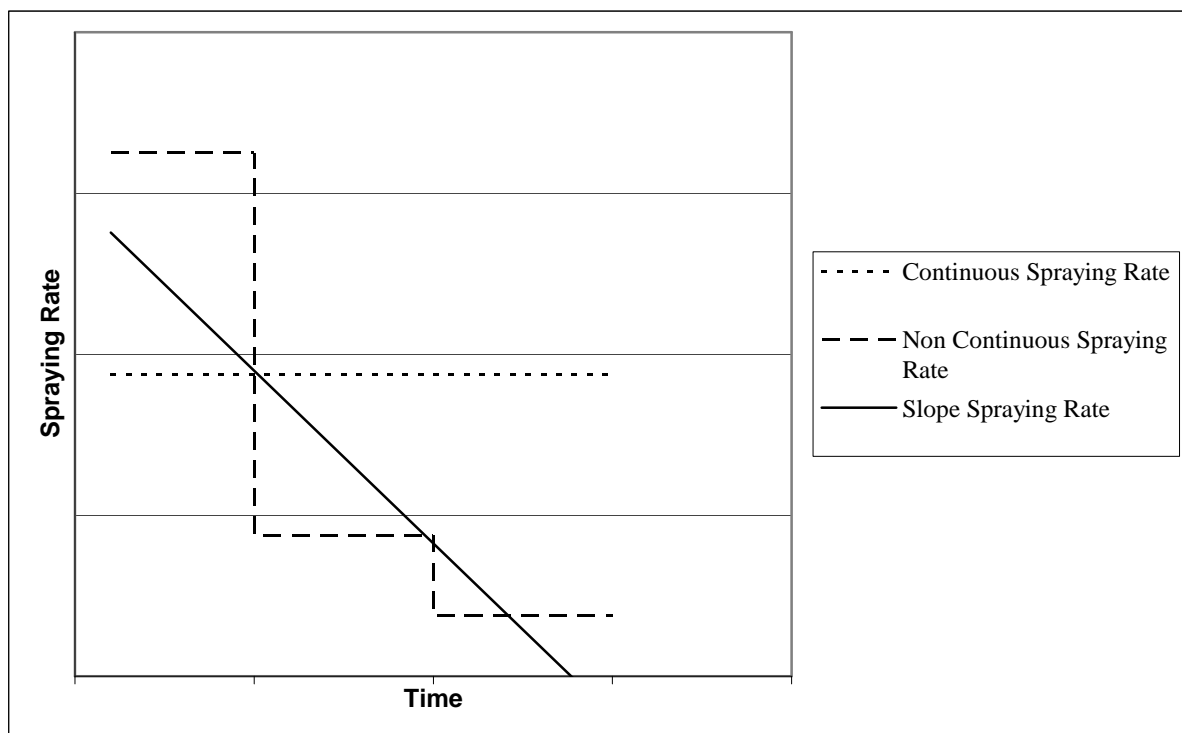


Figure III.1 Variation in spraying rate patterns.
The line represents the relationship between spraying rate and time by linear regression.

Table III.3 Process parameters for the development of Na-CMC micropellets.

Batch	Batch Size [g]	SR ¹ Average [g/min]	SR ² [g/min]	SR ² II [g/min]	SR ² III [g/min]	Binder Amount [g]	Airflow [m ³ /h]	Airflow in SP [m ³ /h]	Airflow DP 1 [m ³ /h]	Inlet Temp [°C]	Inlet Temp DP 1 [°C] ⁵	Inlet Temp DP 2 [°C]	Atomizing Air Pressure [bar]	RS [rpm]	RS Drying Period [rpm]	Rotor Disc	Humidity [g/m ³] ³	Prod. Temp. ³⁴ [°C]
15451/54	750	21	-	-	-	700	42	-	44	45	55	-	1	1305	-	Plane	-	40
15451/55	750	21	-	-	-	700	65	-	65	45	55	-	1	1306	-	Plane	-	41
15451/56	750	21	-	-	-	650	57	-	55	45	55	-	1	1306	-	Plane	-	43
15451/64	500	21	-	-	-	465	42	-	42	45	55	-	1	1305	-	Plane	-	37
15451/65	500	21	-	-	-	465	42	-	42	45	55	-	1	1305	-	Plane	-	38
15451/66	500	16	-	-	-	465	42	-	42	45	55	-	1	1305	-	Plane	-	41
15451/74	500	21	-	-	-	465	42	-	42	45	55	-	1	1500	-	Plane	-	34
15451/75	500	21	-	-	-	465	42	-	42	45	55	-	1	1702	-	Plane	-	40
15451/76	500	18	-	-	-	468	42	-	42	45	55	-	1	1701	-	Plane	-	44
15536/01	500	20	-	-	-	300	52	-	42	30	55	-	3	1427	-	Plane	+(7.2)	-
15536/02	500	22	-	-	-	571	52	-	42	30	55	-	3	1800	-	Plane	+(7.2)	-
15536/03	500	20	-	-	-	465	41	-	42	45	55	-	1	1300	-	Plane	+(7.2)	-
15536/04	500	17	-	-	-	603	41	-	42	30	55	-	3	1405	-	Plane	+(7.2)	-
15536/05	500	>17	-	-	-	432	41	-	42	30	55	-	3	1400	-	Plane	+(7.2)	-
15536/06	500	15	-	-	-	515	41	-	42	30	55	-	3	717	-	Grooved	+(7.2)	-
15536/07	500	24	-	-	-	630	41	-	42	30	55	-	3	710	-	Grooved	+(7.2)	-
15536/08	500	24	-	-	-	630	41	-	42	30	55	-	3	1405	-	Grooved	+(7.2)	-
15536/09	500	27	-	-	-	630	41	-	42	30	55	-	3	1412	-	Grooved	+(7.2)	-
15536/10	500	32	-	-	-	642	41	-	42	30	55	-	3	1412	-	Grooved	+(7.2)	-
15536/11	500	38	-	-	-	635	41	-	42	30	55	-	3	1412	-	Grooved	+(7.2)	-
15536/12	500	38	-	-	-	638	41	-	42	30	55	-	3	1800	-	Grooved	+(7.2)	-
15536/13	500	44	-	-	-	635	41	-	42	30	55	-	3	1800	-	Grooved	+(7.2)	-
15536/14	500	44	-	-	-	501	41	-	42	30	55	-	3	1800	-	Grooved	+(7.2)	-
15536/15	500	44	-	-	-	630	41	30	42	30	55	-	3	1800	-	Grooved	+(7.2)	-
15536/16	500	44	-	-	-	635	52	-	52	30	55	-	3	1800	-	Grooved	+(7.2)	-
15536/17	500	44	-	-	-	635	41	-	42	30	55	-	3	1800	-	Plane	+(7.2)	-
15536/18	500	58	-	-	-	635	41	-	42	30	55	-	3	1800	-	Plane	+(7.2)	-
15536/19	500	58	-	-	-	500	41	-	42	30	55	-	3	1800	-	Plane	+(7.2)	-
15536/20	500	47	57.7 (328)	40.4 (400)	37.6 (630)	630	41	-	42	30	55	-	4	1800	-	Grooved	+(7.2)	-
15536/42	500	45	56 (340)	40 (400)	38 (635)	635	42	-	42	30	55	-	4	1800	-	Grooved	++	25
15536/43	500	40	58 (340)	33.7 (800)	-	800	42	-	42	30	55	-	4	1800	-	Grooved	++	25
15536/44	500	40	58 (340)	33.7 (800)	-	800	42	-	62	30	55	-	4	1800	-	Grooved	++++	26
15536/45	500	40	58 (340)	33.7 (750)	-	750	42	-	42	30	55	-	4	1800	-	Grooved	++++	26

Table III.3 continued

Process parameters for the development of Na-CMC micropellets.

Batch	Batch Size [g]	SR ¹ Average [g/min]	SR ² [g/min]	SR ² II [g/min]	SR ² III [g/min]	Binder Amount [g]	Airflow [m ³ /h]	Airflow in SP [m ³ /h]	Airflow DP 1 [m ³ /h]	Inlet Temp [°C]	Inlet Temp DP 1 [°C] ⁵	Inlet Temp DP 2 [°C]	Atomizing Air Pressure [bar]	RS [rpm]	RS Drying Period [rpm]	Rotor Disc	Humidity ³ [g/m ³]	Prod. Temp. ⁴ [°C]
15536/46	500	40	58 (340)	33.7 (700)	-	700	42	-	42	30	55	-	4	1800	-	Grooved	+++	24
15536/47	500	40	58 (340)	33.7 (635)	-	635	42	-	42	30	55	-	3	1800	-	Grooved	+++	29
15536/48	500	40	58 (340)	33.7 (635)	-	635	42	-	42	30	65	-	3	1800	-	Grooved	++++	26
15536/49	500	40	58 (340)	33.7 (635)	-	635	42	-	42	30	40 (20)	55	3	1800	-	Grooved	++++	28
15536/50	500	45	58 (340)	40 (400)	38 (635)	635	42	-	72	30	40	-	3	1800	-	Grooved	+ (6.48)	27
15536/51	500	45	58 (340)	40 (400)	38 (635)	635	42	-	72	30	30	-	3	1800	-	Grooved	+ (6.56)	30
15536/52	500	40	58 (340)	33.7 (750)	-	750	42	-	72	30	30	-	3	1800	-	Grooved	+ (6.48)	32
15536/53	500	40	58 (340)	33.7 (700)	-	700	42	-	72	30	30	-	3	1800	-	Grooved	+ (6.48)	31
15536/54	500	45	58 (340)	40 (400)	38 (635)	635	42	-	42	30	40	-	3	1800	-	Grooved	+ (6.05)	32
15658/37	500	40	58 (340)	33.7 (750)	-	750	42	-	82	30	37	-	3	1800	-	Grooved	+ (8)	32
15658/39	500	40	58 (340)	33.7 (750)	-	750	42	-	82	30	30	-	3	1800	500	Grooved	+ (7.1)	33
15658/40	500	40	58 (340)	33.7 (750)	-	750	42	-	82	30	30	-	3	1800	-	Grooved	+(7.8)	32
15658/41	500	40	58 (340)	33.7 (750)	-	750	42	-	82	30	30	-	3	1800	-	Grooved	+(8.1)	32

¹ SR average, calculated by amount of liquid used divided by total spraying time.

² In brackets the amount of liquid when the spraying rate was set is given.

³ The inlet air humidity was directly measured when a number is given. In case no numbers but crosses are given, the humidity was assumed since the external measuring equipment was not available.

⁴ Product temperature at the beginning of the spraying period.

⁵ In brackets the time when the spraying rate was set is given.

Table III.4

Characteristic process parameters and batches for the development of Na-CMC micropellets.

Batch	SR° Average ¹ [g/min]	SR° Cont. ² [g/min]	Slope SR ³ [g/min]	Binder Amount [g]	AF* [m ³ /h]	AF* in Sphero- nization [m ³ /h]	RS [rpm]	Rotor Disc	Inlet Air Temp [°C]
15451/64	21	Y	0	465	42	42	1305	plane	45
15536/07	24	Y	0	630	41	41	710	grooved	30
15536/08	24	Y	0	630	41	41	1405	grooved	30
15536/09	27	Y	0	630	41	41	1412	grooved	30
15536/10	32	Y	0	642	41	41	1412	grooved	30
15536/11	38	Y	0	635	41	41	1412	grooved	30
15536/12	38	Y	0	638	41	41	1800	grooved	30
15536/13	44	Y	0	635	41	41	1800	grooved	30
15536/14	44	Y	0	501	41	41	1800	grooved	30
15536/15	44	Y	0	630	41	30	1800	grooved	30
15536/16	44	Y	0	635	52	52	1800	grooved	30
15536/17	44	Y	0	635	41	41	1800	plane	30
15536/18	58	Y	0	635	41	41	1800	plane	30
15536/19	58	Y	0	500	41	41	1800	plane	30
15536/20	47	N	-0.034	630	41	41	1800	grooved	30
15536/50	45	N	-0.032	635	42	42	1800	grooved	30
15536/51	45	N	-0.032	635	42	42	1800	grooved	30
15536/52	40	N	-0.030	750	42	42	1800	grooved	30
15536/53	40	N	-0.034	700	42	42	1800	grooved	30
15536/54	45	N	-0.032	635	42	42	1800	grooved	30
15658/37	40	N	-0.030	750	42	42	1800	grooved	30
15658/40	40	N	-0.030	750	42	42	1800	grooved	30
15658/41	40	N	-0.030	750	42	42	1800	grooved	30

* AF = Air Flow.

°SR = Spraying Rate.

¹ SR average, calculated by amount of liquid used divided by total spraying time.² "Y" means, the spraying rate was constant. "N" means, the spraying rate was not constant. The process was started with a higher spraying rate which was decreased in one or two steps.³ A line of best fit was determined over all different spraying rates.

III.1.2. Na-Alginate Micropellets Production

The equipment used and the procedures applied were identical to Na-CMC micropellets.

III.1.2.1. Initial Screening of the Process Parameters for Na-Alginate Micropellets

In Table III.5 the applied process parameters are presented. The batch size for all trials was set to 754 g. The powder mass was composed of 600g Na-alginate, 150g MCC and 4 g Theophyllin for a 20% MCC content and 525g Na-alginate, 225g MCC and 4 g Theophyllin for a 30% MCC content, respectively. The 5% Kollidon liquid binder was composed of 50g Kollidon in 950g de-ionized water. In all trials atomizing air pressure at 2bar, an 800µm spray nozzle and a plane rotor disc were applied. The trials started with an airflow of 40m³/h. During the trials the airflow was increased along an individual pattern for each experiment. As a comparable parameter the amount of fluidizing air in the liquid addition period is presented in Table III.5. In all experiments raw material was first filled into the GPCG1. Thereafter, the run was started with the preheating phase. After the wet massing the process was stopped and the product was transferred into a drying oven at 40°C for 24h.

Table III.5 Screening of the process parameters for Na-alginate micropellets.

Batch°	RS [rpm] ¹	RS [rpm] ¹	RS [rpm] ¹	RS [rpm] ¹	RS during the Spheronization Period [rpm]	SR [g/min]	Amount of Liquid Binder [g]	Amount of Fluidizing Air in the Liquid Addition Period [m ³]	Spheronization Time [min]	Prod. Temp [°C] ²	MCC Amount in the Pelletization Excipient [%]	Liquid Binder
15176/31	400	1300 (175)	-	-	400	20	400	13	10	35	20	De-ionized Water
15176/32	400	1300 (172)	-	-	400	20	500	18	10	34	20	De-ionized Water
15176/60	400	1300 (115)	1000 (413)	502 (517)	212	21	700	35.1	10	33	20	De-ionized Water
15176/61	400	1300 (112)	1000 (415)	500 (577)	212	21	1001	59	11	31	20	De-ionized Water
15176/34	400	1300 (194)	-	-	400	20 (50)	501	18	10	36	30	De-ionized Water
15176/62	400	1300 (120)	-	-	500	21 (50)	1000	55	11	31	30	De-ionized Water
15176/63	400	1300 (135)	-	-	500	32 (75)	1005	36	11	30	30	De-ionized Water
15176/66	400	1300 (130)	-	-	500	32 (75)	1003	37	22	29	30	5% Kollidon
15176/67	400	1300 (150)	-	-	400	31 (75)	1003	39	22	30	44	5% Kollidon

¹ In brackets the amount of liquid given when the rotor speed was set is given.

² Product temperature at the beginning of the spraying period.

III.1.2.2. Development of the Process Parameters for Na-Alginate Micropellets

The batch size for all batches was set to 500g. The powder mass was composed of 30% MCC and 70% Na-alginate. After 10 minutes, the spraying was started for mixing and temperature calibration. The binder liquid was composed of 15g Theophyllin in 2500g de-ionized water. Spheronization time was set to 10 minutes, airflow to 42m³/h, the inlet temperature to 30°C, the atomizing air pressure to 3bar. The rotor speed during the spheronization time never differed from the rotor speed during the liquid addition period. In all trials a rotor disc was used with the grooves in a hatch pattern. All batches were dried with inlet air at 30°C applying 82m³/h. The following process parameters were varied and are presented in Table III.6: amount of binder, rotor speed, average spraying rate and spraying rate pattern as explained in section “III.1.1.2. Development of the Process Parameters for Na-CMC Micropellets”.

Table III.6 Process parameters for the development of Na-alginate micropellets.

Batch	SR° Average ¹ [g/min]	SR ² I [g/min]	SR ² II [g/min]	SR Cont. ³ [g/min]	Slope SR ⁴	Binder Amount [g]	RS [rpm]	Humi- dity [g/m ³]	Prod. Temp. ⁵ [°C]	Prod. Temp. ⁶ [°C]
15536/55	55	58 (1000)	40 (1200)	N	-0.04545	1200	1800	6.1	30	25
15536/56	93	-	-	Y	-	1300	1800	6.1	31	24
15536/57	93	-	-	Y	-	1200	1800	6.7	34	22
15536/58	93	-	-	Y	-	1032	500	6.7	34	
15536/59	93	-	-	Y	-	1000	500	5.7	30	20
15536/60	93	-	-	Y	-	883	500	5.7	33	21
15536/61	70	93 (500)	55 (954)	N	-0.04226	954	500	5.7	29	19
15658/43	70	93 (500)	55 (954)	N	-0.04226	954	500	6.6	29	17

°SR = Spraying Rate.

¹ SR average, calculated by amount of liquid used divided by total spraying time.

² In brackets the amount of liquid in [ml] is given when the rotor speed was set.

³ “Y” means, the spraying rate was constant. “N” means, the spraying rate was not constant. The process was started with a higher spraying rate which was decreased in one or two steps.

⁴ A line of best fit was determined over all different spraying rates.

⁵ Product temperature at the beginning of the spraying period.

⁶ Product temperature at the end of the spraying period.

III.1.3. Chitosan Micropellets Production

The equipment used and the procedures applied were identical to Na-CMC micropellets.

III.1.3.1. Screening of Process Parameters for Chitosan Micropellets

The batch size for all trials was set to 754 g. The powder mass was composed of 600g Chitosan, 150g MCC and 4 g Theophyllin for a 20% MCC content and 525g Chitosan, 225g MCC and 4 g Theophyllin for a 30% MCC content, respectively. The 6% acetic acid liquid binder was composed of 60g acetic acid (AA) in 940g de-ionized water. The 1.46% chitosan liquid binder was composed of 14.6g chitosan, 60g acetic acid and 925.4g de-ionized water. In all trials atomizing air pressure at 2bar, an 800µm spray nozzle, a plane rotor disc and a spheronization time of 10min were applied. The trials started with an airflow of 40m³/h. During the trials the airflow was increased along an individual pattern for each experiment. As a comparable parameter the amount of fluidizing air in the liquid addition period is

presented in Table III.7. In all experiments raw material was first filled into the GPCG1. Thereafter, the run was started with the preheating phase. After the wet massing the process was stopped and the product was dried in a drying oven at 40°C for 24h.

III.1.3.2. Development of Process Parameters for Chitosan Micropellets

The batch size for all trials was set to 500g. The powder mass was composed of 30% MCC and 70% chitosan. After 10 minutes of preheating, the spraying was started for mixing and temperature calibration. The liquid binders were composed of 15g Theophyllin in 2500g of a solution from 6% (w/w), 10% (w/w), 15% (w/w) or 25% (w/w) acetic acid in de-ionized water. The spheronization time was set to 10min, the airflow to 42m³/h, the inlet air temperature to 30°C, the atomizing air pressure to 3bar. The rotor speed during the spheronization period and the liquid addition period were identical. All batches were dried with inlet air at 30°C and 82 m³/h until the product temperature reached 30°C. Thereafter, the inlet air temperature was increased to 50°C and the product was dried until the outlet air humidity was 1.5 g/m³ lower than the inlet air humidity. The outlet air humidity reached a lower level, since it was composed by the inlet air and drier spraying air. The following process parameters were varied: amount of binder, rotor speed, rotor type, liquid binder, average spraying rate and spraying rate pattern as explained in section III.1.1.2. "Development of the Process Parameters for Na-CMC Micropellets". An overview of the different process runs and the batches produced is given in Table III.8.

Table III.7 Screening of the process parameters of chitosan micropellets.

Batch	RS [rpm] ¹	RS [rpm] ¹	RS [rpm] ¹	RS [rpm] ¹	RS during the Spheronization Period [rpm]	SR ² [g/min]	Amount of Liquid [g]	Amount of Fluidizing Air in the Liquid Addition Period [m ³]	MCC Amount [%]	Liquid Binder	Prod. Temp. [°C] ³
70	409 (0)	1317 (116)	1001 (429)	501 (527)	305	21	801	44	20	6% Acetic Acid	30
71	408 (0)	1315 (125)	1013 (423)	305 (528)	305	18	810	50	20	1.46% Chitosan	30
68	408	1319 (128)	-	-	514	21	1501	101	30	De-ionized Water	27
69	408 (0)	1317 (129)	-	-	378	32	702	18	30	De-ionized Water	31

¹ In brackets the amount of liquid when the rotor speed was set is given.

² SR = Spraying Rate.

³ Product temperature at the beginning of the spraying period.

Table III.8 Process parameters for the development of chitosan micropellets.

Batch	SR ^o Average [g/min]	SR I ² [g/min]	SR II ² [g/min]	SR Cont. ³ [g/min]	Slope ⁴ SR	Binder Amount [g]	RS [rpm]	Rotor Disc	Acetic Acid Conc. [%]	Humidity [g/m ³]	Prod. Temp. ⁵ [°C]	Prod. Temp. ⁶ [°C]
15536/82	41.1	58.1 (340)	33.7 (800)	N	0	800	1800	grooved	6	5.40	35	21
15536/83	93.6	-	-	Y	0	800	1800	grooved	15	5.40	32	23
15536/84	93.6	-	-	Y	0	800	500	grooved	15	5.00	34	19
15536/85	93.6	-	-	Y	0	800	1800	grooved	25	5.00	33	n.d.
15536/86	65.1	93.6 (340)	52.5 (800)	N	-0.04487	800	500	grooved	25	4.85	26	17
15536/87	65.1	93.6 (340)	52.5 (800)	N	-0.04487	800	1000	grooved	25	4.85	27	20
15536/88	65.1	93.6 (340)	52.5 (800)	N	-0.04487	800	1000	plane	25	4.85	27	17
15658/28	93.6	-	-	Y	0	800	1800	grooved	6	8.30	34	24
15658/29	93.6	-	-	Y	0	800	1800	grooved	6	10.60	32	22
15658/30	93.6	-	-	Y	0	800	1800	grooved	10	10.40	32	24
15658/31	93.6	-	-	Y	0	800	1800	grooved	15	11.00	33	n.d.
15658/32	93.6	-	-	Y	0	1000	1800	grooved	15	9.90	32	25
15658/33	93.6	-	-	Y	0	1000	1800	grooved	10	9.99	32	22
15658/34	93.6	-	-	Y	0	890	500	grooved	15	9.99	29	20
15658/35	93.6	-	-	Y	0	1000	1800	grooved	15	9.99	32	23
15658/36	93.6	-	-	Y	0	1130	1800	grooved	15	9.99	32	n.d.
15658/44	93.6	-	-	Y	0	1100	1800	grooved	10	n.d.	32	24
15658/45	93.6	-	-	Y	0	1100	1800	grooved	15	n.d.	32	23

^oSR = Spraying Rate.

¹ SR average, calculated by amount of liquid used divided by total spraying time.

² In brackets the amount of liquid when the rotor speed was set is given.

³ "Y" means, the spraying rate was constant. "N" means, the spraying rate was not constant. The process was started with a higher spraying rate which was decreased in one or two steps.

⁴ A line of best fit was determined over all different spraying rates.

⁵ Product temperature at the beginning of the spraying period.

⁶ Product temperature at the end of the spraying period.

III.1.4. Carbopol® Micropellets Production

The equipment used and the procedures applied were identical to Na-CMC micropellets. In Table III.9 the variable process parameters are presented. The batch size for all trials was set to 500g. The compounds of the different powder masses are presented in Table III.10. The non-acetic acid liquid binder was composed of 15g Theophyllin dissolved in 2500g of de-ionized water. The acetic acid liquid binder was composed of 15g Theophyllin and 125g acetic acid in 2375g de-ionized water. In all trials atomizing air pressure at 3bar, an 800µm spray nozzle and a grooved rotor disc were applied. Furthermore, in all trials, except for batch 15658/1, the inlet air was humidified by placing a boiling water bath in front of the inlet air entrance, to reduce electrostatic product adhesion to the container. The inlet air humidity was close to 100% at room temperature. After the liquid addition phase unconditioned air was used. In all experiments, raw material was first filled into the GPCG1. Thereafter, the run was started with the preheating phase. The product was dried until the outlet air humidity was 1.5 g/m³ lower than the inlet air humidity.

Table III.9 Process parameters for the development of Carbopol® micropellets.

Batch	Spraying Rate [g/min]	Binder Amount [g]	Airflow [m ³ /h]	Inlet Temperature [C°]	Rotor Speed [rpm]	Name Powder Mass from Table III.10
15658/01	54	240	12	30	600	1
15658/02	34	230	12	40	600	2
15658/03	21	236	12	50	500	3
15658/04	21	222	12	50	500	3
15658/05	21	200	12	50	500	3
15658/06	21	200	12	50	500	3
15658/07	21	131	12	50	500	3
15658/08	21	180	12	50	500	3
15658/09	21	180	12	50	500	4
15658/10	83	193	12	50	1800	3
15658/11	83	172	12	50	1800	3
15658/12	83	185	12	50	500	3
15658/13	55	82	12	50	500	4
15658/14	55	52	25	50	500	5
15658/15	55	52	25	50	500	5

Table III.10 Components of the powder masses.

Name	Carbopol® < 90µm	Carbopol® < 70 µm	MCC	Aerosil® 200	Talcum
1	350g	-	150g	-	-
2	250g	-	250g	-	-
3	270g	-	150g	80g	-
4	270g	-	150g	-	80g
5	-	270g	150	-	80g

III.1.5. Noveon Micropellets Production

The equipment used and the procedure applied were identical to Na-CMC micropellets. In Table III.11 the variable process parameters are presented. The batch size for all trials was set to 500g. The powder mass was composed of 280g Noveon AA1, 150g MCC and 80g Aerosil® 200 or 280g Noveon AA1, 150g MCC and 80g talcum. When a batch number is given in the table the product of the batch was taken and used as the starting powder mass. The liquid binder was composed of 15g Theophyllin, 125g acetic acid in 2375g de-ionized water. In all trials atomizing air pressure at 3bar, an 800µm spray nozzle and a grooved rotor disc were applied. In all trials, in which the powder mass type Aerosil® and Talcum were used, the inlet air was humidified by placing a boiling water bath in front of the inlet air entrance to reduce electrostatic sticking of material onto the wall of the product container and

dom. The GPCG1 was preheated for 1 hour with 60°C applying 60m³/h. The inlet air humidity during the preheating phase and the liquid addition phase was close to 100% at room temperature. The water bath was shut off after the liquid addition phase. The raw material was filled after the preheating phase into the GPCG1 and the spraying started directly. The successful products were dried at 40m³/h and 60°C inlet air temperature. The product was dried until the outlet air humidity was 1.5g/m³ lower than the inlet air humidity.

Table III.11 Process parameters for the development of Noveon AA1 micropellets.

Batch	Batch Size [g]	Spraying Rate [g/min]	Binder Amount [g]	Airflow [m ³ /h]	Inlet Temperature [°C]	Rotor Speed [rpm]	Typ of glidants in the Powder Mass
15658/17	500	55	260	13	50	500	Aerosil [®]
15658/18	500	55	225	13	50	500	Aerosil [®]
15658/19	500	55	244	13	50	500	Aerosil [®]
15658/20	500	55	262	13	50	500	Aerosil [®]
15658/21	500	55	282	13	50	500	Aerosil [®]
15658/22	500	55	222	13	50	500	Talcum
15658/23	500	55	272	13	50	500	Aerosil [®]
15658/24	350	55	160	40	30	1800	15658/23 ¹
15658/25	350	83	180	40	30	500	15658/20 ¹
15658/26	350	83	173	40	30	500	15658/19 ¹
15658/27	500	55	262	13	50	500	Aerosil [®]

¹ In this case, the represented batch was used as powder mass without further adding of glidants.

III.2. Characterization of Micropellets

III.2.1. Particle Size Distribution

III.2.1.1. Sieve Analysis

The particle size distribution was performed by sieve analysis. The sieve diameter was 305mm, the amplitude was set to 2.1, the interval time to 15s and the sieving time to 20min. The median (X50), the span and the RRSB parameters of the particle size were calculated with Easysieve Evaluation Software (Retsch). The Span is calculated by [particle diameter at 90% cumulative size (X90)] - [particle diameter at 10% cumulative size (X10)] / [particle diameter at 50% cumulative size (X50)]. The correlation value of RRSB distribution describes the correlation between the calculated particle diameter at 63.2% cumulative size on the RRSB curve and the measured particle diameter. Generally, the X50 value from the sieve analysis is presented.

III.2.1.2. Laser Diffraction

Laser diffraction was performed with dry samples using a Mastersizer 2000 together with the powder feeder Scirocco. Each sample was analyzed 3 times (n=3). The single values of the X50 were not allowed to differ from the mean value by more than 3%, X10 and X90 were not allowed to differ more than 5% from the mean value. The feeding pressure was set to 2.825bar and the feeding rate to 30%. The model “general purpose” was selected.

III.2.2. Tapped Density

The test was carried out with an exact amount of micropellets of a defined particle size range according to European Pharmacopoeia 5.0 (Chapter 2.2.42) for testing tapped density. Each sample was analyzed 3 times (n=3). The particle size ranges were 200-250µm, 250-355 µm and 400-500µm. The equipment used was an ERWEKA PT-TD1.

III.2.3. Friability Testing

Using a Rotating Cylinder, an accurately weighed amount of 10.0g micropellets of a defined particle size range was filled in a 250.0ml graduated cylinder together with 50 glass beads (5mm diameter). The particle size ranges were 200-250µm, 250-355 µm and 400-500µm. The cylinder was mounted to an all purpose motor ERWEKA AR 400 for holding the cylinder. The cylinder was rotated from top to bottom for 10min with 25rpm. Thereafter, the pellets were sieved for 5 minutes using a sieve with mesh size of the smallest particle size of the defined particle size range and weight loss was recorded. All experiments in the rotating cylinder were run with n equal 2-3. Using a Bolatec Friabimat, the test was carried out according to Pharmacopoeia DAB 2004 method 2.9N2 "Abrieb von Pellets und Granulaten: Methode 2 (Schwingapparat)". 10g of accurately weighted micropellets of a particle size between 400 to 500µm were shaken for 240sec at 400 oscillations per minute. Thereafter, the pellets were sieved for 5 minutes using a sieve with 400µm mesh size and weight loss was recorded.

III.2.4. Water Content at the End of the Spraying Period

One sample was drawn during the ongoing process from every batch and analyzed using a halogen drying balance Precisa XM 60 at 105°C applying a booster mode.

III.2.5. Drying Kinetics of the Micropellets

A batch was prepared similarly to 15536/41. After the spraying period, samples were withdrawn, sealed in twist off glass containers and stored at 4°C. The samples were analyzed at 30°C and 50°C using the halogen drying balance Precisa XM 60. Every 2 minutes the loss of water was recorded.

III.2.6. Scanning Electron Microscopy (SEM)

A scanning electron microscope JEOL JSM 840 A type was used. The analysis of the topography of the micropellets was performed using whole undestroyed pellets. For the analysis of the morphology sliced micropellets were used. Shortly before analysis, the samples were coated with a thin gold layer (25nm).

III.2.7. True Density

An accurately weighted amount of micropellets of a particle size range of 250µm-600µm was filled into the pycnometer of a known volume. The pycnometer was filled with petroleum ether and weighted. Afterwards, the pycnometer was cleaned and filled with petroleum ether (blanc) and was weighted again. The true density was calculated using the following equation:

$$\rho = \frac{m_1 \times m_2}{(m_2 - m_3) \times V}$$

m_1 = Weight of the sample

m_2 = Weight of the petroleum ether inside the pycnometer

m_3 = Weight of sample plus the petroleum ether inside the pycnometer

V = Volume of the pycnometer

III.2.8. Estimation of the Surface Area with the Modified Blaine Method

The Blaine method was modified according to Gupte (Gupte, 1976) with an increased air volume (Friedrich manometer) and powder bed (see Figure III.2.). A sample equivalent to 100-130g was accurately weighed into the glass tube of a length of 50cm and a diameter of 2.6cm. The tube was attached to a tapping volumeter JEL ST 2 and tapped 1250 times. The resulting volume was recorded. The glass tube was connected to the manometer. The fluid was risen with an electric pipette Pipetus to the uppermost mark Y_1 by opening tap B and closing tap A. By closing tab B and opening tap A, the liquid level dropped and drew a defined air volume through the product bed. The time taken for the liquid level to drop from mark Y_2 to mark Y_3 (corresponding to about 100 cm³) was recorded automatically. The volume-related specific surface area ($S_v = \text{cm}^2/\text{cm}^3$) was calculated according to the following equation:

$$S_v = \frac{\sqrt{\varepsilon^3 \times K}}{(1 - \varepsilon)^2 \times L \times \eta} \times \sqrt{t - t_0} \text{ (cm}^{-1}\text{)}$$

ε = porosity of the product bed (ratio of pore volume to bulk volume)

K = equipment constant

L = length of product bed in the direction of flow

η = viscosity of the flow medium (for air at 23°C: 0.01834 mPa s)

t = time taken for liquid level to drop from Y_2 to Y_3 (in sec)

t_0 = flow time without sample

$$\varepsilon = \frac{V}{V_b} = \frac{V_b - V_p}{V_b}$$

V = pore volume

V_b = bulk volume or tapped volume

V_p = true volume or pore free volume

$$V_p = \frac{m}{D}$$

m = weight of the sample

D = true density g/cm³

$$S_M = \frac{S_v}{D}$$

S_M = mass-related specific surface area

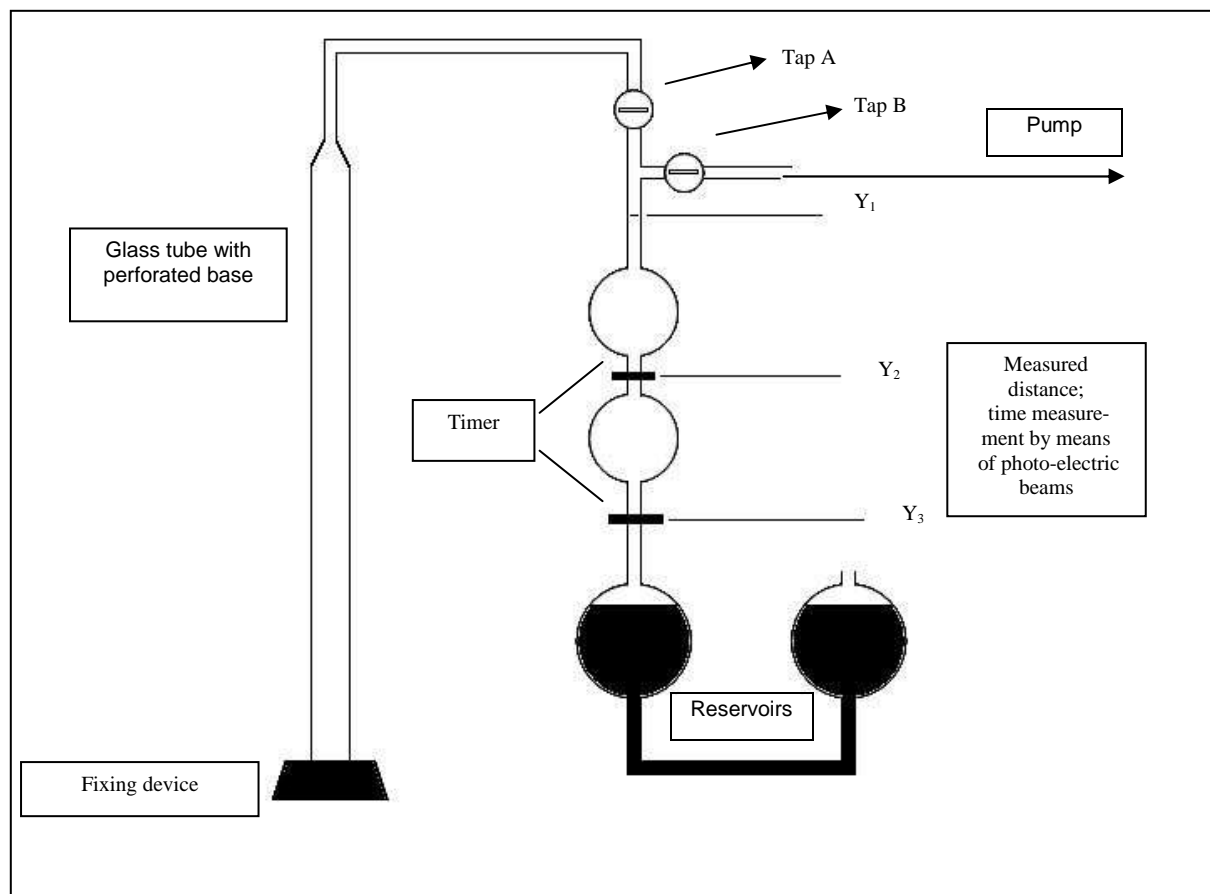


Figure III.2 Apparatus for estimation of the surface area.

III.2.9. NMR for Acetic Acid Content in the Chitosan Micropellets

For sample preparation, 10mg Chitosan pellets were suspended in 2ml D₂O. The polymer was dissolved by adding 30mg citric acid. The remaining carrier material was separated by centrifugation. The NMR-experiments were performed on a PFT-NMR-Spectrometer Varian Unity Inova 400 equipped with a switchable multinuclear 5mm probe. ¹H-NMR spectra were recorded by taking a few hundred scans using a recycle delay of 5 seconds at 30°C.

III.2.10. Content Uniformity of Theophyllin within Micropellets by HPLC

For the **sample preparation**, 400mg micropellets, 15ml acetone and 5ml double distilled water were mixed and extracted for 17 hours at 50°C. Thereafter, the volume of the sample was adjusted to 50.0ml with double distilled water. 10ml clear supernatant of the solution was withdrawn and 10ml of 0.25 molar sodium perchlorate solution was added. The resulting precipitate was removed by centrifugation.

The **HPLC conditions** were as follows:

Eluent:	Methanol: phosphate buffer (0.05 M) pH 3.5	20:80 (V/V)
Column:	Nucleosil-100, C18 7µm, 120/4.6mm	
Flow rate:	2ml/min	
Wave length:	273nm	
Injection volume:	10µl	

The quantification was performed with an external standard.

III.2.11. Statistical Analysis

The statistical analysis was performed using Statistica. A central composite design was applied and an ANOVA test was carried out taking the process parameters as given in Table III.4 as factors and the microparticle properties particle size (X50), span, friability and tapped density as responses. The following parameters were used for statistical programming:

Spraying rate constant “yes”	→ Code	-1
Spraying rate constant “no”	→ Code	1
Plane rotor disc	→ Code	-1
Grooved rotor disc	→ Code	1

III.3. Enteric Coating of the Micropellets

III.3.1. Terminology

The term “micropellets with XX% EUDRAGIT® film layer means that the percentage was calculated based on the dry EUDRAGIT® polymer and the uncoated micropellet. For example, 20% coating means:

Uncoated batch size:	150g
Mass of dry EUDRAGIT® Polymer	$= \frac{150g \times 20}{100} = 30g$
Mass of the coated batch	= 180g + mass of plasticizer + mass of glidants + mass of emulsifier.

The term “solid content” includes all substances which remain in the film after drying, for example, triethyl citrate (plasticizer) and polysorbate 80.

III.3.2. Formulation of the Spraying Suspension

The EUDRAGIT® L 30D-55 formulation with 15% solid content lead to 702g spraying suspension (10% plasticizer and 5% glidant calculated based on dry polymer).

Suspension A:	
De-ionized water	294g
EUDRAGIT® L 30 D-55	300g
Triethyl citrate (plasticizer)	9g

EUDRAGIT® L 30 D-55 was first poured through a sieve (mesh size 100µm) to avoid lumps in the spraying solution. De-ionized water and triethyl citrate were added to the EUDRAGIT® L 30 D-55 while stirring with a magnetic stirring device.

Suspension B:	
De-ionized water	74.25g
Polysorbate 80 (emulsifier)	1.50g
Glycerol monostearate (glidant)	3.75g

Water, polysorbate 80 (Tween 80) and glycerol monostearate were heated above 70°C and were homogenized using an Ultra Turr ax applying moderate speed. The suspension was cooled down while stirring with a magnetic stirring device. After suspension B was cooled off, both suspensions (A and B) were combined while still stirring. Shortly before spraying, the suspension was again passed through a sieve (mesh size 100µm).

The **EUDRAGIT® L 30D-55 formulation with 20% solid content** lead to 614.25g spraying suspension (10% plasticizer and 5% glidant calculated based on dry polymer).

Suspension A:
De-ionized water 138.25g
EUDRAGIT® L 30 D-55 350.00g
Triethyl citrate 10.50g

Suspension B:
De-ionized water 103.95g
Polysorbate 80 6.30g
Glycerol monostearate 5.25g

The preparation procedure is identical to the preparation described above.

The **EUDRAGIT® L 30D-55 formulation with 25% solid content** lead to 491.4g spraying suspension (10% plasticizer and 5% glidant calculated based on dry polymer).

Suspension A:
De-ionized water 15.40g
EUDRAGIT® L 30 D-55 350.00g
Triethyl citrate 10.50g

Suspension B:
De-ionized water 103.95g
Polysorbate 80 6.30g
Glycerol monostearate 5.25g

The preparation procedure is identical to the preparation described above.

The **EUDRAGIT® FS 30D 55 formulation with 15% solid content** lead to 784g spraying suspension (5% plasticizer and 5% glidant calculated based on dry polymer).

Suspension A:
De-ionized water 138.25g
EUDRAGIT® FS 30 D 350.00g
Triethyl citrate 5.25g

Suspension B:
De-ionized water 103.95g

Polysorbate 80	6.30g
Glycerol monostearate	5.25g

The preparation procedure is identical to the preparation described above.

III.3.3. Enteric Coating using the Mini-Glatt

The coating was performed using a Mini-Glatt equipped with a Wurster insert and a 600µm spray nozzle. The upper end of the Wurster cylinder was located 0.3cm above the fixing device of the Wurster cylinder. The test batch for determining the process parameters for mucoadhesive micropellets was composed by pooling the micropellets of a particle size between 250µm–600µm (batches 15536/47, 15536/48, 15536/49 and 15658/39). This new batch was termed “dummy” batch.

In the following the manufacturing specifications of different formulations are described.

20% EUDRAGIT® L 30 D-55 Coating of Na-CMC Micropellets (Batch 15658/46a):

Spraying Suspension:	EUDRAGIT® L 30 D-55 with 20% solid content
Micropellets:	Dummy Batch
Batch size:	150g
Amount of Spraying Susp.:	234g
Product Temperature:	27.5°C–29.5°C
Inlet Air Temperature:	The inlet air temperature was adjusted to maintain a product temperature between 27.5°C and 29.5°C
Atomizing Air Pressure:	0.8bar
Fluidizing Air Pressure:	0.55bar
Spraying Time:	150 minutes
Spraying Rate:	The process was started with a spraying rate of 0.27g/min and was increased every 2min by approx. 0.055 g/min. After reaching a spraying rate of 0.65g/min, the spraying rate was increased every 3.3 minutes by approx. 0.07 g/min to reach a final spraying rate of 2.17g/min.

At the final spraying rate of 2.17g/min the fluidized bed collapsed and the Wurster cylinder was blocked. A successful coating was achieved by reducing the spraying rate to 1.96 g/min. The product was dried for 12 minutes in the airstream.

It was necessary to start with a slow spraying rate (dry process) to create on one hand an isolation layer outside the mucoadhesive pellets preventing twin formation and on the other hand to realize slowly growing particles characterized by a higher surface. This enabled an increase of the spraying rate afterwards without the risk of agglomeration.

30% EUDRAGIT® L 30 D-55 Coating with a Second Coating of 15658/46a (Batch 15658/46b):

Spraying Suspension:	EUDRAGIT® L 30 D-55 with 20% solid content
----------------------	---

Micropellets:	15658/46a
Batch Size:	100g
Amount of Spraying Susp.:	54.29g
Product Temperature:	30°C–31°C
Inlet Air Temperature:	The inlet air temperature was adjusted to maintain a product temperature between 30°C and 31°C
Atomizing Air Pressure:	0.8bar
Fluidizing Air Pressure:	0.55bar
Spraying Rate:	1.1g/min
Spraying Time:	60 minutes

The product was dried for 12 minutes.

50% EUDRAGIT® L 30 D-55 Coating of Na-CMC Micropellets (Batch 15658/47):

Spraying Suspension:	EUDRAGIT® L 30 D-55 with 15% solid content
Micropellets:	Dummy Batch
Batch Size:	150g
Amount of Spraying Susp.:	585g
Product Temperature:	29.8°C-31.5°C
Inlet Air Temperature:	33°C
Atomizing Air Pressure:	0.8bar
Fluidizing Air Pressure:	0.5bar
Spraying Rate:	The process was started with a spraying rate of 0.40g/min and was increased every 5min by approx. 0.07g/min to reach a final spraying rate of 1.47g/min.

At the final spraying rate of 1.47g/min the fluidized bed collapsed and the Wurster cylinder was blocked. The process was aborted.

50% EUDRAGIT® L 30 D-55 Coating of Na-CMC Micropellets (Batch 15658/48a):

Spraying Suspension:	EUDRAGIT® L 30 D-55 with 15% solid content
Micropellets:	Dummy Batch
Batch Size:	150g
Amount of Spraying Susp.:	585g
Product Temperature:	30°C-31.5°C
Inlet Air Temperature:	33°C
Atomizing Air Pressure:	0.8bar
Fluidizing Air Pressure:	0.5bar
Spraying Rate:	The process was started with a spraying rate of 0.40g/min and was increased every 5min by approx. 0.07g/min to reach a final spraying rate of 1.05g/min.

At a spraying rate of 1.05 g/min the fluidized bed collapsed, the Wurster cylinder was blocked, and the process was aborted.

50% EUDRAGIT® L 30 D-55 Coating of Na-CMC Micropellets (Batch 15658/48b):

Spraying Suspension:	EUDRAGIT [®] L 30 D-55 with 25% solid content
Micropellets:	Dummy Batch
Batch Size:	150g
Amount of Spraying Susp.:	351g
Product Temperature:	31.2°C–31.8°C
Inlet Air Temperature:	The inlet air temperature was adjusted to maintain a product temperature between 31-32°C.
Atomizing Air Pressure:	0.6bar
Fluidizing Air Pressure:	0.5bar
Spraying Rate:	The process was started with a spraying rate of 0.40g/min and was increased in 3 steps up to 0.7g/min during 21min. After 30min the spraying rate was decreased to 0.56g/min.

After 32 minutes the fluidized bed collapsed, the Wurster cylinder was blocked, and the process was aborted.

50% EUDRAGIT[®] L 30 D-55 Coating of Na-CMC Micropellets (Batch 15658/49a):

Spraying Suspension:	EUDRAGIT [®] L 30 D-55 with 15% solid content
Micropellets:	Dummy Batch
Batch Size:	150g
Amount of Spraying Susp.:	585g
Product Temperature:	32°C
Inlet Air Temperature:	33°C
Atomizing Air Pressure:	0.8bar
Fluidizing Air Pressure:	0.5bar
Spraying Rate:	The process was started with a spraying rate of 0.40g/min and was increased every 5min by approx. 0.07g/min to reach a final spraying rate of 0.61g/min.

At the final spraying rate of 0.61g/min the spraying nozzle was blocked and the batch was aborted.

50% EUDRAGIT[®] L 30 D-55 Coating of Na-CMC Micropellets (Batch 15658/49b):

Spraying Suspension:	EUDRAGIT [®] L 30 D-55 with 15% solid content
Micropellets:	Dummy Batch
Batch Size:	150g
Amount of Spraying Susp.:	585g
Product Temperature:	32°C
Inlet Air Temperature:	33°C
Atomizing Air Pressure:	0.8bar
Fluidizing Air Pressure:	0.5bar
Spraying Rate:	The process was started with a spraying rate of 0.40g/min and was increased every 5min by approx. 0.07g/min to reach a final spraying rate of 0.61g/min.

At the final spraying rate of 0.61g/min the spraying nozzle was blocked and the batch was aborted.

III.3.4. Enteric Coating using the Hüttlin Mycrolab®

The coating was performed in a Hüttlin Mycrolab® with a 600µm spray nozzle. Only micropellets with a particle size between 250µm – 600µm were selected. The test batch for determining the process parameters for mucoadhesive micropellets were composed by pooling the micropellets of a particle size between 250µm – 600µm (batches 15536/47, 15536/48, 15536/49 and 15658/39) to a new batch which was termed “dummy” batch. For Na-CMC the batches 15536/52, 15658/37, 15658/40 and 15658/41 were pooled and termed 15658/53. For Na-alginate the batches 15536/61 and 15658/43 were pooled and termed 15658/60.

III.3.4.1. Determination of the Process Parameters using the Hüttlin Mycrolab®

In the following section the manufacturing specifications of different formulations are described.

50% EUDRAGIT® L 30 D-55 Coating of Na-CMC Micropellets (Batch 15658/51):

Spraying Suspension:	EUDRAGIT® L 30 D-55 with 20% solid content
Micropellets:	Dummy Batch
Batch Size:	150g
Amount of Spraying Susp.:	438.75g
Product Temperature:	27°C–29°C
Inlet Air Temperature:	The inlet air temperature was adjusted to maintain a product temperature between 27°C-29°C
Atomizing Air Pressure:	0.8bar
Microclimate:	0.3bar
Airflow:	20m ³ /h
Spraying Rate:	see Table III.12.

Table III.12 Spraying rates for batch 15658/51.

Time [min]	0-2	2-4	4-8	8-25	25-32	32-48	48-187
Spraying Rate [g/min]	0.46	0.92	1.38	1.84	2.3	2.76	2.99

The product was dried for 10 minutes applying an inlet air temperature of 33°C.

65% EUDRAGIT® L 30 D-55 Coating with a Second Coating of Batch 5658/51 (Batch 15658/52):

Spraying Suspension:	EUDRAGIT® L 30 D-55 with 20% solid content
Micropellets:	15658/51
Batch Size:	100g
Amount of Spraying Susp.:	55.36g
Product Temperature:	28°C–29°C
Inlet Air Temperature:	39°C
Atomizing Air Pressure:	0.8bar

Microclimate: 0.4bar
 Airflow: 20m³/h
 Spraying Rate: see Table III.13.

Table III.13 Spraying rates for batch 15658/52.

Time Point [min]	0-2	2-4	12-23
Spraying Rate [g/min]	1.84	2.3	2.76

After the termination of the spraying period at 23 minutes, the product was dried for 10 minutes applying an inlet air temperature of 33°C.

70% EUDRAGIT® L 30 D-55 Coating of Na-CMC Micropellets (Batch 15658/54):

Spraying Suspension: EUDRAGIT® L 30 D-55 with 20% solid content
 Micropellets: 15658/53
 Batch Size: 150g
 Amount of Spraying Susp.: 614.25g
 Product Temperature: 28°C–29°C
 Inlet Air Temperature: The inlet air temperature was adjusted to maintain a product temperature between 28°C-29°C
 Atomizing Air Pressure: 0.8bar
 Microclimate: 0.3bar
 Airflow: 20m³/h
 Spraying Rate: see Table III.14.

Table III.14 Spraying rates for batch 15658/54.

Time [min]	0-6	6-8	8-10	10-44	44-54	54-66	66-86	86-95
Spraying Rate [g/min]	0.8	1.2	1.6	2.6	2.8	3.2	3.6	4.0

After 95 minutes the experiment was aborted.

III.3.4.2. Final Process Parameters for the Enteric Coating of Mucoadhesive Micropellets

In the following section the manufacturing specifications of the desired formulations is described.

70% EUDRAGIT® L 30 D-55 Coating of Na-CMC Micropellets (Batch 15658/56):

Spraying Suspension: EUDRAGIT® L 30 D-55 with 20% solid content
 Micropellets: 15658/53
 Batch size: 150g
 Amount of Spraying Susp.: 614.25g
 Product Temperature: 28°C–29.5°C
 Inlet Air Temperature: The inlet air temperature was adjusted to maintain a product temperature between 28°C-29°C
 Atomizing Air Pressure: 0.8bar
 Microclimate: 0.3bar
 Airflow: 20m³/h
 Spraying Rate: see Table III.15.

Table III.15 Spraying rates for batch 15658/56.

Time [min]	0-2	2-4	4-8	8-58	58-77	77-118	118-276
Spraying Rate [g/min]	0.4	0.8	1.2	1.6	2.0	2.4	2.6

The spraying period was finished after 276 minutes. The product was dried for 10 minutes applying an inlet air temperature of 36°C.

140% EUDRAGIT L 30 D-55 Coating of Na-alginate Micropellets (Batch 15658/57):

Spraying Suspension: EUDRAGIT[®] L 30 D-55 with 20% solid content
 Micropellets: 15658/60
 Batch Size: 150g
 Amount of Spraying Susp.: 1228.5g
 Product Temperature: 27°C–28.5°C
 Inlet Air Temperature: The inlet air temperature was adjusted to maintain a product temperature between 27°C-28.5°C
 Atomizing Air Pressure: 0.8bar
 Microclimate: 0.3bar
 Airflow: 17.5m³/h
 Spraying Rate: see Table III.16.

Table III.16 Spraying rates for batch 15658/57

Time [min]	0-5	5-10	10-22	22-145	145-188	188-213	213-397	397-438	438-602
Spraying Rate [g/min]	0.4	0.8	1.2	1.6	2.0	2.3	2.5	2.8	2.6

The spraying period was finished after 602 minutes. The product was dried for 10 minutes applying an inlet air temperature of 36°C.

70% EUDRAGIT[®] FS 30 D Coating of Na-CMC Micropellets (Batch 15658/58):

Spraying Suspension: EUDRAGIT[®] FS 30 D with 15% solid content
 Micropellets: 15658/53
 Batch Size: 136g
 Amount of Spraying Susp.: 710g
 Product Temperature: 28°C–29.5°C
 Inlet Air Temperature: The inlet air temperature was adjusted to maintain a product temperature between 28°C-29°C
 Atomizing Air Pressure: 0.8bar
 Microclimate: 0.6bar
 Airflow: 20m³/h
 Spraying rate: see Table III.17.

Table III.17 Spraying rates for batch 15658/58

Time [min]	0-2	2-7	7-16	16-18	18-73	73-332
Spraying Rate [g/min]	0.42	0.84	1.26	1.68	2.1	2.56

The spraying period was finished after 332 minutes. The product was dried for 10 minutes applying an inlet air temperature of 33°C.

85% EUDRAGIT L 30 D-55 Coating of Chitosan Micropellets (Batch 15658/59):

Spraying Suspension:	EUDRAGIT® L 30 D-55 with 20% solid content
Micropellets:	15658/32
Batch Size:	150g
Amount of Spraying Susp.:	745.88g
Product Temperature:	28°C–29.5°C
Inlet Air Temperature:	The inlet air temperature was adjusted to maintain a product temperature between 28°C-29°C
Atomizing Air Pressure:	0.8bar
Microclimate:	0.3bar
Airflow:	20m ³ /h
Spraying Rate:	see Table III.18.

Table III.18 Spraying rates for batch 15658/59.

Time [min]	0-2	2-5	5-13	13-17	17-62	62-94	94-126	126-325
Spraying Rate [g/min]	0.45	0.9	1.35	1.8	1.6	1.8	2.2	2.7

The spraying period was terminated after 325 minutes. The product was dried for 10 minutes with an inlet air temperature of 33°C.

III.4. Dissolution Testing

III.4.1. Screening of Dissolution Methods for Mucoadhesive Micropellets

III.4.1.1. Dissolution Methods

Four different dissolution apparatus were evaluated:

The USP Apparatus 1 (APP. 1), Basket Apparatus Erweka DT6R

The USP Apparatus 2 (APP. 2), Paddle Apparatus Erweka DT7R

The USP Apparatus 3 (APP. 3), Reciprocating Cylinder Biocontrol B3 Release Tester

The USP Apparatus 4 (APP. 4), Flow-through cell Dissotest Type C 610 and Dissotest type CY-6-V (pump).

III.4.1.2. Dissolution Medium

Solution A:

KH₂PO₄ 54.44g

De-ionized Water ad 2000ml

Solution B:	
NaOH	80.00g
De-ionized Water	ad 2000ml

1250ml of solution A and 140ml of solution B were combined and de-ionized water was added ad 5000ml. The pH was adjusted with H₃PO₃ (85%) or 6N NaOH solution to 6.0 ± 0.05.

III.4.1.3. Dissolution Procedure

For a comparison of the methods, uncoated Na-CMC micropellets of batches 15536/11 and 15536/12 were pooled. The sample amount for dissolution testing was 2g. The particle size range of the micropellets was between 250µm and 600µm. Six samples were tested from each batch for App.1 to 3. For App. 4 five samples were tested for each batch. Six aliquots were withdrawn for analysis and were replaced with equal volumes of fresh dissolution medium, for the specific time points and volumes see below adequate dissolution procedure. The total amount of drug released was obtained by correcting for the amount of drug lost in the dissolution samples.

The samples were analyzed using a UV/VIS spectrometer type Lambda 20 at 273nm and the drug concentration was calculated based on a calibration curve. The 100% content was set as the content after homogenization for 5 minutes using an Ultra-Turrax at a high speed for APP. 1, APP. 2 and for APP. 3. For APP. 2 and App. 3, the baskets were emptied inside the vessels and homogenization took place thereafter. The 100% content for APP. 4 was calculated based on the results of the total content of APP. 1.

The samples of App. 1 – 3 were passed through a 5µm membrane filter type FP 30/5.0 CN before measuring. After leaving the cell, the samples of APP. 4 passed automatically a glass micro fiber filter type GF/D with a particle retention capacity larger than 2.7 µm.

III.4.1.4. Dissolution Testing using Different Methodologies

Ten different or modified trials applied are described in the following section. For convenient differentiation they are numbered D1 to D10.

Paddle Apparatus (D1)

For the dissolution, App. 2 was used. The vessels were filled with 1l of dissolution medium at 37°C and the paddle speed was set to 100rpm. Samples of 5ml were taken at 1min, 2min, 5min, 10min, 15min, 20min, 30min, 45min, 60min, 90min, 120min, 150min and 180 minutes.

Modified Paddle Apparatus containing a 250µm (D2 & D3) or a 360µm (D4)

Sieve Inlay

Method D1 was modified as follows: A 250µm or a 360µm mesh size sieve bottom (Figure III.3) was inserted 40mm above the vessel bottom in App. 2. This sieve bottom is described in US. Patent 5412979 (Fassihi, 1995) with a suggested mesh size of 370µm. The formulation was put on the top of the sieve. The distance from the paddle to the sieve was set with a standard calibration device. The sieve bottom is supposed to avoid creation of a dead zone below the paddle at the bottom of the dissolution vessel where the dispersion of the product would be minimal due to low convective forces. Samples were taken up to 2h. In case of method D2 the

micropellet size was between 250µm-600µm in case of method D4 the micropellets size was between 400-500µm.

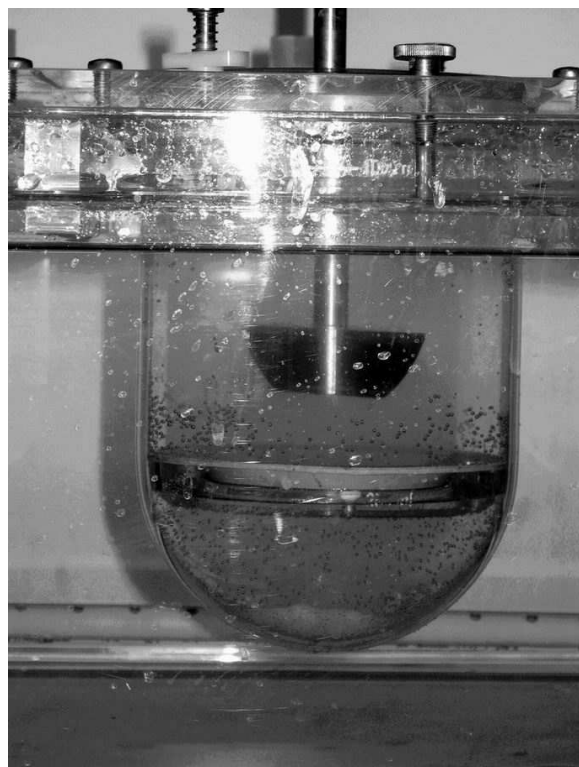


Figure III.3 Vessel with sieve inlay.

Basket Apparatus (D5)

For the dissolution, App. 1 was used. The vessels were filled with 1l of dissolution medium. The basket speed was set to 100rpm. Samples were taken at 1min, 2min, 5min, 10min, 15min, 20min, 30min, 45min, 60min, 90min, 120min, 150min, 180min, 240min and 21.75h.

Reciprocating Cylinder (D6)

For the dissolution, App. 3 was used. The vessels were filled with 250ml dissolution medium. Comparable to USP the method a dip rate of 25 per minute was applied. The vessel rows (1-6) were changed as outlined in Table III.19. Samples were taken after 1, 2, 5, 10, 15, 20, 30, 45, 60, 90, 120, 150, 180, 240, 300min and 23h, respectively.

Table III.19 Timing for the change of the rows of the reciprocating cylinder.

Row	1	2	3	4	5	6
Time [min]	0-15	15-60	60-120	120-180	180-240	240-end

Flow-Through Cell (D7-D10)

For the dissolution, App.4 with the tablet cell (22.6mm diameter) was used. The flow rate was set to 10ml/min for trials D7, D8 and D10 and to 20ml/min for trial D10. 15g glass beads were carefully mixed with the micropellets for the trials D7-D9 and 18g of glass beads were used for trial D10. The accurately weighted amount of micropellets was 2 g for the trial D7 and 0.5g for the trials D8-D10. Sampling vessels were changed after 1, 2, 5, 10, 15, 30, 45, 60, 75 and 90min.

Dissolution Test for Enteric Coated Micropellets

The dissolution test was carried out in 0.1N hydrochloric acid (HCl) using the USP App. 2 Erweka DT6 at a stirring speed of 100 rpm. The samples were withdrawn automatically, passed through a Poroplast 10µm filter, quantified using a flow-through spectrophotometer Lambda 20 at 271nm. The eluate from the spectrophotometer was directed back to the dissolution vessels. The 100% content was set as the dry content following homogenization for 5 minutes using an Ultra-Turrax at high speed.

III.4.2. Dissolution of the Developed and Manufactured Micropellets using App. 2 and App. 4

The screening of the dissolution methods exhibit, that App. 2 and App. 4 are the most appropriate for characterizing the dissolution of mucoadhesive micropellets. Therefore, the finally produced micropellets were dissolved using these methods. For the evaluation of the influence of the paddle speed on the dissolution profile of APP. 2 also different paddle velocities were applied. The dissolution media for all micropellets coated with EUDRAGIT® L 30 D55 was 0.1 N HCL during the initial two hours and thereafter buffer pH 6.0. The dissolution medium for all micropellets coated with EUDRAGIT® FS 30 D was 0.1 N HCL for the initial two hours and thereafter phosphate buffer pH 7.2. The uncoated micropellets were directly dissolved in buffer of pH 6.0 or 7.2. An overview of all applied dissolution conditions is presented in Table III.19.

III.4.2.1. Formulations used for Dissolution Testing

15658/32: Chitosan with 30% microcrystalline cellulose micropellets
15658/53: Na-CMC with 30% microcrystalline cellulose micropellets
15658/60: Na-alginate with 30% microcrystalline cellulose micropellets
15658/56: 15658/53 coated with 70% EUDRAGIT® L 30 D55
15658/57: 15658/60 coated with 140% EUDRAGIT® L 30 D55
15658/58: 15658/53 coated with 70% EUDRAGIT® FS 30D
15658/59: 15658/32 coated with 85% EUDRAGIT® L 30D55

III.4.2.2. Dissolution Media

A) 0.1N HCl	1 Package Titrisol® for 1l 1N HCl is diluted to 10l
B) 2N HCl	2 Packages Titrisol® for 1l 1N HCl are diluted to 1l
C) 2N NaOH	2 Packages Titrisol® for 1l 1N NaOH are diluted to 1l
D) Buffer 6.0	0.1 N HCL Tri-natriumphosphate-dodecahydrate 7500ml De-ionized water 150.80g ad 10000ml
E) Buffer 7.2	0.1 N HCl Tri-natriumphosphate-dodecahydrate 7500ml De-ionized water 213.5g ad 10000ml

III.4.2.3. Dissolution Profiles Using the USP Paddle Apparatus

Dissolution Procedure

For all experiments in APP. 2, 1l dissolution medium was used together with 2g accurately weighted sample. The temperature was set to 37°C. Dissolution medium, paddle speed and sampling times were varied. At the end of the dissolution test, the dissolution medium was homogenized using the Ultra Turrax at maximum speed for 5 minutes. The samples after homogenization were used as the 100% reference value. In Table III.18., a summary of the batches and dissolution methods is shown.

All experiments with Na-CMC and Na-alginate micropellets were performed in a dissolution tester Erweka DT 80 at a rotor speed of 150 rpm. Samples of 5ml were withdrawn at different time points and filtered through a 0.45 µm filter. The aliquots were not replaced and therefore, the concentration in the remaining dissolution fluid was corrected by calculation. The samples were measured using a Lambda 20 UV/VIS spectrometer at 271nm and the total drug content was calculated based on a calibration curve.

All trials of Na-CMC and Na-alginate micropellets with a rotor speed of 100rpm and 50rpm were performed in a dissolution tester Erweka DT6. The samples were withdrawn automatically, passed through a Poroplast 10µm filter, their absorbance was measured using a flow-through spectrophotometer Lambda 20 at 271nm. The effluent was circulated back into the dissolution vessels. The total content was calculated based on a calibration curve.

All dissolution experiments with chitosan micropellets were performed in a dissolution tester type Erweka DT6. Samples of 5ml were withdrawn and 50µl of 2N HCl was added to each sample. The sample was mixed and passed through a 0.45 µm filter RC-45/25. The aliquots were not replaced and therefore, the concentration in the remaining dissolution fluid was corrected by calculation. The samples were measured using a spectrometer Lambda 20 at 271nm and the total drug content was calculated based on a calibration curve.

Eight modified methods applied are described in the following section. For convenient differentiation they are numbered D11 to D18.

Dissolution without a change of the pH of the dissolution medium (D11 & D12)

The dissolution period was set to 240 minutes using phosphate buffer pH 6.0 (Trial D11) or pH 7.2 (Trial D12) as dissolution medium (see Chapter III.4.2.2.). Different paddle velocities were applied.

Dissolution at pH 1 and pH 6.0 (D13) or pH 7.2 (D14) – Delayed Release

This method is the modified USP method <724> Drug Release, Delayed Release, Method A. The dissolution starts in 750ml 0.1N hydrochloric acid for 2 hours. Thereafter, 250ml of either a 60.3 g/l (Trial D13) or a 85.4g/l (Trial D14) Na₃PO₄*12H₂O solution is added to the 750ml 0.1N HCl to reach pH 6.0 or 7.2 respectively. The dissolution time was set to 360 minutes. To maintain the pH, 2N HCl or NaOH solution was used. Different paddle velocities were applied.

III.4.2.4. Dissolution Profiles using the USP Flow- Through Cell

Dissolution Procedure

All trials were performed using a flow-through cell Dissotest type C 610 and Dissotest type CY-6-V (pump). A tablet cell with a diameter of 22.6mm was used, the flow rate was set to 20ml/min. 18g glass beads (1mm) were carefully mixed with 0.5g micropellets and filled into the cell. The medium was deaerated using a membrane filter with a pore size of 0.45µm. The tablet dissolution cell was equipped with a Whatman filter type GF/D. The samples were analyzed using a spectrometer Lambda 20 at 273nm. The samples of the chitosan micropellets were centrifuged at 11000rpm using a centrifuge type 5834R (Eppendorf). In all dissolution tests with coated micropellets (methods D17 and D18), the fluid volumes of the first fraction following a change in the dissolution medium were adjusted to pH 6.0 (method D17) and pH 7.2 (method D18) with 2N NaOH. In Table III.19, a summary of the batches and dissolution methods is shown.

Dissolution without a change of the pH of the dissolution medium (D15 & D16)

The dissolution was carried out for 164 minutes in phosphate buffer pH 6.0 or pH 7.2. Fraction collection vessels were changed after appropriate time intervals to describe the dissolution profile.

Dissolution at pH 1 and pH 6.0 (D17) or pH 7.2 (D18)

The method is similar to trial D15 or D16, but during the first 2h, 0.1N HCl was used as dissolution fluid. Thereafter, a buffer pH 6.0 (Trial D17) or pH 7.2 (Trial D 18) was used. The dissolution was carried out for 220 minutes.

Table III.19 Summary of the micropellet batches tested and dissolution methods employed.

Trial (rpm)	15658/32	15658/53	15658/60	15658/56	15658/57	15658/58	15658/59
D11(50rpm)	-	-	X	-	-	-	-
D11 (100rpm)	-	-	X	-	-	-	-
D11 (150rpm)	X	-	X	-	-	-	-
D12 (150rpm)	-	X	-	-	-	-	-
D13 (50rpm)	-	-	-	X	X	-	X
D13 (100rpm)	-	-	-	X	X	-	X
D13 (150rpm)	-	-	-	X	X	-	X
D14 (50rpm)	-	-	-	-	-	X	-
D14 (100rpm)	-	-	-	-	-	X	-
D14 (150rpm)	-	-	-	-	-	X	-
D15	X	X	X	-	-	-	-
D16	-	X	-	-	-	-	-
D17	-	-	-	X	X	-	X
D18	-	-	-	-	-	X	-

III.4.3. Dynamic Hydration Properties of Excipients for Mucoadhesive Micropellets

The dynamic hydration was investigated by means of a modified “Enslin” apparatus. Instead of the frit G3 with a diameter of 2cm, a frit Por 3 with a diameter of 3.57 cm and a capacity of 50ml was used. The frit was connected via an approximately 40cm vacuum hose with a diameter of 0.75 cm to a 10.00 ml burette. The reading accuracy was 0.02ml. The burette was adjusted, such that the top edge of the burette was on the same height as the membrane of the frit. For verification, a water-level and a band were used. The modified Enslin apparatus is presented in Figure III.4.

For filling, the burette stopcock was closed, and the accurate amount of the designated substance was filled into the frit. The substance in the frit should be plane. The stopcock was opened and consumption of water against time was read of the burette. The “Enslin” number was defined as the amount of water that was soaked within a maximum period of 15min. Each experiment was repeated three times.

Two modified set ups were applied and are numbered H1 and H2 for convenient differentiation.

Method H1

The dynamic hydration properties of Carbopol 71G, Chitosan, Na-alginate, Na-CMC, Noveon AA1 and MCC were evaluated with 3.24g of excipient and de-ionized water as hydration medium. In an additional experiment 3.24g chitosan was evaluated with 6% acetic acid in de-ionized water as a hydration medium.

Method H2

The dynamic hydration properties of Carbopol 71G, Chitosan, Eudispert hv, Na-alginate, Na-CMC, Noveon AA1 and MCC were evaluated using 1g of excipient and acetate buffer pH 5.5 or phosphate buffer pH 6.0 and 7.2 respectively as hydration media. In order to reduce the pH shift of the buffer, the amount of substance was reduced from 3.24g to 1g according to method H1. The selected buffers were modified USP buffers with a ten times higher concentration of buffering salt resulting in an increased buffer capacity.



Figure III.4 Modified Enslin apparatus.

Hydration Media

A) 6% Acetic acid		
	Acetic Acid	60g
	De-ionized water	940g
B) Acetate Buffer pH 5.5		
	NaC ₂ H ₃ O ₂ x 3H ₂ O	299g
	2N CH ₃ COOH	150ml
	De-ionized water	ad 5000ml
C) Phosphate Buffer pH 6.0		
	KH ₂ PO ₄	340g
	1N NaOH	280ml
	De-ionized water	ad 5000ml
D) Phosphate Buffer pH 7.2		
	KH ₂ PO ₄	340g
	1N NaOH	1750ml
	H ₂ O	ad 5000ml

III.4.4. Electron Dispersive X-Ray Method for Proving the Separation of an Enteric Coating Layer from a Mucoadhesive Matrix Layer

III.4.4.1. Background

An EDX-analysis in combination with Scanning Electron Microscopy (SEM) allows the topographical and morphological analysis of multiple layers in addition to locally dissolved element analysis. With EDX-analysis, a high energy containing electron beam is focused onto the surface of the probe. Out of all possible physical interactions, the most important is generating the Roentgen quanta. When electrons with sufficient energy pass the probe, it is possible that electrons are accelerated from the inner bowl and become ejected. The gaps generated have to be occupied by electrons from the outer bowls. Since the electrons have a higher energy being further away from the nucleus, they loose energy for the transition into an inner bowl. Their energy appears by emission of a Roentgen quant or "Auger" electron. The developing X-ray spectrum consists of two different spectra. A continuous X-ray spectrum related to the slowing down of the electrons as a result of interaction with atomic envelope, and the continuous loss of kinetic energy in terms of radiation. These spectra contain little analytic information and are regarded as background. The second spectrum is the "discrete" or "characteristic" X-ray spectrum of interest. This spectrum consists of a quantity of lines, whose positions are characteristic for the respective element. In accordance with this method, a qualitative and semi-quantitative analysis for all elements of a higher ordinal number than 4 (boron) is possible, e.g. titan and iron. In combination with a SEM analysis it is possible to assign the differential localization of the elements to specific surface areas or layers of the probe. The EDX analysis in combination with SEM was shown to be an appropriate method for testing the separation of the two functional layers *in vitro* (Knoell, 2004).

The purpose of the experiment was to evaluate, whether the enteric coating layer separated completed from the mucoadhesive matrix underneath.

III.4.4.2. Proof of Separation of Poured Films (Method X1)

For simulating the coated matrix, a three layer system was developed, (Figure III.5). Initially, 100ml of a solution containing EUDRAGIT L 30D-55 or EUDRAGIT FS 30D as enteric coating layer was poured onto a glass plate. After drying, the mucoadhesive inner layer (Chitosan, Na-Alginate, Na-CMC) was poured on top of the enteric coating layer. The poured solutions of the mucoadhesive layer were adjusted to an acidic pH to prevent the EUDRAGIT layer from dissolving. To the chitosan solution NaCl was added since nitrogen as component of chitosan is not a sufficient marker element for EDX. After drying, a defined circular area was punched out of the two layer film composite and was attached onto an adhesive backing layer facing the functional inner layer. The idea was to prohibit the functional inner layer from dissolving first, thus simulating a real matrix system. This three layer film (Figure III.5.) preparation was then fixed on a disc of the Paddle-over-Disc apparatus. This disc was exposed to buffer pH 6.0 or pH 7.2 for EUDRAGIT L 30 D-55 and EUDRAGIT FS 30D coated films, respectively, and different discs were removed at specified time points. The stirring rate was 100rpm in an APP. 2 DT6. The buffers are described in Chapter III.4.2.2. The probes were analyzed before dissolution as well as after the dissolution test using SEM in combination with EDX and an electron microscope.

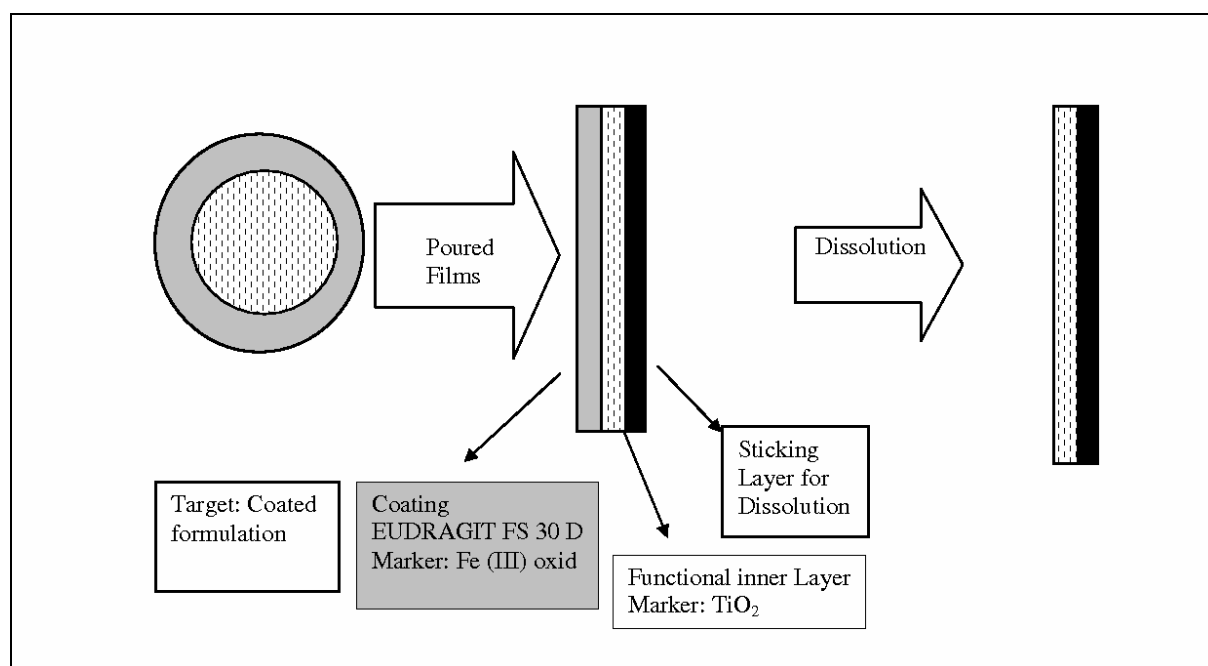


Figure III.5 Three layer film model.

Preparation of the Film Suspensions

The enteric films were composed of suspension A, the components are given below, with either a suspension of EUDRAGIT[®] L30 D-55 or EUDRAGIT[®] FS 30 D. The mucoadhesive polymers were directly dissolved in the diluents. The concentration of the EUDRAGIT[®] polymers was selected to achieve a film thickness comparable to an enteric resistant coating. The highest concentration of the mucoadhesive polymer was selected where the solution was also able to spread homogeneously over the glass plate.

Suspension A:	
Tween 80 (33.33 % ¹)	4.3g
GMS	3.6g
De-ionized water I	346.0g
De-ionized water II	<u>1646.1g</u>
Total	2000.0g

¹ 33.33g Tween 80 is diluted in 67.67 de-ionized water.

346g water together with the Tween 80 (33.33%) solution and the glycerolmonostearate were heated above 70°C and were homogenized with an Ultra-Turrax at moderate speed. The suspension was cooled down under continuous stirring with a magnetic stirring device and 1646.1g water was added.

Suspension B:	
EUDRAGIT [®] L 30 D-55	239.5g
TEC	7.2g
De-ionized water	<u>2153.3g</u>
Total	2400.0g

Suspension C:	
EUDRAGIT [®] FS 30 D	239.5g
TEC	3.6g
De-ionized water	<u>2156.9g</u>
Total	2400.0g

Acetic Acid Buffer pH 5.1 USP:	
Na-Acetate Tri-Hydrate	5.08g
2N Acetic Acid	6.30ml
De-ionized Water	ad 1000ml

Formulation of the EUDRAGIT[®] L 30 D-55 Film

Suspension A	47.07g
Suspension B	<u>52.93g</u>
Total	100.00g

Formulation of the EUDRAGIT[®] FS 30 D Film

Suspension A	47.07g
Suspension C	<u>52.93g</u>
Total	100.00g

Formulation of the Chitosan Film

Chitosan	12.0g
Acetic acid 96%	48.0g
NaCl	0.6g
De-ionized water	<u>340.0g</u>
Total	400.6g

Formulation of the Na-CMC Film

16.0g of Na-CMC were dissolved in 340g de-ionized water. The pH was adjusted to 5.1 with 0.1N acetic acid. The solution was filled with acetic buffer of pH 5.1 to 400.0g.

Formulation of the Na-Alginate Film

4.0g Na-alginate were dissolved in 372g de-ionized water. The pH was adjusted to 5.1 with 0.1N acetic acid. The solution was filled with acetic buffer of pH 5.1 to 400.0g.

III.4.4.3. Proof of Separation with Coated Micropellets (Method X2)

Micropellets of batches 15658/56, 15658/57, 15658/59 were stirred at 100rpm in APP. 2 DT6 in a phosphate buffer pH 6.0 (see Chapter III.4.2.2.). The experiments were stopped at different time points and the micropellets were dried. The samples were analyzed before dissolution as well as after the dissolution test using SEM in combination with EDX as described above.

III.4.5. Improving the Solubility of Lipophilic Drugs by Adjusting the Hydrophilic Lipophilic Balance (HLB Value) of the Drug Carrier System

III.4.5.1. Theoretical Estimation of (HLB) Value

Estimation of the Drug HLB

For the estimation of a drug HLB a correlation between the logP value and the HLB value was developed. For the correlation the known HLB value of different emulsifiers were plotted against calculated logP values. The different logP values of emulsifiers were calculated with ALOGPS 2.1 program (Tetko, 2002) or the S+logP and the MlogP (the Moriguchi logP) were calculated with QMPRPlus. In the case where the emulsifier is composed of different diastereomeres, a representative structural formula was selected. The different calculated logP values were plotted against the HLB values reported in the literature (Voigt, 2000). The coefficient of determination was calculated and the best fitting logP, the Moriguchi logP was selected. The equation of the best fitting straight line was calculated.

The Moriguchi logP of the drug was calculated. The log P value of the drug was transferred into the HLB value using the linear equation between the HLB value and the logP of the emulsifier and the HLB of the drug was calculated with the linear equation of the plot of logP against the HLB of the emulsifier.

Estimation of the HLB of the Lipid Matrix

The HLB of the mono-, di-, or tri- glyceride lipid matrices was calculated by the following equation reported by (Martin, 2002):

$$HLB = 20 \times \left(1 - \frac{SV}{AV}\right)$$

SV = Saponification value

AV = Acid value of the fatty acid of the glyceride

Most of the glycerides are composed of different fatty acids. Therefore the acid value was calculated as average of the fatty acids.

$$AV_{Average} = \left(\frac{X\%}{100}\right) \times AV_A + \left(\frac{X\%}{100}\right) \times AV_B + \left(\frac{X\%}{100}\right) \times AV_C + \left(\frac{X\%}{100}\right) \times AV_D + \left(\frac{X\%}{100}\right) \times AV_n$$

$AV_{Average}$ = The average acid value of all fatty acids of the glyceride.

$AV_A - AV_n$ = Acid value of the single fatty acid.

$$X\% = \frac{FA_A (molar)}{FA_{Total} (molar)} \times 100$$

FA_A = Amount of specific fatty acid in moles.

FA_{Total} = Amount of all fatty acids in moles.

Estimation of the HLB Value of a Matrix Composed of two Components

$$HLB_{Total} = \frac{Component_A [g]}{Matrix [g]} \times HLB_A + \frac{Component_B [g]}{Matrix [g]} \times HLB_B$$

Component_A [g] = Mass of the component A

Component_B [g] = Mass of the component B

Matrix [g] = Mass of the matrix

HLB_A = HLB value of component A

HLB_B = HLB value of component B

III.4.5.2. Solubility of Spironolacton in Fatty Matrices

Single Component Matrix

Imwitor 308, Imwitor 312, Imwitor 742, Softisan 138, Softisan 154, Vitamine E acetate and Vitamine E TPGS were melted on a water bath, mixed with different fractions of Spironolacton and cooled down while stirring. From each compound, samples were prepared with 0%, 5%, 10%, 20%, 30%, 40% and 50% content of Spironolacton. The samples and pure Spironolacton were analyzed using differential scanning calorimetry (DSC).

Double Component Matrix

14.31g Softisan 138 was melted together with 5.69g Vitamine E TPGS using a water bath and cooled down under stirring.

13.44g Softisan 154 was melted together with 6.56g Vitamine E TPGS using a water bath and cooled down under stirring. From each blend samples were

prepared with 5%, 10%, 15%, 20%, 25%, 30%, 40%, 50% content of Spironolacton as described above. The samples were analyzed with DSC.

Analysis by Differential Scanning Calorimetry

The DSC-Thermograms were recorded using the power compensation calorimeter Pyris 1 (Perkin Elmer) at a heating rate of 10Kmin^{-1} in a nitrogen atmosphere. The heat flux calorimeter DSC 910 has been used for problematic samples. The samples were scanned from -50 to 250°C in closed pans. Some samples yielded increased pressure under heating due to vaporizable components. The reported values of melting temperature and melt enthalpy have been evaluated according to ISO 11357-1.

CHAPTER IV RESULTS

In this section the results with production and characterization of micropellets produced with Na-CMC, Na-alginate, Chitosan, Carbopol and Noveon are presented.

IV.1. Production of Na-CMC Micropellets in the GPCG1 Rotary Processor

IV.1.1. Screening of Process Parameters

The process parameters described in Chapter III.1.1.1. were applied producing Na-CMC micropellets using 20 and 30% MCC.

Upon evaluation of the produced micropellets it turned out that their friability, tapped density and reproducibility was insufficient. Furthermore, even though batches 15176/49 15176/50 and 15176/51 were produced under the same conditions they showed pronounced differences in their span and amount of oversized particles. The friability and tapped density were insufficient even though as much as 800ml of liquid binder had been added. A comparison between batch 15176/54 and 15176/57 indicates that a decrease in rotor speed leads to an increase in particle size. On the other hand, the influence of the spheronization time seems to be negligible. In Table IV.1 the micropellet properties of the screening of the process parameters with 20% MCC are presented and in Table IV.2 with 30% MCC, respectively. The morphology and topographical quality of the results is presented in Figures IV.1 and IV.2.

Table IV.1 Properties of micropellets formulated with 20% MCC. Screening of process parameters. For process parameter see Chapter III.1.1.1.

Batch	X50 [μm]	Span	Oversized Particles >2000 μm [%]	Correlation Factor ¹	Tapped Density (200-250 μm) [g/ml]	Friability (200-250 μm) [%]	Over All Yield Particles [%]
15176/30	139.2	0.868	0	1.000	n.d.	n.d.	98
15176/39	233.6	0.907	0.08	0.974	n.d.	n.d.	94
15176/41	299.9	3.525	7.12	0.950	n.d.	n.d.	100
15176/42	178.0	1.209	0.18	0.996	n.d.	n.d.	100
15176/46	319.8	1.202	4.06	0.921	0.36	24.5	100
15176/47	302.3	1.324	2.60	0.949	0.37	29.5	99
15176/48	277.6	1.201	1.72	0.952	n.d.	n.d.	100
15176/49	350.2	5.615	11.76	0.939	n.d.	n.d.	100
15176/50	288.9	7.024	12.22	0.910	n.d.	n.d.	100
15176/51	352.7	1.187	3.32	0.958	n.d.	n.d.	100
15176/52	282.7	1.205	0.90	0.980	n.d.	n.d.	100
15176/53	269.7	1.325	0.42	0.982	0.37	32.7	100
15176/54	318.9	1.160	0.92	0.987	n.d.	n.d.	100
15176/56	530.4	1.215	3.44	0.950	n.d.	n.d.	100
15176/57	444.3	1.299	0.74	0.991	n.d.	n.d.	98
15176/58	194.3	0.937	0.02	1.000	n.d.	n.d.	99
15176/59	370.5	1.023	0.15	0.994	0.36	32.5	100

¹ Correlation between the RRSB line and particle diameter at 63.2% cumulative size distribution. If the correlation is 1, the distribution follows RRSB distribution perfectly.

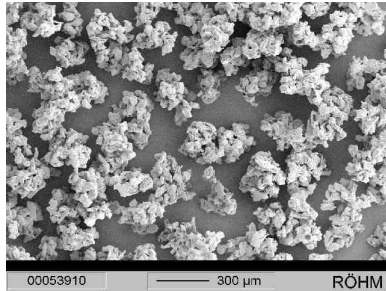
Table IV.2

Properties of micropellets formulated with 30% MCC.
Screening of process parameters. For process parameters see Chapter III.1.1.1.

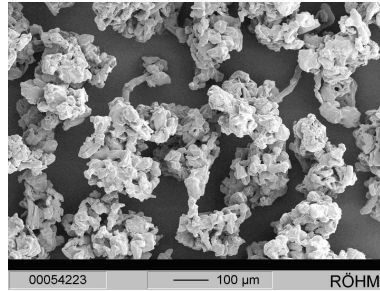
Batch	X50 [μm]	Span	Oversized Particles >2000 μm [%]	Correlation Factor ¹	Over All Yield Particles [%]
15176/23	170.3	1.258	0	0.996	96
15176/26	376.4	1.203	0	0.999	97
15176/28	172.2	2.601	0	0.964	100
15176/29	133.4	0.938	0	0.997	100

¹ Correlation between the RRSB line and particle diameter at 63.2% cumulative size distribution. If the correlation is 1, it follows RRSB distribution.

15176/39



15176/53



15176/59

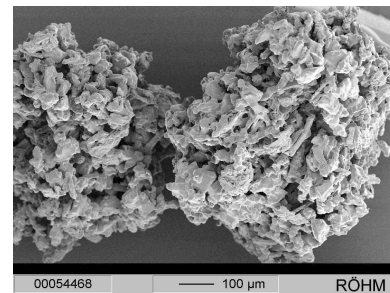
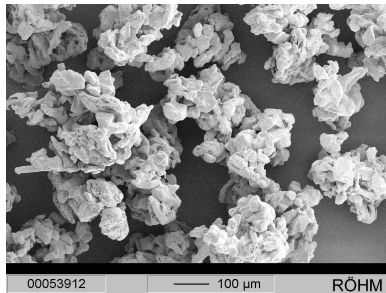
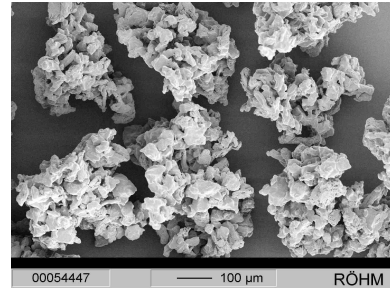


Figure IV.1

Morphology and topographical quality of micropellets formulated with 20% MCC.
For process parameters see Chapter III.1.1.1. The scale of the picture is to be taken into consideration.
All micropellets demonstrated an expressed fluffy body structure, independent of the process parameters.

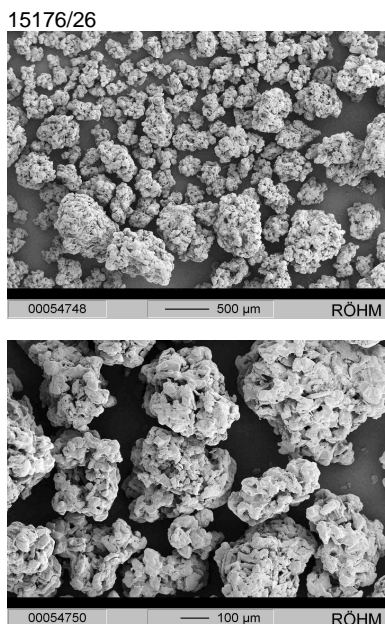


Figure IV.2 Morphology and topographical quality of micropellets formulated with 30% MCC. For process parameters see Chapter III.1.1.1. The scale of the picture is to be taken into consideration. The micropellets demonstrated an expressed fluffy body structure, independent of the process parameters.

All micropellets demonstrated an expressed fluffy body structure. Based on the screening experiments it was concluded that it will be necessary to maintain the airflow at a low starting setting of 42m³ per h in order to avoid the extensive evaporation of water. It can be expected that this measure will also lead to a higher reproducibility because fewer changes of the process parameters during the process support the stable process. Furthermore, the rotor speed should be maintained at one defined level without any change during the process to decrease the particle size. The spheronization time should be set to 10 minutes. As a result of the insufficient micropellet properties the higher level of the binder microcrystalline cellulose (MCC 30%) was selected for further experiments to assist in the pelletization process.

IV.1.2. Development of Process Parameters for Na-CMC Micropellets

The development of Na-CMC micropellets with suitable friability, tapped density, particle size and yield to be used in a subsequent coating process was successful. In Table IV.3 the micropellet properties during the process development phase are presented. Particle size and friability are influenced by the spraying rate, amount of binder, airflow, inlet air temperature, rotor speed and type of rotor disc (Table IV.3). Except for the rotor speed and type of rotor disc, the parameters mentioned above are also determinants for the tapped density. The span is impacted by airflow and rotor speed. Process parameters leading to batches 15536/52, 15658/37, 15658/40 and 15658/41 turned out to be optimum leading to products within defined particle size ranges. In addition, these micropellets showed improved friability in comparison with the commercially available Cellets[®] (5.7% versus 41.5%) and a high tapped density of 0.934g/ml. The particle size distribution of the micropellets did not always follow a RRSB distribution as can be seen from the correlation factor (Table IV.3). This was seen for batches with a high x50 value where two independent particle size distributions were detected combined with independent growth. Therefore, it can be concluded that particle growth was not homogenous.

Table IV.3. Properties of micropellets formulated with 30% MCC during the development phase.
For process parameters see Chapter III.1.1.2.

Batch	X50 [μm]	Span	Oversized Particles >2000 μm [%]	Correlation Factor ¹	Tapped Density 400-500 μm [250-350 μm] {200-250 μm } [g/ml]	Friability 400-500 μm [250-350 μm] {200-250 μm } [%]	Water Content ² [%]	Yield [%]
15451/54	552	2.729	5.86	0.985	[0.43] {0.47}	[7.92] {9.42}	39.8	100
15451/55	332	1.717	6.66	0.939	{0.40}	{16.01}	31.9	100
15451/56	248	1.557	3.00	0.943	{0.39}	{27.83}	30.0	97.2
15451/64	491	3.974	13.33	0.878	0.46 [0.49]	24.83 [2.95]	n.d. ³	90.0
15451/65	477	3.577	8.63	0.980	[0.39] {0.42}	[14.40] {14.71}	41.3	98.6
15451/66	250	1.036	2.62	0.925	[0.34] {0.37}	[36.20] {32.60}	29.9	100
15451/74	459	4.232	12.83	0.879	[0.46]	[6.37]	n.d.	95.4
15451/75	360	0.993	3.67	0.911	[0.42] {0.46}	[13.03] {9.27}	37.2	93.2
15451/76	351	0.958	0.59	0.998	[0.36] {0.40}	[34.92] {35.42}	31.6	100
15536/01	154	1.374	0	1	{0.32}	n.d.	n.d.	100
15536/02	232	1.099	1.62	0.989	{0.36}	n.d.	n.d.	100
15536/03	284	1.279	1.24	0.985	0.28	n.d.	n.d.	100
15536/04	540	1.942	10.13	0.905	0.36	n.d.	34.9	100 ⁴
15536/05	496	3.591	7.70	0.905	0.36	n.d.	n.d.	99.1 ⁴
15536/06	495	1.056	5.59	0.934	0.33	n.d.	32.0	99.0
15536/07	757	2.698	19.80	0.889	0.58	11.11	44.0	100
15536/08	489	0.886	2.50	0.903	0.56	20.27	45.1	96.0
15536/09	498	0.889	2.05	0.906	0.67	15.97	46.0	88.6
15536/10	526	0.950	1.97	0.966	0.67	13.77	48.0	93.0

¹ Correlation between the RRSB line and particle diameter at 63.2% cumulative distribution. In case the correlation is 1, it follows RRSB distribution perfectly.

² Water content at the end of the spraying period.

³ n.d. = not determined.

⁴ The fluid bed collapsed.

Table IV.3. continued

Properties of micropellets formulated with 30% MCC during the development phase.
For process parameters see Chapter III.1.1.2.

Batch	X50 [μm]	Span	Oversized Particles >2000 μm [%]	Correlation Factor ¹	Tapped Density 400-500 μm [250-350 μm] {200-250 μm } [g/ml]	Friability 400-500 μm [250-350 μm] {200-250 μm } [%]	Water Content ² [%]	Yield [%]
15536/11	565	0.895	1.35	0.991	0.73	8.31	48.6	86.4
15536/12	481	0.818	1.29	0.995	0.72	14.00	49.2	90.6
15536/13	493	0.905	0.96	0.998	0.71	12.64	n.d. ³	90.0
15536/14	484	0.920	0.57	0.997	0.60	14.82	44.0	88.0
15536/15	499	0.960	2.84	0.908	0.70	12.26	48.0	85.8
15536/16	458	1.104	2.09	0.950	0.47	25.21	41.0	n.d.
15536/17	576	1	7.72	0.916	0.72	7.57	n.d. ³	90.2
15536/18	745	0.897	7.25	0.917	0.80	4.64	53.0	82.5
15536/19	582	3.062	11.97	0.918	0.70	12.01	46.0	94.98
15536/20	490	0.805	1.59	0.996	0.74	14.50	50.6	82.0
15536/42	494	0.545	1.25	0.999	0.83	6.55	n.d. ³	77.0
15536/43	523	0.597	0.90	0.997	0.92	1.98	n.d. ³	61.0
15536/44	869	1.892	13.60	0.862	n.d. ³	n.d. ³	61.9	60.0
15536/45	568	0.613	0.31	0.987	0.93	1.96	61.2	37.0
15536/46	505	0.762	3.75	0.907	0.86	8.88	55.9	66.0
15536/47	498	0.470	0.93	0.999	0.82	9.78	54.8	56.4
15536/48	535	0.587	0.12	0.997	0.87	5.77	56.2	46.0
15536/49	530	0.610	0.18	0.996	0.86	7.86	n.d. ³	60.0
15536/50	518	0.591	0.68	0.998	0.83	10.47	55.0	82.2
15536/51	492	0.603	0.50	0.998	0.83	12.87	54.8	84.0
15536/52	501	0.603	1.25	0.995	0.91	7.68	55.5	82.0
15536/53	470	0.509	0.75	0.998	0.83	14.37	54.1	86.0
15536/54	470	0.509	1.49	0.999	0.80	15.77	54.0	88.0

¹ Correlation between the RRSB line and particle diameter at 63.2% cumulative distribution. In case the correlation is 1, it follows RRSB distribution perfectly.

² Water content at the end of the spraying period.

³ n.d. = not determined.

Table IV.3. continued

Properties of micropellets formulated with 30% MCC during the development phase.
For process parameters see Chapter III.1.1.2.

Batch	X50 [μm]	Span	Oversized Particles >2000 μm [%]	Correlation Factor ¹	Tapped Density 400-500 μm [250-350 μm] {200-250 μm } [g/ml]	Friability 400-500 μm [250-350 μm] {200-250 μm } [%]	Water Content ² [%]	Yield [%]
15658/37	525	0.596	0.25	0.999	0.93	5.39	54.6	92.6
15658/39	563	0.649	3.30	0.923	0.88	4.15	53.8	96.0
15658/40	526	0.662	0.37	0.923	0.95	5.11	55.9	84.2
15658/41	543	0.611	1.18	0.998	0.95	4.68	55.5	82.6
Celllets [®]	n.d. ³	n.d. ³	n.d. ³	n.d. ³	0.916	41.5	n.d. ³	n.d.

¹ Correlation between the RRSB line and particle diameter at 63.2% cumulative distribution. When the correlation is 1, it follows RRSB distribution perfectly.

² Water content at the end of the spraying period.

³ n.d. = not determined.

IV.1.2.1. Process Parameters Affecting Micropellet Properties

Several process parameters exhibit distinctive influence on the final quality of the micropellets manufactured. The results of experiments showing the influence of average spraying rate, continuous/non-continuous spraying rates, rotor speed, type of rotor disc, liquid binder amount, airflow, batch size onto the properties are reported in the following paragraphs. In addition, inlet air humidity and drying air temperature are shown to have an impact on the yield. Finally, the reproducibility of the production process is characterized.

It was shown that an increase of the average spraying rate results in an increase of particle size and tapped density, combined with a decrease of friability of the micropellets (Table IV.4).

Table IV.4 Effect of the average spraying rate of liquid binder on particle size, tapped density and friability. The composition of the pellets is given in Chapter III.1.1.2.

Batch	Average Spraying Rate [g/min]	X50 [μm]	Tapped Density 400-500 μm [g/ml]	Friability 400-500 μm [%]
15536/8	23.8	489	0.56	20.27
15536/9	26.5	498	0.67	15.97
15536/10	32.1	526	0.67	13.77
15536/11	37.5	565	0.73	8.31

The influence of the average spraying rate was statistically significant as presented in Figure IV.3. In the statistical analysis the influence of the rotor speed and the binder amount were also shown to be significant. On the basis of the insufficient retrospective design of the statistical analysis it was not possible to show statistical significance for other process parameters with respect to the particle size.

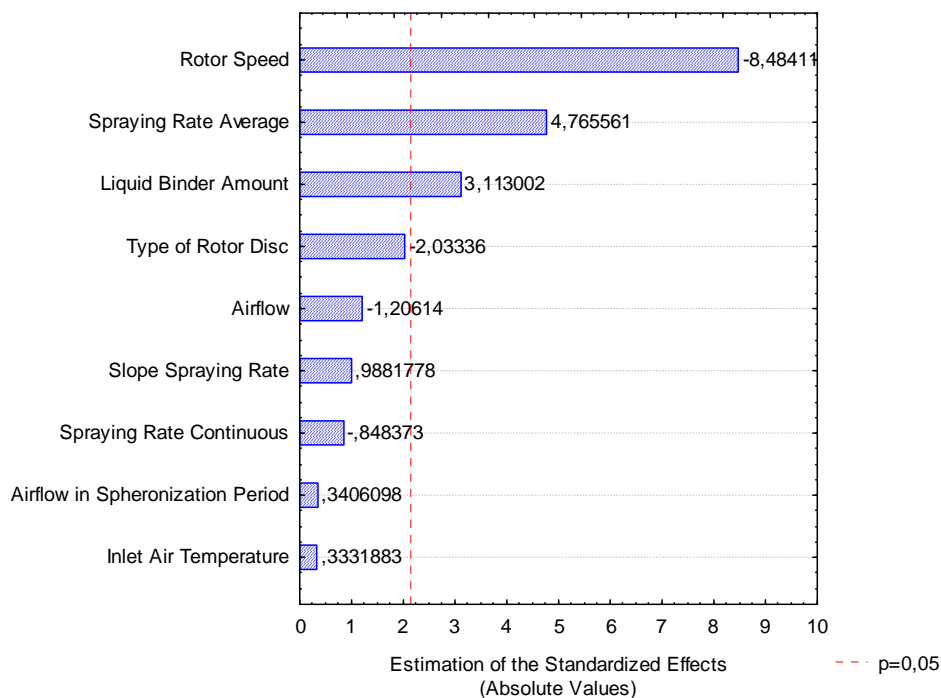


Figure IV.3 Pareto diagram of the standardized variables. Response variable was the particle size. The confidence interval is 95%, values higher than the dotted p value ($p=0.05$; 2.16039) are statistically significant.

The average spraying rate used for the production of batch 15536/50 (45g/min) was comparable to that for batch 15536/13 (44g/min). Therefore, the effect of **non-continuous** (batch 15536/50) **versus continuous spraying rate** can be investigated. A non-continuous spraying rate leads to lower span (0.59 versus 0.91), slightly increased tapped density (0.83g/ml versus 0.71g/ml) and slightly decreased friability (10.47% versus 12.64%).

A higher initial **rotor speed** (1400rpm versus 710rpm) leads to smaller particles (489µm versus 757µm) which are less mechanically stable and thus demonstrate a higher friability (20.27% versus 11.11%). In addition, the span of the particle size distribution is smaller (0.886 versus 2.698) and the fraction of oversized particles is reduced (2.6% versus 19.8%). In Figure IV.4 the statistically significant influence of the rotor speed on the span of the particle size distribution is shown. The rotor speed has no measurable effect on the particle density. The same effect can be seen by comparing batch 15536/11 versus 15536/12.

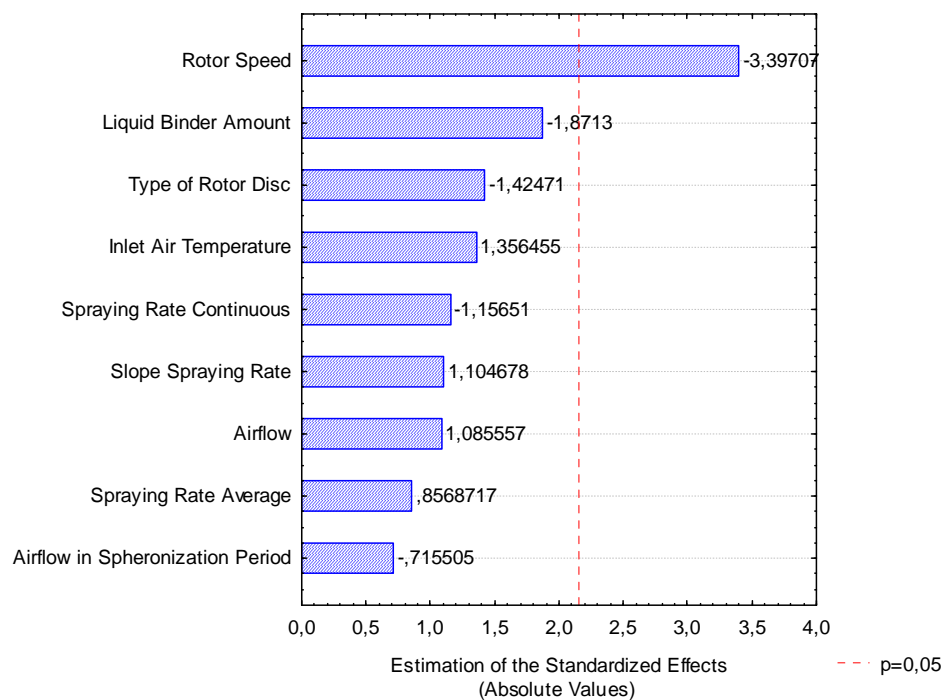


Figure IV.4 Pareto diagram of the standardized variables. Response variable was the span. The confidence interval is 95%, values higher than the dotted p value (p=0.05; 2.16039) are statistically significant.

The influence of the **type of rotor disc** in terms of changing a plane rotor disc to a grooved rotor disc has a similar effect as an increase in rotor speed. The grooved rotor disc leads to smaller particles (493µm versus 576µm) with a higher friability (12.64% versus 7.57%). The span of the particle size distribution is smaller (0.905 versus 1) and the fraction of oversized particles is reduced (0.96% versus 7.72%). The rotor type has no measurable effect on particle density.

An Influence of the **rotor speed** during the drying period can also be demonstrated by comparing batches 15658/37 and /39, where a decrease of rotor speed (500rpm to 1800rpm) leads to an increase in particle size (563µm versus 535µm).

Furthermore, an influence of the **liquid binder amount** on the quality of the product was found. An increase in the amount of liquid binder (from 700ml batch 15536/53 to 750ml batch 15536/52) results in an increase in particle size (501µm versus 470µm), span (0.603 versus 0.509) and amount of oversized particles (1.25%

versus 0.75%). In addition, the tapped density of the micropellets was increased (0.91g/ml versus 0.83g/ml) whereas the friability of the micropellets was significantly decreased by approximately 50% (7.68% versus 14.37%) as presented in Figure IV.5. In addition, the airflow, the average spraying rate, the slope of the spraying rate, the rotor speed and the spraying pattern were proven to have a significant influence. In contrast, both the type of the rotor disc and the inlet air temperature also influence the friability. It was however not possible to demonstrate statistical significance for these effects due to the design of the experiments.

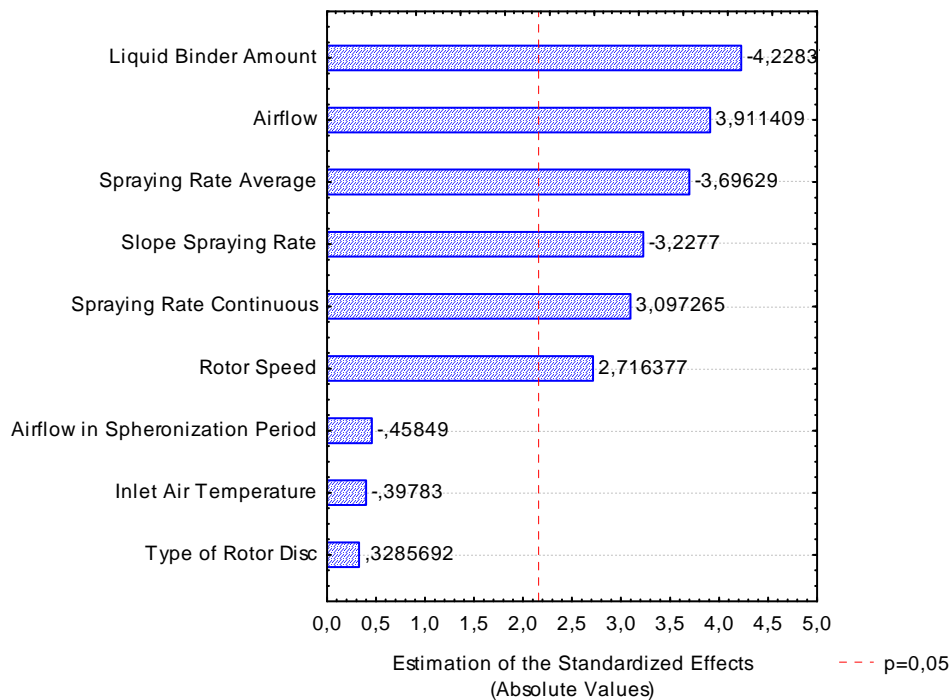


Figure IV.5 Pareto diagram of the standardized variables. Response variable was the friability. The confidence interval is 95%, values higher than the dotted p value ($p=0.05$; 2.16039) are statistically significant.

An increase in **airflow** (52m³/h batch 15536/16 versus 42m³/h batch 15536/13) results in a decrease of particle size (470µm versus 493µm) and tapped density (0.47g/ml versus 0.71g/ml), combined with an increase of friability (25.21% versus 12.64%), span (1.104 versus 0.905) and amount of oversized particles (2.09% versus 0.96%). In Figure IV.6 a significant influence of the airflow on the tapped density is shown. Figure IV.6 exhibits also a significant influence of the following process parameters: liquid binder amount, continuous spraying rate versus non-continuous, slope of the spraying rate and average spraying rate on tapped density of the micropellets. Based on the insufficient number of experiments with different inlet air temperatures, no significant influence of the inlet temperature can be demonstrated.

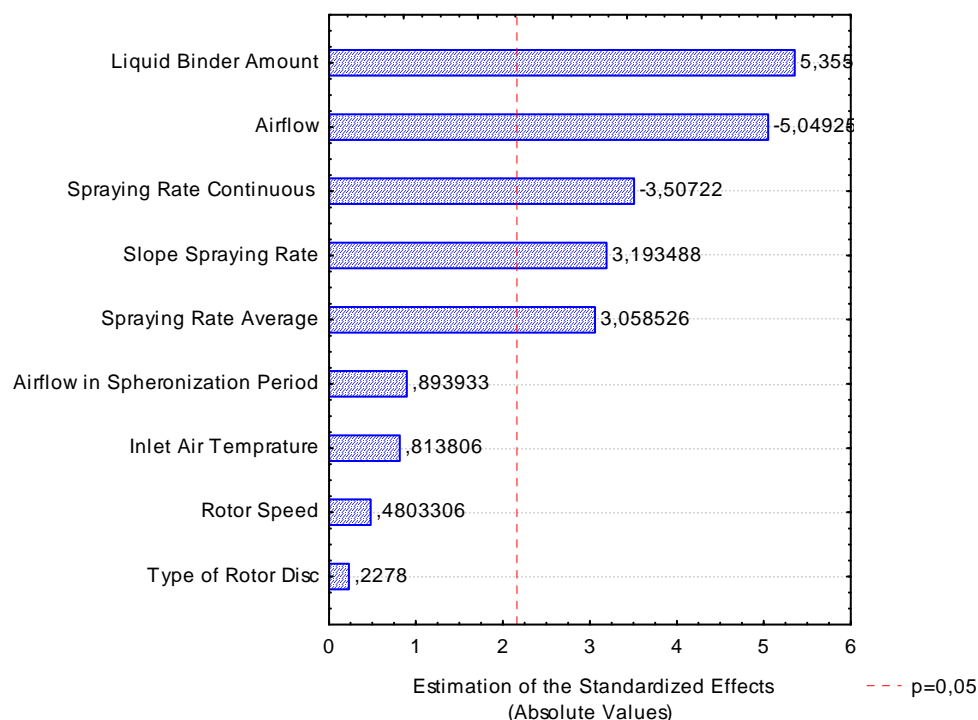


Figure IV.6 Pareto diagram of the standardized variables. Response variable was the tapped density. The confidence interval is 95%, values higher than the dotted p value ($p=0.05$; 2.16039) are statistically significant.

Batch size represented a further factor to consider where a decrease of batch size (from 750g batch 15658/54 to 500g batch 15536/64) in combination with a proportional increase of liquid resulted in a decrease of particle size (491 μ m versus 552 μ m) and friability (2.95% versus 7.92%), combined with an increase of tapped density (0.46g/ml versus 0.43g/ml), span (3.974 versus 2.729) and amount of oversized particles (13.33% versus 5.86%) of the product.

The **inlet air humidity** has a pronounced impact on **the yield**. This is demonstrated by a comparison of batch 15536/42 with batch 15536/47 where inlet air humidity was controlled by a hygrometer. Whereas the batch /42 was manufactured at an average spraying rate of 45.0g/min, batch /47 was produced at lower spraying rate (40.2g/min). Against the expectations, the yield of batch 15536/42 was greater than the yield of batch 15536/47. As cause of this result, a higher inlet air humidity may be assumed. An increase of the inlet air humidity can also led to an addition increase of the outlet humidity, which is also at low inlet humidities at a very high level. The high relative humidity of the outlet air can cause a recondensation of water at the cold shell of the GPCG1. The micropellets can stick permanent at the shell and are lost for the further process. The current weather conditions have therefore to be taken into consideration during the processing period.

The impact of the **drying air temperature** on the yield was studied comparing batch 15536/48 and batch 15536/49 produced on the same day under conditions of high inlet air humidity. An increase of the drying air temperature (40 $^{\circ}$ C to 65 $^{\circ}$ C) lead to a decrease of the yield (60% to 46%).

In addition, the yield is highly reduced by high **inlet air humidity** in combination with high **drying temperature**. On the other hand, an increase of the inlet air humidity lead to an increase in tapped density together with particle size, and to a decrease of friability. Both phenomena are depicted in Table IV.5.

Table IV.5 Influence of the inlet air humidity on friability and tapped density of micropellets and impact of the inlet air humidity in combination with the drying air temperature on the yield.

Batch	Inlet Air Humidity [g/m ³]	Drying Air Temperature 1 [°C]	X50 [µm]	Tapped Density 400-500µm [g/ml]	Friability 400-500µm [%]	Yield [%]
15536/45	+++++	55	568	0.93	1.96	37
15536/48	++++	65	535	0.87	5.77	46
15536/49	++++	40	530	0.86	7.86	60
15536/52	+	30	501	0.91	7.68	82

The **reproducibility of the manufacturing process** for Na-CMC micropellets is satisfactory in terms of particle size, particle density, friability, and yield. The process is thus robust under the condition that the most critical manufacturing variables, i.e. inlet air humidity and the starting product temperature are tightly controlled. Suggested boundary values for these parameters are 6.56g/m³ to 8.10g/m³ for inlet air humidity and 32°C to 34°C for the starting product temperature, respectively. Characteristic product properties following variation of these critical manufacturing variables in the production are presented in Table IV.5.

Table IV.5 Reproducibility of the Na-CMC micropellets manufacturing process.

Batch	Inlet Air Humidity [g/m ³]	Starting Product Temperature [°C]	X50 [µm]	Tapped Density 400-500µm [g/ml]	Friability 400-500µm [%]	Yield [%]
15536/52	6.56	32	501	0.91	7.68	82
15658/37	8.00	34	525	0.93	5.39	93
15658/40	7.80	32	526	0.95	5.11	84
15658/41	8.10	32	542	0.95	4.68	82

IV.1.2.2. Morphology and Topographical Quality of Na-CMC Micropellets

SEM photographs of Na-CMC micropellets are presented in Figure IV.7 Batch 15451/64 was prepared at a high inlet air temperature, a low amount of liquid binder and a low spraying rate as compared to the other batches. Batch 15536/13 was prepared at a continuous spraying rate and batch 15658/41 was prepared at a non continuous spraying rate. The amount of liquid binder added to batch 15536/13 was less than to batch 15658/41. The morphology and topographical quality is improved from batch 15451/64 via 15536/13 to 15658/41. The micropellets appear more spherical since the structure of the micropellets changes from a granule style to a smooth gliding surface. The process parameters for each batch were presented in Table III.3 (page 46f).

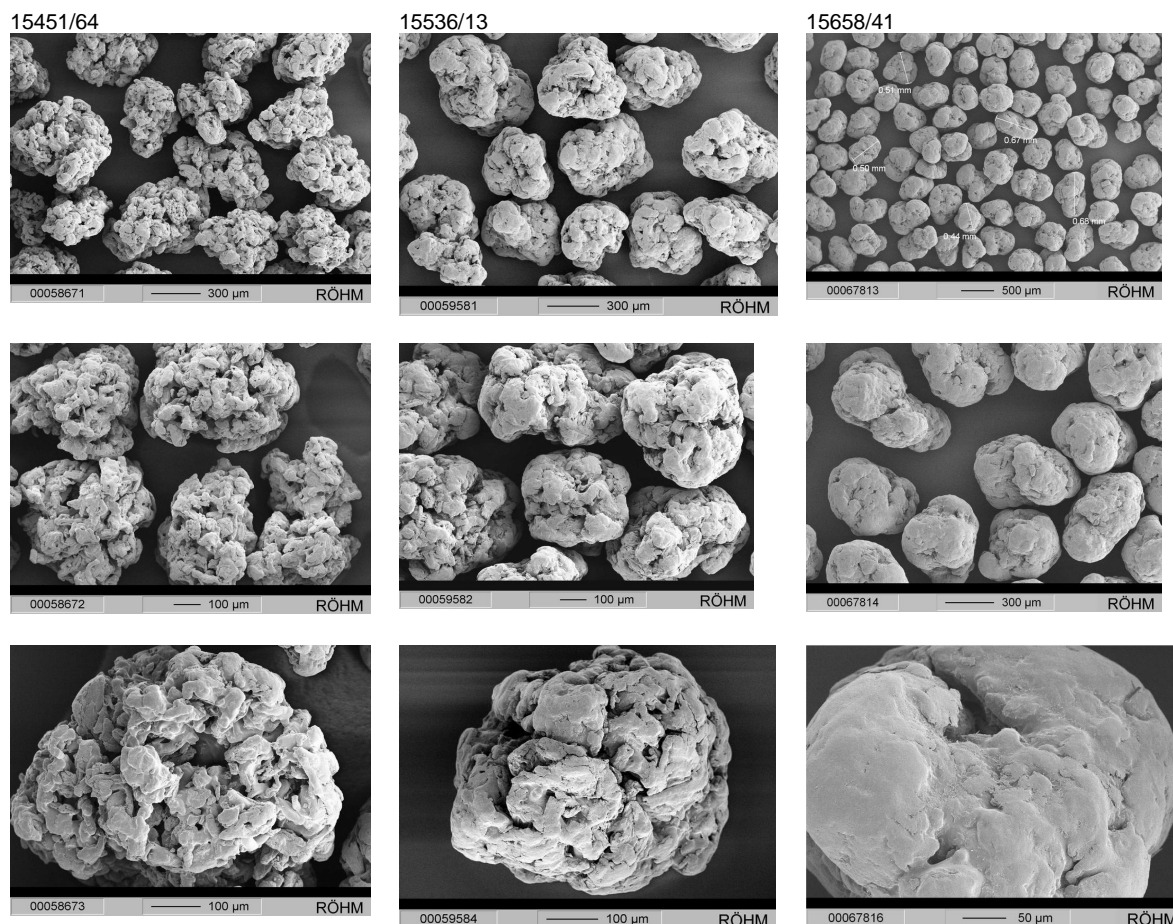


Figure IV.7 Morphology and topographical quality of selected batches of Na-CMC micropellets. The shape of the micropellets appears more spherical for batch 15658/41 since the structure of the micropellets changes from a granule style to a smooth gliding surface. The different scales of the photographs need to be taken into consideration.

IV.2. *Na-Alginate Micropellets Production in the GPCG1 Rotary Processor*

IV.2.1. *Screening of Process Parameters*

The process parameters described in Chapter III.1.2.1. were applied to the production of Na-alginate micropellets. It was shown that friability, tapped density and particle size of the presented micropellets were insufficient. A comparison between batches 15176/32 and 15176/34 in which, except for the MCC content, all other variables were kept constant, indicates that there is negligible impact of the MCC content on particle size. From the batches 15176/33, 15176/34 and 15176/62 it can be concluded that an increase of the binder amount lead to an increase in particle size. Furthermore it can be observed that an increase of the average spraying rate lead to larger particles with slightly lower friability as can be seen from a comparison of batch 15658/62 versus 15658/63. The use of a Kollidon[®] solution instead of de-ionized water as liquid binder resulted in particles of the same size but with higher tapped density, friability and reduced span (batch 15568/63 versus 15658/66).

All micropellets presented a very fluffy body structure. Micropellets with a higher MCC content or those prepared with Kollidon[®] solution as liquid binder seem to have a more defined core structure. The backdraft of the micropellets prepared

with Kollidon® is their higher friability which excluded the Kollidon® solution as a liquid binder from further development. As a result of the insufficient micropellet properties of the formulation with the lower MCC content, the product with the higher level of MCC was selected for further experiments. For the development of the process parameters the experience gained in the formulation of Na-CMC micropellets and the screening experience of the process parameters for Na-alginate micropellets were combined.

In Table IV.6 the micropellet properties of the screening of the process parameters with 20% MCC are presented and in Table IV.7 the results with 30% MCC and 44% MCC, respectively. The morphology and topographical quality of the products is shown in Figures IV.8 and IV.9.

Table IV.6. Properties of Na-alginate micropellets. Screening of process parameters with 20% MCC. For process parameters see Chapter III.1.2.1.

Batch	X50 [µm]	Span	Oversized Particles >2000µm [%]	Correlation Factor ¹	Yield [%]
15176/31	115.4	0.917	0	0.995	89.9
15176/32	121.0	0.881	0	0.998	94.8
15176/60	165.1	0.761	0	0.999	100.0
15176/61	184.3	0.692	0	0.999	99.2

¹Correlation between the RRSB line and particle diameter at 63.2% cumulative size distribution. In case the correlation is 1, it follows RRSB distribution perfectly.

Table IV.7 Properties of Na-alginate micropellets. Screening of process parameters with 30% and 44% MCC, respectively. For process parameters see Chapter III.1.2.1.

Batch	X50 [µm]	Span	Oversized Particles >2000µm [%]	Correlation Factor ¹	Tapped Density (200-250µm) [g/ml]	Friability (200-250) [%]	Yield [%]
15176/33	111.7	1.004	0	0.995	n.d. ²	n.d. ²	93.6
15176/34	120.3	0.945	0	0.997	n.d. ²	n.d. ²	95.5
15176/62	151.3	0.622	0	0.998	0.41	67.62	93.9
15176/63	203.7	0.708	0.08	0.920	0.42	64.60	89.7
15176/66	207.2	0.518	0.16	0.998	0.48	82.90	83.8
15176/67	204.0	0.552	0.01	0.996	0.46	84.41	84.5

¹ Correlation between the RRSB line and particle diameter at 63.2% cumulative size distribution. In case the correlation is 1, it follows RRSB distribution perfectly.

² n.d. = not determined.

15176/60

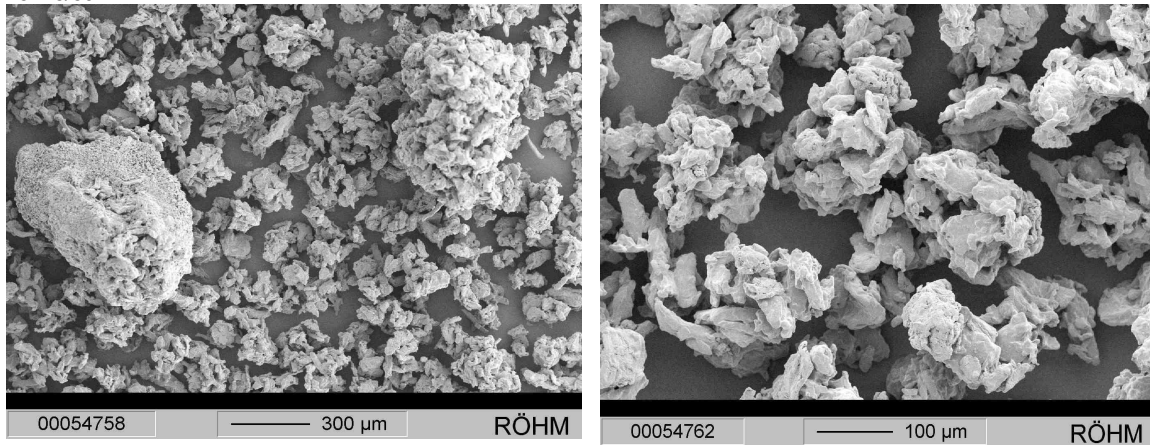
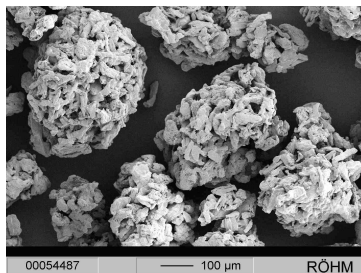
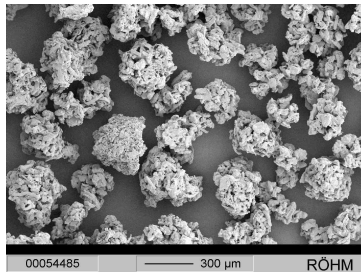
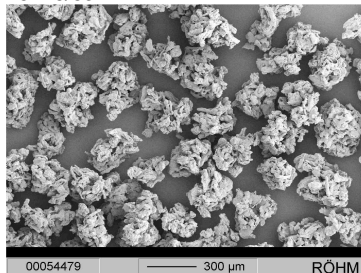


Figure IV.8

Morphology and topographical quality as a result of screening of the process parameters of Na-alginate micropellets with 20% MCC. Batch 15176/60 is presented where the micropellets presented a very fluffy body structure. The process parameters are given in Table III.5. The scale of the picture should be taken into consideration.

15176/63



15176/66

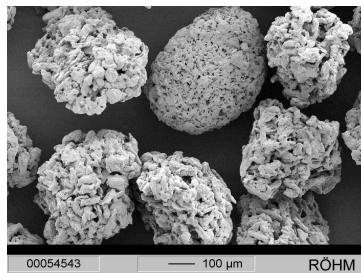
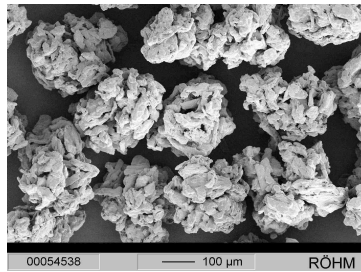
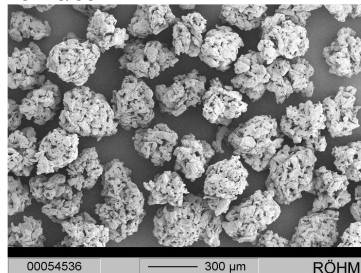


Figure IV.9

Morphology and topographical quality as a result of screening of the process parameters of Na-alginate micropellets with 30% MCC. Micropellets of batch 15176/63 are depicted on the left, and micropellets of batch 15176/66 on the right. Batch 15176/66 was prepared with a Kollidon solution as a liquid binder, batch 15176/63 with de-ionized water. The remaining process parameters (Table III.5) were identical. All micropellets presented a very fluffy body structure. Micropellets with a higher MCC content or those prepared with Kollidon® solution as liquid binder seem to have a more defined core structure. The scale of the picture should be taken into consideration.

IV.2.2. Development of Process Parameters for Na-Alginate Micropellets

The development of Na-alginate micropellets with acceptable friability, tapped density, particle size and yield to be used in subsequent coating processes was successful. In Table IV.8 the micropellet properties and the parameters which varied during the process development are presented. Particle size, tapped density and friability are influenced by the same process parameters as shown for Na-CMC micropellets. The process parameters applied for the production of batches 15536/61 and 15658/43 lead to the most promising micropellets of defined particle size range. These micropellets had a very low friability of 13.11 to 17.04% and also a high tapped density of 0.72g/ml. For better reproducibility, the liquid spraying amount should be reduced since 950ml of liquid binder as employed in these experiments was nearly leading to a collapse of the fluidized bed. At this point the risk is very high to produce an over-wetted area followed by the formation of lumps. This happened in the case of batch 15658/43. The particle size distribution did not always follow RRSB distribution as can be seen from the correlation value. Therefore, it can be concluded that the particle growth is not homogenous. This was seen for batches with a high x50 value where two independent particle size distributions were detected combined with independent growth.

Table IV.8 Properties of Na-alginate micropellets produced during development of the process parameters.
For process parameters see Chapter III.1.2.2.

Batch	X50 [μm]	Span	Oversized Particles >2000 μm [%]	Correlation Factor ¹	Tapped Density 400-500 μm , [250-350 μm] [g/ml]	Friability 400-500 μm [250-350 μm .] [%]	Water Content ² [%]	Yield [%]	Incidents
15536/55	224.5	1.008	0	1	[0.98]	[18.28]	67.8	88	-
15536/57	272.2	1.552	0.19	0.993	[0.99]	[11.65]	72.07	88	-
15536/58 ³	442.9	3.033	7.40	0.906	0.89 [0.94]	13.30 [3.57]	67.5	96	Collapse of the fluid bed
15536/59	482.8	4.026	12.95	0.905	0.82	18.81	67.6	108	
15536/60	350.1	1.176	2.42	0.919	0.7	16.18	61.1	96.44	-
15536/61	364.8	1.385	3.11	0.906	0.73	17.04	66.2	96.44	-
15358/43	371.0	3.584	6.25	0.919	0.72	13.11	65.93	95	-
Celllets [®]	n.d. ⁴	n.d. ⁴	n.d. ⁴	n.d. ⁴	0.916	41.50	n.d. ⁴	n.d. ⁴	-

¹ Correlation between the RRSB line and particle diameter at 63.2% cumulative size distribution. In case the correlation is 1, it follows RRSB distribution perfectly.

² Water content at the end of the spraying period.

³ The fluidized bed collapsed. The GPCG1 was opened, big particles were broken by hand, and the GPCG1 was started again. This batch is only affiliated in the table for comparison;

⁴ n.d. = not determined.

IV.2.2.1. Process Parameters affecting Micropellet Properties

Several process parameters exhibit a distinctive influence on the final quality of the micropellets manufactured. As follows, the results of experiments showing the influence of average spraying rate, liquid binder amount and rotor speed on the properties of micropellets are summarized.

An increase of the **average spraying rate** lead to an increase in particle size as well as span. Furthermore, a decrease of friability resulted and a slight increase of tapped density. The data are given in Table IV.9.

Table IV.9 Influence of the average spraying rate on the quality of the micropellets.

Batch	Average Spraying Rate [g/min]	X50 [μm]	Span	Tapped Density 250-355 μm [g/ml]	Friability 250-355 μm [%]
15536/55	54.7	224.5	1.008	0.98	18.28
15536/57	93.0	272.2	1.552	0.99	11.65

An increase in the **liquid binder amount** lead to an increase in particle size, span, tapped density and to a decrease of friability as can be seen from Table IV.10.

Table IV.10 Influence of the Liquid Binder Amount on the quality of the micropellets.

Batch	Liquid Binder Amount [g]	X50 [μm]	Span	Tapped Density 400-500 μm [g/ml]	Friability 400-500 μm [%]
15536/58	1032	442.9	3.033	0.89	13.30
15536/60	883	350.1	1.176	0.70	16.18

A decrease in the **rotor speed**, even if accompanied with a decrease of the amount of binder, lead to an increase in particle size, span and an increase in friability (Table IV.11).

Table IV.11 Influence of the rotor speed on the quality of the micropellets.

Batch	Rotor Speed [rpm]	Liquid Binder Amount [g]	X50 [μm]	Span	Tapped Density 250-355 μm [g/ml]	Friability 250-355 μm [%]
15536/57	1800	1200	272.2	1.552	0.99	11.65
15536/58	500	1032	442.9	3.033	0.89	13.30

IV.2.2.2. Morphology and Topographical Quality of Na-Alginate Micropellets

The micropellets of batch 15536/61 and 15658/43 were optimized concerning the yield, friability, tapped density and body structure. The particles of batch 15536/59 were prepared by applying a higher spraying rate and a higher amount of binder. Their body structure was improved in comparison to batch 15536/61, however, the yield of micropellets between 250 μm to 600 μm was hreduced from 78% to 61%. The process parameters are presented in Table III.6. Figure IV.10 shows the morphology and topographical quality of the Na-alginate micropellets.

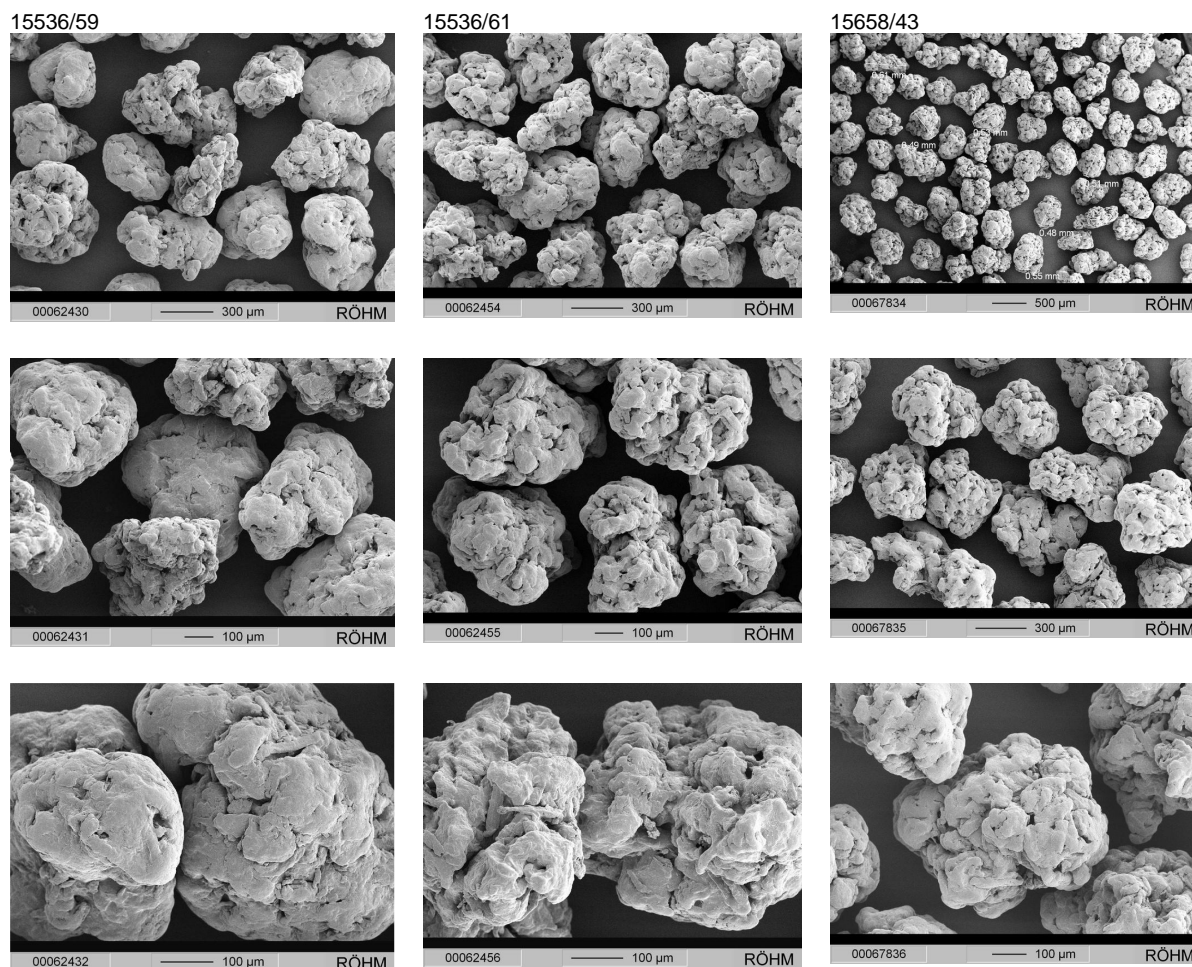


Figure IV.10 Morphology and topographical quality of Na-alginate micropellets. Micropellets of batch 15536/59 are depicted on the left, micropellets of batch 15536/61 in the middle and micropellets of batch 15658/43 at the right. The particles of batch 15536/59 were prepared by applying a higher spraying rate and a higher binder amount than the others. Its body structure was improved in comparison to batch 15536/61 and 15658/43. For process parameters see Table III.6. The scale of the picture needs to be taken into consideration.

IV.3. *Production of Chitosan Micropellets in the GPCG1 Rotary Processor*

IV.3.1. *Screening of Process Parameters*

The same process parameters as described in Chapter III.1.3.1. (Table III.7.) were applied to the production of Chitosan micropellets. The batches 15176/68 and 15176/69 were prepared applying a content of 20% MCC and de-ionized water as liquid binder. Batches 15176/70 and 15176/71 were prepared using a content of 30% MCC and 6% acetic acid solution (batch 15176/70) or a solution of 1.46% chitosan in acetic acid 6% (batch 15176/71) as a liquid binder.

No build up of particles was seen in case of the batches 15176/68 and 15176/69. The friability, tapped density and particle size of the micropellet batches 15176/70 and 15176/71 were not sufficient. A comparison of these batches showed that the use of a solution of chitosan in acetic acid lead to an increase in particle size and a decrease of friability.

The micropellet properties following screening of the process parameters are presented in Table IV.12. The morphology and topographical quality of the micropellets is presented in Figure IV.11.

Table IV.12 Properties of chitosan micropellets.
Screening of process parameters. For process parameters see Chapter III.1.3.1.

Batch	X50 [µm]	Span	Oversized >2000 [%]	Correlation Factor ¹	Tapped Density (200-250µm) [g/ml]	Friability (200-250) [%]	Yield Over all Particles [g] ²
15176/68	63.6	1.367	0	1	n.d. ³	n.d. ³	666.1
15176/69	67.2	1.257	0.01	1	n.d. ³	n.d. ³	746.0
15176/70	211.7	1.055	0.08	0.973	0.25	53.73	781.8
15176/71	288.5	1.198	0	0.999	0.23	41.17	805.0

¹ Correlation between the RRSB line and particle diameter at 63.2% cumulative size distribution. In case the correlation is 1, it follows RRSB distribution perfectly.

² The batch size was 750g. For chitosan only the yield of the mass is presented because the amount of remaining acid in the product is unknown.

³ n.d. = not determined.

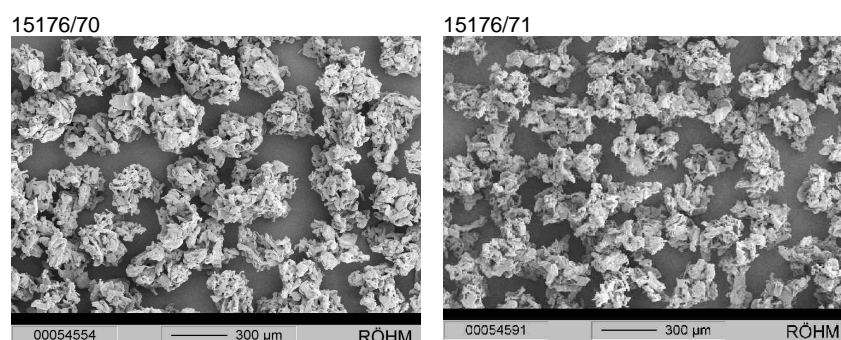


Figure IV.11 Morphology and topographical quality as a result of screening of the process parameters of chitosan micropellets. Micropellets of batch 15176/70 (prepared with acetic acid as liquid binder) are depicted on the left, the micropellets of batch 15176/71 (prepared with a solution of chitosan in acetic acid) are shown on the right. The core structure of the micropellets prepared with the chitosan solution appears less solid and more fragmented than the micropellets prepared with acetic acid. For process parameters see Table III.7.

The core structure of the micropellets prepared with the chitosan solution appears more fragmented than the micropellets prepared with acetic acid. Therefore, for further development of micropellets, different concentrated acetic acid solutions were used as the liquid binder.

IV.3.2. Development of Process Parameters for Chitosan Micropellets

During the development phase a successful method was established to produce chitosan micropellets with acceptable friability, tapped density, particle size and yield to be used in subsequent coating processes. In Table IV.13, properties of all micropellets prepared during the process development are presented. Particle size, tapped density and friability are influenced by the same process parameters as described for the Na-CMC micropellets. The process parameters of batch 15658/32 lead to the most promising micropellets of defined particle size range. The micropellets had a very low friability of 6% as compared to Cellets[®] (41.5%) and a high tapped density (0.72 g/ml). As it can be seen from the correlation value the particle size distribution did not always follow RRSB distribution. Batches with a high x50 value showed two independent particle size distributions which are characteristic for a non homogenous particle growth.

Table IV.13 Development of process parameters for chitosan micropellets. Properties of micropellets.
For process parameters see Chapter III.1.3.2.

Batch	X50 [μm]	Span	Oversized Particles >2000 μm [%]	Correlation Factor ¹	Tapped Density 400-500 μm [250-350 μm] [g/ml]	Friability 400-500 μm [250-350 μm] [%]	Water Content ² [%]	Yield [g] ³	Incidents
15536/82	266.4	0.885	1.19	0.999	[0.67]	[7.84]	53.68	465	-
15536/83	358.9	0.935	0.69	0.997	0.60 [0.68]	7.59 [5.14]	51.08	560	-
15536/84	599.6	2.468	8.16	0.968	0.56	7.48	52.47	557	-
15536/85	375.2	0.988	0.25	0.999	0.59	11.31	49.71	536	-
15536/86	541.6	1.643	3.87	0.970	0.50	7.75	45.03	558	-
15536/87	457.7	1.164	2.99	0.950	0.51	10.24	48.46	581	-
15536/88	498.9	3.584	8.49	0.934	0.51	8.47	48.11	564	-
15658/28	296.0	0.969	0.81	0.996	0.63	14.39	59.13	420	-
15658/29	294.5	0.969	0.99	0.985	0.62	11.76	59.01	420	-
15658/30	396.3	0.969	0.19	0.998	0.62	10.66	54.22	560	-
15658/31	358.1	0.890	0.25	0.995	0.66	10.93	52.12	603	-
15658/32	464.1	0.668	0.19	0.998	0.91	6.05	51.86	530	-
15658/33	460.5	0.586	0.43	0.999	0.87	9.63	57.91	535	-
15658/34	n.d. ⁵	n.d. ⁵	n.d. ⁵	n.d. ⁵	n.d. ⁵	n.d. ⁵	52.15	n.d. ⁵	Collapsed ⁴
15658/35	479.0	0.802	0.50	0.999	0.85	7.20	51.87	565	-
15658/36	n.d. ⁵	n.d. ⁵	n.d. ⁵	n.d. ⁵	n.d. ⁵	n.d. ⁵	n.d. ⁵	n.d. ⁵	Collapsed ⁴
15658/44	449.8	0.489	0.25	0.998	0.87	13.49	59.85	525	-
15658/45	453.2	0.513	0.31	0.999	0.87	8.87	58.86	532	-
Celllets [®]	n.d. ⁵	n.d. ⁵	n.d. ⁵	n.d. ⁵	0.92	41.50	n.d. ⁵	n.d. ⁵	-

¹ Correlation between the RSBB line and particle diameter at 63.2% cumulative size distribution. In case the correlation is 1, it follows RRSB distribution perfectly.

² Water content at the end of the spraying period.

³ The starting batch size was 750g. For chitosan only the yield of the mass is presented because the amount of remaining sprayed acetic acid in the product is unknown.

⁴ The fluidized bed collapsed. The manufacturing of the batch was aborted.

⁵ n.d. = not determined.

IV.3.2.1. Process Parameters Affecting Properties of Chitosan Micropellets

The **average spraying rate** was shown to have a visible impact on micropellet particle size. An increase of the spraying rate from 41.1g/min (batch 15536/82) to 93.6 g/min (batch 15658/28) resulted in a growth of the particles by approximately 30 μ m (266.4 μ m to 296.0 μ m).

In the trials examining the effect of **rotor speed** two different spraying rates were applied: a high spraying rate (65.1 g/min) and a very high rate (93.6 g/min). A higher rotor speed combined with a high spraying rate lead to smaller particles with a high friability. Upon application of a very high spraying rate the particle size decreased and the friability remained unchanged at higher rotor speed. Thus an interaction between rotor speed and spraying rate is obvious. With both spraying rates the span of the particle size distribution was smaller and the fraction of the oversized particles was reduced at higher rotor speed. The rotor speed had no effect on micropellet density. The data are shown in Table IV.14.

Table IV.14 Influence of the rotor speed and average spraying rate on properties of chitosan micropellets.

Batch	Rotor Speed [rpm]	Average Spraying Rate [g/min]	X50 [μ m]	Span	Oversized Particles >2000 μ m [%]	Tapped Density 400-500 μ m [g/ml]	Friability 400-500 μ m [%]
15536/83	1800	93.6	358.9	0.935	0.69	0.60	7.59
15536/84	500	93.6	599.6	2.468	8.16	0.56	7.48
15536/86	500	65.1	541.6	1.643	3.87	0.50	7.75
15536/87	1000	65.1	457.7	1.164	2.99	0.51	10.24

The influence of the **type of rotor disc** from a plane rotor disc to one with a grooved surface is similar to increasing the rotor speed. The grooved rotor disc lead to smaller particles with higher friability. The span of the particle size distribution was smaller and the fraction of oversized particles was reduced. The rotor type had no effect on micropellet density. The results are depicted in Table IV.15.

Table IV.15 Influence of the type of rotor disc on properties of chitosan micropellets.

Batch	Rotor Type	X50 [μ m]	Span	Oversized Particles >2000 μ m [%]	Tapped Density 400-500 μ m [g/ml]	Friability 400-500 μ m [%]
15536/87	grooved	457.7	1.164	2.99	0.51	10.24
15536/88	plane	498.9	3.584	8.49	0.51	8.47

During these experiments it was shown that the liquid binder amount also presents an influencing variable on the micropellet characteristics (see Table IV.16.). An increase in the **amount of liquid binder** resulted in increases in particle size, and tapped density, combined with a decrease of micropellet friability.

Table IV.16 Influence of the amount of liquid binder on properties of chitosan micropellets.

Batch	Binder Amount	X50 [μ m]	Span	Oversized Particles >2000 μ m [%]	Tapped Density 400-500 μ m [g/ml]	Friability 400-500 μ m [%]
15658/31	800	358.1	0.890	0.25	0.66	10.93
15658/32	1000	464.1	0.668	0.19	0.91	6.05

Not only the amount of liquid binder but also the **acetic acid concentration** within the liquid binder preparation was influencing the final product, however the effect was rather unpredictable. Using a 10% acetic acid in comparison to a 6% solution (Table IV.17) the particle size increased. In contrast, the particle size decreased using a 15% acetic acid solution in comparison to a 10% solution. The friability was to a large extent unaffected by an increase in the acetic acid

concentration. The tapped density appeared to increase by increasing the acetic acid concentration. These results were obtained using a volume of 800ml of liquid binder. At an addition of 1000ml liquid binder, the particle size remained nearly constant, the friability decreased and the tapped density increased by increasing the acetic acid concentration. However, this effect was reversible since the friability was increased in some exploratory experiments using an acetic acid solution at a concentration of 25% (volume of liquid binder 800ml). The most appropriate acetic acid concentration needs to be optimized in conjunction with the liquid binder amount.

Table IV.17 Influence of the acetic acid concentration of the liquid binder on properties of chitosan micropellet.

Batch	Acetic Acid Conc. [%]	Binder Amount [ml]	X50 [μm]	Span	Oversized Particles >2000 μm [%]	Tapped Density 400-500 μm [g/ml]	Friability 400-500 μm [%]
15658/29	6	800	294.5	0.969	0.99	0.62	11.77
15656/30	10	800	396	0.969	0.19	0.62	10.67
15658/31	15	800	358.1	0.890	0.25	0.66	10.93
15658/32	15	1000	460.5	0.668	0.19	0.87	9.63
15658/33	10	1000	464.1	0.586	0.43	0.91	6.05

IV.3.2.2. Morphology and Topographical Quality of Chitosan Micropellets

Regarding the batches produced the optimal results were received with the micropellets of batch 15658/32 which was optimized concerning yield, friability, tapped density and core structure. The particles were characterized by a nearly spherical shape, homogenous size and smooth surface with reduced amount of pores. In comparison to this batch, the micropellets of batch 15536/82 and /83 showed a more conventional granule structure which was still homogenous (Figure IV.12). The first batch of these two was prepared with a lower spraying rate, binder amount and acetic acid concentration and the second batch (15536/83) was prepared with the same spraying rate and acetic acid concentration, however with a lower binder amount compared to batch 15658/32.

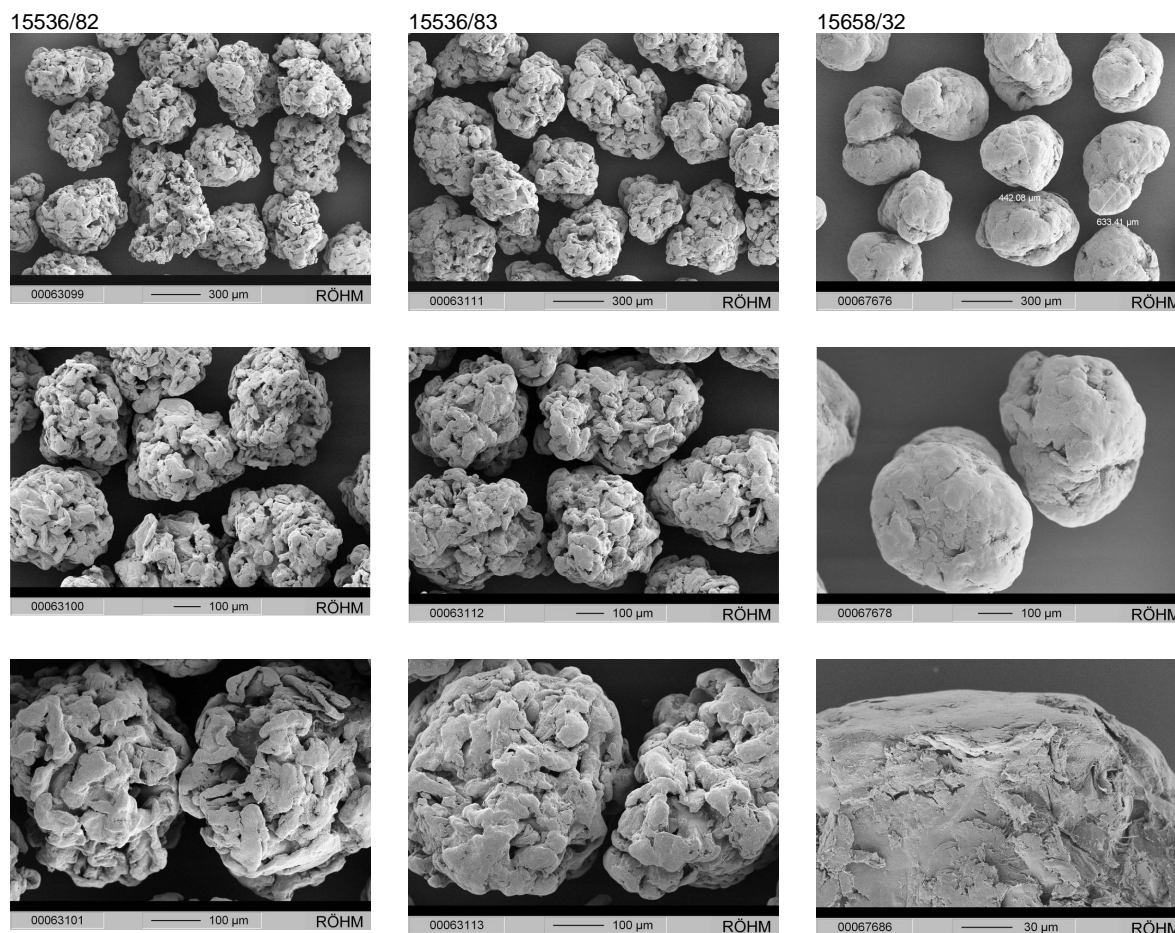


Figure IV.12 Morphology and topographical quality of the chitosan micropellets. The scale of the picture needs to be taken into consideration. Batch 15658/32 to the right is the most promising product characterized by nearly spherical shape, homogenous size and smooth surface with reduced amount of pores, produced with optimized processing conditions (see above). For process parameters see Table III.8.

IV.3.2.3. Acetic Acid Content of Chitosan Micropellets

The acetic acid content of the most promising batch of chitosan micropellets, which was used for subsequent coating processes, was determined by NMR spectroscopy as described in Chapter III.2.9. Batch 15658/32 contained 160% free acetic acid or acetate calculated on the molar basis of the monomer of chitosan. This amounts to approximately 22% (w/w) free acid or acetate in the micropellet formulation.

IV.4. Carbopol® Micropellet Production in the GPCG1 Rotary Processor

Despite several experimental efforts, the development of carbopol micropellets was not successful (see Table IV.18). One of the problems was the adhesion of the pellet material to the wall of the pelletizer. It was possible to reduce that “sticking” phenomenon of by increasing the inlet air humidity. On the other hand, it was not possible to develop micropellets of the defined particle size mainly because of the drastic influence of the amount of liquid binder: Either nearly not non-granulated powder resulted in the experiments or completely oversized particles were received applying only small additional volumes. This fact would lead to difficulties in accurately handling a manufacturing process. In Figure IV.13, samples of batches 15658/10 and 15658/11 are displayed. In batch 15658/11 172g of liquid

binder and in the batch 15658/10 193g of liquid binder were added. In case of batch 15658/11, the result was a powder and in case of batch 15658/10, dramatically oversized particles were produced. In addition, the process development was hampered due to Carbopol® blocking the window to the process chamber. A further drawback of the formulation was the high content of non mucoadhesive polymer and the high content of Aerosil® to reduce the sticking.

Table IV.18 Properties of Carbopol® micropellets.
For process parameters see Chapter III.1.4.

Batch	Description of the Product	Figure	X50 [µm]
15658/01	one big lump	-	n.d. ⁴
15658/02	one big lump	-	n.d. ⁴
15658/03	Balls ¹	IV.13	n.d. ⁴
15658/04	Balls ¹		n.d. ⁴
15658/05	aborted		n.d. ⁴
15658/06	Balls ¹	IV.13	n.d. ⁴
15658/07	Powder ²	-	n.d. ⁴
15658/08	Powder with granules	-	n.d. ⁴
15658/09	one big lump	-	n.d. ⁴
15658/10	Balls ¹	IV.13	n.d. ⁴
15658/11	Powder with granules	IV.13	91 ³
15658/12	Powder	-	n.d. ⁴
15658/13	Balls ¹	-	n.d. ⁴
15658/14	Balls ¹	-	n.d. ⁴
15658/15	Balls ¹	-	n.d. ⁴

¹ Particles larger than 2500µm.

² Particles finer than 100µm.

³ Measured with the laser diffraction method.

⁴ n.d. = not determined.

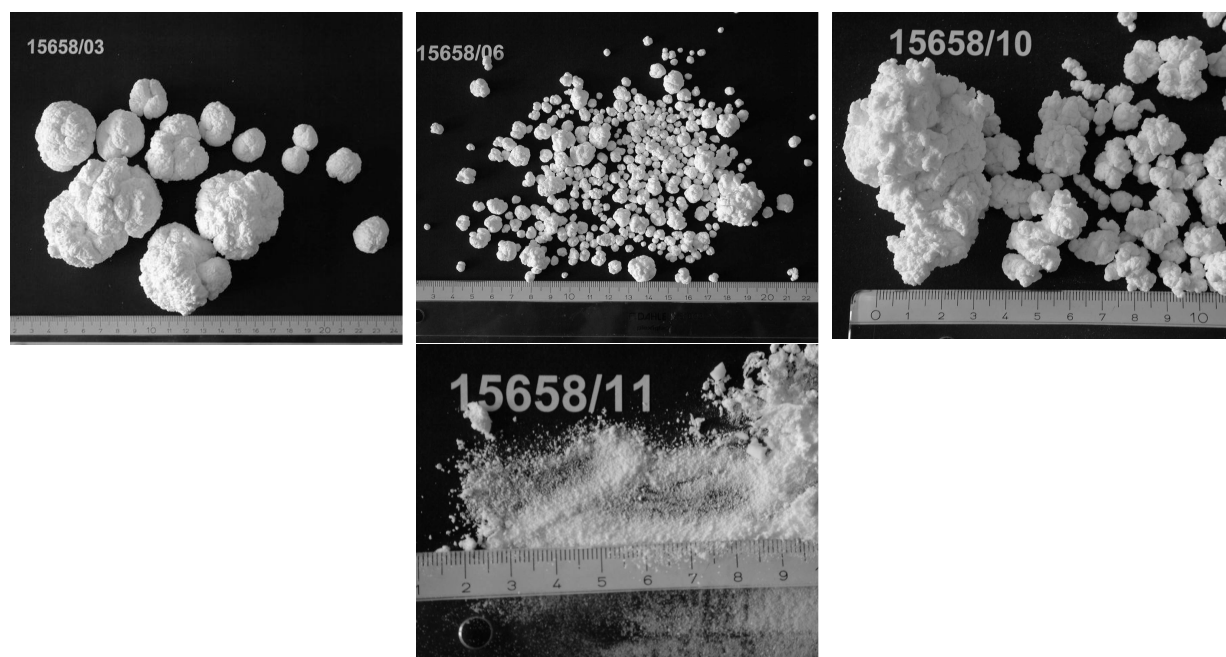


Figure IV.13 Size comparison of the attempts to form micropellets with Carbopol®. The batch numbers are given in each photograph, the scale on every photograph is 1cm. A production of Carbopol® micropellets was not possible. Minor variation of the liquid binder volume lead to drastic changes of the particle size (batch 15658/10 versus 15658/11). The complete process parameters are given in Table III.9.

IV.5. Noveon® AA1 Micropellet Production in the GPCG1 Rotary Processor

Noveon® AA1 micropellets were also manufactured in the GPCG1 rotary processor. Similar to the Carbopol® micropellets the development of Noveon AA1 micropellets was difficult and not successful due to the close overlap of the chemical structure of both polymers (Table IV.19). The problem of sticking of the material to the wall was solved by increasing the inlet air humidity, however, it was not possible to develop micropellets of the defined particle size in a sufficient yield.

Table IV.19 Noveon® AA1 micropellet properties.
For process parameters see Chapter III.1.5.

Batch	Description of the Product	Figure	X50 [μm]
15658/17	Powder ² with granules	-	n.d. ⁴
15658/18	Powder ² with granules	-	n.d. ⁴
15658/19	Powder ²	IV. 14	n.d. ⁴
15658/20	Powder ²	-	n.d. ⁴
15658/21	Balls ¹	IV.14	n.d. ⁴
15658/22	Balls ¹	-	n.d. ⁴
15658/23	Powder with fine granules	-	n.d. ⁴
15658/24	Powder with granules	IV.14	n.d. ⁴
15658/25	Granules	IV.14	299 ¹
15658/26	Granules	IV.14	121 ¹
15658/27	Balls with fine	-	n.d. ⁴

¹ Particles larger than 2500 μm .

² Particles finer than 100 μm .

³ Measured by sieving.

⁴ n.d. = not determined.

The balance between the liquid binder amount added leading to either nearly non-granulated powder or to completely oversized particles was too narrow. Typical products are presented in Figure IV.14. For the batches 15658/24, 15658/25 and 15658/26 210g, 180g and 173g of liquid binder, respectively, were used. 210g of liquid binder lead to oversized particles, 180g to granules and 173g to very fine granules. The difference of the amount of liquid binder is therefore too small to allow successful production of batches with acceptable reproducibility. In addition, the visualization of the process was hampered due to the blockage of the window to the process chamber by Noveon® AA1. This could possibly be circumvented by a two step granulation process in which initially small pre-granules are produced and thereafter the final granules. A further drawback of the formulation was the high content of non mucoadhesive polymer and the high content of Aerosil® to reduce the sticking between particles.

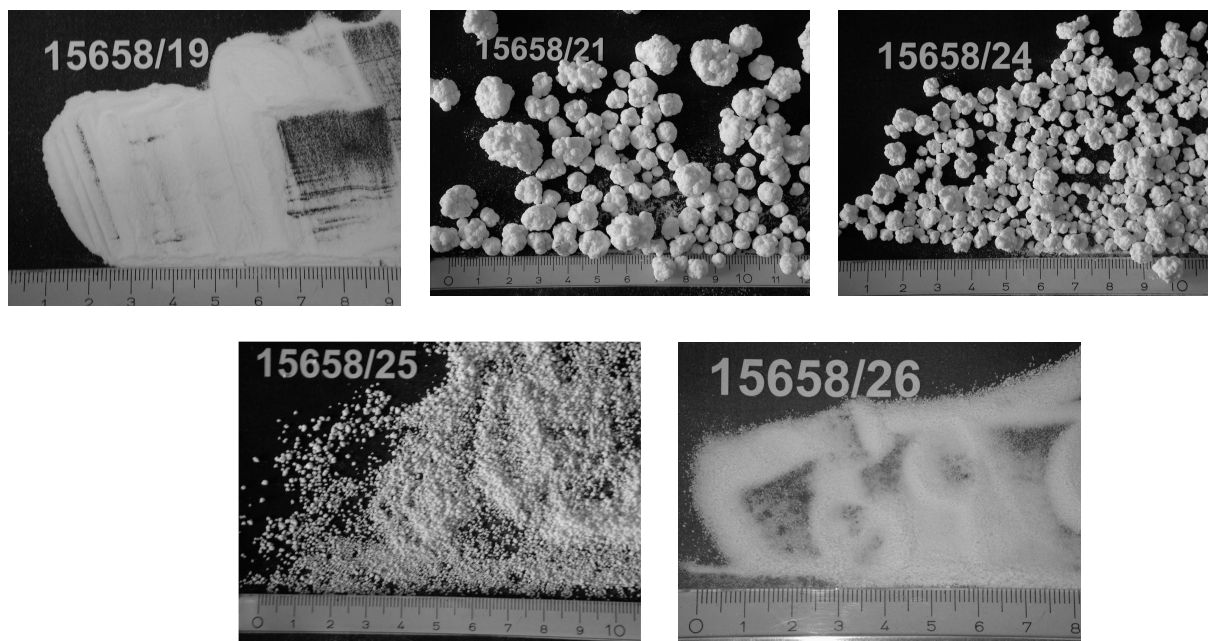


Figure IV.14 Size comparison of the attempts to form micropellets with Noveon® AA1. The batch numbers are given in each photograph, the scale on every photograph is 1cm. A production of Noveon® AA1 micropellets was not possible. Minor variation of the liquid binder volume lead to strong changes of the particle size (batch 15658/24, /25, and /26). The complete process parameters are given in Table III.11.

Yield and tapped density of the particles between 250 and 600µm of batch 15658/25 were insufficient. The friability of the particles (49.8%) was worse than the standard Cellets® (41.5%). However, it was still sufficient for a subsequent coating process. The span of the particles was 2.89 and the tapped density amounted to 0.47g/ml (Cellets® 0.916g/ml). The yield, defined as the percentage of particles between 250µm – 600µm was only 33.1% and thus insufficient.

IV.6. Comparison between Rotating Cylinder and the Bolatec Friabimat for Friability Measurements

The micropellets are subjected to greater mechanical stress in the rotating cylinder when compared to the Bolatec Friabimat. Therefore, the friability data presented in Table IV.20 are higher for the rotating cylinder. At higher friability values, as described for Cellets®, the difference was neglectable.

Table IV.20 Comparison of friabilities between the rotating cylinder and the Bolatec Friabimat.

Batch	Rotating Cylinder [%] ²	Bolatec Friabimat [%] ²	Ratio RC/BF ¹
15658/32	6.0	3.8	0.63
15658/40	5.1	2.2	0.43
15658/41	4.7	1.9	0.41
15658/43	13.1	5.1	0.39
Cellets®	41.5	39.1	0.94

¹ Friability, measured using the Bolatec Friabimat (BF) divided by the friability measured using the rotating cylinder (RC).

² The standard deviation of both methods varied between 2.5-8% of the values.

IV.7. Rotor Torque Measurement for Monitoring the Pelletization Process as In Process Control

The torque measurements of the rotor were performed using selected batches of the **Na-CMC** micropellets production. The data is presented in Figure IV.15. Batch 15536/50 was prepared at an average spraying rate of 45g/min, a liquid binder amount of 635g and a water content of 55% at the end of the spraying period. Batch 15536/51 was prepared identical to batch 15536/50, whereas only the water content at the end of spraying period was 54.8%. The curve of batch 15536/51 displayed this lack of water by a delayed increase in combination with a decrease of the maximum by maintaining the same slope. The batches 15536/52 and 15536/53 were prepared at a spraying rate of 40.2g/min. Batch 15536/52 was prepared at 750g liquid binder and had a water content of 55.5% at the end of the spraying period. Batch 15536/53 was prepared using 700g of liquid binder and had a water content of 54.1% at the end of the spraying period. The curve of batch 15536/52 exactly matched the one of 15536/53, except for the maximum which was higher for batch 15536/54 because of the extended spraying time.

It can be concluded (Figure IV.15 and IV.16) that the rotor measurement was an appropriate method for the determination of the product water content. Furthermore the method was also sensitive to the rate of binder addition. Batches with the same liquid addition rate showed the same slope of torque increase. Even the reduction of the spraying rate during the process was visible with a decrease of the slope at the 15 minutes time point.

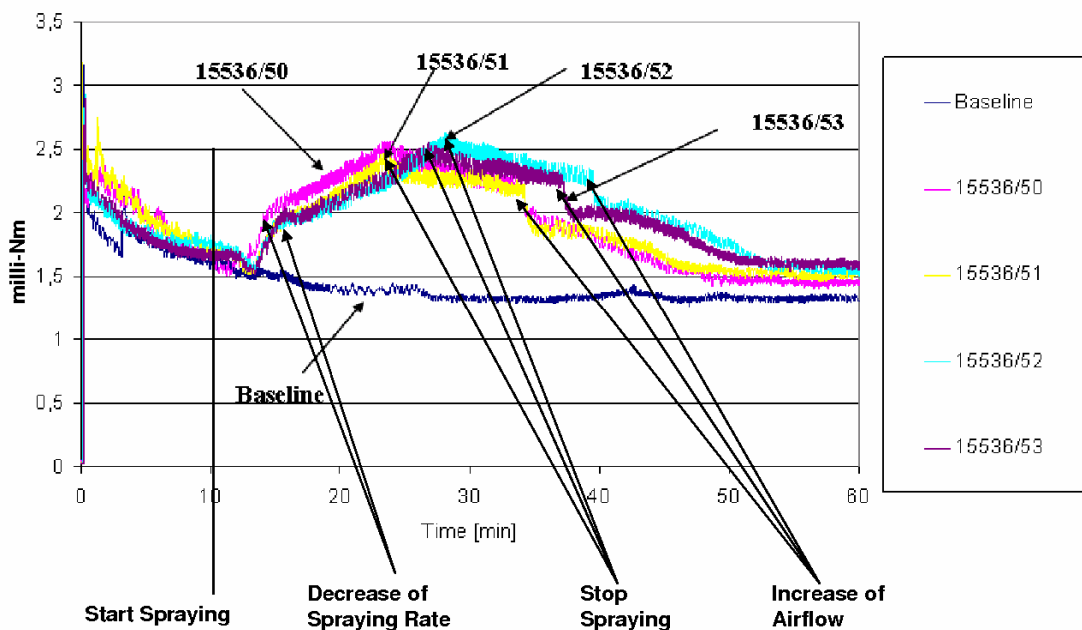


Figure IV.15 Rotor torque measurement during the production of Na-CMC micropellets. The batch 15536/50 was prepared with an average spraying rate of 45g/min, a liquid binder amount of 635g and a water of 55% content at the end of the spraying period. The batch 15536/51 was prepared identical to batch 15536/50 only the water content at the end of spraying period was 54.8%. The batches 15536/52 and 15536/53 were prepared with a spraying rate of 40.2g/min. 15536/52 was prepared with 750g liquid binder and had a water content of 55.5% at the end of the spraying period and 15536/53 was prepared with 700g liquid binder and had a water content at the end of the spraying period of 54.1%.

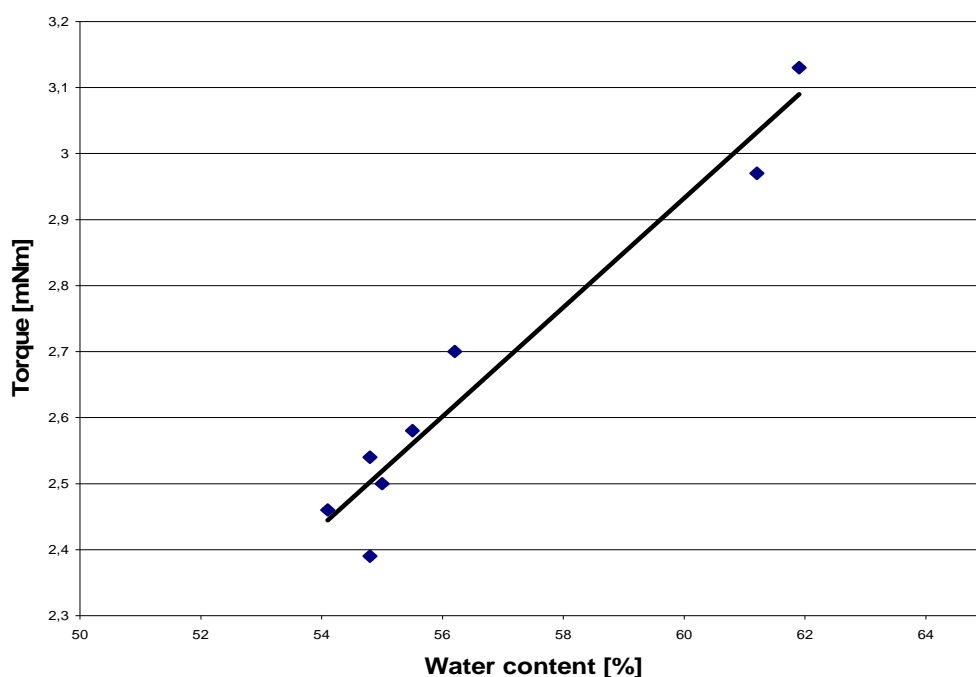


Figure IV.16 Relationship between water content at the end of the spraying period and maximum torque during Na-CMC micropellet production ($R^2=0.9432$).

The torque measurements for the rotor were also performed with selected batches of **chitosan** micropellets. These were prepared using identical process parameters except for the amount of binder. Batches 15658/31, 15658/32 and 15658/45 were prepared with 800ml, 1000ml and 1100ml of liquid binder, respectively. The torque measurements of the rotor for chitosan micropellets exhibit similarly promising results as for Na-CMC micropellets (Figure IV.17). Changes in the process directly result in changes of the torque curve. For example, a higher liquid binder amount led to higher rotor torque values.

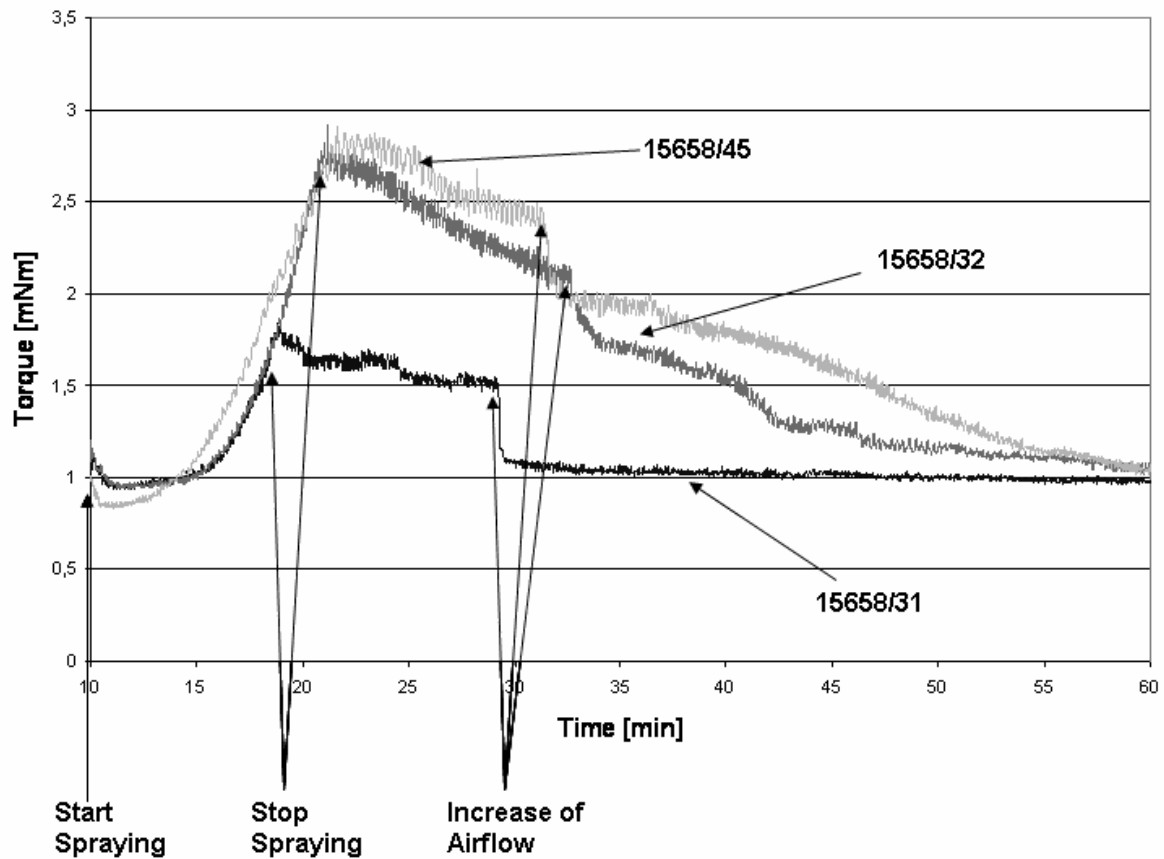


Figure IV.17 Torque measurement of the rotor for chitosan micropellets. The chitosan micropellets were prepared with identical process parameters except for amount of binder. 15658/31, 15658/32 and 15658/45 were prepared with 800ml, 1000ml and 1100ml of liquid binder, respectively.

IV.8. Measurements of Air Humidity

IV.8.1. Differences between Inlet and Outlet Air Humidity in Relationship to Product Temperature

Since it is known that air humidity is a crucial parameter in fluidized bed processing, the inlet and outlet air humidity was measured to gain a better process understanding and controlling. The water content differences between the in- and outlet air of batches 15658/37, 15658/39, 15658/40 and 15658/41 are presented in Figure IV.18. Batch 15658/37 was produced applying an inlet air humidity of 8g/m^3 , a starting product temperature of 34°C and a rotor speed during the drying period of 1800rpm. Batch 15658/39 was produced using an inlet air humidity of 7.2g/m^3 , a starting product temperature of 33°C and a rotor speed during the drying period of 500rpm, respectively. The batches 15658/40 and 15658/41 were produced with starting product temperatures of 32°C and a rotor speed during the drying period of 1800rpm. In these cases, the inlet air humidity was 7.8g/m^3 and 8.1g/m^3 , respectively.

The higher starting product temperature of batches 15658/37 and 15658/39 lead to a higher water content difference during the spraying period compared to the batches with lower starting product temperature as is depicted in Figure IV.18.

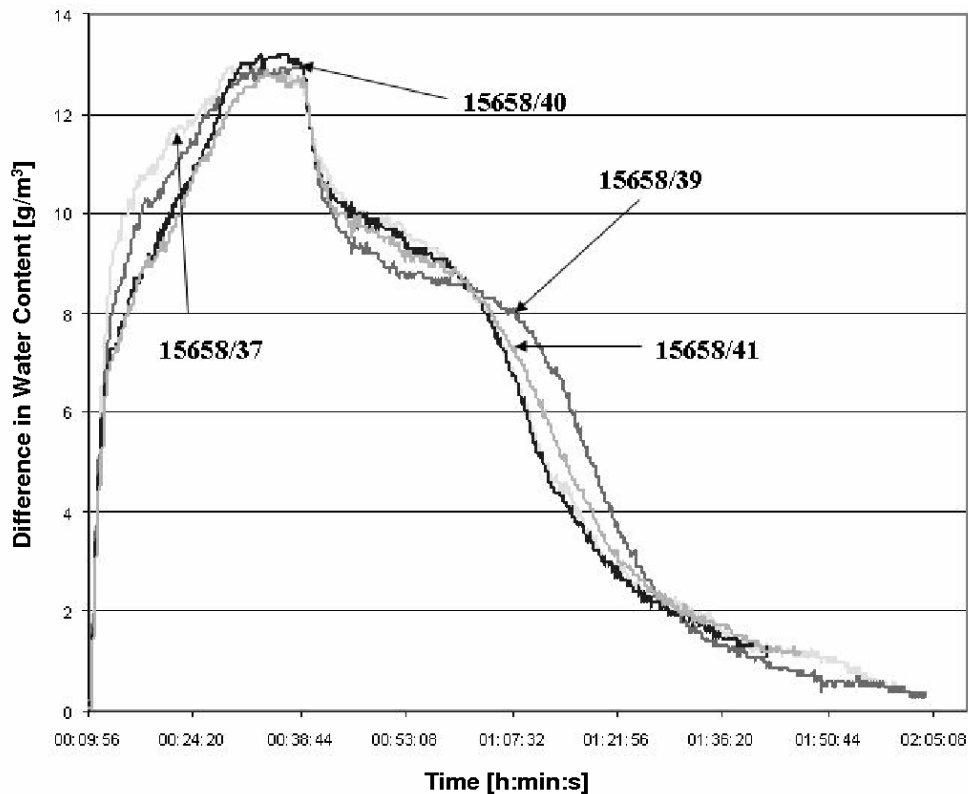


Figure IV.18 Differences between air humidities in inlet and outlet. Batch 15658/37 was produced applying an inlet air humidity of 8g/m^3 , a starting product temperature of 34°C and a rotor speed during the drying period of 1800rpm. Batch 15658/39 was produced at an inlet air humidity of 7.2g/m^3 , a starting product temperature of 33°C and a rotor speed during the drying period of 500rpm. Batches 15658/40 and 15658/41 were produced at a starting product temperature of 32°C and a rotor speed during the drying period of 1800rpm. The inlet air humidity was 7.8g/m^3 and 8.1g/m^3 , respectively.

IV.8.2. Dependence of Outlet Air Humidity on Rotor Speed

In addition to the product temperature, the drying capacity of the system is also indirectly controlled by the rotor speed. In Figure IV.19 the dependence of absolute outlet air humidity on rotor speed is presented. The time point of the rotor speed reduction is marked with the arrow. Beyond this time point, the humidity of the outlet air in the non-continuous process drops clearly below the humidity of the outlet air when the equipment is operated in the continuous batch mode at 1800rpm. An increase of the outlet humidity is related to a higher drying capacity of the system and leads to a lower water content of the product at the same time point. The difference is caused by the lack of waste heat from the rotor engine.

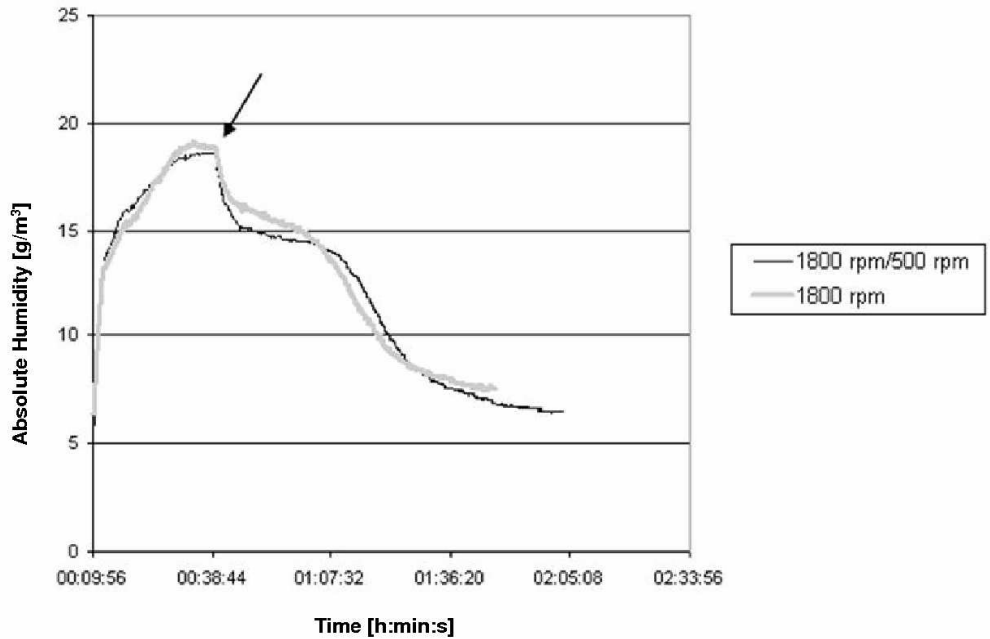


Figure IV.19 Dependence of outlet air humidity on rotor speed of the GPCG1. For obtaining the grey dotted curve, the rotor speed was adjusted to 1800rpm. The black curve was obtained by adjusting to 1800rpm initially, thereafter it was set to 500rpm (arrow). Both curves drop that, because the airflow was also increased at this time point which lead to a lower absolute outlet air humidity.

IV.8.3. Water Content of Outlet Air

The maximum relative humidity measured in the outlet air was close to 100% at a temperature of 23°C. The high relative humidity of the outlet air can lead to a condensation of water at cold spots, especially at high differences between in and outlet air temperature in the drying phase. Water may condensate at the cold metal of the wall and material may consequently stick to the wall. The relative humidity during one entire production process is depicted in Figure IV.20.

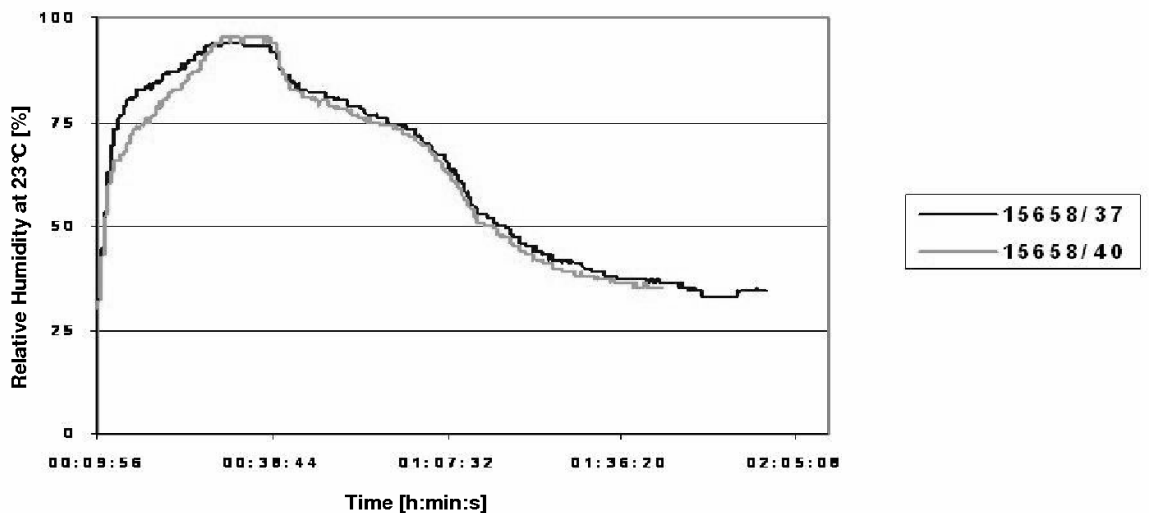


Figure IV.20 Relative humidity of the outlet air at 23°C during an entire production process.

IV.8.4. Total Water Added at Different Inlet Air Humidities

The influence of the inlet air humidity on the amount of total added water can be seen in Figure IV.21. Batch 15658/28 was produced at an inlet air humidity of 8.3g/m^3 . For batch 15658/29 it was 10.6g/m^3 . The total water added was nearly concurrent for batches 15658/28 and 15658/29 during the spraying and the spheronization period, but different during the drying period. Based on this information it can be concluded, that the greatest impact of the inlet air humidity occurs during the drying period.

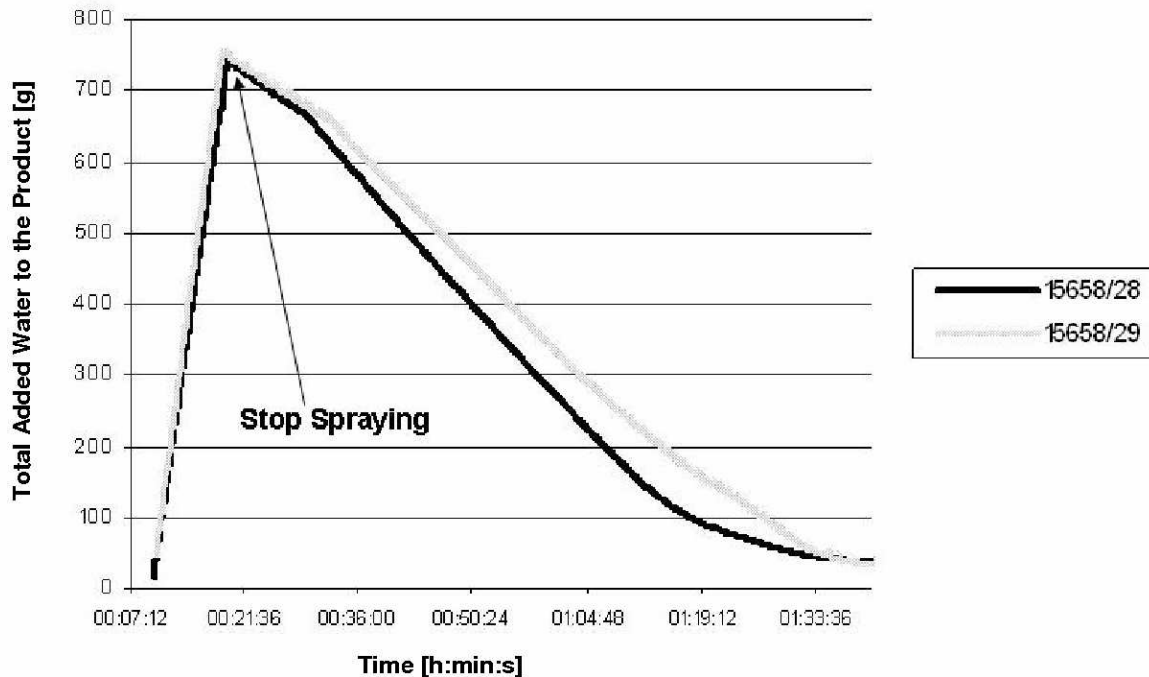


Figure IV.21 Impact of the inlet air humidity onto the product water content. The water content of the product was calculated by following equation: water content = added water by spraying minus lost water by drying. The lost water by drying was calculated by the difference of the in- and outlet water content. Batch 15658/28 was produced applying an inlet condition of 8.3g/m^3 and batch 15658/29 of 10.6g/m^3

IV.9. Drying Kinetics of the Na-CMC Micropellets

The drying kinetics of the Na-CMC micropellets is homogenous. The dependence of the product water content on the drying temperature is shown in Figure IV.22. At 50°C , the time to reach a 10% humidity level within the product was 10 hours more rapid than at 30°C .

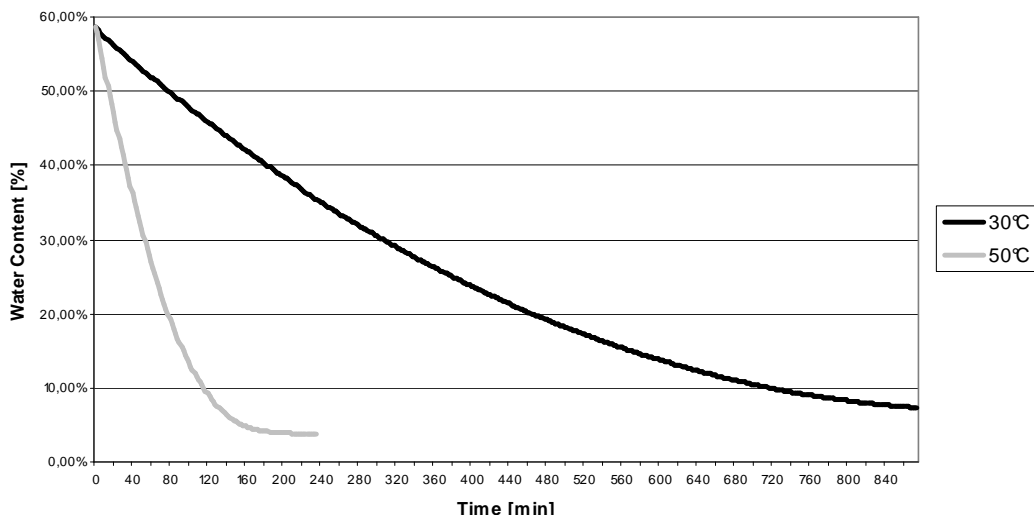


Figure IV.22 Drying kinetics of Na-CMC micropellets using a drying balance.

IV.10. True Density and Estimation of Surface Area of the Micropellets

True density and surface area of the micropellets were determined by a pycnometer and a modified Blaine method, respectively. The results are presented in Tables IV.21 and IV.22. Whereas the ranking in terms of tapped density was chitosan > Na-CMC > Na-alginate micropellets, the densities did not reflect the true densities of the micropellets which were ranked Na-CMC > Na-alginate > chitosan micropellets. The ranking of the tapped density is corresponding to the smoothness of the surface of the micropellets. Micropellets with a smoother surface are able to reach denser packing during tapping with lesser residual air holes, thus explaining the difference between the ranking of tapped density and the true density.

Table IV.21 True density of the mucoadhesive micropellets measured using the pycnometer method.

Batch	Mucoadhesive Polymer	True Density [g/cm ³]
15658/53	Na-CMC	1.425
15658/60	Na-alginate	1.417
15658/32	Chitosan	1.329

The surface area determination reflected mainly the differences in particle size, however the loose core structure of the Na-alginate micropellets is also expressed in its high surface area (see Table IV.22). As stated in the Materials and Method section, the modified Blaine method was calibrated with glass beads of 1mm diameter. The method is theoretically able to measure pores but it loses accuracy, by increasing the difference between the calibration standard and the measured sample.

Table IV.22 Surface area of the mucoadhesive micropellets measured by a modified Blaine method.

Batch	Mucoadhesive Polymer	Surface area [cm ² /g]
15658/53	Na-CMC	97.0
15658/60	Na-Alginate	192.0
15658/32	Chitosan	113.5

IV.11. Content Uniformity of the Batches

The content uniformity of Theophyllin between the different particle sizes of Na-alginate (15536/61) and chitosan micropellets (15658/32) was good, the values

are presented in Table IV.23. For the Na-CMC micropellets, however, a trend was obvious towards larger particles showing higher drug content. An explanation may be given by the fact that larger particles have reserved more liquid binder for their superior growth. Since the drug has been dissolved in the liquid binder, this may explain the higher drug content of the larger particles.

Table IV.23 Content uniformity of Theophyllin of coated and uncoated mucoadhesive micropellets. The batches 15658/37, 15658/53 and 15658/58 consist of Na-CMC, the batches 15536/61, 15658/60 and 15658/59 of Na-alginate.

Batch	Coated/Uncoated	Particle Size [μm]	Theoretical Content [%]	Content [%]
15536/61	Uncoated	200-250	1.132	1.097
	Uncoated	500-600	1.132	1.118
	Uncoated	600-800	1.132	1.084
	Uncoated	800-2000	1.132	1.093
	Uncoated	>2000	1.132	1.107
15658/32	Uncoated	250-600	0.927	0.792
	Uncoated	250-355	0.927	0.816
	Uncoated	400-500	0.927	0.827
15658/37	Uncoated	250-355	0.892	0.777
	Uncoated	400-500	0.892	0.814
	Uncoated	500-600	0.892	0.829
	Uncoated	600-800	0.892	0.834
15658/53	Uncoated	250-600	0.892	0.857
15658/56	Coated	Complete batch	0.525	0.483
15658/57	Coated	Complete batch	0.472	0.419
15658/58	Coated	Complete batch	0.525	0.448
15658/59	Coated	Complete batch	0.482	0.429
15658/60	Uncoated	250-600	1.132	1.127

Analysis of content uniformity for coated versus uncoated batches revealed no surprises, since the content ratios were close to the theoretical value based on the contents of each batch. The results are presented in Table IV.24. These values indicate a successful coating process with high yields, no loss of active material or change of water content.

Table IV.24 Comparison between the theoretical ratio of the content between coated and uncoated microparticles and the determined ratio. The observed ratio was calculated by dividing the total content of the coated micropellets by the total content of the uncoated micropellets. The theoretical ratio was calculated by dividing the total content of the uncoated micropellets by the theoretical content of the coated micropellets after increasing the mass of the micropellets by coating.

Batches $\frac{\textit{coated}}{\textit{uncoated}}$	Observed Ratio $\frac{\textit{coated}}{\textit{uncoated}}$	Theoretical Ratio
$\frac{15658/56}{15658/53}$	1.77	1.82
$\frac{15658/57}{15658/60}$	2.69	2.64
$\frac{15658/58}{15658/53}$	1.91	1.78
$\frac{15658/59}{15658/32_{(250-600\mu\text{m})}}$	1.85	1.99

IV.12. **Dynamic Hydration Properties of Excipients used for the Manufacture of Mucoadhesive Micropellets**

The kinetics of water uptake determines the rate of swelling of mucoadhesive polymers used in the formulation of micropellets. Thus these investigations should aid in the selection of excipients with acceptable dynamic hydration properties and their ability to form round pellets with high density. As mucoadhesive polymers, Na-CMC, Na-alginate, Noveon AA1, Carbopol, chitosan and the pelletizing aid microcrystalline cellulose were tested. Polymers with a similar dynamic hydration profile behave similarly in their pellet forming properties in the GPCG1 rotary processor.

The hydration rates in de-ionized water are presented in Figure IV.23 below. In the case of chitosan, diluted acetic acid was used as hydration medium. The hydration rate in the case of microcrystalline cellulose, an excellent pellet forming excipient, is several fold greater than the one of poor pellet-forming mucoadhesive polymers. Chitosan behaves differently since it does not form granules with water, yet it showed a high hydration rate. In contrast, using acetic acid solution, the hydration rate of chitosan was very slow, nevertheless it formed pellets. The poor hydration properties seem to be due to the formation of a gel which acts as a diffusion barrier to the penetrating liquid. Therefore, a similar diffusion barrier on top of the starting particles during the granulation process may preclude pelletizing aid properties of the mucoadhesive polymers.

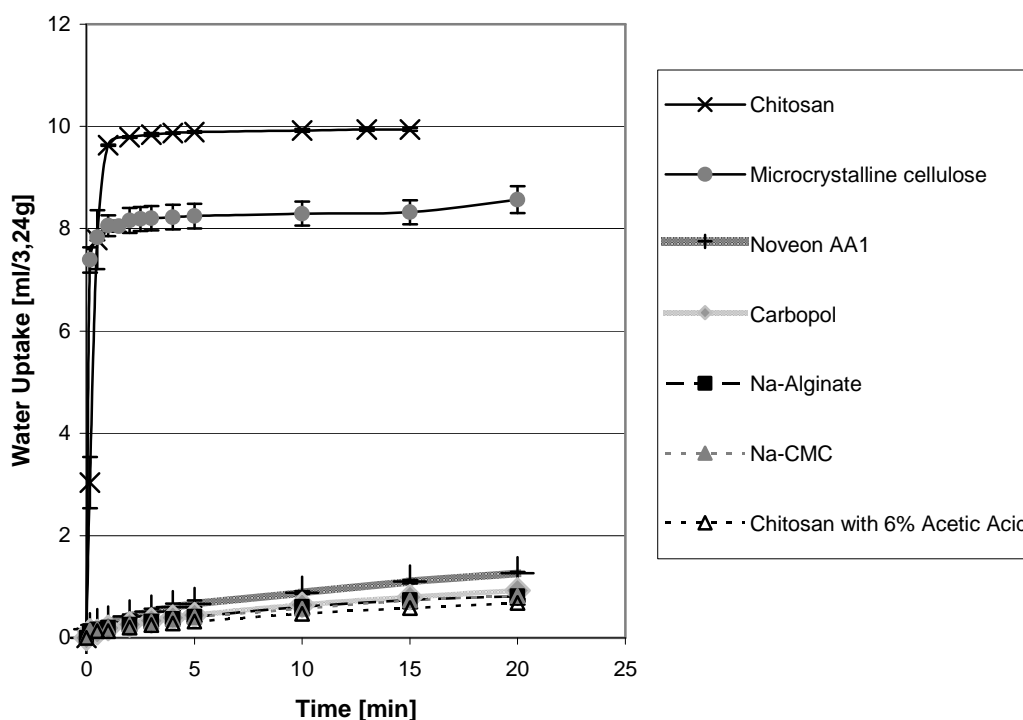


Figure IV.23 Dynamic hydration properties of mucoadhesive polymers (described as method H1). The hydration medium was de-ionized water except for chitosan, where diluted acetic acid served as hydration medium.

As shown in Figures IV.24 - IV.26 the pH value has an impact on the dynamic hydration of Carbopol, chitosan, Na-alginate and Noveon AA1, whereas no influence was observed for Na-CMC and microcrystalline cellulose. An increase of the pH value clearly increased the dynamic hydration of chitosan whereas for Na-

alginate only a slight increase was seen. The dynamic hydration of the polyacrylic acid polymers Carbopol and Noveon AA1 is highest at pH 5.5 and lowest at pH 6.0 compared to Figure IV.27. The low dynamic hydration at pH 6.0 was unexpected, since a minimum hydration capacity was predicted at pH 7.2. This may be due to the different viscosity or solubility of the polymers at different pH values. As discussed above, the slow and inefficient hydration seems to be due to the gel formation by the mucoadhesive polymers. Hence it can be concluded, that a lower dynamic hydration rate is the result of a faster gel forming process and the swelling of the polymer.

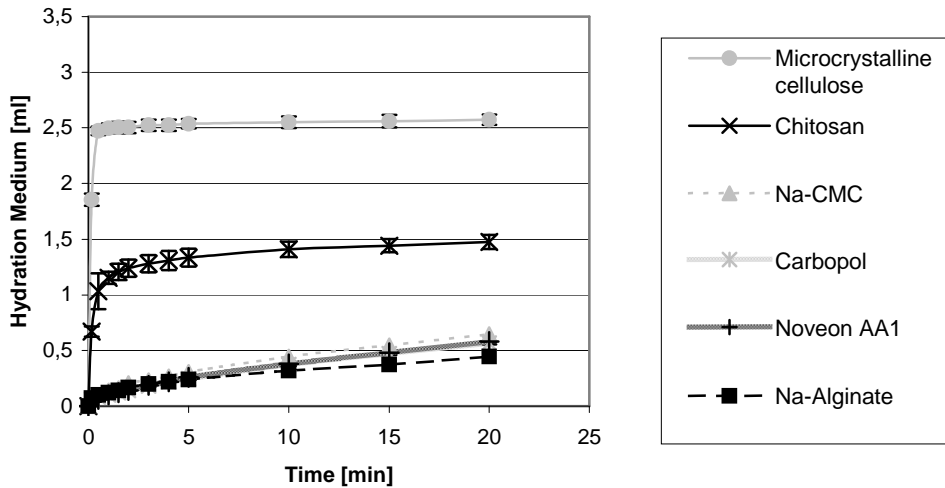


Figure IV.24 Dynamic hydration properties of mucoadhesive polymers (described as method H2). The hydration medium was acetate buffer pH 5.5.

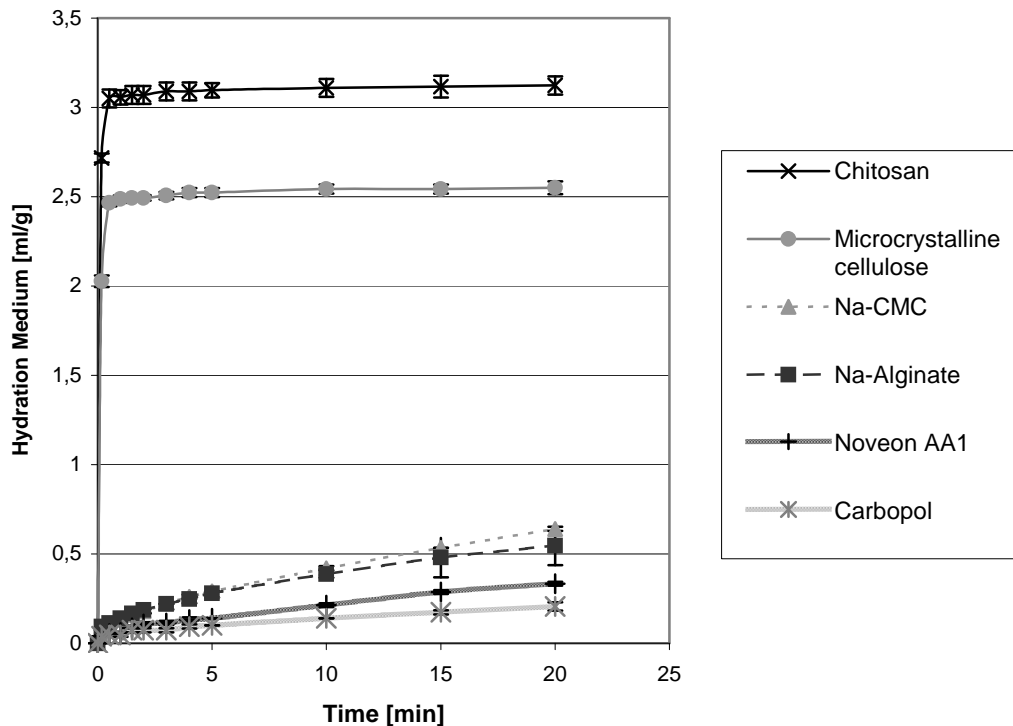


Figure IV.25 Dynamic hydration properties of mucoadhesive polymers (described as method H2). The hydration medium was phosphate buffer pH 6.0.

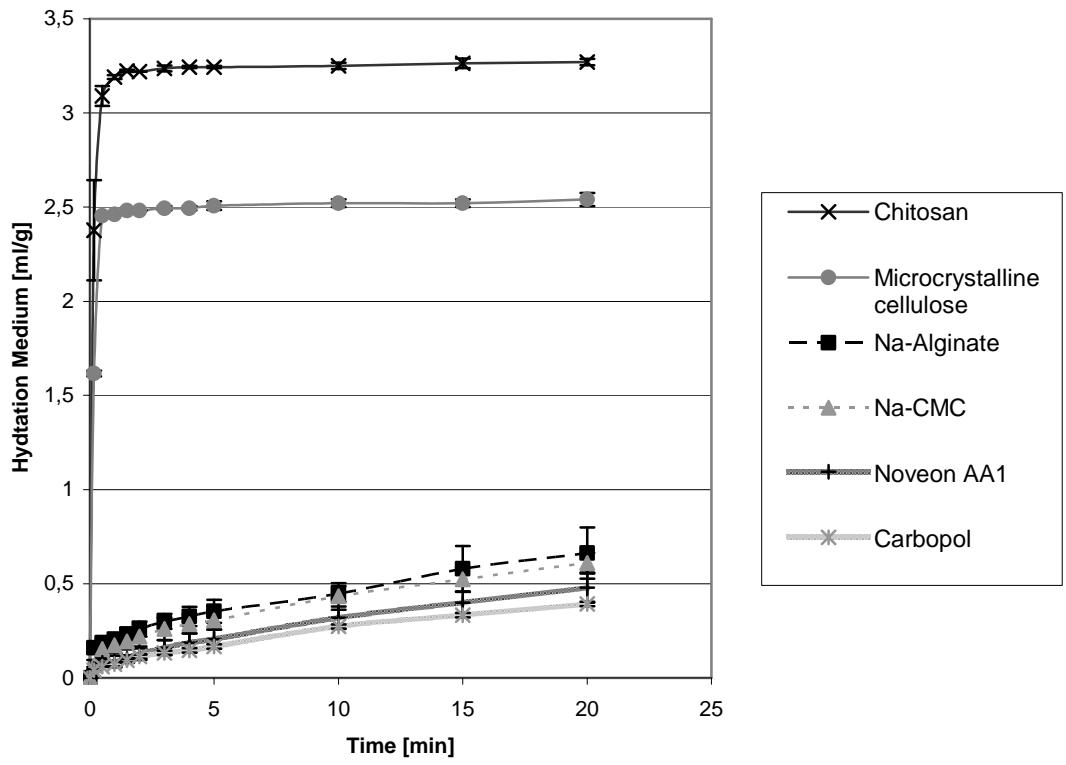


Figure IV.26 Dynamic hydration properties of mucoadhesive polymers (described as method H2). The hydration medium was phosphate buffer pH 7.2.

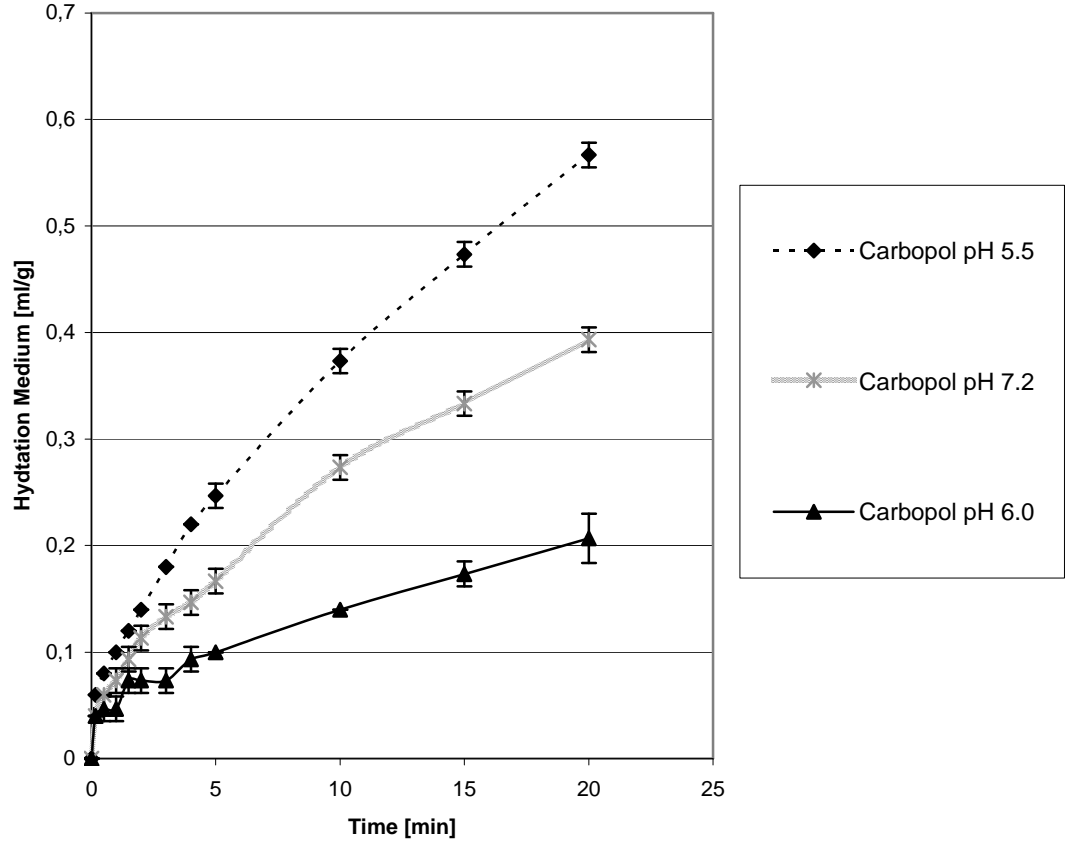


Figure IV.27 Dynamic hydration properties of Carbopol at different pH (described as method H2).

IV.13. Enteric Coating of Mucoadhesive Micropellets

IV.13.1. Coating of Na-CMC Micropellets with EUDRAGIT® L 30 D-55 using the Mini-Glatt

IV.13.1.1. Not Acceptable Manufacturing Results

The coating of the micropellets was generally not successful in the Mini-Glatt, although two successful batches 15658/46a (containing 20% coating layer) and 15658/46b (containing 30% coating layer) were produced. However, their production was not reproducible. The maximum spraying rate reached was also very slow, 1.96g/min and 1.1g/min respectively. The slow spraying rate caused very long process times of 150 minutes for batch 15658/46a and 210 minutes for batch 15658/48b. The batches 15658/47 to batch 15658/49 were aborted since the wurster insert was blocked.

The thickness of the coating layer of the micropellets with 20% coating measured between 9 and 22µm. At a 30% coating layer the thickness varied between 11 and 25µm. An enteric fluid residence would require a coating layer thickness of approximate 40µm. The structures of both films were homogenous without any holes as presented in Figures IV.28 and IV.29, the process time in the Mini-Glatt® was too long and the process was not reproducible.

IV.13.1.2. SEM Pictures of the Enteric Coating using the Mini-Glatt

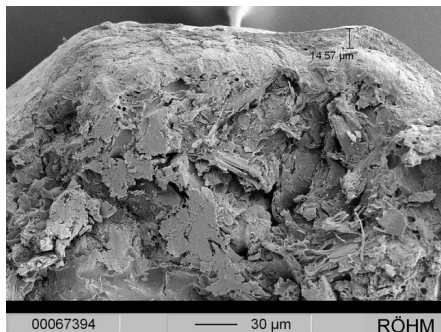


Figure IV.28 Na-CMC micropellets coated with a 30% coating layer (batch 15658/46a).

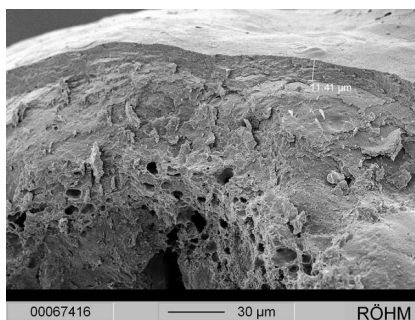
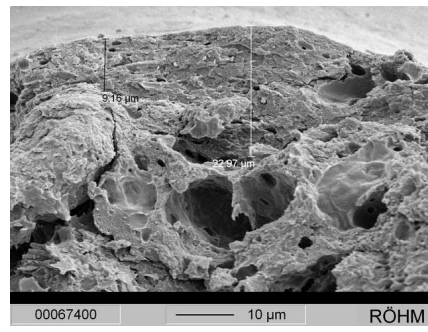
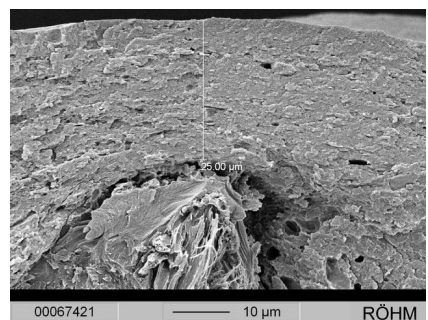


Figure IV.29 Na-CMC micropellets coated with a 30% coating layer (batch 15658/46b).



IV.13.2. Enteric Coating using the Hüttlin Mycrolab®

IV.13.2.1. Estimation of the Required Percentage of Coating

The following equation was used to estimate the required percentage of coating:

$$C_{\%} = S \times \rho \times T \times 100$$

$C_{\%}$ = Percentage of coating in terms of weight of uncoated pellets.

S = Surface area per gram determined by the modified Blaine method.

ρ = Density of the enteric film (1.04g/cm³ for EUDRAGIT®).

T = Thickness of the film (a minimum of 0.004cm for an enteric resistant coating).

For the Na-CMC micropellets, a minimum coating level of 40% was calculated. An additional 10% overhead was added.

IV.13.2.2. Development of Process Parameters for the Enteric Coating of Na-CMC Mucoadhesive Micropellets

The coating of mucoadhesive micropellets using a maximum spraying rate of 2.99g/min was successful in the Hüttlin Mycrolab®. The particle size, as given in Table IV.25 in combination with the process parameters, was increased only by means of thickness of the enteric coating layer. No twins or agglomeration of the particles was detectable. On the contrary, a spraying rate of 4g/min was too rapid. The spraying time in the Hüttlin Mycrolab® was much shorter than in the Mini-Glatt due to superior technology of the Diskjet compared to the Wurster inlet.

Table IV.25 Screening of process parameters for enteric coating

Batch	Coating Level [%]	Spraying Time [min]	Maximum Spraying Rate [g/min]	Particle ² size before coating [µm]	Particle ² size after Coating [µm]
15658/51	50	187	2.99	536	570
15658/52	65	210 ¹	2.76	-	-
15658/54	Aborted ³	-	4	-	-

¹ Sum of spraying times for batches 15658/51 and 15658/52, since batch 15658/51 was used for further coating.

² The X50 value presented was measured using the mastersizer.

³ The spraying rate was too high. Twins and agglomerates were produced.

The dissolution profile displayed in Figure IV.30 shows that no gastric resistance was reached by applying a 50% coating level of EUDRAGIT® L 30D-55. A gastric resistance was reached, however, by applying a 65% coating of EUDRAGIT® L 30 D-55 polymer.

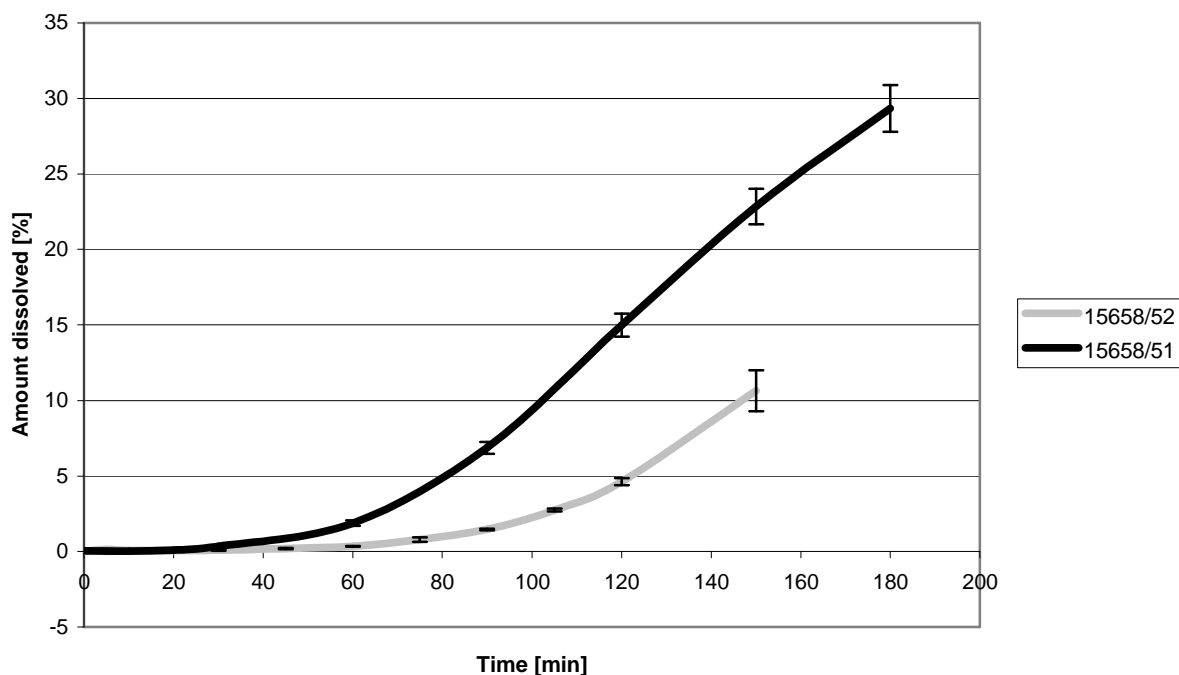


Figure IV.30 Dissolution test for gastric resistance of the mucoadhesive theophyllin micropellets in 1000ml of 0.1N HCl. The agitation rate of the paddle was 100rpm. Batch 15658/51 was manufactured with a 50% coating of Eudragit® L 30D-55, batch 15658/52 with a 65% coating of Eudragit® L 30D-55. Gastric resistance is defined according to the European Pharmacopea as a maximum of 10% dissolved drug after 2 hours.

The thickness of the film layers as presented in Figure IV.31 was between 23µm and 35µm and thus not sufficient for gastric resistant coating. The body structure of the film was excellent. The film was homogenous, no bubbles or sponge structures were detectable. Furthermore, no particle agglomeration was observed. An explanation for the discrepancy between the calculated and required amount of enteric coating is the false estimation of the surface area with the modified Blaine method. The Blaine apparatus was calibrated with glass beads of 1mm diameter, defined as complete spherical without any pores. The tested micropellets only had a diameter between 250µm and 600µm with many pores. This high discrepancy can explain the loss of accuracy of the method. The accuracy of the determination of the surface area from the micropellets should be increased by the use of smaller calibration glass beads or by a change from the modified Blaine method to a mercury pycnometer.

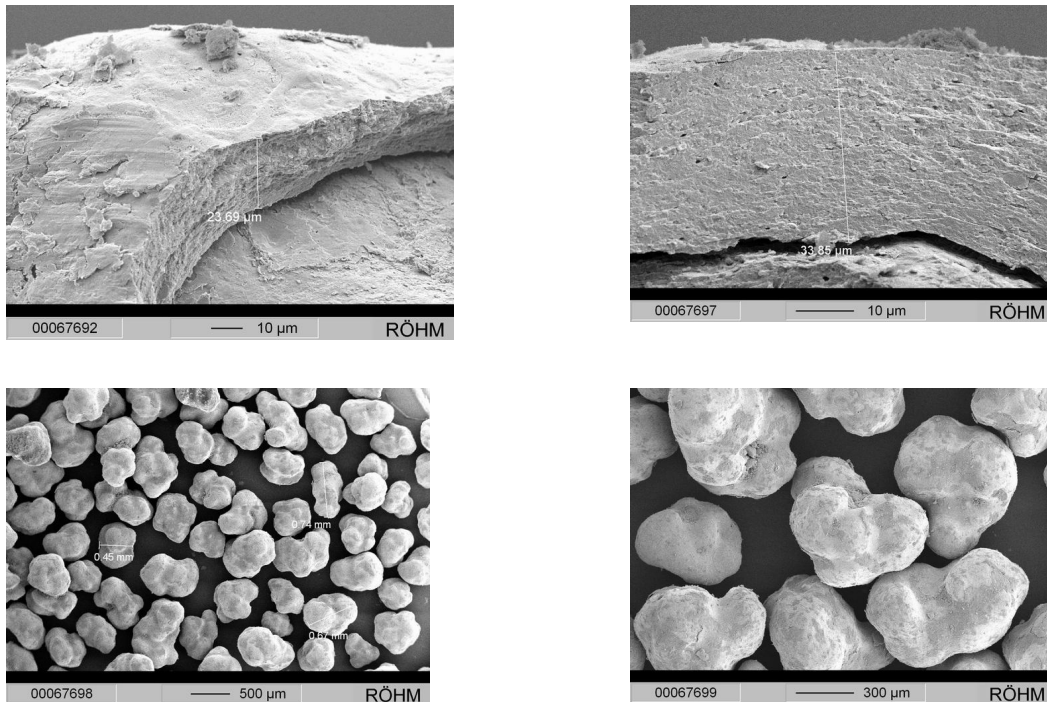


Figure IV.31 Na-CMC micropellets coated with EUDRAGIT® L 30D-55 (batch 15658/51). The coating level was 50% (w/w) based on uncoated pellet weight.

IV.13.2.3. Final Formulation for Enteric Coated Mucoadhesive Micropellets

Based on the previous experience a 70% coating level was selected for the Na-CMC micropellets to ensure gastric resistance and to minimize the amount dissolved to less than 5%. The coating level for the Na-alginate and chitosan micropellets was calculated by the ratio of the surfaces of the uncoated Na-alginate or chitosan micropellets to the uncoated Na-CMC micropellets and rounded to the next number which could be divided by 5. The surface of the Na-CMC micropellets was used similarly as a correction factor, based on the knowledge that the determined surface area of the modified Blaine method was too small.

$$C_{\%} = \frac{S_{micropellet}}{S_{Na-CMC}} \times 0,7 \times 100\% \times \text{weight of the micropellet [g]}$$

$C_{\%}$ = percentage of coating;
 S_{Na-CMC} = Surface area of the uncoated Na-CMC micropellets per gram;
 $S_{micropellet}$ = Surface area of the uncoated Na-alginate or chitosan micropellets per gram

All coatings performed in the Hüttlin Mycrolab® were successful. The spraying rate used for the production of batch 15658/57 was temporarily too high during the experiment, which lead to some particle growth by agglomeration. Also for batch 15658/58 a slight growth occurred by agglomeration. On the other hand the micropellets of batches 15658/56 and 15658/59 mainly grew due to the increase of their enteric layer. The production yield was very close to the 100% theoretical yield demonstrating that very little coating material was lost during the process. In Table IV.26 the main manufacturing parameters of the final formulation are summarized. For the entire process parameters see Chapter III.3.4.2.

Table IV.26 Main manufacturing parameters of the final enteric coating formulation of mucoadhesive micropellets.

Batch	Coating level of Enteric Polymer [%]	Mucoadhesive Polymer	Spraying Time [min]	Maximum Spraying Rate [g/min]	Particle ³ Size before Coating [μm]	Particle ³ Size after Coating [μm]	Theoretical Yield [g]	Practical Yield [g]
15658/56	70% of L ¹	Na-CMC	276	2.6	542	627	273	275
15658/57	140% of L ¹	Na-Alginate	602	2.8 (2.6) ⁴	398	560	395	390
15658/58	70% of FS ²	Na-CMC	325	2.7	542	698	268	266
15658/59	85% of L ¹	Chitosan	332	2.56	491	602	299	293

¹ EUDRAGIT® L 30 D-55.

² EUDRAGIT® FS 30 D.

³ The X50 value presented was measured in the mastersizer.

⁴ The maximum spraying rate of 2.8g/min was only applied for a short period; after twins were visible the spraying rate was reduced to 2.6 g/min.

SEM pictures of product batches 15658/56, 15658/57, 15658/58 and 15658/59 are presented in Figures IV.32 - IV.35.

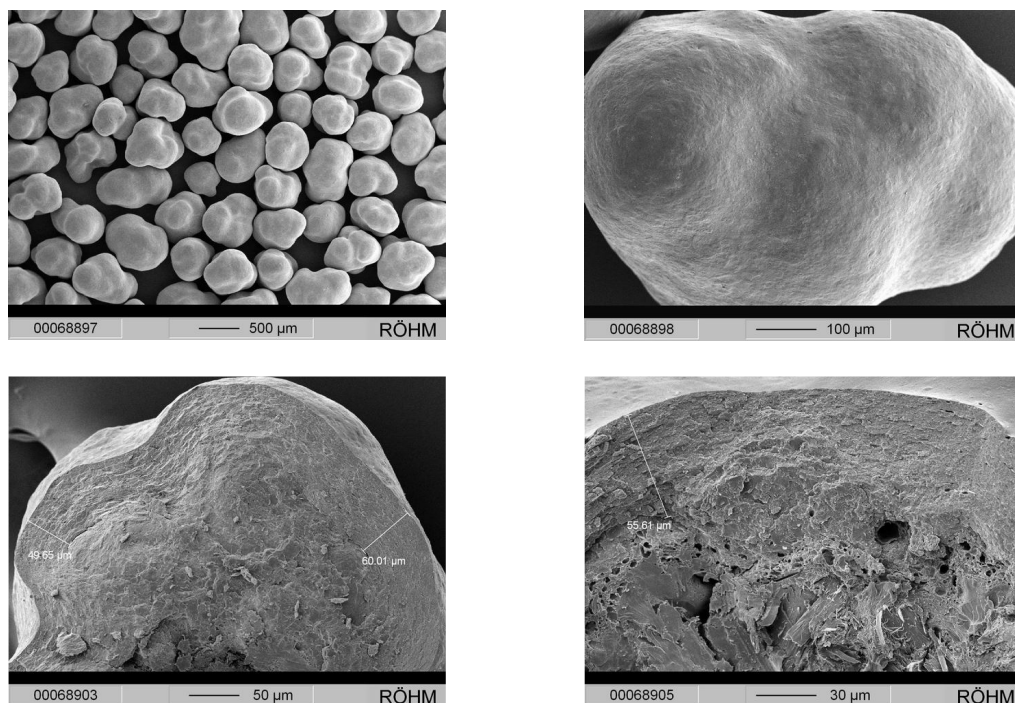


Figure IV.32 Na-CMC micropellets coated with EUDRAGIT® L 30D-55 (batch 15658/56). The coating level was 70% (w/w) based on uncoated pellet weight.

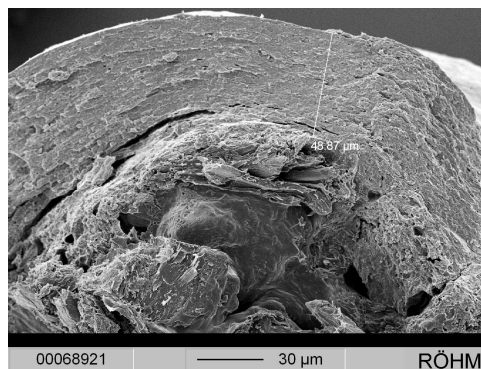
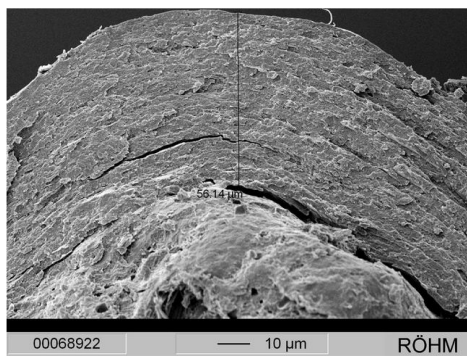


Figure IV.33 Na-alginate micropellets coated with EUDRAGIT® L 30D-55 (batch 15658/57). The coating level was 140% (w/w) based on uncoated pellet weight.

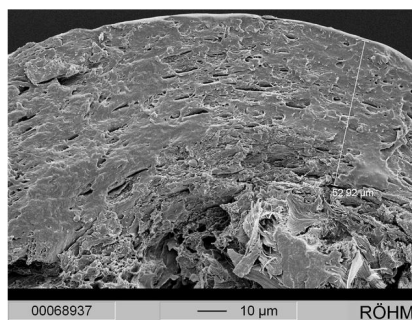
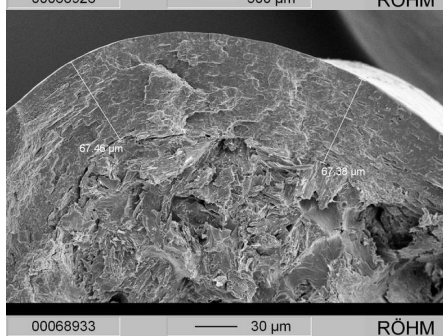
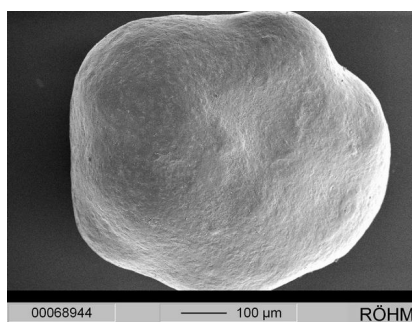
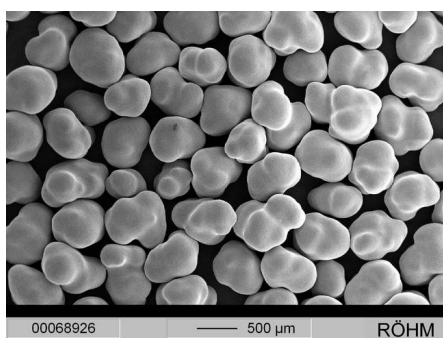


Figure IV.34 Chitosan micropellets coated with EUDRAGIT® L 30D-55 (batch 15658/58). The coating level was 85% (w/w) based on uncoated pellet weight.

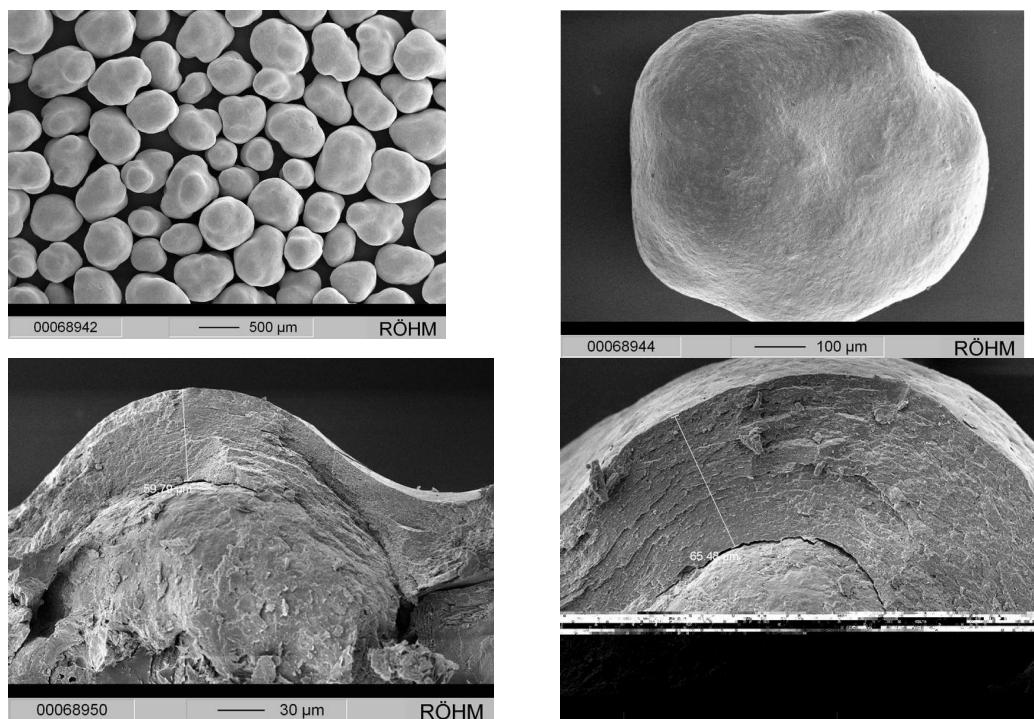


Figure IV.35 Na-CMC micropellets coated with EUDRAGIT® FS 30D (batch 15658/59).
The coating level was 70% (w/w) based on uncoated pellet weight.

The thickness of each film is clearly greater than 40 μ m. In general, film thickness ranged between 50 and 65 μ m. The films are homogenous, neither bubbles nor a spongetype structure is detectable. Furthermore, no particle agglomeration is seen.

IV.14. Results of the Dissolution Tests

IV.14.1. Comparison of the Different Dissolution Apparatus

In Figures IV.36 - IV.46 the results of experiments carried out in the different dissolution apparatus are presented. Also, different conditions for the Flow-through cell were compared to define an appropriate method for the dissolution of mucoadhesive micropellets in this system. In all dissolution apparatus an uncoated Na-CMC micropellet dummy batch of a particle size between 250 μ m-600 μ m was dissolved at pH 6.0 for comparison.

IV.14.1.1. Dissolution in the Paddle Apparatus (USP Apparatus Type 2)

In Figure IV.36, the dissolution profile in the paddle apparatus at an agitation of 100rpm is presented. The mucoadhesive theophyllin containing pellets dissolved fast and homogenously. The standard deviation calculated over all dissolution points was 3.87%.

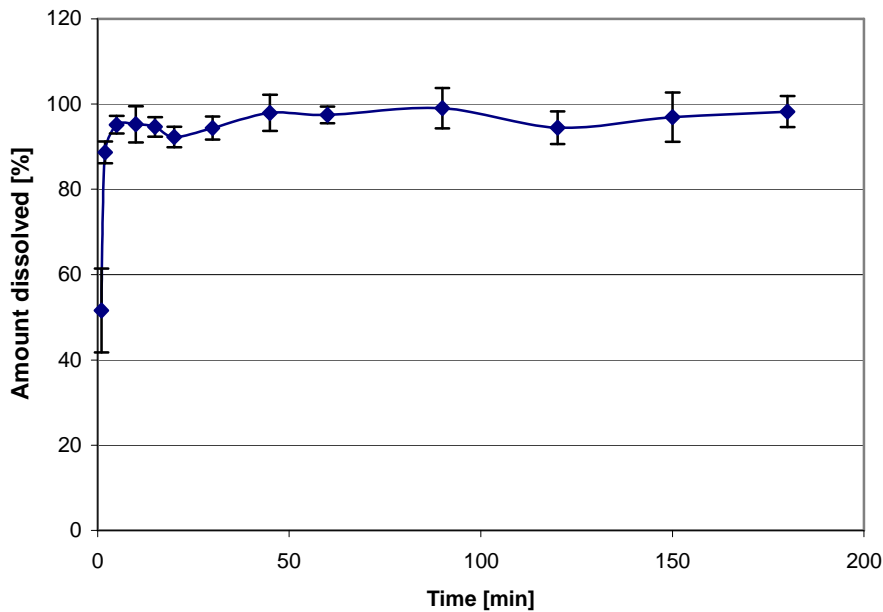


Figure IV.36 Dissolution profile of theophyllin containing Na-CMC micropellets using APP.2 at 100rpm, described as D1 (n=6).

The apparatus type 2 has been modified with a 250 μ m sieve inlay in case of the experiment displayed in Figure IV.37. The agitation rate of the paddle was 100rpm and theophyllin containing Na-CMC micropellets were dissolved. The mucoadhesive pellets also show very fast release, however, the sieve seems to inhibit a free mixing of the dissolution medium in the vessels. This is indicated by amounts released exceeding 100% at the beginning of the dissolution test, indicating that the medium underneath the sieves is excluded from the dissolution process at the beginning of the test due to the barrier function of the sieve. After an appropriate equilibration time the medium in the vessels is completely mixed and the values approach 100%. The standard deviation calculated over all dissolution points was 5.11%.

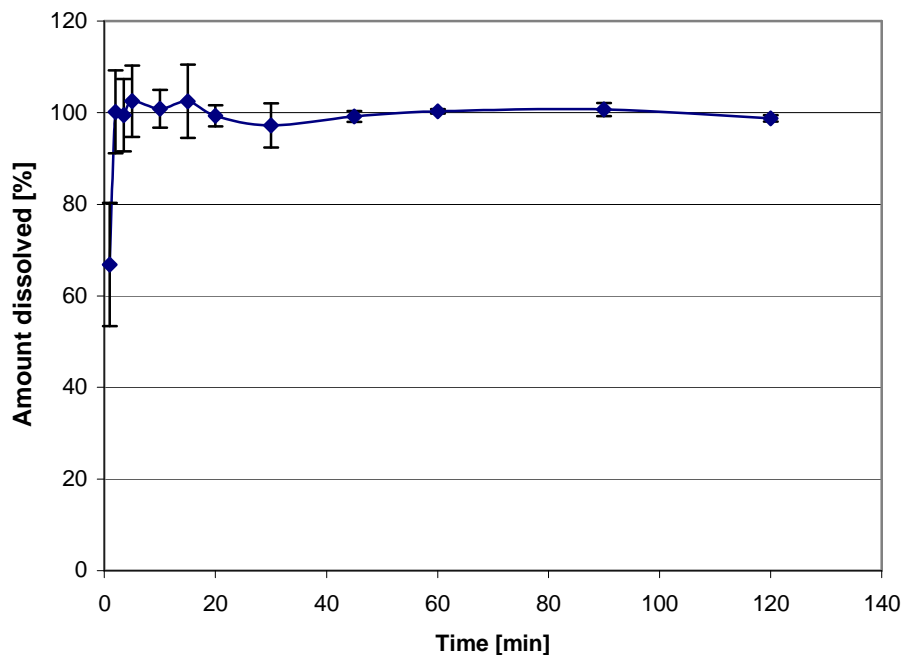


Figure IV.37 Dissolution profile of theophyllin containing Na-CMC micropellets using APP.2 modified with a 250 μ m sieve inlay at 100rpm, described as D2 (n=6).

The dissolution profile of theophyllin pellets with a defined particle size range from 400 μ m to 500 μ m using the APP.2 with an agitation rate of the paddle of 100rpm and a sieve inlay of 250 μ m is presented in Figure IV.38. The same but more pronounced mixing problem failure appeared as described for dissolution method displayed in Figure IV.37. The standard deviation calculated over all dissolution points was 3.81%.

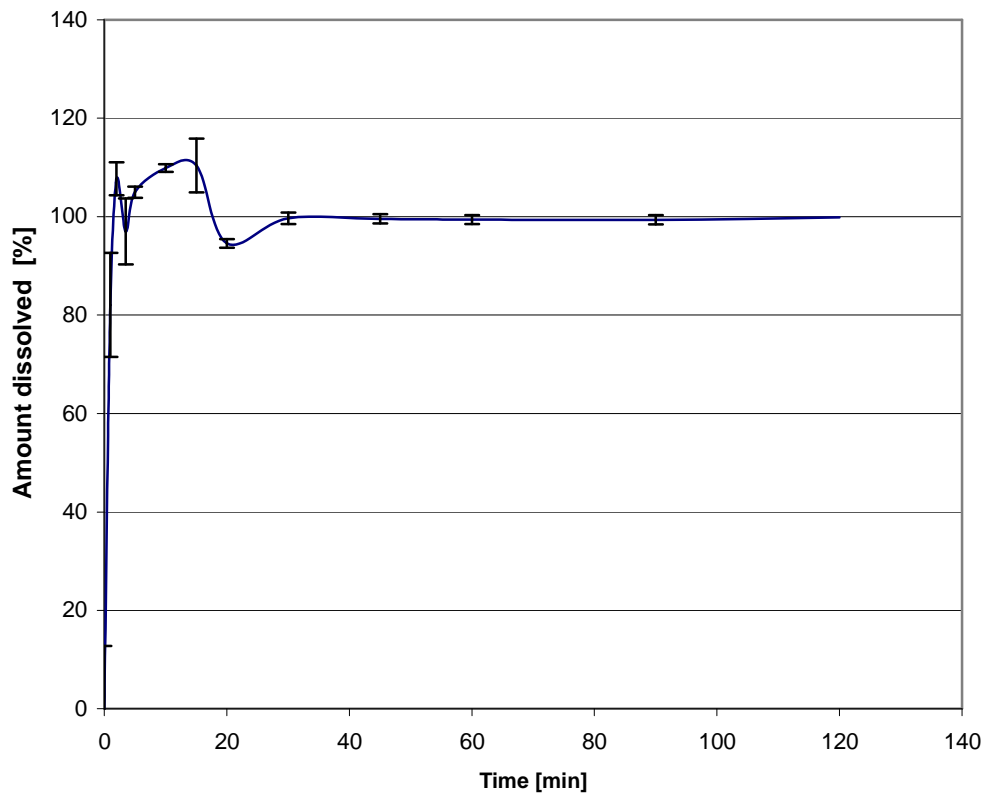


Figure IV.38 Dissolution profile of theophyllin containing Na-CMC micropellets between 400 μ m and 500 μ m using APP.2, modified with a 250 μ m sieve inlay at 100rpm, described as D3 (n=6).

The effect of an increase in the mesh size of the sieve inlay is demonstrated in Figure IV.39. The dissolution was performed in the APP.2 with an agitation of the paddles of 100rpm and a sieve inlay of 360 μ m. The mucoadhesive theophyllin pellets were between 400 μ m and 500 μ m. The problems with insufficient mixing which occurred in methods D2 & D3 (Figures IV.37 and IV.38) did not occur. The standard deviation calculated over all dissolution points was 2.46%.

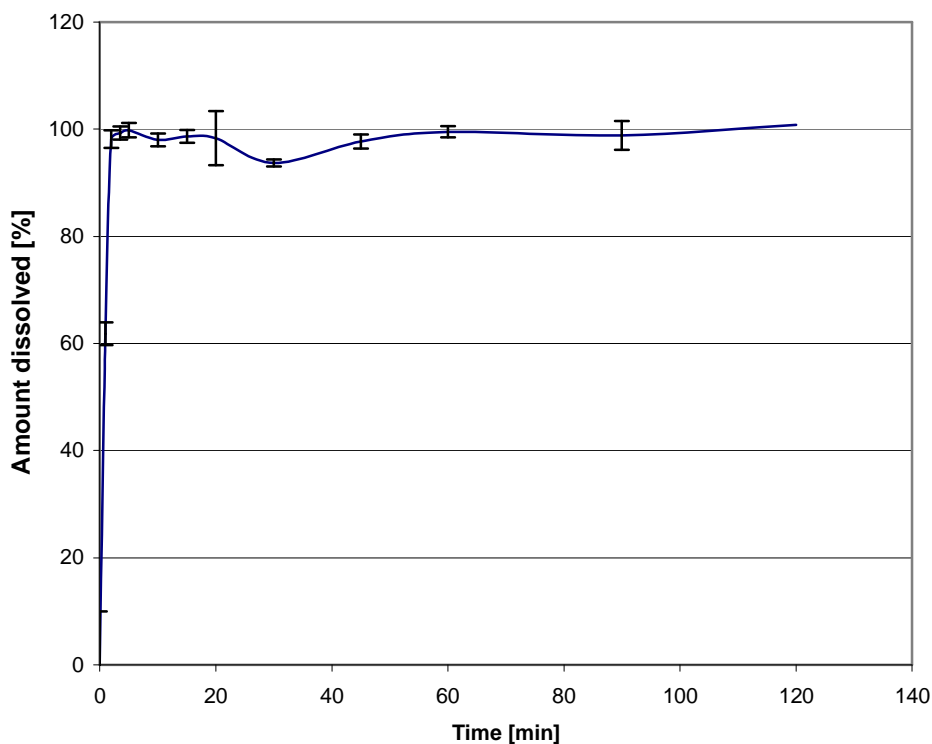


Figure IV.39 Dissolution profile of theophyllin containing Na-CMC micropellets between 400 μ m and 500 μ m using APP.2, modified with a 360 μ m sieve inlay at 100rpm, described as D4 (n=6).

IV.14.1.2. Dissolution using the Basket Apparatus (USP Apparatus Type 1)

The micropellets dissolved very slowly but homogeneously in the basket apparatus (Figure IV.40). The low dissolution rate was caused by the formation of a homogenous gel by the pellets inside the basket. The standard deviation calculated over all dissolution points was 0.97%.

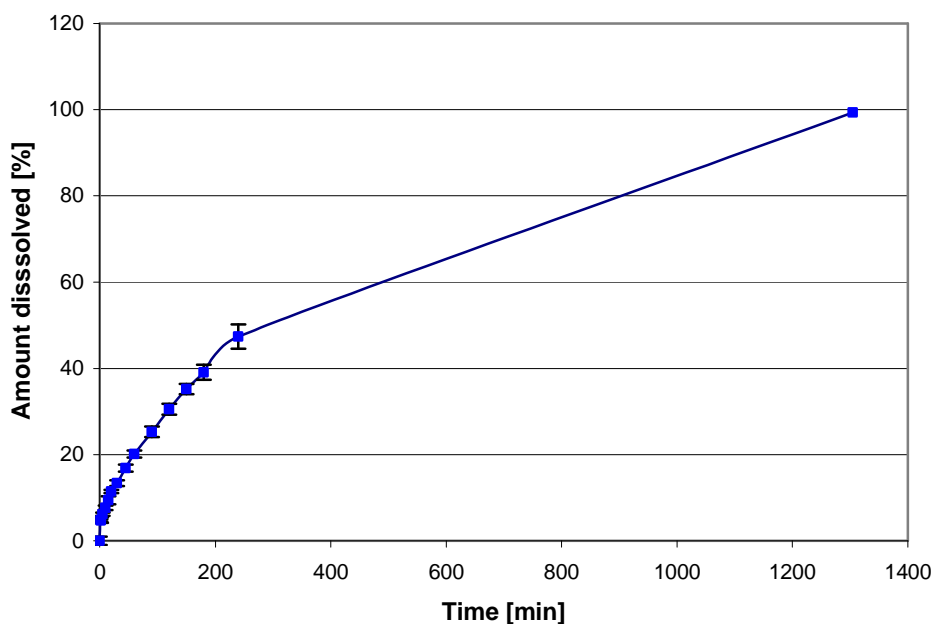


Figure IV.40 Dissolution profile of theophyllin containing Na-CMC micropellets using APP.1 at 100rpm, described as D5 (n=6).

IV.14.1.3. Dissolution in the Reciprocating Cylinder (USP Apparatus Type 3)

The Reciprocating Cylinder dissolution profile shows a very slow and variable release of the micropellets (Figure IV.41). The inhomogeneous release is due to the cross contamination between the single dissolution vessels. Comparable to the dissolution in the basket apparatus a coalescence of the single pellets to a homogeneous gel occurs. This gel blocks the sieve at the bottom of the cylinder and buffer remains inside after the drip off time, as presented in Figure IV.42. This buffer is subsequently transferred to the next row or is lost between the rows. Thus it is concluded that the reciprocating cylinder is not an appropriate apparatus for determining the dissolution of mucoadhesive pellets. This is also obvious from the high standard deviation calculated over all dissolution points (10.88%).

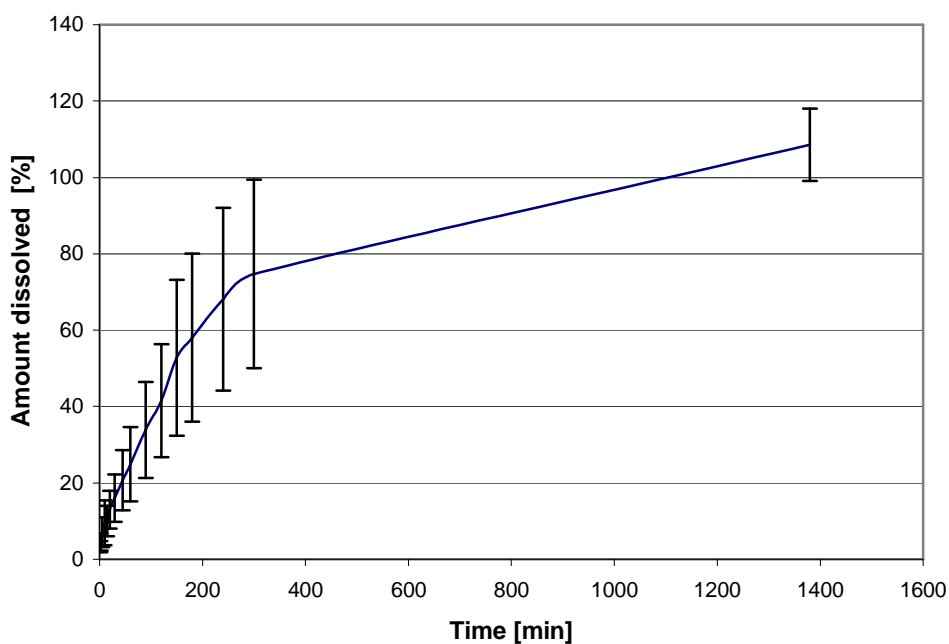


Figure IV.41 Dissolution profile of theophyllin containing Na-CMC micropellets using APP.1 at 25 dips per minute, described as D6 (n=6).



Figure IV.42 Dissolution of theophyllin containing Na-CMC micropellets in the reciprocating cylinder apparatus. The cylinders are still filled with buffer after the drip off time, because they are blocked by the mucoadhesive micropellets.

IV.14.1.4. Dissolution in the Flow-Through Cell (USP Apparatus Type 4)

As presented in Figure IV.43 the flow-through cell is overloaded and consequently blocked. For further experiments the loading needed to be reduced.



Figure IV.43 Dissolution profile of theophyllin containing Na-CMC micropellets using APP.4 at a flow rate of 10g/min. A blocked dissolution vessel of the APP.4 is observed by a loading of 2g micropellets together with 15g of glass beads (flow rate 10ml/min), described as D7 (n=5).

In the subsequent trials the loading of the micropellets was reduced to 0.5g. The dissolution profile of the combination of the reduced loading together with 15g glass beads and an adjusted flow rate of 10ml/min is presented in Figure IV.44. This method leads to a dissolution profile which is located between the basket and paddle

method with a standard deviation over all dissolution points of 6.21%. After 90min the release of the drug was not complete.

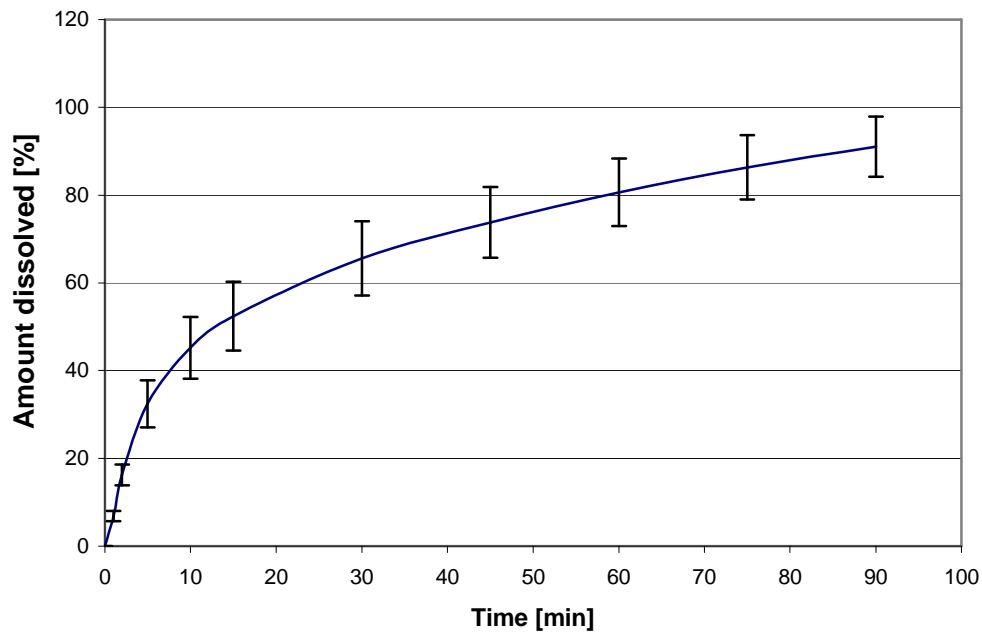


Figure IV.44 Dissolution profile of 0.5g theophyllin containing Na-CMC micropellets using APP.4 at a flow rate of 10ml/min, described as D8 (n=5). The micropellets were mixed with 15g glass beads.

An increase of the flow rate from 10ml/min (Figure IV.44) to 20ml/min (Figure IV.45) by keeping the loading of the micropellets and the glass beads constant at 0.5g and 15g, a more rapid dissolution rate and a smaller standard deviation occurred over all dissolution points (3.92%).

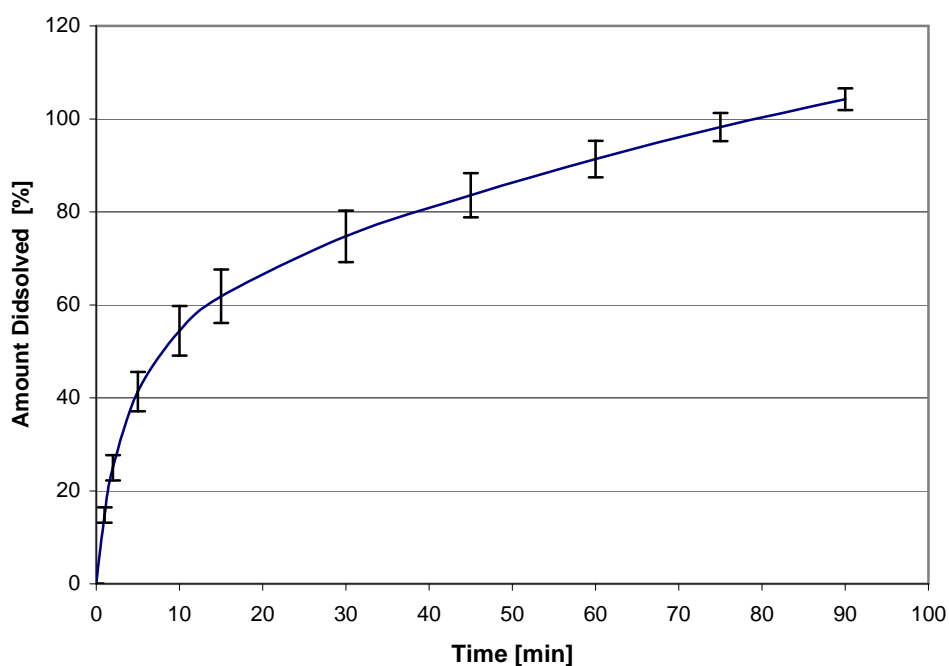


Figure IV.45 Dissolution profile of 0.5g theophyllin containing Na-CMC micropellets using APP.4 at a flow rate of 20ml/min, described as D9 (n=5). The micropellets were mixed with 15g glass beads.

The effect of an increase in glass beads on drug release is demonstrated in Figure IV.46. In this case a micropellet loading of 0.5g micropellets and 18g glass beads at a flow rate of 10ml/min has been evaluated. Described as D10, a faster release and smaller standard deviation in comparison to D8 is obvious. The standard deviation calculated over all dissolution points was 3.69%.

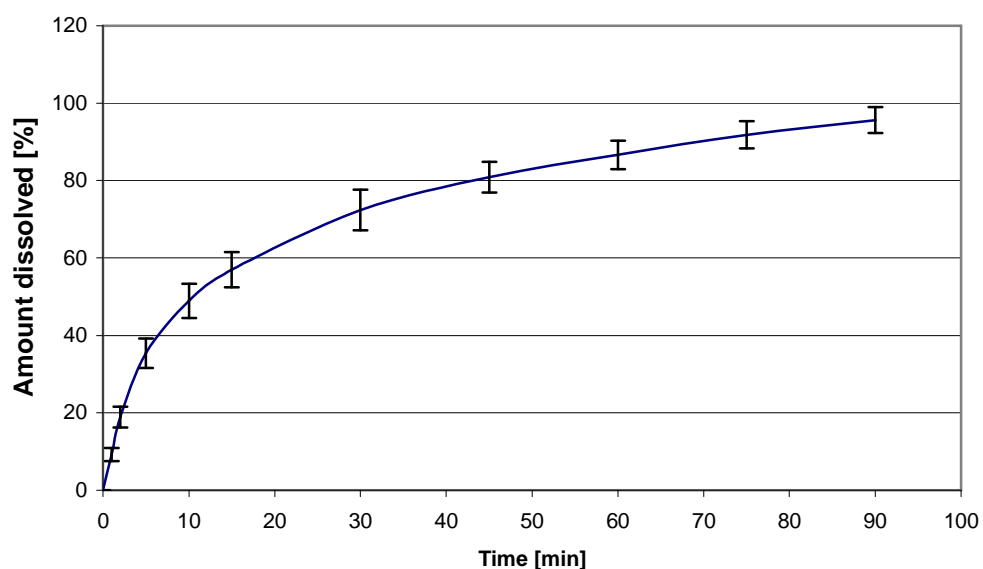


Figure IV.46 Dissolution profile of 0.5g theophyllin containing Na-CMC micropellets using APP.4 at a flow rate of 10ml/min, described as D10 (n=5). The micropellets were mixed with 18g glass beads.

IV.14.1.5. Summary of the Comparison of the Different Dissolution Apparatus

The different methods result in large differences in the dissolution rate. Using the paddle apparatus, 100% was released within 5 minutes. Using the Basket Apparatus, 100% was released within 21.75 hours. All methods except of the Reciprocating Cylinder show high conformity. The most qualified methods seem to be the unmodified paddle apparatus and the Flow-through cell employing a large cell, 18g of glass beads and a flow rate of 20ml/min. The conditions of the Flow-through cell are a combination of D9 and D10.

IV.14.2. Dissolution of the Final Batches and Comparison of Different Agitation Rates using the Paddle Apparatus and Flow-Through Cell

Based on the results described in Chapter IV.14.1, dissolution testing of different mucoadhesive micropellets with and without enteric coating was performed using the paddle apparatus at 50rpm, 100rpm and 150rpm, and the flow-through cell.

IV.14.2.1. Na-CMC Dissolution Profiles

The dissolution profiles of coated and uncoated Na-CMC micropellets are presented in Figures IV.47 to IV.50. Micropellets which were coated with EUDRAGIT[®] L 30D-55 were dissolved at pH 6.0, micropellets which were coated with EUDRAGIT[®] FS 30 D were dissolved at pH 7.2. The pH values were selected to simulate a drug delivery to the upper part of the small intestine for the EUDRAGIT[®] L 30D-55 formulation and drug delivery to the upper part of the colon for the EUDRAGIT[®] FS 30 D formulation. In Figure IV.47 the dissolution profile of Na-CMC micropellets coated with EUDRAGIT[®] L 30D-55 using the paddle apparatus with different agitation rates is presented. In all cases an initial burst was observed. The following release kinetics depended on the paddle velocity. During the start of the dissolution test or shortly after changing the pH of the medium, all micropellets were separated from each other. During the ongoing dissolution test, the pellets started to swell, they formed a gel and lumped together. These processes lead to an increase in the diffusion distances and thereby to a decrease in the release rate. The higher shearing capacity at higher paddle speed inhibited the formation of lumps from the mucoadhesive pellets. Furthermore, it caused a faster breakdown of the pellets.

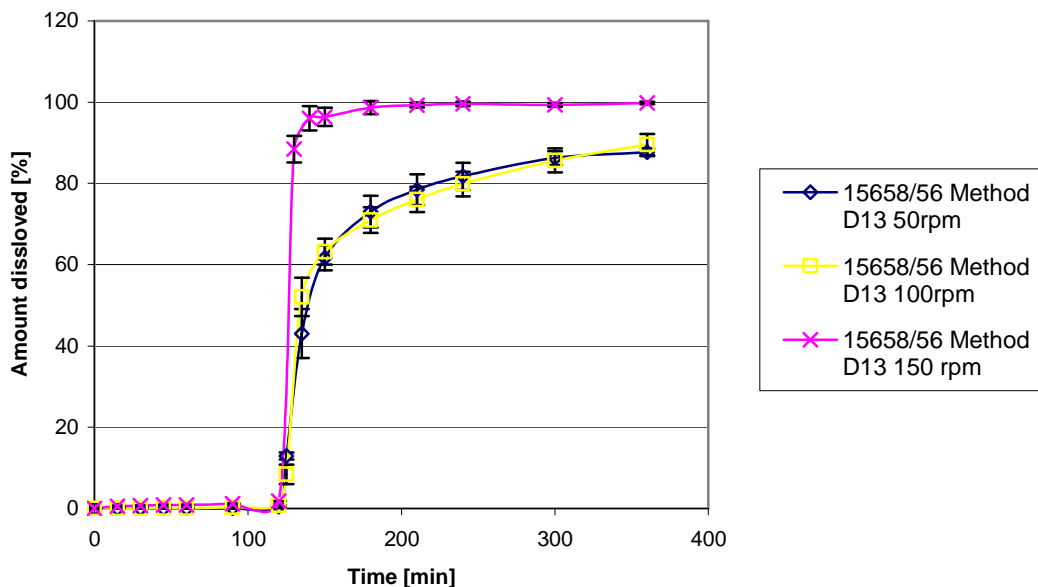


Figure IV.47 Dissolution profile of batch 15658/56: theophyllin containing Na-CMC micropellets coated with EUDRAGIT L 30D-55 using App.2 and applying different agitation rates (D13). The dissolution medium was changed after two hours from 0.1 N HCl to phosphate buffer pH 6.0 in accordance with compendial procedures (n=6).

The dissolution profile using the same formulation and the Flow-through cell is presented in Figure IV.48. The profile is similar to the one obtained in the paddle apparatus. A high initial burst release is followed by a slow diffusion-controlled release rate. During the starting phase of the dissolution process the micropellets were separated from the glass beads. At later points in time the pellets started to coalesce. Therefore, the release kinetics was decreased. All dissolution profiles proved that an enteric resistant coating, in terms of less than 10% release in 0.1 N HCl solution during 2h, was achieved.

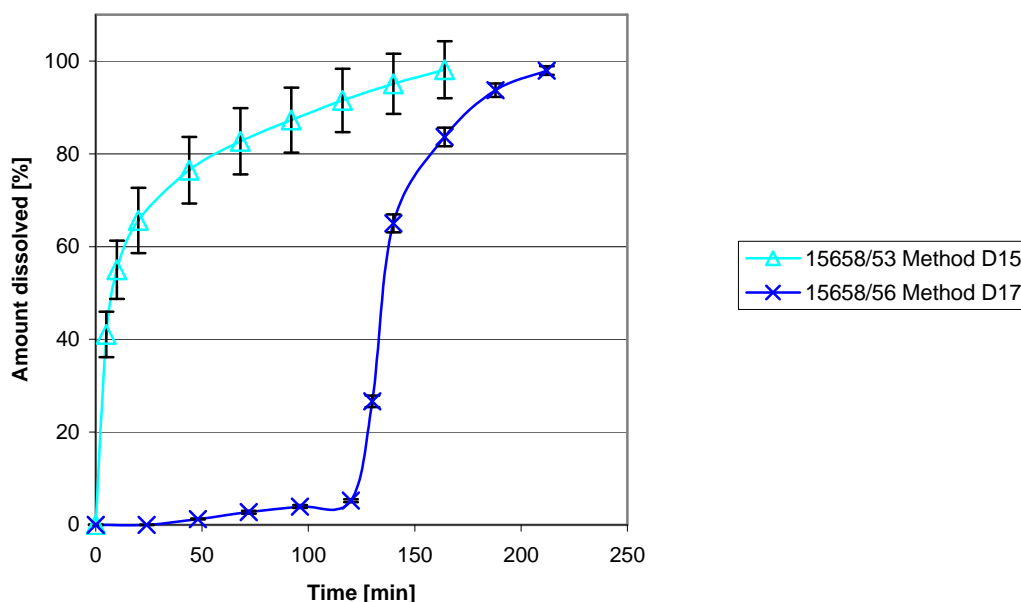


Figure IV.48 Dissolution profile of Na-CMC uncoated and EUDRAGIT® L 30D-55 coated theophyllin containing micropellets using App.4 (D15 and D 17). Batch 15658/53 was uncoated and batch 15658/56 was the coated formulation. In D15 phosphate buffer pH 6.0 was used during the entire dissolution test. In D17, 0.1N HCl was used during the first two hours and thereafter phosphate buffer pH 6.0 (n=5).

The dissolution profiles of Na-CMC micropellets coated with EUDRAGIT FS 30D using the paddle apparatus are presented in Figure IV.49. The influence of the paddle speed shows pronounced differences in release rates. The dissolution of the uncoated micropellets was slower compared to the coated micropellets, which may be caused by a higher tendency to form lumps upon transfer into the dissolution vessels. At the first sampling point a relatively high standard deviation for D14 with a paddle velocity of 150 rpm was observed. An explanation of this phenomenon may be the high shearing forces of the paddles at 150rpm which can cause a non uniform breaking of the coating in the different vessels. Another explanation may be small changes of the medium pH which were not carried out at the defined time point, resulting in a shift in the dissolution profile. All dissolution profiles proved that an enteric resistant coating was achieved since the amount released within 2h in 0.1N HCl was less than 10% of the dose.

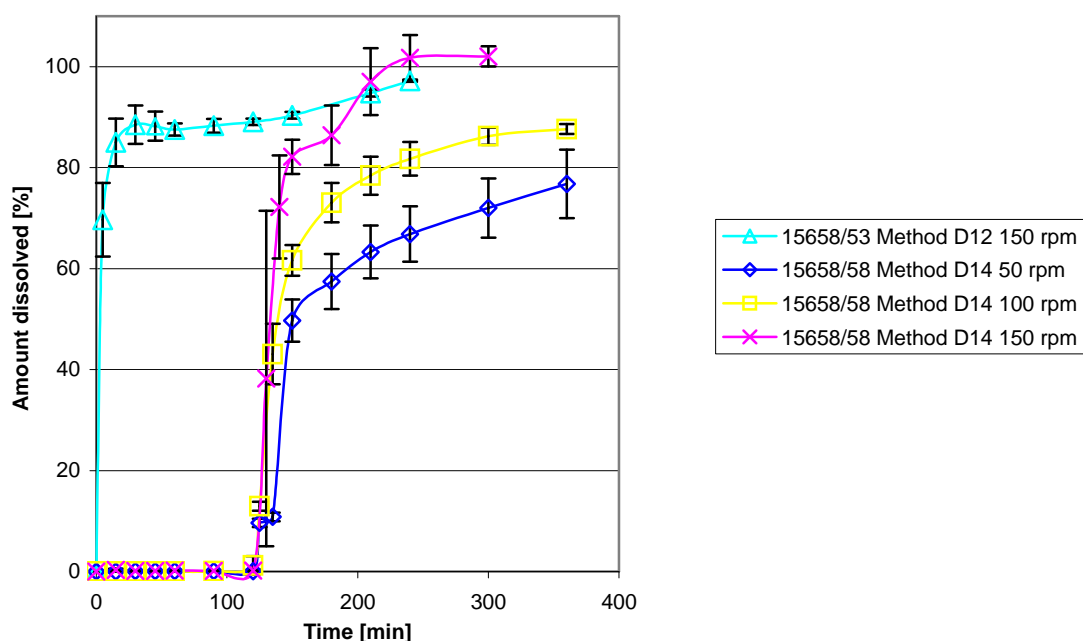


Figure IV.49 Dissolution profile of Na-CMC uncoated and EUDRAGIT® FS 30D coated theophyllin containing micropellets using APP.2 (D12 and D14). Batch 15658/53 was uncoated and batch 15658/58 was the coated formulation. In D12 phosphate buffer pH 7.2 was used during the entire dissolution test. In D14, 0.1N HCl was used during the first two hours and thereafter phosphate buffer pH 7.2 (n=6).

The dissolution profile of the EUDRAGIT® FS 30D coated micropellets using the flow-through cell is presented in the Figure IV.50. It shows high analogy to the results generated by the paddle apparatus at 100rpm. Although the dissolution profiles using the flow-through cell at pH 6.0 and 7.2 are quite similar, a decrease of the dissolution rate at pH 7.2 compared to pH 6.0 was detectable due to the pH dependent solubility of theophyllin. Theophyllin has a higher solubility at lower pH.

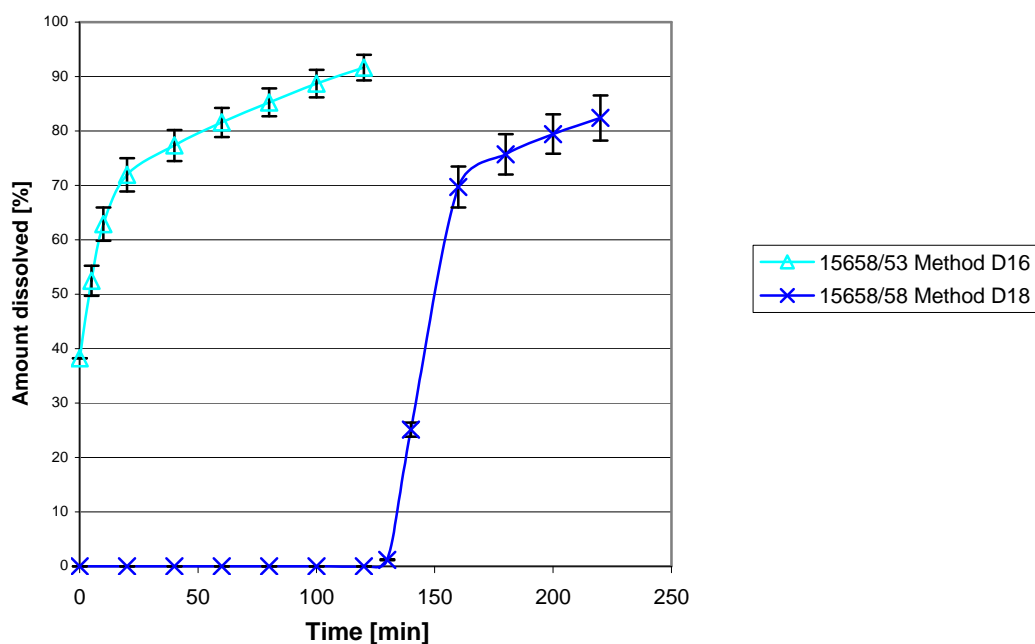


Figure IV.50 Dissolution profile of Na-CMC uncoated and EUDRAGIT® FS 30D coated theophyllin containing micropellets using APP.4 (D16 and D18). Batch 15658/53 was uncoated and batch 15658/58 was the coated formulation. In D16 phosphate buffer pH 7.2 was used during the entire dissolution test. In D18, 0.1N HCl was used during the first two hours and thereafter phosphate buffer pH 7.2 (n=5).

IV.14.2.2. Na-Alginate Dissolution Profiles

Dissolution profiles of coated and uncoated Na-alginate micropellets are presented in Figures IV.51 to IV.53. The dissolution profiles of the uncoated Na-alginate micropellets in the Paddle Apparatus applying different agitation rates are presented in Figure IV.50. The profiles are similar to the coated Na-CMC micropellets using the Paddle Apparatus. There was no influence of paddle velocity at 100rpm and 150rpm, however, the standard deviation at 100rpm was smaller than at 150rpm.

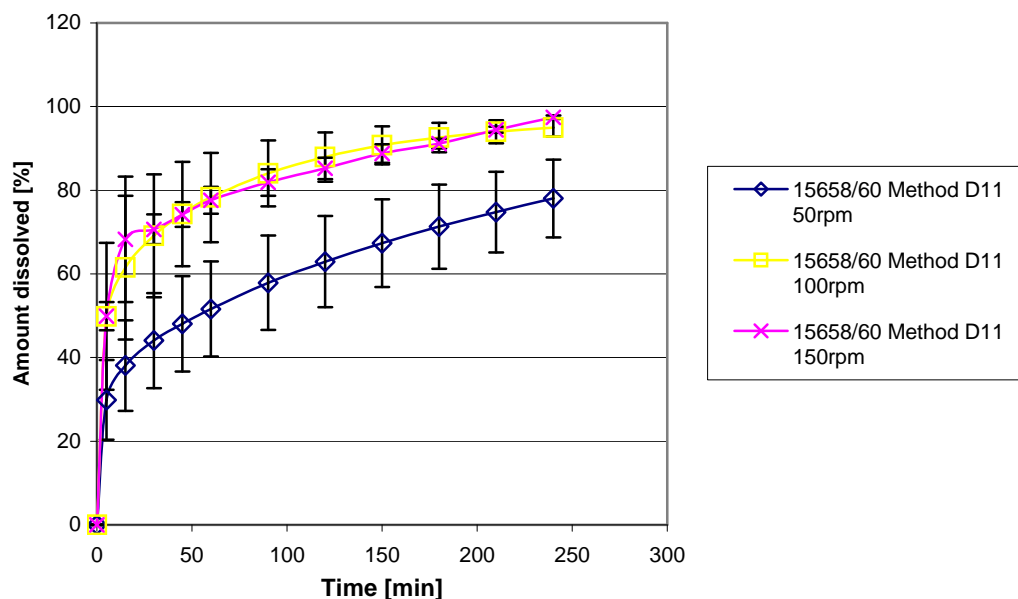


Figure IV.51 Dissolution profile of theophyllin containing uncoated Na-alginate micropellets (batch 15658/60) using App.2 and applying different agitation rates (D11). In D11 a phosphate buffer pH 7.2 was used during the entire dissolution test (n=6).

The dissolution profiles of the coated Na-alginate micropellets in the Paddle Apparatus at different agitation rates are presented in Figure IV.52. Similar to Na-CMC, the dissolution profile was dependent on the agitation rate. All dissolution profiles showed that an enteric resistant coating was achieved.

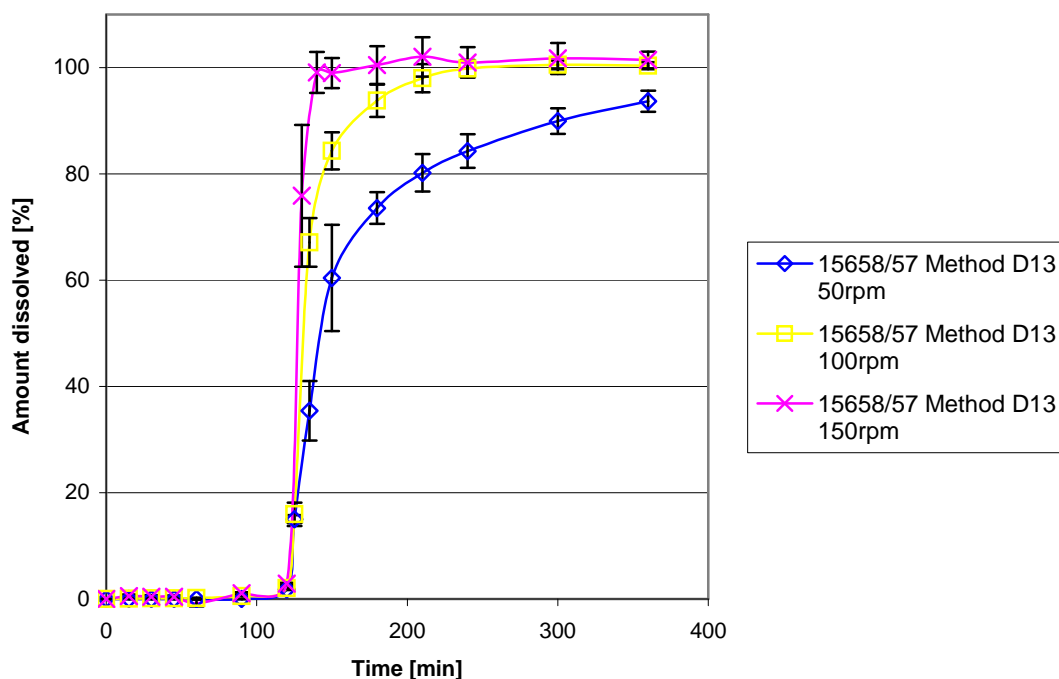


Figure IV.52 Dissolution profile of batch 15658/57 theophyllin containing Na-alginate micropellets coated with EUDRAGIT L 30D-55 using App.2 and applying different agitation rates (D13). The dissolution medium was changed after two hours from 0.1 N HCl to the buffer pH 6.0 in accordance with compendial procedures (n=6).

On the one hand the dissolution profile of the uncoated micropellets in Figure IV.53 using the flow-through cell is similar to applying the paddle apparatus at 50rpm, on the other hand this similarity was not obvious for the coated micropellets. The release rate of the coated micropellets using the flow-through cell is slower than applying App.2 at 50rpm. Therefore, it can be concluded, that general applicable dissolution conditions of the flow-through cell to obtain similar profiles compared to the paddle apparatus do not exist. Using the Flow-through cell, the dissolution profiles of the Na-alginate micropellets are slower compared to the Na-CMC micropellets. The average particle size of the Na-alginate preparation is reduced in comparison to Na-CMC microparticles. Hence the Na-alginate micropellets slip faster through the gaps between glass beads and the coalescence of the micropellets is more pronounced. All dissolution profiles showed that an enteric resistant coating was achieved.

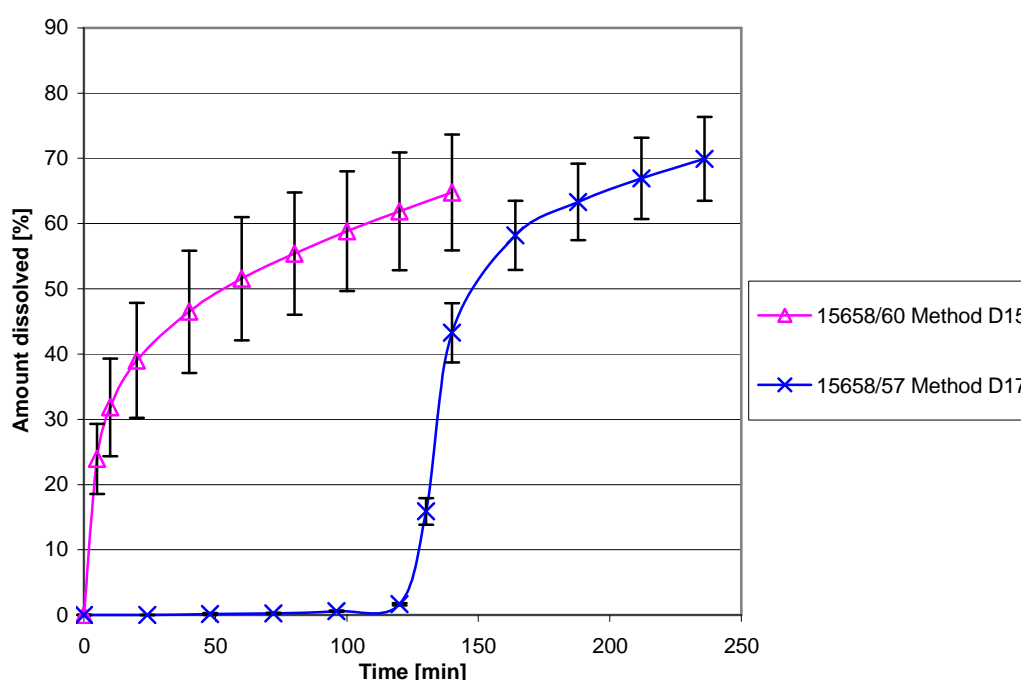


Figure IV.53 Dissolution profile of Na-alginate uncoated and EUDRAGIT® L 30D 55 coated theophyllin containing micropellets using APP.4 (D15 and D17). Batch 15658/60 was uncoated and batch 15658/57 was the coated formulation. In D15 phosphate buffer pH 6.0 was used during the entire dissolution test. In D17, 0.1N HCl was used during the first two hours and thereafter phosphate buffer pH 6.0 (n=5).

IV.14.2.3. Chitosan Dissolution Profiles

Dissolution profiles of coated and uncoated Chitosan micropellets are presented in Figures IV.54 to IV.56.

In Figure IV.54, the dissolution profile of uncoated chitosan micropellets using the Paddle Apparatus is presented. The release rate of theophyllin from the chitosan micropellets was the fastest among the formulations. Hence, the influence of the dissolution method was not as pronounced as compared to the other formulations. Nevertheless, the method with the highest shear capacity led to the fastest dissolution rate and smallest standard deviation.

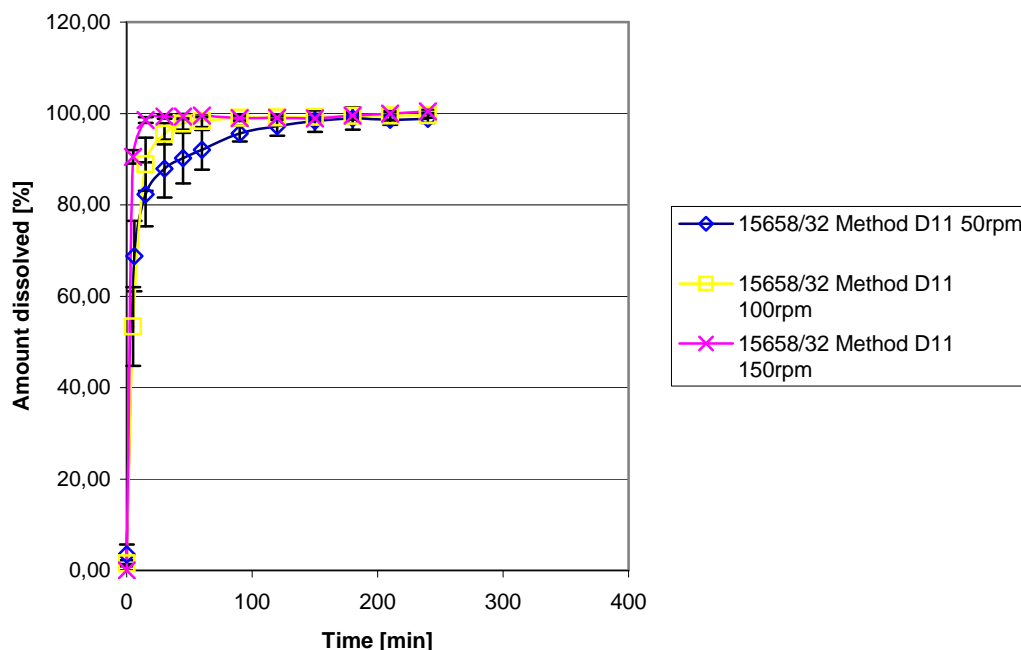


Figure IV.54 Dissolution profile of theophyllin containing chitosan micropellets (batch 15658/32) using App.2 and applying different agitation rates (D11). In D11 phosphate buffer pH 6.0 was used during the entire dissolution test (n=6).

The dissolution profiles of the coated chitosan micropellets are presented in Figure IV.55. At 150rpm the dissolution was more rapid as compared to 100rpm or 50rpm. All dissolution profiles proved that an enteric resistant coating was achieved.

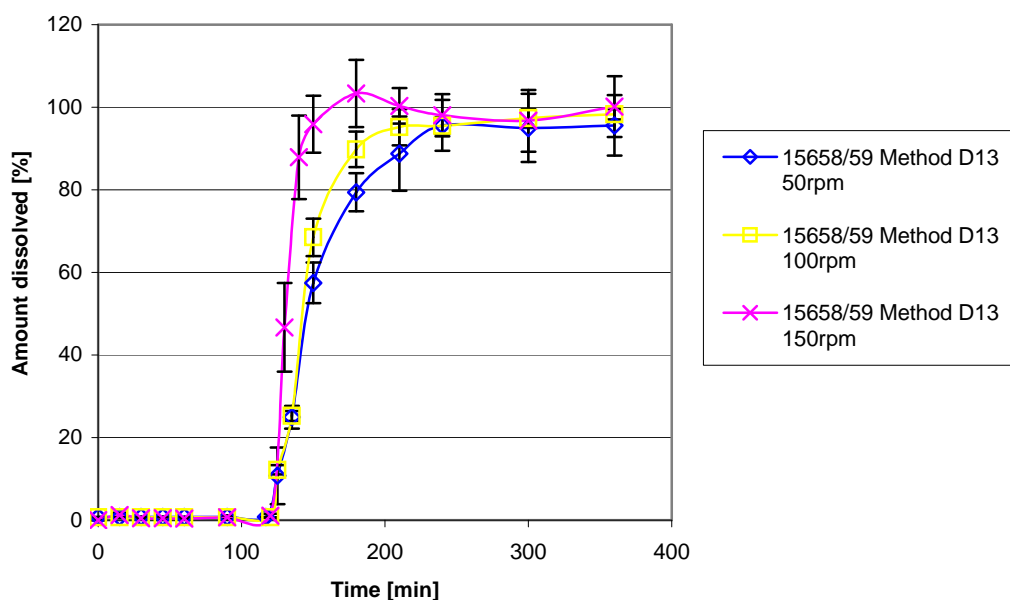


Figure IV.55 Dissolution profile of theophyllin containing chitosan micropellets (batch 15658/59) coated with EUDRAGIT L 30D-55 using App.2 and applying different agitation rates (D13). The dissolution medium was changed after two hours from 0.1 N HCl to the phosphate buffer pH 6.0 in accordance with compendial procedures (n=6).

The dissolution profile of the uncoated micropellets presented in Figure IV.5, using the flow-through cell showed high analogy to the results achieved with the paddle apparatus at 50rpm. The shape of the dissolution profile is similar to the dissolution profile of the Na-CMC micropellets in the flow-through cell caused by

coalescence of the micropellets. Nevertheless the release rate remains very fast in contrast to the Na-CMC micropellets. The dissolution profile in App.4 also proved that an enteric resistant coating was achieved.

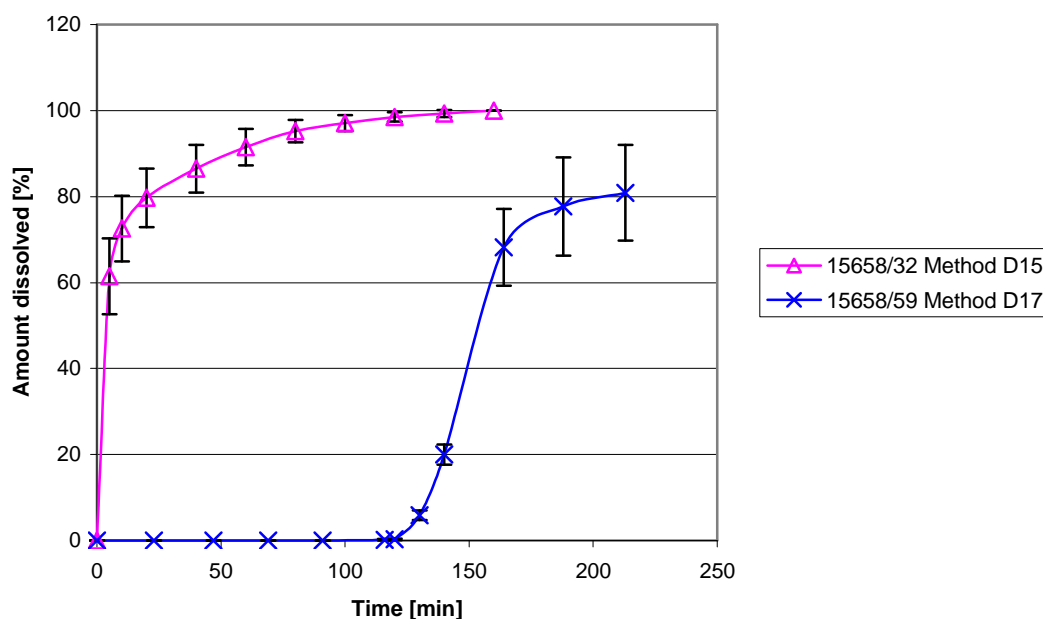


Figure IV.56 Dissolution profile of chitosan uncoated and EUDRAGIT® L 30D 55 coated theophyllin containing micropellets using APP.4 (D15 and D17). Batch 15658/32 was uncoated and batch 15658/59 was the coated formulation. In D15 phosphate buffer pH 6.0 was used during the entire dissolution test. In D17, 0.1N HCl was used during the first two hours and thereafter phosphate buffer pH 6.0 (n=5).

IV.14.3 Summary of the Dissolution Results

For all coated micropellets gastric resistance was achieved during manufacturing. The applied dissolution methods had a high impact on the dissolution profiles. Depending on the method, the dissolution profile changed from immediate release to a slow release pattern for the same dosage form. All dissolution profiles showed an initial burst release followed by a slower release phase due to diffusion-controlled release. The dissolution profile using the Paddle Apparatus (App.2) is highly depending on the agitation rate whereas the dissolution profile using the flow-through cell is highly depending on the particle size of the micropellets. Smaller micropellets can easier slip between the gaps of the glass beads thus pronouncing the coalescence of the smaller micropellets. Consequently the diffusion distance of the drug is increased and the release of the drug is delayed.

IV.15. Evaluation of the Separation of an Enteric Coating Layer from a Mucoadhesive Matrix Layer by Electron Dispersive X-Ray

IV.15.1. Method X1, Evaluation of the Separation of Poured Films

IV.15.1.1. Separation of EUDRAGIT[®] L 30D-55 from Layer Chitosan Film at pH 6.0

The separation of the EUDRAGIT[®] L 30D-55 film from the poured chitosan during the dissolution test is presented in Figure IV.57 (see below). The chitosan film layer was marked with chloride ions. Thus, the EUDRAGIT[®] film layer is characterized by a low chloride concentration and the chitosan film layer is the one with the high chloride concentration. After 2.5 minutes, hardly any EUDRAGIT[®] film was dissolved. After 20 minutes, the EUDRAGIT[®] film was partly dissolved. Furthermore, the remaining thicker parts of the EUDRAGIT[®] layer appear as soft residues compared to their status at the beginning of the test. It can be concluded that the film had swollen, dried and left some cavities and, after 20 minutes, the separation of both layers was not yet complete.

The separation of poured Na-alginate from an EUDRAGIT[®] L 30D-55 film during a dissolution test is presented in Figure IV.58. The Na-alginate film layer exhibits a high concentration of sodium. The EUDRAGIT[®] film layer which is displayed in the Figure on the left hand side contains a low sodium concentration. The Na-alginate film layer, which is displayed on the right hand side exhibited a distinct swelling with the duration of the dissolution process. The film layer increased in thickness along with a decrease of sodium concentration as displayed in the plot of Na⁺-counts versus distance from the surface where the Na⁺-counts decreased from 70 to 10. After 20 minutes of dissolution the EUDRAGIT[®] film was still present.

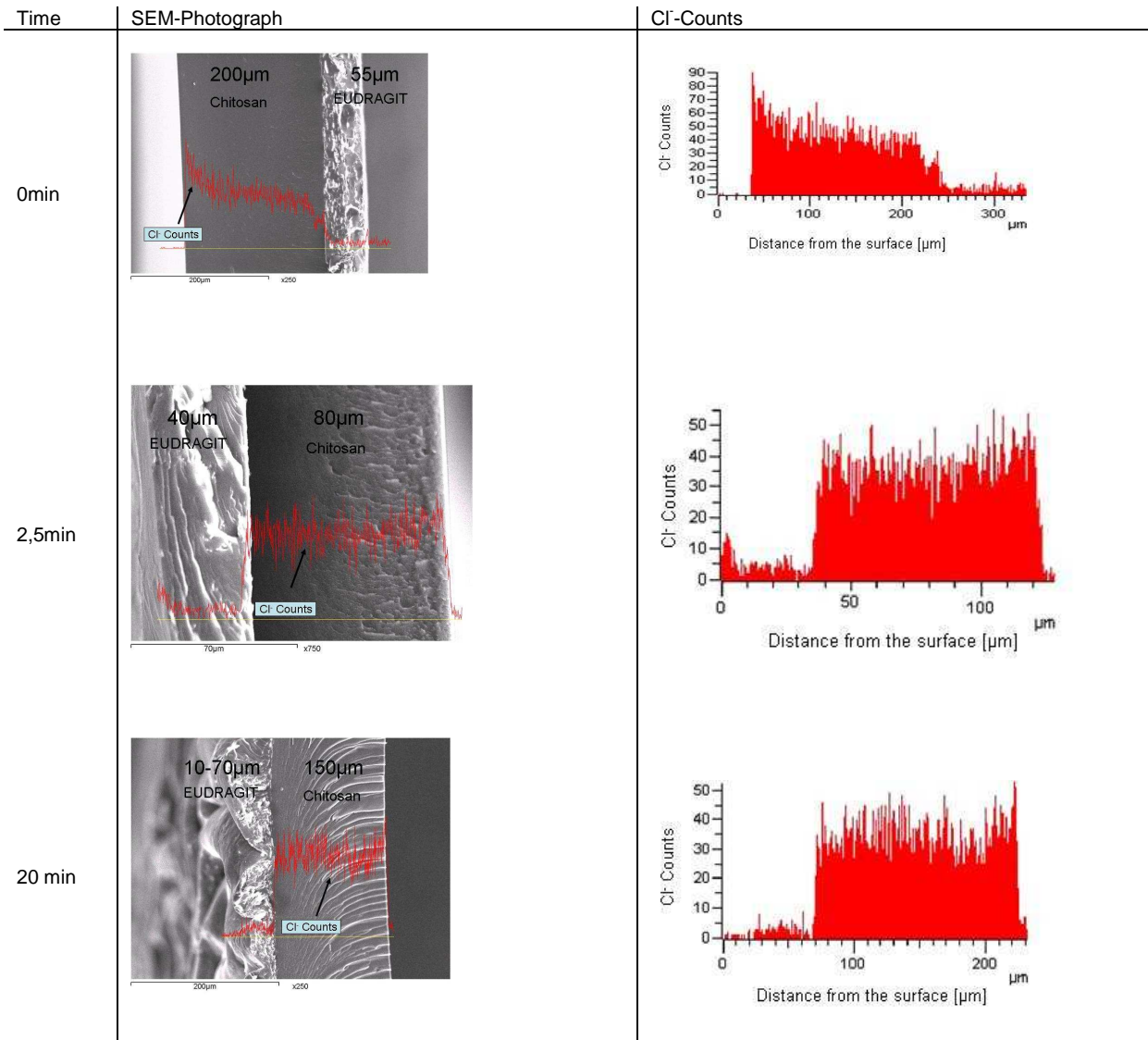


Figure IV.57

EDX of poured EUDRAGIT® L 30D-55 over chitosan film before and following dissolution. In the very left column, the dissolution times are given. In the middle column the SEM-photographs are presented and in right column the counts of chloride are plotted against the distance of the surface. Even after 20 minutes the EUDRAGIT® layer was not completely dissolved from the chitosan layer.

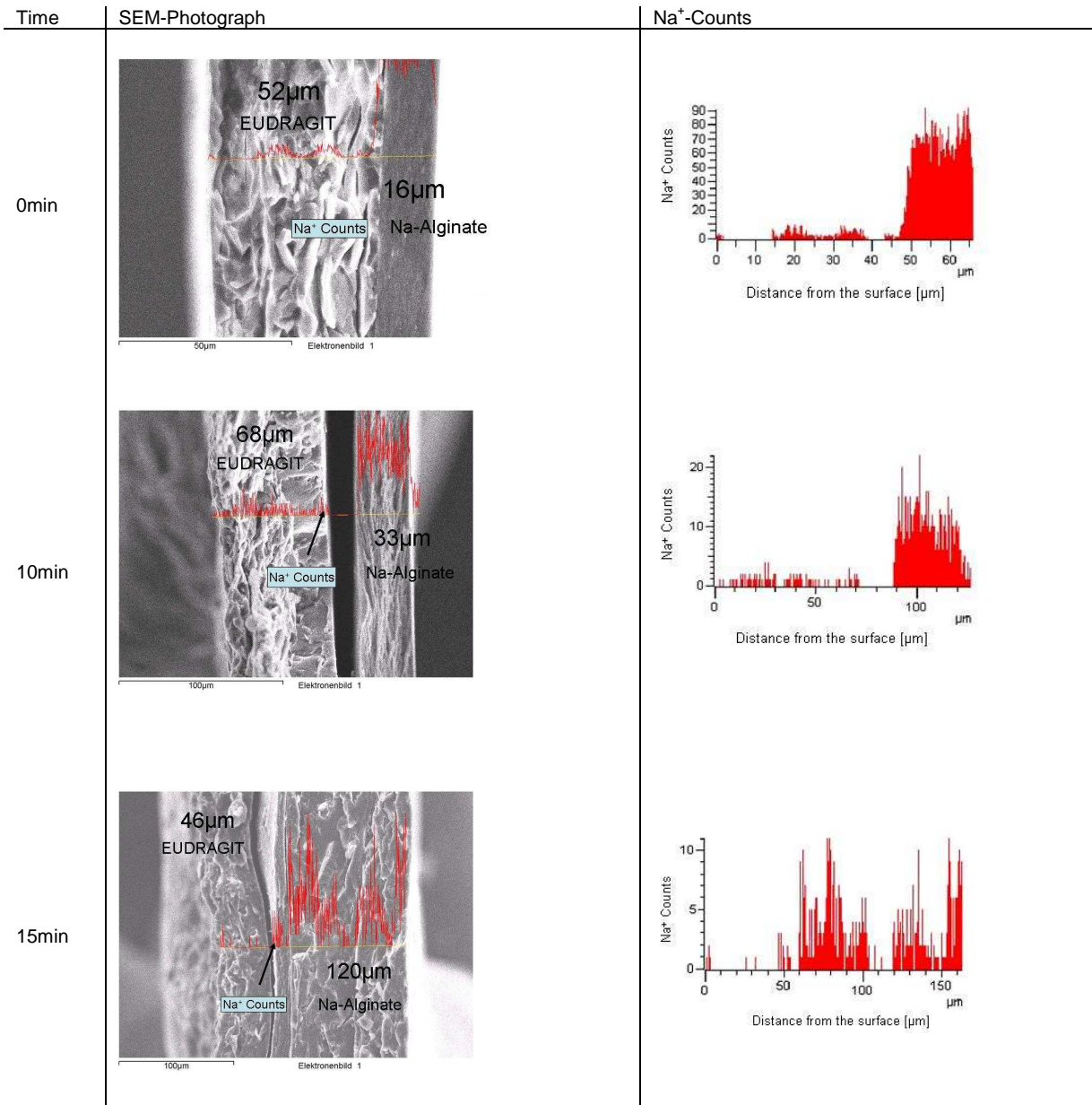


Figure IV.58 EDX of poured EUDRAGIT[®] L 30D-55 over Na-alginate film before and following dissolution. In the very left column, the dissolution times are given. In the middle column the SEM-photographs are presented and in right column the counts of sodium are plotted against the distance of the surface. Even after 15 minutes the EUDRAGIT[®] layer was not completely dissolved from the Na-alginate layer.

IV.15.1.3. Separation of EUDRAGIT[®] FS 30D Layer from Na-CMC Film at pH 7.2

The separation of the poured Na-CMC film from a EUDRAGIT[®] FS 30D layer is presented in Figure IV.59. The EUDRAGIT[®] film layer is displayed in the Figure on the left hand side identified by the low sodium concentration, whereas the Na-CMC film layer is displayed on the right hand side characterized by its high sodium concentration. The EUDRAGIT[®] FS 30D film dissolved completely within 10 to 15 minutes. After 5 minutes the film was partly dissolved and porous. After 10 minutes, a residual 50µm film layer was still remaining (data not shown). At 15 minutes following the start of the dissolution, the EUDRAGIT[®] film layer has completely disappeared.

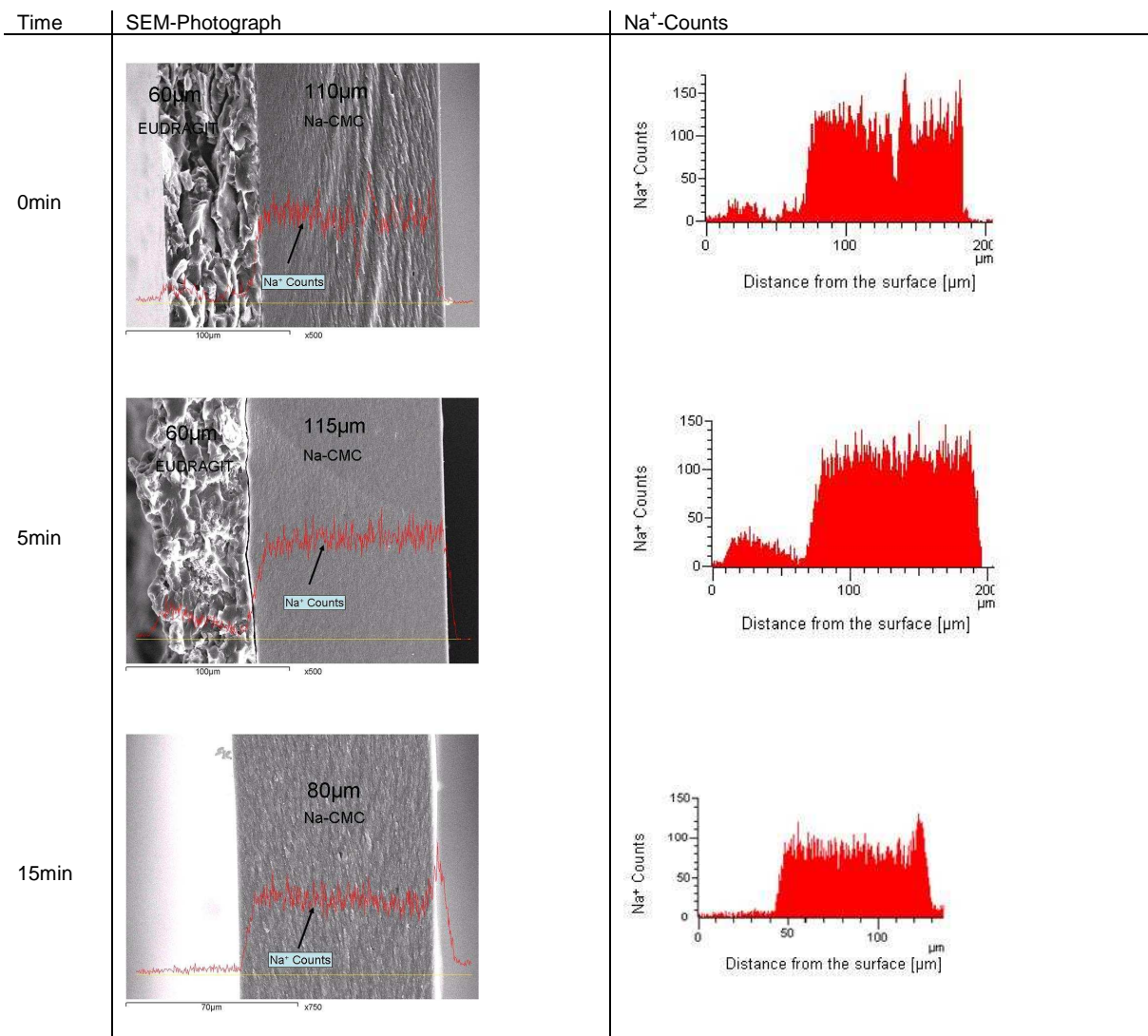


Figure IV.59 EDX of poured EUDRAGIT[®] FS 30D over Na-CMC film before and following dissolution. In the very left column, the dissolution times are given. In the middle column the SEM-photographs are presented and in right column the counts of sodium are plotted against the distance of the surface. The EUDRAGIT[®] FS 30D layer dissolved completely from the Na-CMC layer.

IV.15.2. Method X2, Evaluation of Separation of Multifunctional Polymers using Coated Micropellets

IV.15.2.1. Separation of EUDRAGIT[®] L 30D-55 from Na-CMC Micropellets

The dissolution at pH 6.0 of Na-CMC micropellets coated with EUDRAGIT[®] L 30D-55 is presented in Figure IV.60. The inner core of Na-CMC exhibits a high sodium concentration. Eight minutes following the start of dissolution, the EUDRAGIT[®] layer still remains in place. After 10 minutes, the micropellet is destroyed and no definite conclusion can be drawn with respect to the fate of the EUDRAGIT[®] layer. It may be speculated though that the inner core consisting of swellable Na-CMC expands leading to a burst of the EUDRAGIT[®] film. Therefore, parts of the film may still remain in place while the core is accessible to the dissolution medium.

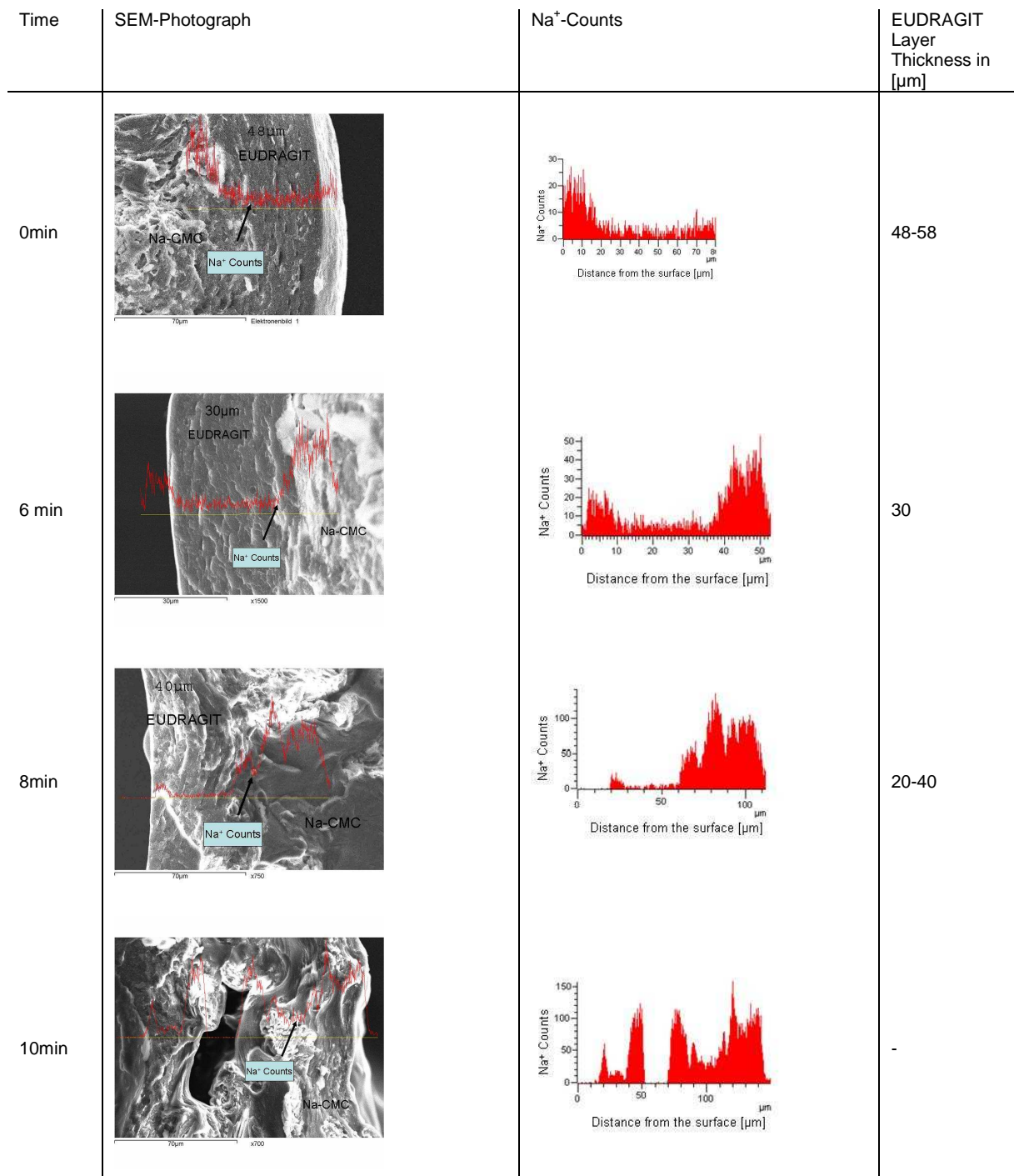


Figure IV.60 EDX of Na-CMC micropellets coated with EUDRAGIT[®] L 30D-55 before and following dissolution. In the very left column, the dissolution times are given. In the middle column the SEM-photographs are presented and in right column the counts of sodium are plotted against the distance of the surface. Eight minutes following the start of dissolution, the EUDRAGIT[®] layer still remains in place. After 10 minutes, the micropellet is destroyed and no definite conclusion can be drawn with respect to the fate of the EUDRAGIT[®] layer

IV.15.2.2. Separation of EUDRAGIT L 30D-55 Layer from Chitosan Micropellets

The dissolution of chitosan micropellets coated with EUDRAGIT[®] L 30D-55 is presented in Figure IV.61. In the Figure, only SEM pictures are presented since nitrogen, the marker element of the chitosan layer was not detectable by EDX,

because the emitted spectrum is weaker of the nitrogen and simultaneously overlapped from the carbon and oxygen spectra. In addition, both elements also have a higher concentration within the chitosan. Nevertheless, the two layers can be differentiated by their structure. The EUDRAGIT[®] layer dissolved slowly. After 12.5 minutes a layer still remained. After 15 minutes one part of the pellets burst (see first picture next page) whereas some still remain intact while showing initial signs of burst. As can be seen on the fourth picture of the row displaying bursting micropellets, some EUDRAGIT[®] still remained in place following a burst of the pellets.

Time	SEM-Photograph	EUDRAGIT Layer Thickness in [μ m]	Comments
0min		50-70	Solid EUDRAGIT layer before dissolution
10min		20-25	More than 50% of the EUDRAGIT are dissolved
12min 30sec		10-25	Micropellet with thin EUDRAGIT layer
15min		5-20	Micropellets with initial sign of burst

Figure IV.61/1 SEM of Chitosan micropellets coated with EUDRAGIT[®] L 30D-55 before and following dissolution. In the very left column, the dissolution times are given. In the middle left column the SEM-photograph is presented and in middle right column the thickness of the EUDRAGIT[®] layer is given. EUDRAGIT[®] still remained in place following a burst of the pellets.

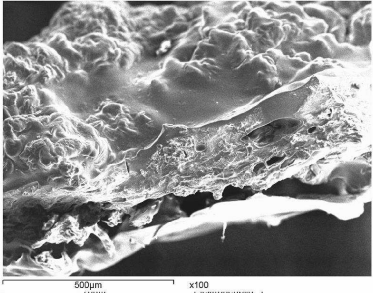
Time	SEM-Photograph	EUDRAGIT Layer Thickness in [μm]	Comments
15min		-	Bursting micropellet

Figure IV.61/2 SEM of Chitosan micropellets coated with EUDRAGIT[®] L 30D-55 before and following dissolution. In the very left column, the dissolution times are given. After 15 minutes one part of the pellets burst whereas some still remain intact while showing initial signs of burst. EUDRAGIT[®] still remained in place following a burst of the pellets.

IV.15.2.3. Separation of EUDRAGIT L 30D-55 from Na-Alginate Micropellets

The dissolution of Na-alginate micropellets coated with EUDRAGIT L 30D-55 is presented in Figure IV.62. In the Figure, only SEM pictures are presented due to failure of the EDX method. Nevertheless, the two layers can be differentiated by their structure. After 5 minutes of dissolution, a layer of EUDRAGIT[®] ranging 10-45 μm in thickness still remained. Beyond the 5 minutes time point the micropellets coalesce such that differential analysis was not undertaken.

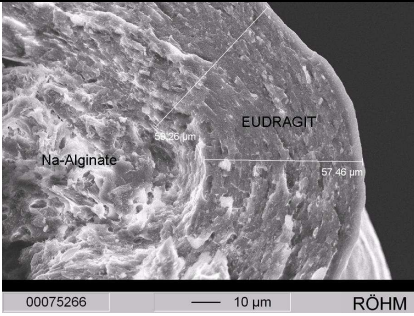
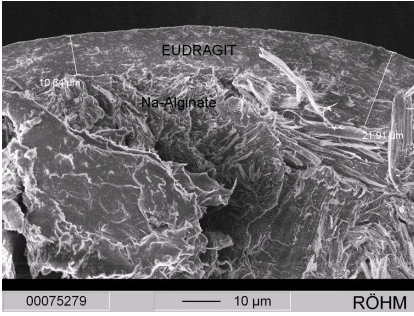
Time	SEM-Photograph	EUDRAGIT [®] Layer Thickness [μm]
0min		57
5min		10-45

Figure IV.62 SEM of Na-alginate micropellets coated with EUDRAGIT[®] L 30D-55 before and following dissolution. In the very left column, the dissolution times are given. In the middle column the SEM-photographs are presented and in right column the thickness of the EUDRAGIT[®] layer is given.

IV.15.3. Summary on Separation of an Enteric Layer from the Mucoadhesive Polymer

The EUDRAGIT[®] FS 30D layer dissolved completely at pH 7.2 within 15 minutes from the mucoadhesive layer. Hence mucoadhesion may in principle be operative after 15 minutes. An even earlier onset of mucoadhesion would be achieved in case the enteric coating layer was constructed to be thinner. In contrast, the dissolution of EUDRAGIT[®] L 30D-55 was slow at pH 6.0. Thus even after 20 minutes, in the case of a poured film, EUDRAGIT[®] remained on the surface. Presumably, the mucoadhesive micropellets burst before the complete EUDRAGIT[®] film was dissolved, which was caused by the high swelling capacity of the mucoadhesive polymer within the core of the micropellets.

IV.16. Improving the Solubility of Lipophilic Drugs in Lipid Matrices

The dissolution of a drug in aqueous solvents might be improved when the matrix, within the drug is dispersed, has a similar lipophilicity as the drug. As characteristic values for lipophilicity the logP and the HLB value were selected. The logP is accessible by calculation using different computer programs as described in Chapter III.4.5.1. In contrast, the logP of lipids is not accessible by calculation since most lipids are mixtures of mono-, di-, and triglycerides of different fatty acids. In these cases, the HLB value - instead of the logP - is accessible by calculation as described in the same Chapter. To combine the system of logP and HLB, logP values of emulsifiers with known HLB values were calculated and plotted. On the basis of the correlation between HLB and logP, one of each variable thus may be calculated from the other.

IV.16.1. Correlation Between HLB and logP

In Figures IV.63 to IV.68, different logP values were plotted against the HLB values to determine the most appropriate logP value of different emulsifiers presented in Table IV.27.

Table IV.27 HLB values and LogPs of different emulsifiers.

Emulsifier	HLB	M logP ²	S+log P	A LOGPs	X logP	C LOGP	Kowwin ³
Polyoxyethylen10cetylolether (Brij 56)	12.90	0.84	4.05	4.23	4.30	5.97	3.99
Polyoxyethylen10oleylether (Brij 96)	12.40	1.05	4.38	4.93	4.71	6.54	4.76
Polyoxyethylen10stearylether (Brij 76)	12.40	1.19	4.68	4.80	5.23	7.03	4.97
Polyoxyethylen20cetylolether (Brij 58)	15.70	-2.87	4.27	2.62	2.40	4.61	1.25
Polyoxyethylen20oleylether (Brij 98)	15.30	-2.72	4.58	3.01	2.81	5.19	2.01
Polyoxyethylen20stearylether (Brij 78)	15.30	-2.57	4.76	3.02	3.33	5.67	2.23
Polyoxyethylen2cetylolether (Brij 52)	5.30	3.73	6.03	7.13	5.82	7.05	6.19
Polyoxyethylen2oleylether (Brij 92)	4.90	4.03	6.46	7.69	6.23	7.63	6.95
Polyoxyethylen2stearylether (Brij 72)	4.90	4.17	6.73	7.93	6.75	8.11	7.17
Polyoxyethylen40stearat (Myrj 52)	16.90	-10.69	4.95	1.80	-0.78	2.90	-3.44
Polyoxyethylen423aurylether (Brij 35)	16.90	-4.58	3.50	1.53	1.03	2.09	-1.54
Polyoxyethylen4laurylether (Brij 30)	9.70	2.14	3.93	4.48	4.64	4.67	3.67
Polyoxyethylen50stearat (Myrj 53)	17.90	-14.63	4.87	1.61	-2.68	n.a. ¹	-6.19
Polyoxyethylen8stearat (Myrj 45)	11.10	1.46	4.90	5.50	5.30	7.24	5.34
Polyoxythylen20sorbitanmonolaurat (Tween 20)	16.70	-6.04	1.70	0.85	-0.56	1.45	-3.40
Polyoxythylen20sorbitanmonooleat (Tween 80)	15.00	-5.28	3.15	2.09	0.65	4.14	-0.67
Polyoxythylen20sorbitanmonopalmitat (Tween 40)	15.60	-5.46	2.85	1.66	0.23	3.57	-1.43
Polyoxythylen20sorbitanmonostearat (Tween 60)	14.90	-5.18	3.39	2.07	1.16	4.62	-0.45
Polyoxythylen20sorbitantrioleat (Tween 85)	11.00	-1.51	8.62	6.81	n.d.	21.89	16.22
Polyoxythylen20sorbitantristearat (Tween 65)	10.50	-1.25	8.8	6.49	n.d.	23.34	16.87
Polyoxythylen4sorbitanmonolaurat (Tween 21)	13.30	-0.46	1.95	2.73	2.48	3.62	0.99
Polyoxythylen4sorbitanmonostearat (Tween 61)	9.60	0.70	4.18	4.85	4.20	6.79	3.94
Polyoxythylen5sorbitanmonooleat (Tween 81)	10.00	0.24	3.48	4.72	3.50	6.17	3.45
Saccharosediesterat	7.00	2.15	7.51	7.85	11.19	14.57	13.86
Saccharosedioleat	7.20	1.97	6.88	7.58	10.16	13.6	13.43
Saccharosedipalmitat	7.40	1.51	6.64	7.00	9.34	12.45	11.90
Saccharosemonooleat	11.20	-0.63	1.86	3.33	2.84	5.38	5.00
Saccharosemonolaurat	13.00	-1.70	0.18	1.17	1.63	2.69	2.27
Saccharosemonomyristat	12.30	-1.30	0.84	1.82	1.50	3.74	3.25
Saccharosemonopalmitat	11.70	-0.90	1.55	2.70	2.43	4.80	4.23
Saccharosemonostearat	11.20	-0.52	2.28	3.42	3.35	5.86	5.22
Sorbitanmonolaurat (Span 20)	8.60	0.77	2.40	3.12	3.88	4.09	3.15
Sorbitanmonooleat (Span 80)	4.30	1.99	4.53	5.25	5.09	6.78	5.89
Sorbitanmonopalmitat (Span 40)	6.70	1.68	4.11	4.61	4.68	6.21	5.12
Sorbitanmonostearat (Span 60)	4.70	2.10	4.91	5.42	5.61	7.27	6.10
Sorbitantrioleat (Span 85)	1.80	7.08	11.29	10.34	19.30	23.79	21.71
Sorbitantristearat (Span 65)	2.10	7.34	11.61	10.22	20.85	25.25	22.35

¹ n.a. :The software was not able to calculate the value.² Moriguchi logP.³ Kowwin logP.

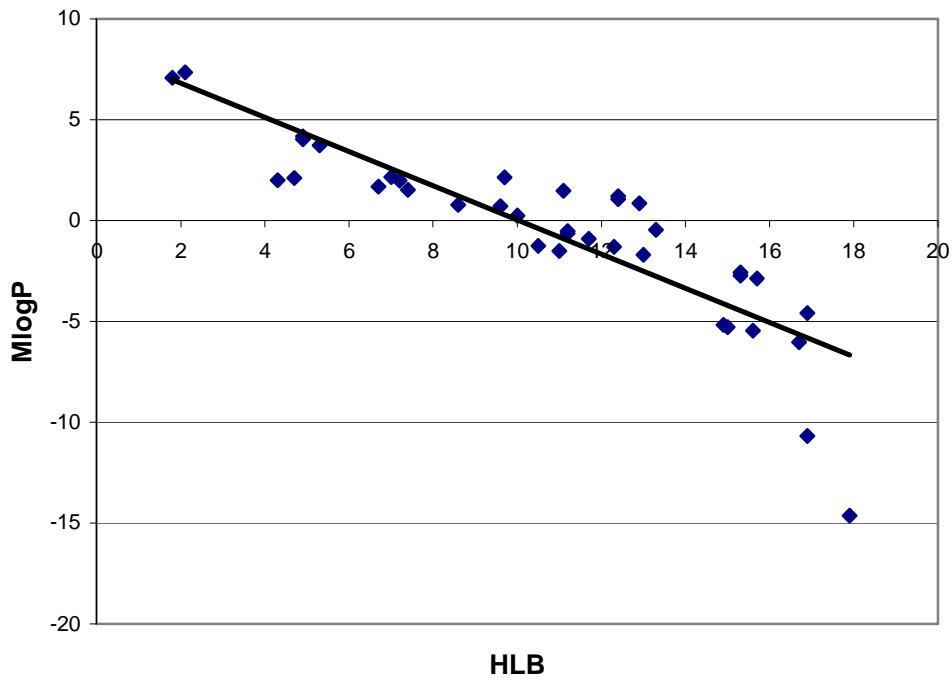


Figure IV.63 Relationship between HLB value and Moriguchi logP of the different emulsifiers presented in Table IV.28. The coefficient of determination was 0.7257, the linear equation was $y = -0.8479x + 8.5079$.

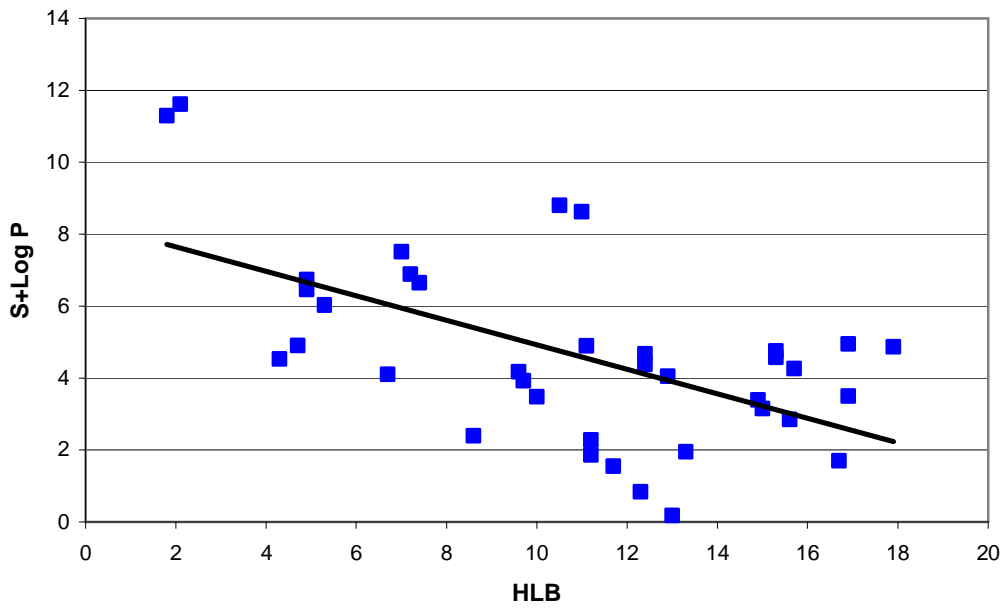


Figure IV.64 Relationship between HLB value and S+logP of the different emulsifiers presented in Table IV.28. The coefficient of determination was 0.3363, the linear equation was $y = -0.3398x + 8.320$.

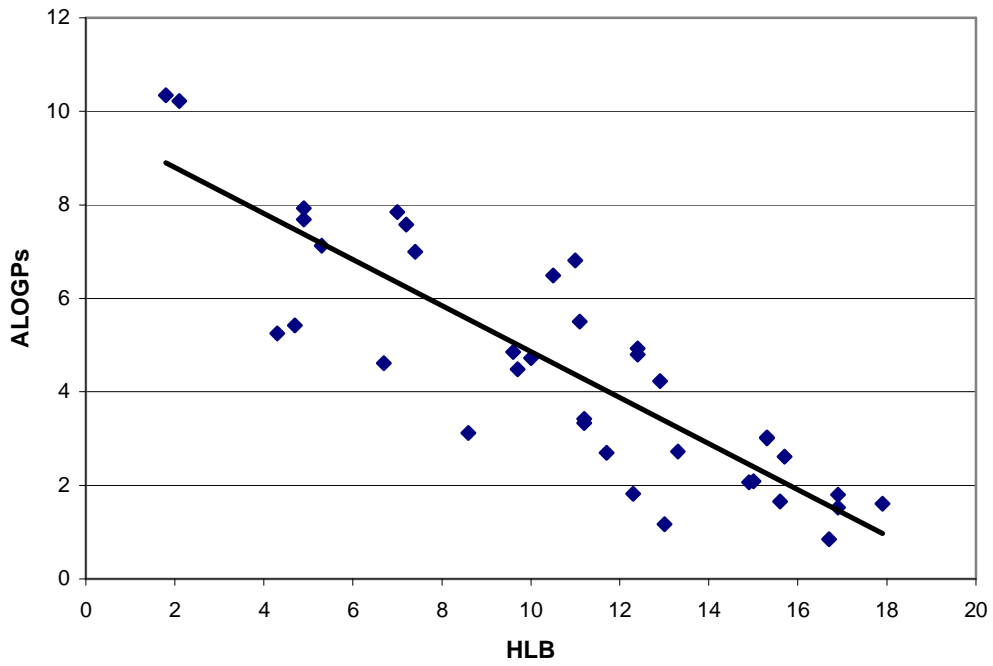


Figure IV.65 Relationship between HLB Value and ALOGPs of the different emulsifiers presented in Table IV.28. The coefficient of determination was 0.7441, the linear equation was $y = -0.4919x + 9.78$.

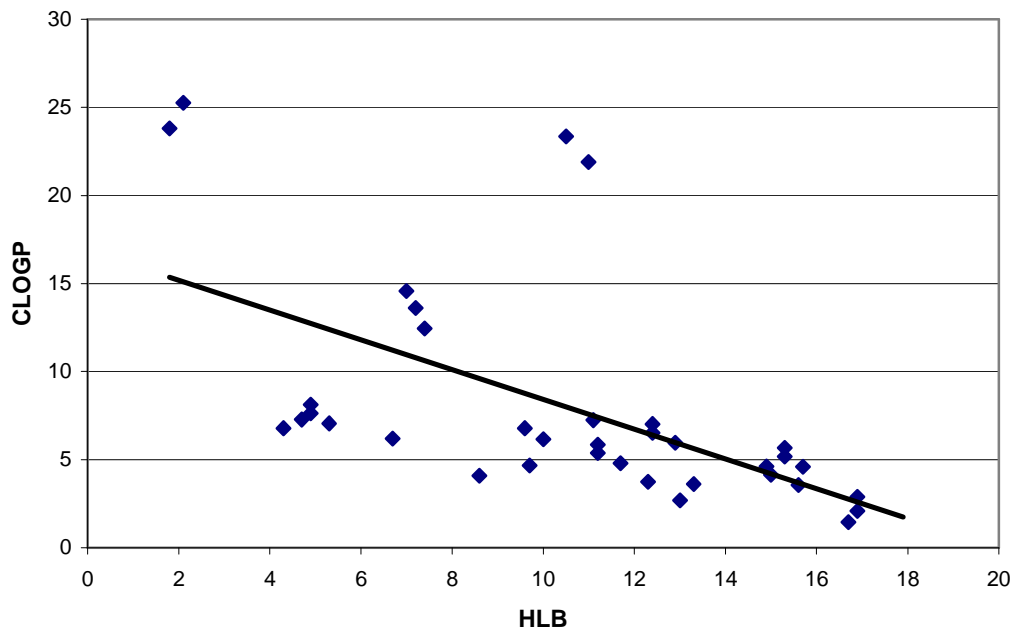


Figure IV.66 Relationship between HLB value and CLOGP of the different emulsifiers presented in Table IV.28. The coefficient of determination was 0.339. The linear equation was $y = -0.8454x + 16.877$.

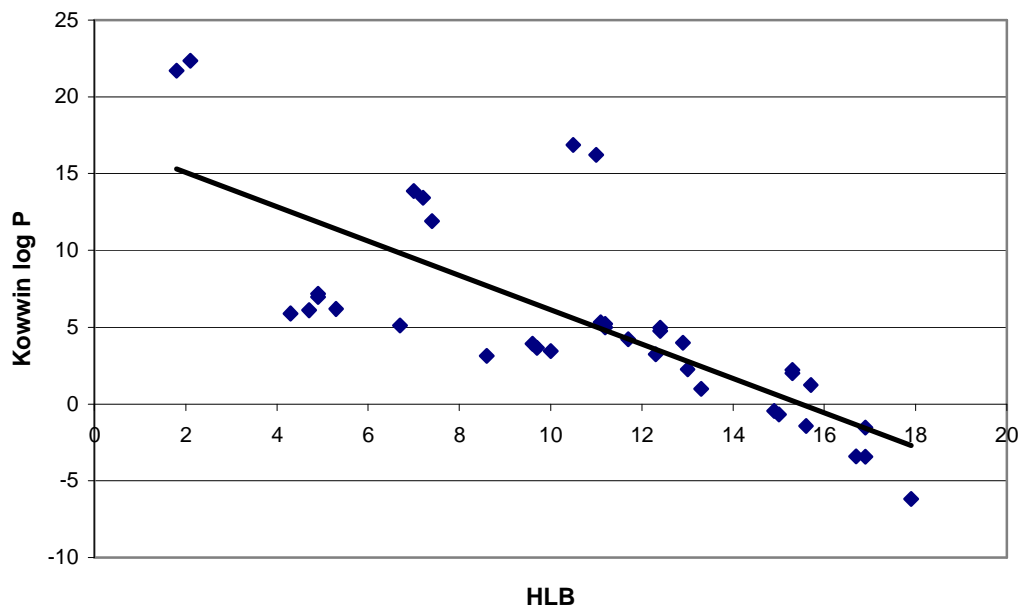


Figure IV.67 Relationship between HLB value and Kowwin LogP of the different emulsifiers presented in Table IV.28. The coefficient of determination was 0.5748, the linear equation was $y = -1.1176x + 17.31$.

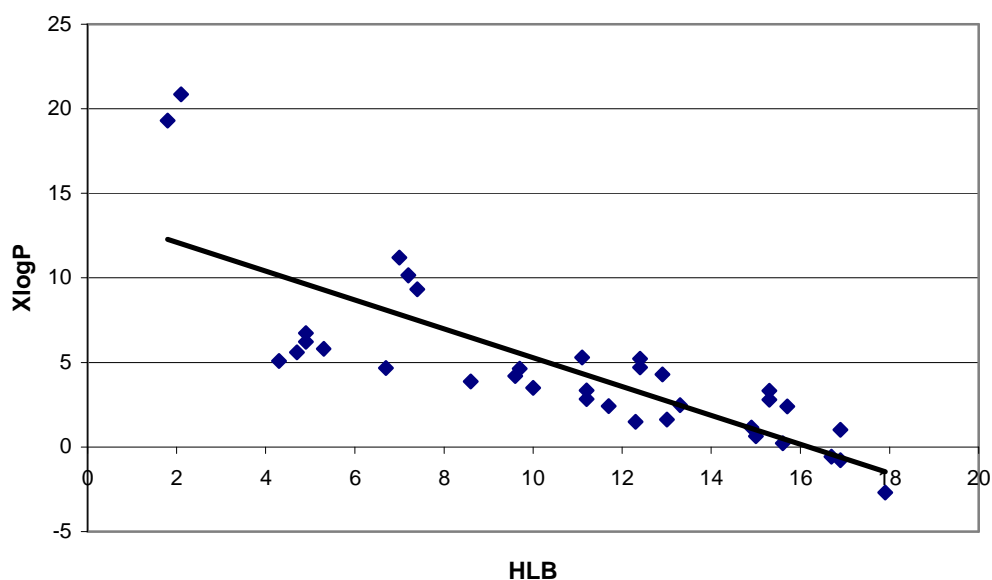


Figure IV.68 Relationship between HLB value and XLOGP of the different emulsifiers presented in Table IV.28. The coefficient of determination was 0.6432, the linear equation was $y = -0.8538x + 13.815$.

The correlation between Moriguchi logP and HLB appears to present the most representative method. This is based on the fact that the calculation of the Moriguchi logP leads to negative logP values for hydrophilic compounds, e.g. Tween 80, whereas the ALOGPS always result in positive values. Furthermore a Moriguchi logP of 0 is equivalent to an HLB value of 10. A logP of 0 reflects that a substance is as soluble in water as in the lipophilic phase, an HLB value of 10 in contrast reflects, that the molecular structure is characterized by 50% of lipophilic structures and by 50% of hydrophilic structures.

IV.16.2. Estimation of the HLB Value of Different Lipid Matrices and of Spirolactone

The HLB values presented in Table IV.28 are given by the manufacturer of the lipid matrices or were calculated by the following equation explained in Chapter III.4.5.1.

Table IV.28 HLB Values of Different Lipid Matrices.

Compound	HLB Value (manufacturer)	HLB Value (calculated)
Imwitor 308	4-5	
Imwitor 312	3-4	
Imwitor 742	3-4	
Softisan 138		1.71
Softisan 158		0.72
Vitamin E TPGS	17-19	

$$HLB = 20 \times \left(1 - \frac{SV}{AV} \right)$$

SV = Saponification value;

AV= Acid value of the fatty acid of the glyceride.

For vitamin E acetate and spironolactone the Moriguchi logP was calculated first and then a HLB of 2.84 for vitamin E acetate and 6.06 for spironolactone was calculated based on the linear equation between the Moriguchi logP and HLB.

IV.16.3. Determination of the Solubility of Spirolactone in Different Single Lipid Matrices

Blends with contents ranging from 5 to 50% of spironolactone and six single lipid matrices were prepared. These six lipids were: Imwitor 308, a glycerol monocaprylate with a monoester content higher as 80% listed in the USP as glyceryl caprylate; Imwitor 312, a glycerol monolaurate with a monoester content higher than 90%; Imwitor 742, a blend of mono-, di-and triglycerides mainly containing caprylic and capric acid listed in the DAB as "mittelkettige Partialglyceride"; Softisan 138, a hard fat registered as hydrogenated palm oil with a melting point of 38°C and two Vitamin E derivatives: Vitamin E acetate and Vitamin E TPGS. The blends, the lipids and spironolactone alone were analysed using the DSC method. In blends with a single endothermic peak near the melting peak of the lipid, spironolactone was completely soluble. In contrast in blends with two melting peaks, spironolactone was not completely soluble.

In Figure IV.69, the DSC curve of the pure spironolactone is presented.

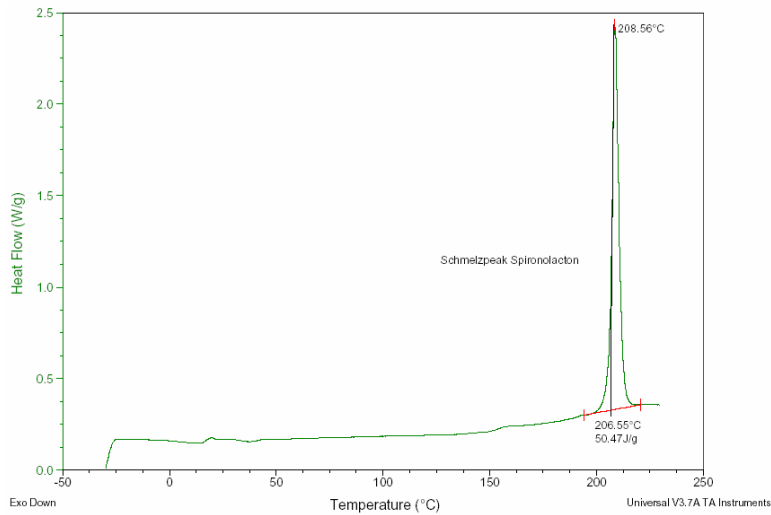


Figure IV.69 DSC curve of pure spironolactone. Spironolactone has an endothermic melting peak of 50.47 J/g at an onset of 206.55°C.

IV.16.3.1. Estimation of the Solubility of Spironolactone in Softisan 138

In the Figures IV.70 – IV.75, the DSC curves of different blends of Softisan 138 and spironolactone are presented.

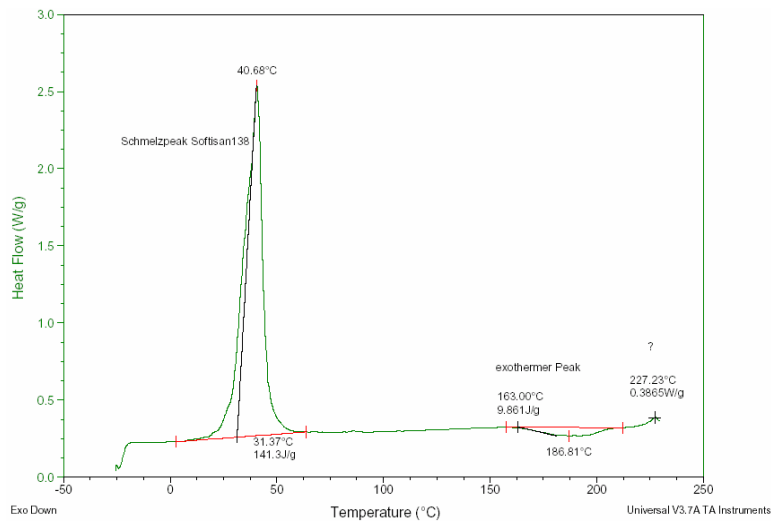


Figure IV.70 DSC curve of Softisan 138. Softisan 138 has an endothermic melting peak of 141.3 J/g at an onset of 31.37°C and an exothermic peak of decomposition of 9.861 J/g at an onset of 163°C.

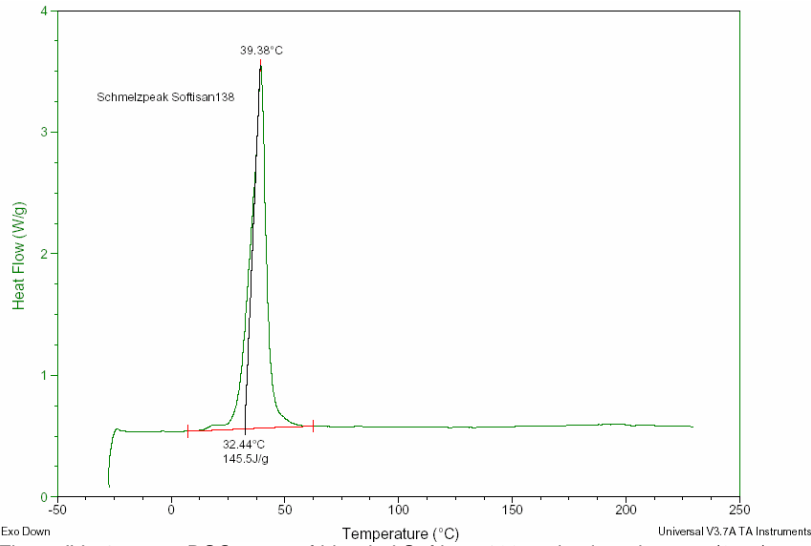


Figure IV.71 DSC curve of blended Softisan 138 and spirinolactone (95:5). The blend has an endothermic melting peak from Softisan 138 of 145.5 J/g at an onset of 32.44°C.

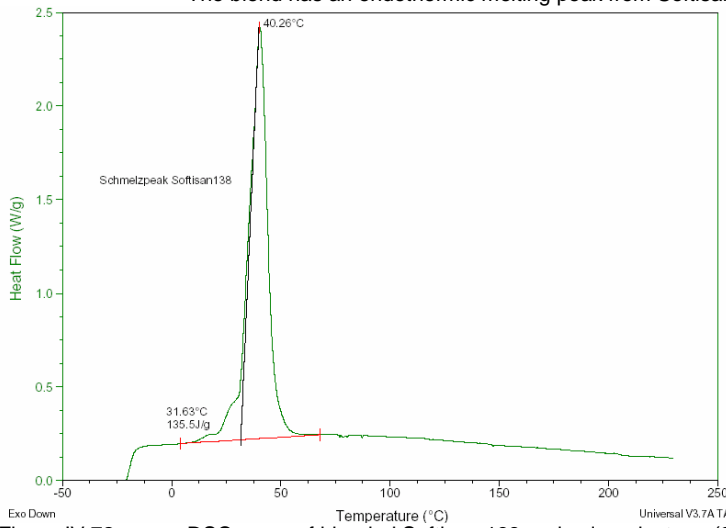


Figure IV.72 DSC curve of blended Softisan 138 and spirinolactone (90:10). The blend has an endothermic melting peak from Softisan 138 of 135.5 J/g at an onset of 31.63°C.

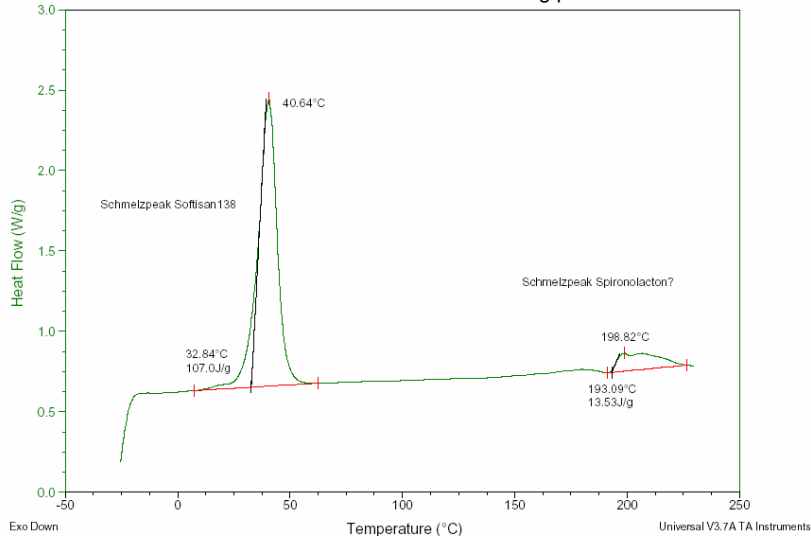


Figure IV.73 DSC curve of blended Softisan 138 and spirinolactone (70:30). The blend has an endothermic melting peak from Softisan 138 of 107.5 J/g at an onset of 32.84°C and a second endothermic melting peak from spirinolactone of 13.53 J/g at an onset of 193.09°C.

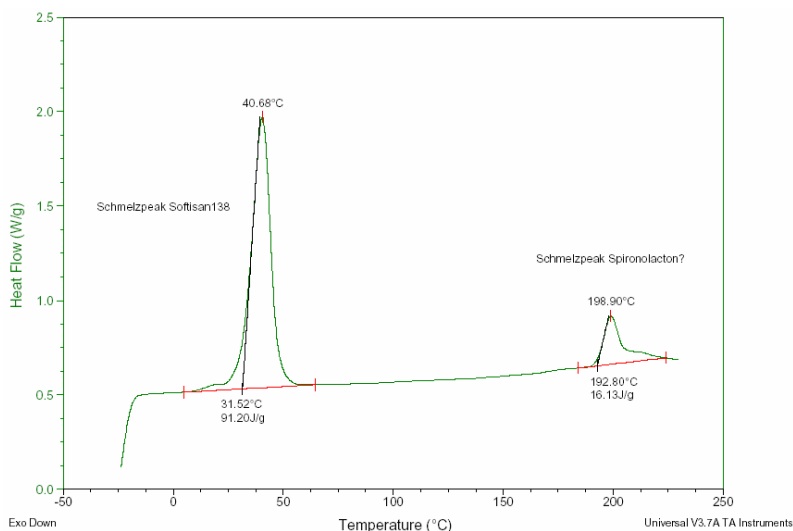


Figure IV.74 DSC curve of blended Softisan 138 and spironolactone (60:40). The blend has an endothermic melting peak from Softisan 138 of 91.20 J/g at an onset of 31.52°C and a second endothermic melting peak from spironolactone of 16.13 J/g at an onset of 192.80°C.

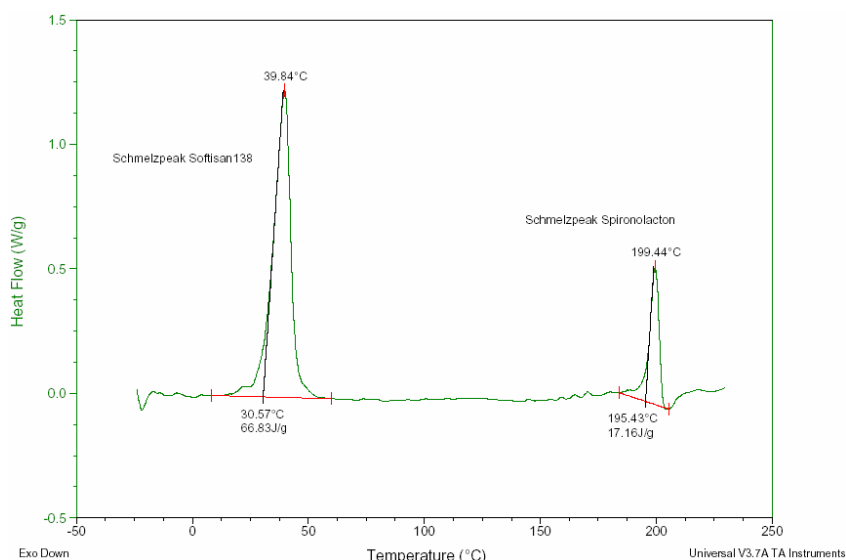


Figure IV.75 DSC Curve of blended Softisan 138 and Spironolactone (50:50). The blend has an endothermic melting peak from Softisan 138 of 66.83 J/g at an onset of 30.57°C and a second endothermic melting peak from spironolactone of 17.16 J/g at an onset of 195.43°C.

The DSC curve of Softisan showed an exothermic peak at 186.81°C which was close to the endothermic melting peak of spironolactone at 206.55°C. The exothermic peak is not obvious at 5% and 10% spironolactone concentration. Therefore, an interference cannot be excluded. Assuming no relevant interference, the borderline of the solubility of spironolactone in Softisan 138 is estimated between 10% and 30% in Softisan 138. In opposite by assuming, that the exothermic decomposition peak of Softisan 138 in Figure IV.71 and IV.72 was erased exactly by the endothermic melting peak of spironolactone, the the borderline of the solubility of spironolactone in Softisan 138 would be only ranging at 0% to 5%. The exothermic peak may display decomposition by pyrolysis, polymerization or hydration.

IV.16.3.2. Solubility of Spironolactone in Softisan 154

In Figure IV.76, the DSC curve of Softisan 154 is presented. In Figures IV.77 – IV.82, the DSC curves of different blends of Softisan 154 and spironolactone are presented.

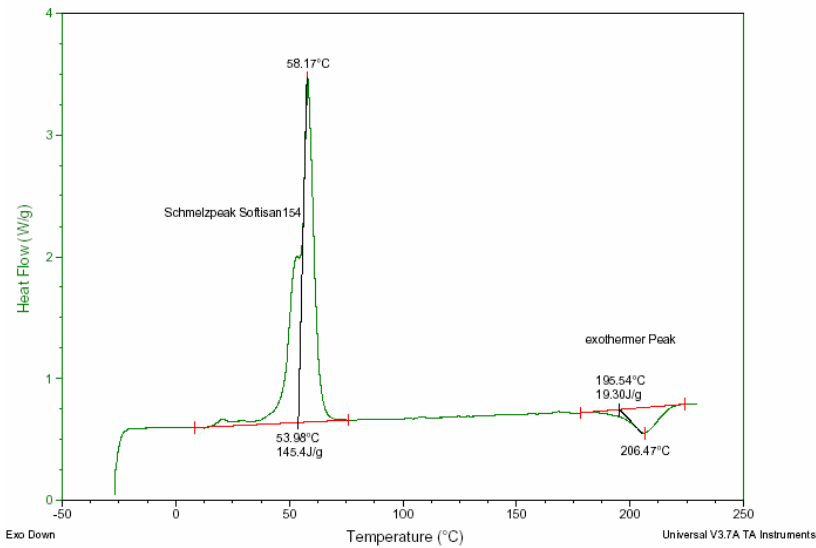


Figure IV.76 DSC curve of Softisan 154. Softisan 154 has an endothermic melting peak of 145.4 J/g at an onset of 53.98°C and an exothermic peak of decomposition of 19.30 J/g at an onset of 195.54°C.

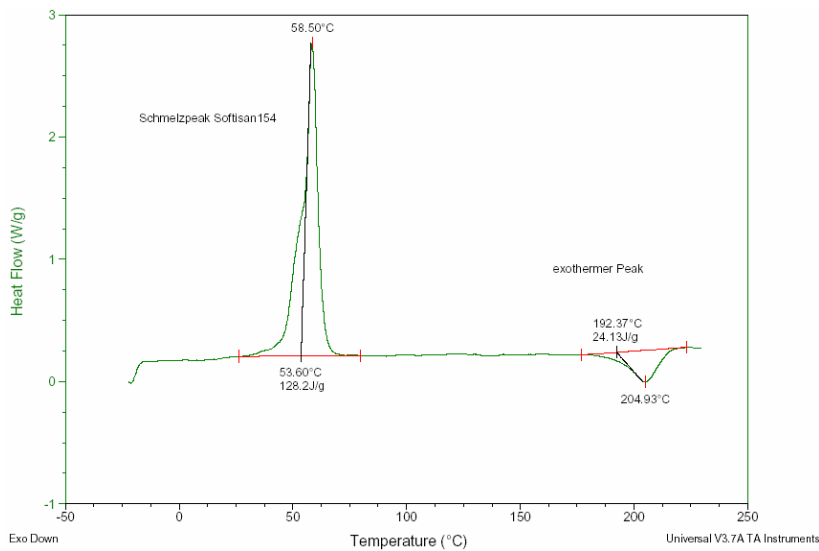


Figure IV.77 DSC curve of blended Softisan 154 and spirinolactone (95:05). The blend has an endothermic melting peak from Softisan 154 of 145.4 J/g at an onset of 53.98°C and an exothermic peak of decomposition of 24.13 J/g at an onset of 192.37°C.

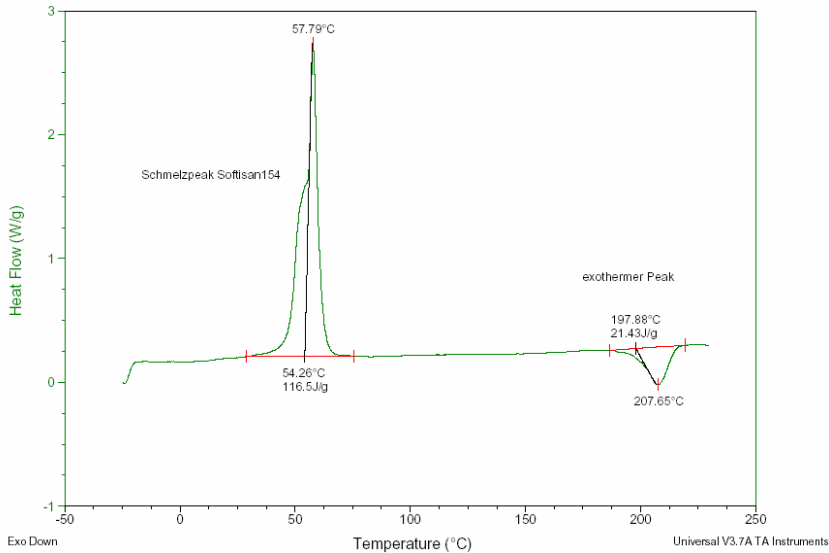


Figure IV.78 DSC curve of blended Softisan 154 and spirinolactone (90:10). The blend has an endothermic melting peak from Softisan 154 of 116.5 J/g at an onset of 54.26°C and an exothermic peak of decomposition of 21.43 J/g at an onset of 197.88°C.

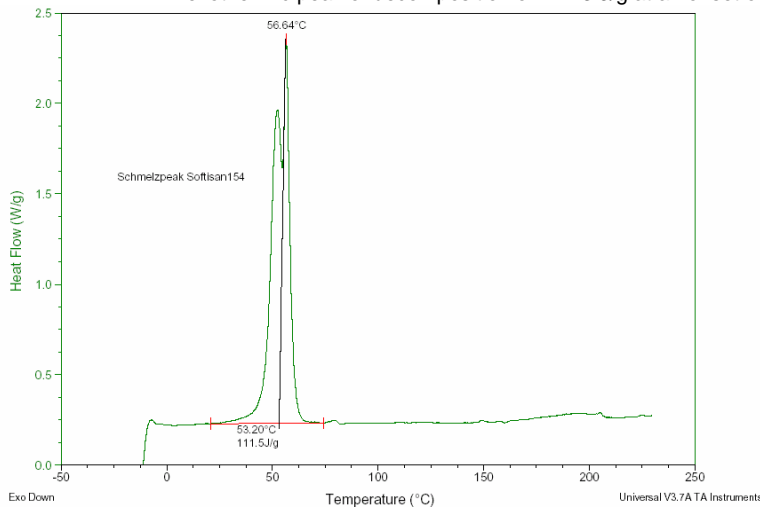


Figure IV.79 DSC curve of blended Softisan 154 and spirinolactone (80:20). The blend has an endothermic double melting peak from Softisan 154 of 111.5 J/g at an onset of 53.20°C and no further exothermic peak of decomposition.

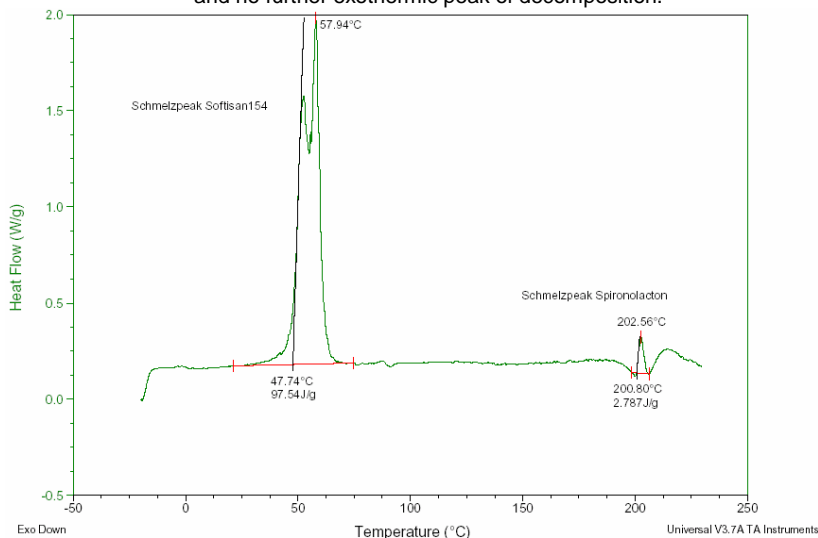


Figure IV.80 DSC curve of blended Softisan 154 and spirinolactone (70:30). The blend has an endothermic double melting peak from Softisan 154 of 111.5 J/g at an onset of 47.74°C and an exothermic peak of decomposition overlapped by a second endothermic melting peak from spirinolactone of resulting 2.79 J/g at an onset of 200.80 °C.

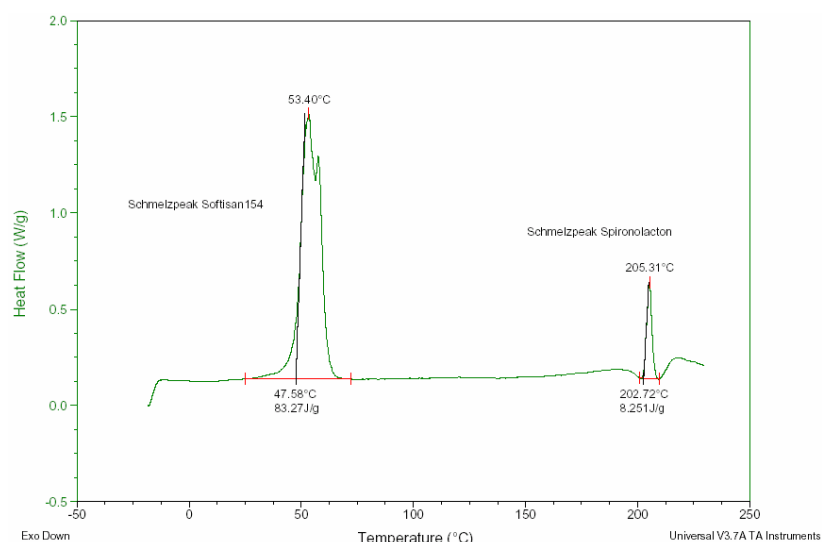


Figure IV.81 DSC curve of blended Softisan 154 and spirinolactone (60:40). The blend has an endothermic double melting peak from Softisan 154 of 83.27 J/g at an onset of 47.58°C and an exothermic peak of decomposition overlapped by a second endothermic melting peak from spirinolactone of resulting 8.25 J/g at an onset of 202.72°C.

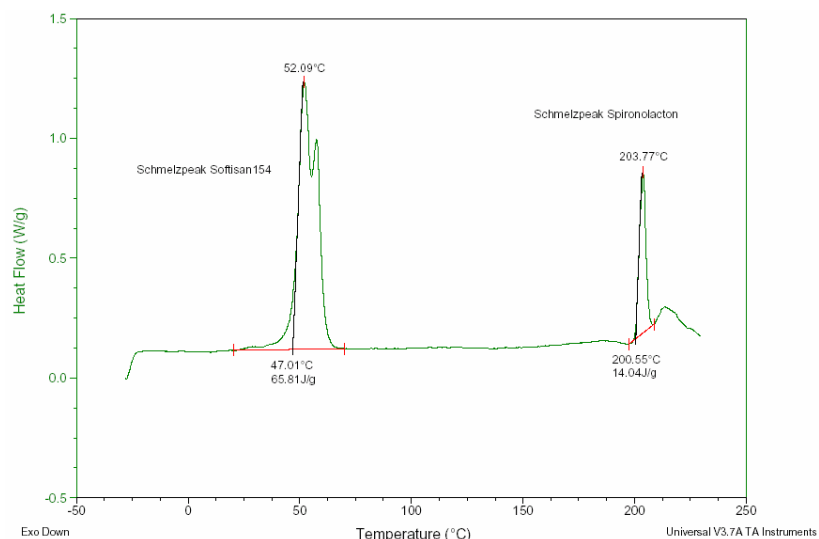


Figure IV.82 DSC curve of blended Softisan 154 and spirinolactone (50:50). The blend has an endothermic double melting peak from Softisan 154 of 65.81 J/g at an onset of 47.01°C and an exothermic peak of decomposition overlapped by a second endothermic melting peak from spirinolactone of resulting 14.04 J/g at an onset of 200.55°C.

The DSC curve of Softisan 154 showed an exothermic peak at 205°C, which was directly overlapping the endothermic melting peak of spirinolactone. The exothermic peak did not appear in the DSC curve at a spirinolactone content of 20%. Assuming no interferences in the DSCs of lipid matrix and spirinolactone the solubility of spirinolactone in the lipid matrix is estimated between 20% and 30% by weight. In contrast, by assuming that the exothermic decomposition peak was erased by the endothermic melting peak of spirinolactone, the borderline of the solubility of spirinolactone in Softisan 154 can be estimated between 10% and 20% by weight. The exothermic peak may display decomposition by pyrolysis, polymerization or hydration.

IV.16.3.3. Solubility of Spirolactone in Vitamin E TPGS

In Figure IV.83, the DSC curve of Vitamin E TPGS is presented. In Figures IV.84 – IV.89, the DSC curves of different blends of Vitamin E TPGS and spironolactone are presented.

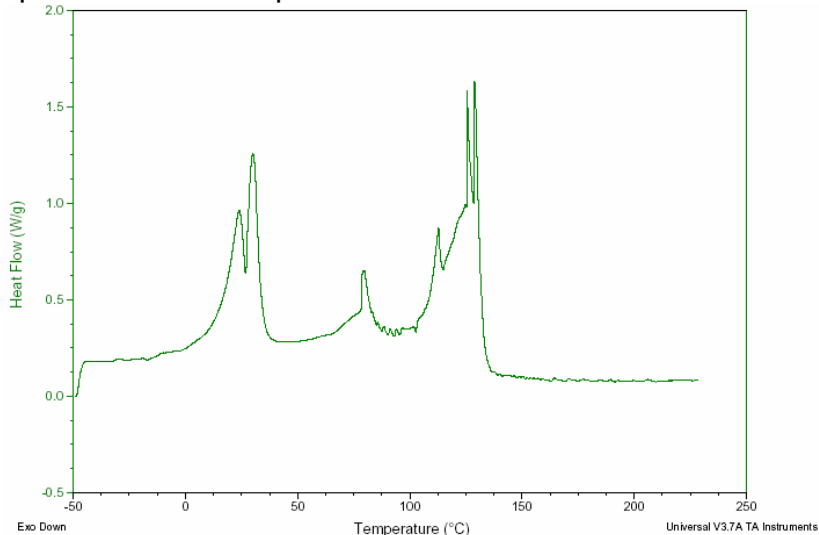


Figure IV.83 DSC curve of vitamin E TPGS.

The vitamin E TPGS has no definite melting point and exhibits different endothermic peaks over a broad temperature range which can be caused by different modifications or chain lengths of the vitamin E TPGS.

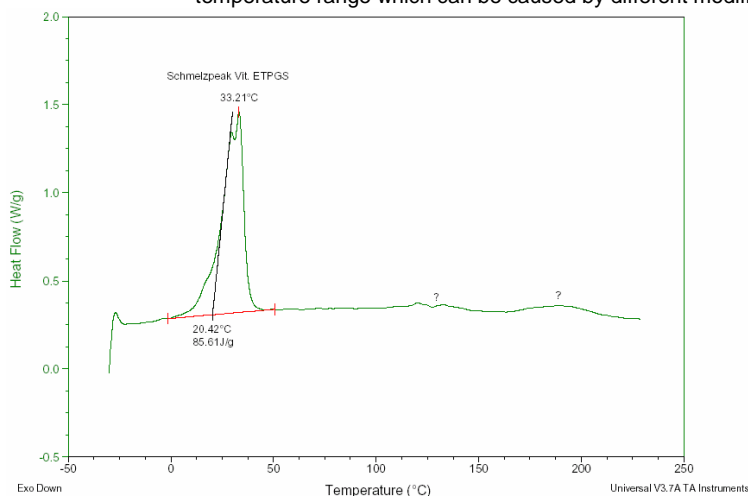


Figure IV.84 DSC curve of blended vitamin E TPGS and spironolactone (95:05).

However, the blend has a single endothermic melting peak from vitamin E TPGS of 85.61 J/g at an onset of 20.42°C and two small endothermic waves marked by question mark.

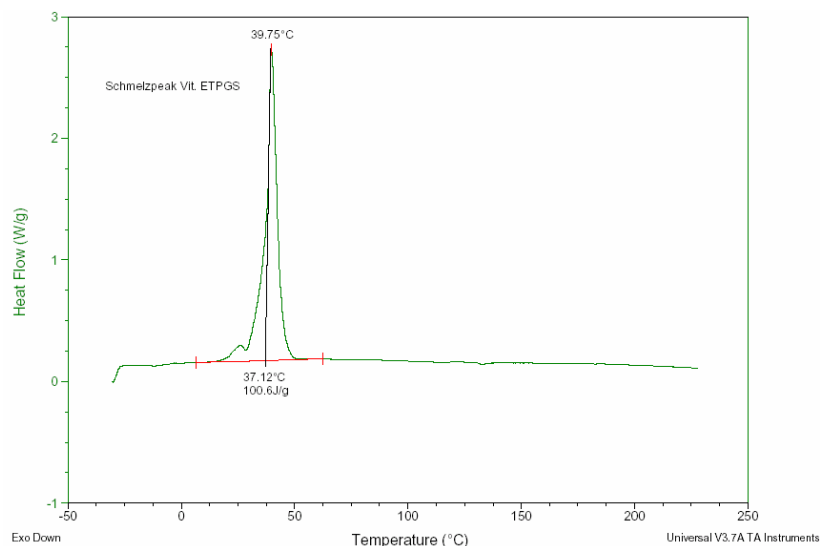


Figure IV.85 DSC curve of blended vitamin E TPGS and spironolactone (90:10). The blend has a single endothermic melting peak from vitamin E TPGS of 100.6 J/g at an onset of 37.12°C and no further exothermic peak of decomposition.

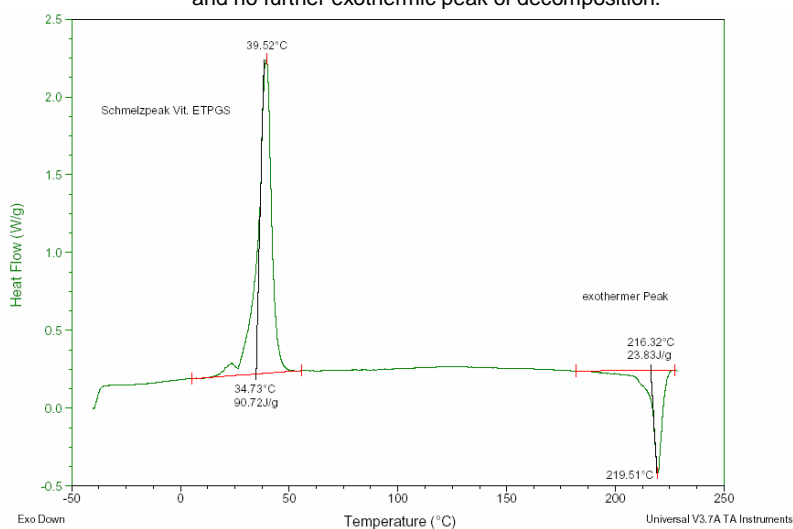


Figure IV.86 DSC curve of blended vitamin E TPGS and spironolactone (80:20). The blend has an endothermic melting peak from vitamin E TPGS of 90.72 J/g at an onset of 34.73°C and an exothermic peak of decomposition of 23.83 J/g at an onset of 216.32°C.

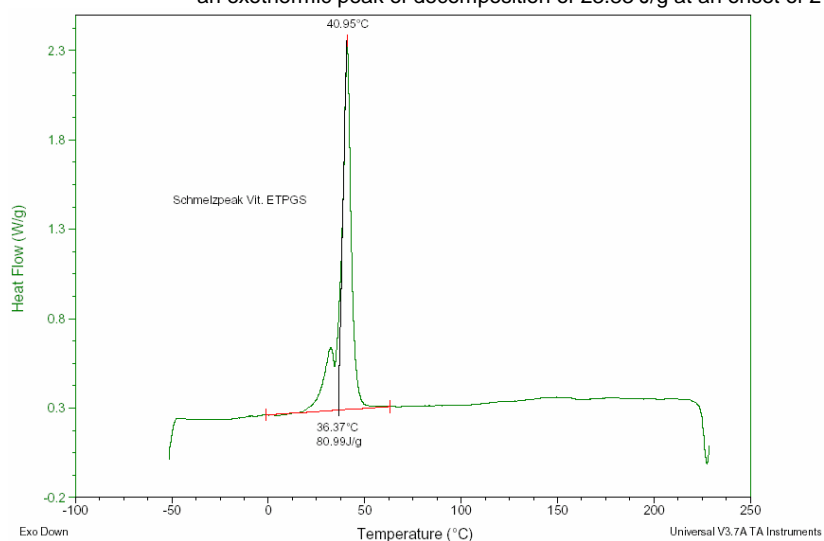


Figure IV.87 DSC curve of blended vitamin E TPGS and spironolactone (70:30). The blend has an endothermic melting peak from vitamin E TPGS of 80.99 J/g at an onset of 36.37°C and a further exothermic peak of decomposition at the end of the range of the method.

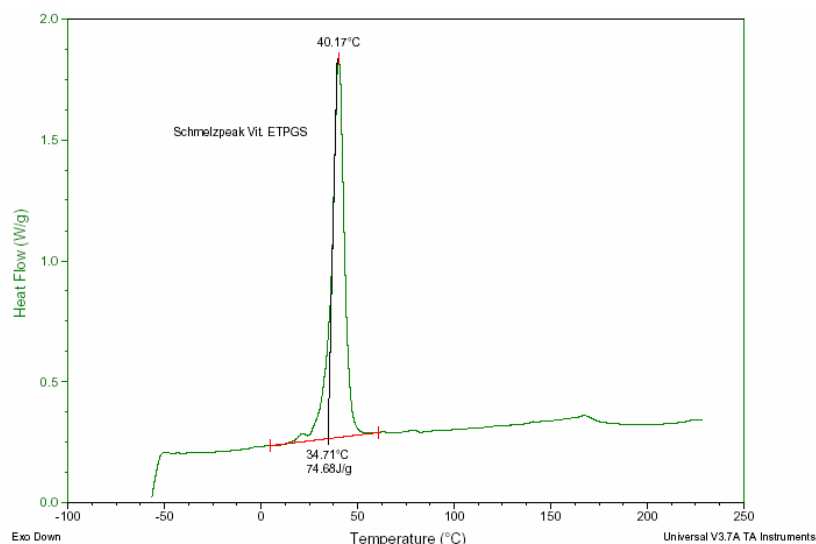


Figure IV.88 DSC curve of blended vitamin E TPGS and spironolactone (60:40). The blend has an endothermic melting peak from the vitamin E TPGS of 74.68 J/g at an onset of 34.71°C and no further exothermic peak of decomposition.

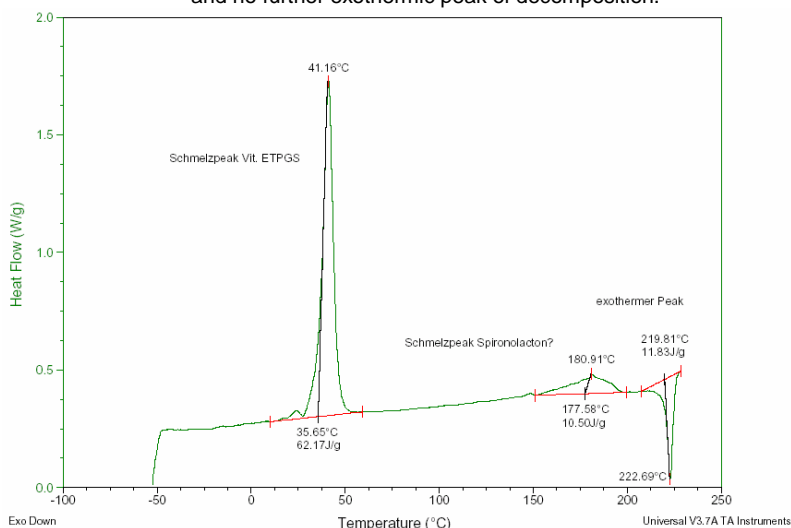


Figure IV.90 DSC curve of blended vitamin E TPGS and spironolactone (50:50). The blend has an endothermic melting peak from the vitamin E TPGS of 62.17 J/g at an onset of 35.65°C, a second endothermic melting peak from spironolactone of 10.50 J/g at an onset of 177.58°C and an exothermic peak of decomposition of 11.83 J/g at an onset of 222.69°C.

The DSC curve of vitamin E TPGS did not show an exothermic peak at 217°C, which might have overlapped the endothermic melting peak of spironolactone. The exothermic peak is lacking at a content of 0%, 5%, 10% and 40% of spironolactone. At 5% spironolactone concentration, two very small endothermic peaks are visible, which do not appear at higher concentrations. Upon assumption of no interference in the DSC's the borderline of the solubility of spironolactone is estimated between 40% and 50% by weight. The appearance of the exothermic peak at the high temperature about 220°C may be caused by decomposition of the matrix by pyrolysis, polymerization or hydration.

IV.16.3.4. Solubility of Spironolactone in Different Imwitor Types and Vitamin E Acetate

The DSC curves of all Imwitor types and vitamin E acetate were not evaluable due to the DSC interferences. The figures are presented in the Appendix.

IV.16.4. Solubility of Spironolactone in Mixtures of Lipid Matrices with Adjusted HLB

Softisan 138 and Softisan 154 were blended with vitamin E TPGS in a ratio to approach the calculated HLB value of spironolactone. Softisan 138 and vitamin E TPGS were blended in the ratio 71.55% and 28.45%, respectively, by weight and Softisan 154 and vitamin E TPGS in the ratio 67.20% and 32.80%, respectively, by weight. These blends were mixed with spironolactone at concentrations ranging from 5-50%. The blends, the mixtures and spironolactone alone were analyzed using DSC.

IV.16.4.1. Solubility of Spironolactone Softisan 138/ Vitamin E TPGS Blend

In Figure IV.90, the DSC curve of a blend of Softisan 138/vitamin E TPGS (71.55:28.45) is presented. In the Figures IV.91 – IV.98, the DSC curves of different blends of Softisan138/vitamin E TPGS and spironolactone are shown.

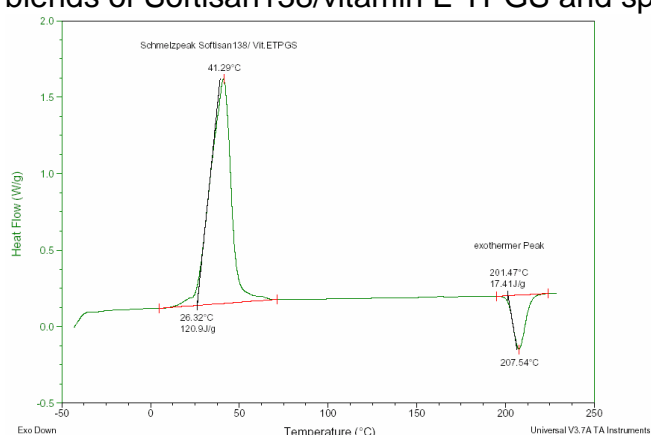


Figure IV.90 DSC curve of blended Softisan 138 and vitamin E TPGS (71.55:28.45). The mixture has an endothermic melting peak from the blend of Softisan 138 and vitamin E TPGS of 120.9 J/g at an onset of 26.32°C and an exothermic peak of decomposition of 17.41 J/g at an onset of 201.47°C.

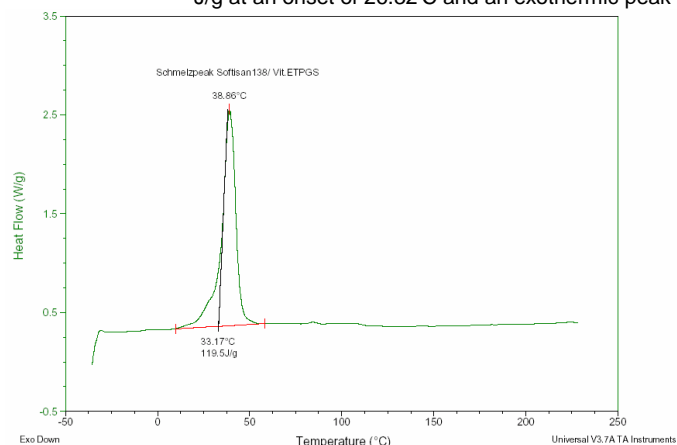


Figure IV.91 DSC curve of blended Softisan 138 and vitamin E TPGS (71.55:28.45) containing 5% spironolactone. The mixture has an endothermic melting peak from the blend of Softisan 138 and vitamin E TPGS of 119.5 J/g at an onset of 33.17°C and however, no further exothermic peak of decomposition about 200°C.

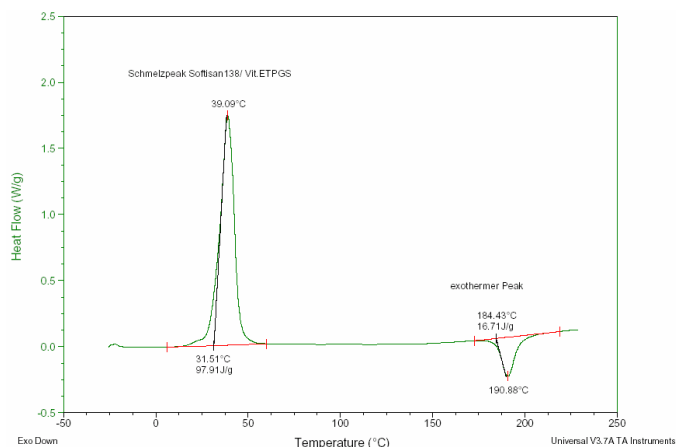


Figure IV.92 DSC curve of blended Softisan 138 and vitamin E TPGS (71.55:28.45) containing 10% spironolactone. The mixture has an endothermic melting peak from the blend of Softisan 138 and vitamin E TPGS of 97.91 J/g at an onset of 31.51°C and an exothermic peak of decomposition of 16.71 J/g at an onset of 184.43°C.

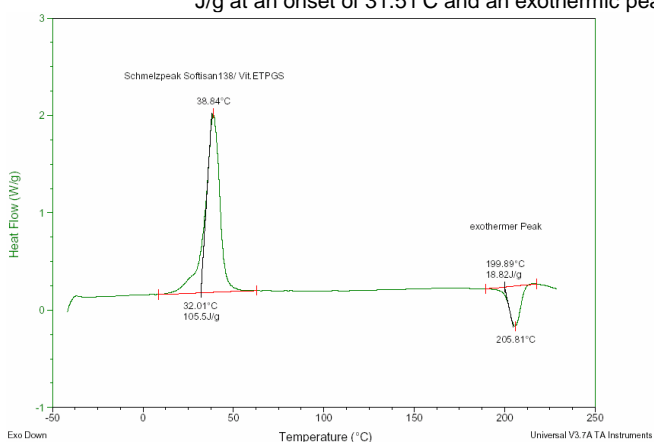


Figure IV.93 DSC curve of blended Softisan 138 and vitamin E TPGS (71.55:28.45) containing 15% spironolactone. The mixture has an endothermic melting peak from the blend of Softisan 138 and vitamin E TPGS of 105.5 J/g at an onset of 32.01°C and an exothermic peak of decomposition of 18.82 J/g at an onset of 199.89°C.

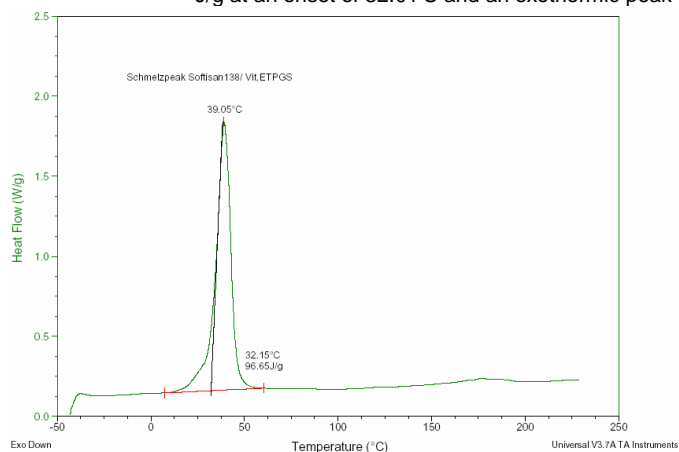


Figure IV.94 DSC curve of blended Softisan 138 and vitamin E TPGS (71.55:28.45) containing 20% spironolactone. The mixture has an endothermic melting peak from the blend of Softisan 138 and vitamin E TPGS of 96.65 J/g at an onset of 32.15°C and however, no further exothermic peak of decomposition about 200°C.

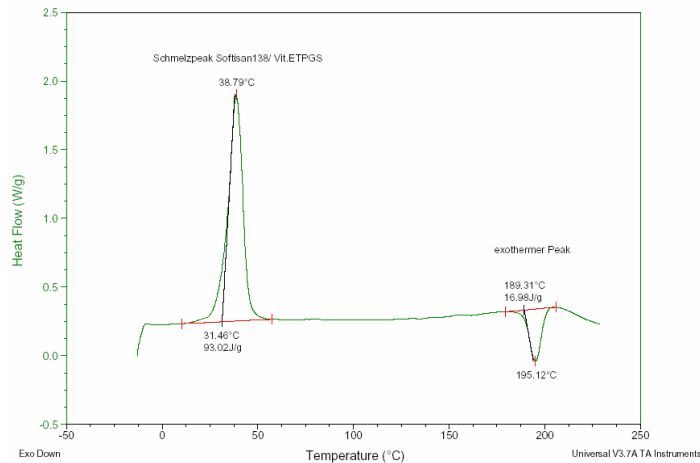


Figure IV.95 DSC curve of blended Softisan 138 and vitamin E TPGS (71.55:28.45) containing 25% spironolactone. The mixture has an endothermic melting peak from the blend of Softisan 138 and vitamin E TPGS of 93.02 J/g at an onset of 31.46°C and an exothermic peak of decomposition of 16.98 J/g at an onset of 189.31°C.

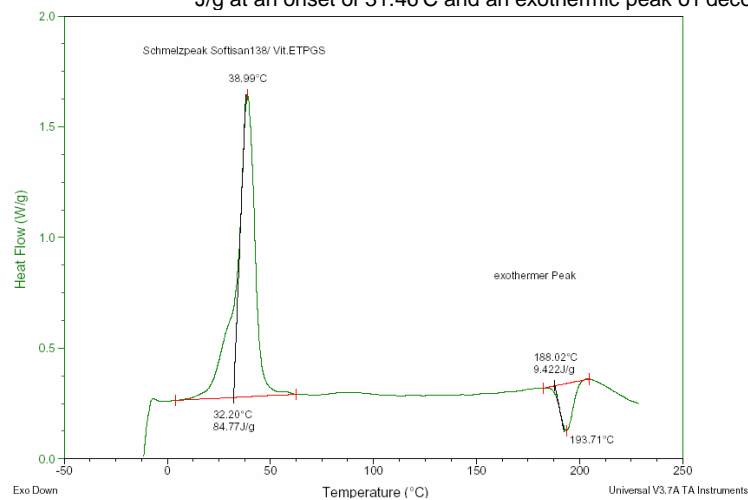


Figure IV.96 DSC curve of blended Softisan 138 and vitamin E TPGS (71.55:28.45) containing 30% spironolactone. The mixture has an endothermic melting peak from blend Softisan 138 and vitamin E TPGS of 84.77 J/g at an onset of 32.20°C and a second endothermic melting peak from spironolactone overlapped by an exothermic peak of decomposition of resulting 9.42 J/g at an onset of 188.02°C.

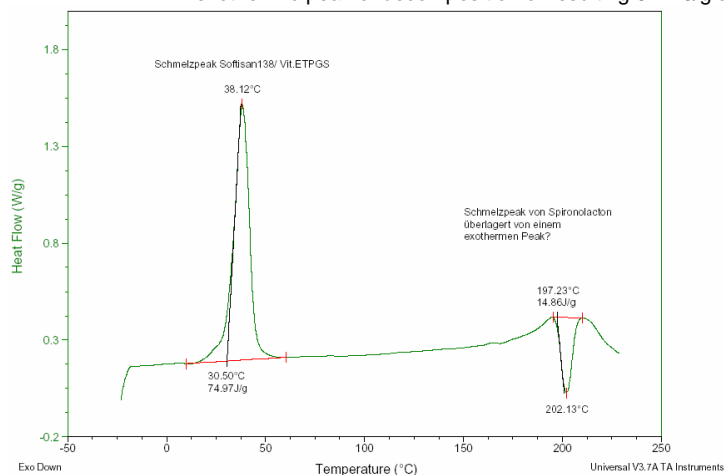


Figure IV.97 DSC curve of blended Softisan 138 and vitamin E TPGS (71.55:28.45) containing 40% spironolactone. The mixture has an endothermic melting peak from blend Softisan 138 and vitamin E TPGS of 74.97 J/g at an onset of 30.50°C and a second endothermic melting peak from spironolactone overlapped by an exothermic peak of decomposition of resulting 14.86 J/g at an onset of 197.23°C.

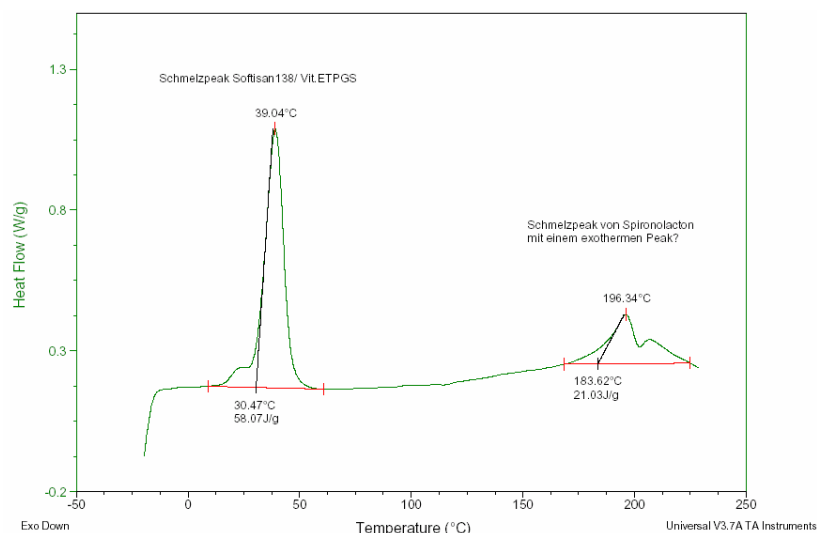


Figure IV.98 DSC curve of blended Softisan 138 and vitamin E TPGS (71.55:28.45) containing 50% spironolactone. The mixture has an endothermic melting peak from blend Softisan 138 and vitamin E TPGS of 58.07 J/g at an onset of 30.47°C and a second endothermic melting peak from spironolactone of 21.03 J/g at an onset of 188.62°C properly overlapped by an exothermic peak of decomposition.

The DSC curve of Softisan 138/vitamin E TPGS showed an exothermic peak at approximately 200°C, which was directly overlapping the endothermic melting peak of spironolactone. The area of the exothermic peak is not reproducible, the peak is lacking completely at a content of 5% and 20% of spironolactone respectively. Furthermore, at concentrations in excess of 15% of spironolactone endothermic shoulders appeared, indicating an overlapped endothermic melting peak. Hence, it is not possible to determine the solubility of spironolactone with sufficient accuracy. Pyrolysis, polymerization or hydration can be the circumstance for the exothermic peak of decomposition.

IV.16.4.2. Estimation of the Solubility of Spironolactone Softisan154/Vitamin E TPGS Blend

In Figure IV.99, the DSC curve of the Softisan 154/vitamin E TPGS (67.20:32.80) lipid matrix is presented. In the Figures IV.99 – IV.106, the DSC curves of different blends of Softisan154/vitamin E TPGS and spironolactone are shown.

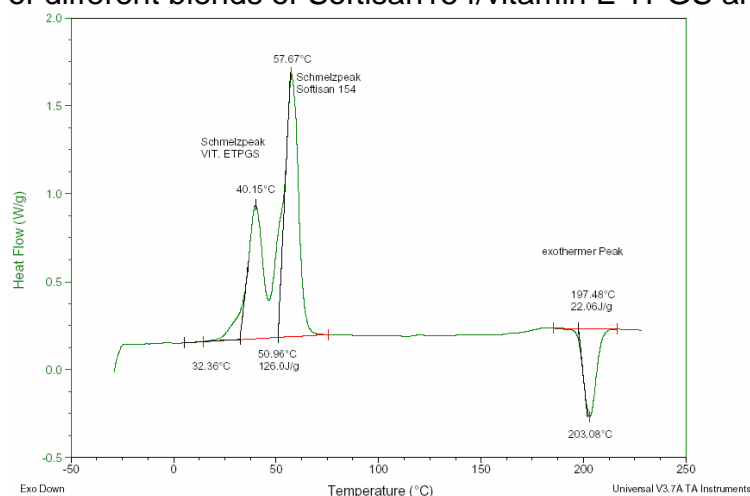


Figure IV.99 DSC curve of blended Softisan 154 and vitamin E TPGS (67.20:32.80). The mixture has endothermic melting double peak from the blend of Softisan 154/vitamin E TPGS of 126.0 J/g at an onset of 32.36°C and an exothermic peak of decomposition of 22.06 J/g at an onset of 197.48°C.

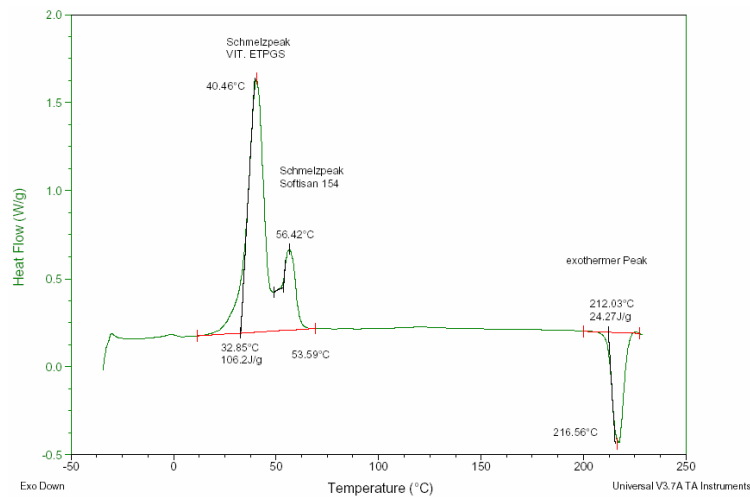


Figure IV.100 DSC curve of blended Softisan 154 and vitamin E TPGS (67.20:32.80) containing 5% spironolactone. The mixture has endothermic melting double peak from the blend of Softisan 154/vitamin E TPGS of 106.2 J/g at an onset of 32.85°C and an exothermic peak of decomposition of 24.27 J/g at an onset of 212.03°C.

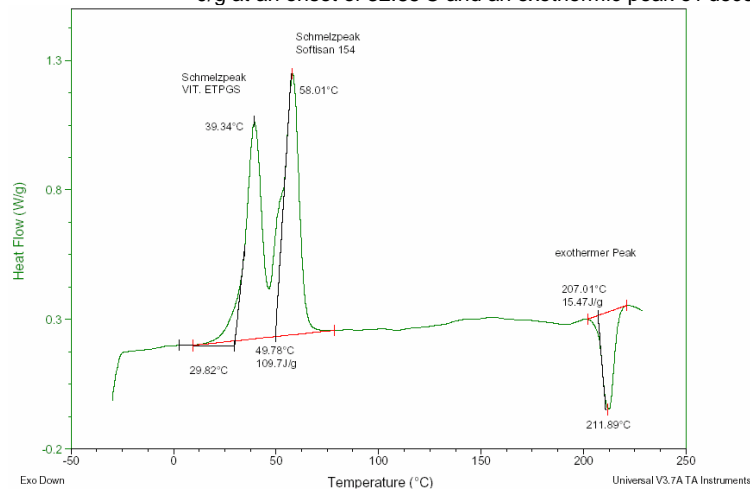


Figure IV.101 DSC curve of blended Softisan 154 and vitamin E TPGS (67.20:32.80) containing 10% spironolactone. The mixture has endothermic melting double peak from the blend of Softisan 154/vitamin E TPGS of 109.7 J/g at an onset of 29.82°C and an exothermic peak of decomposition of 15.47 J/g at an onset of 207.01°C.

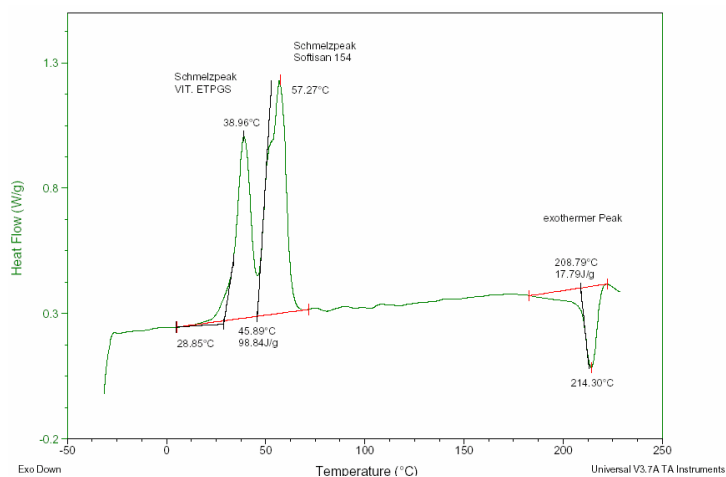


Figure IV.102 DSC curve of blended Softisan 154 and vitamin E TPGS (67.20:32.80) containing 15% spironolactone. The mixture has endothermic melting double peak from the blend of Softisan 154/vitamin E TPGS of 98.84 J/g at an onset of 28.85°C and an exothermic peak of decomposition of 17.79 J/g at an onset of 208.79°C.

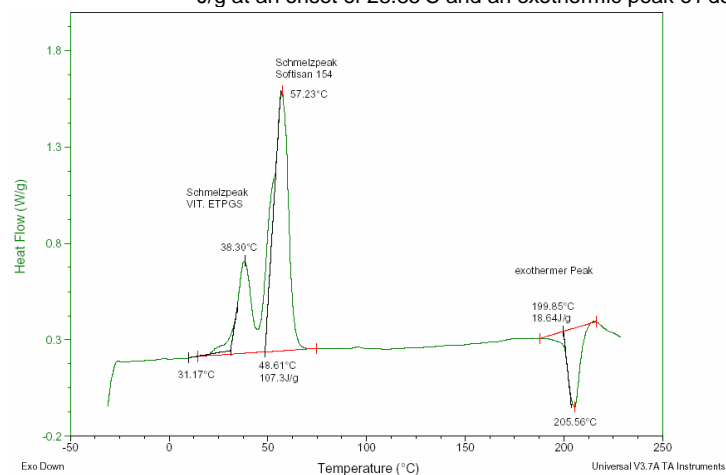


Figure IV.103 DSC curve of blended Softisan 154 and vitamin E TPGS (67.20:32.80) containing 20% spironolactone. The mixture has endothermic melting double peak from blend Softisan 154 and vitamin E TPGS of 107.30 J/g at an onset of 31.17°C and further endothermic melting peak from spironolactone overlapped by an exothermic peak of decomposition of resulting 18.64 J/g at an onset of 199.85°C.

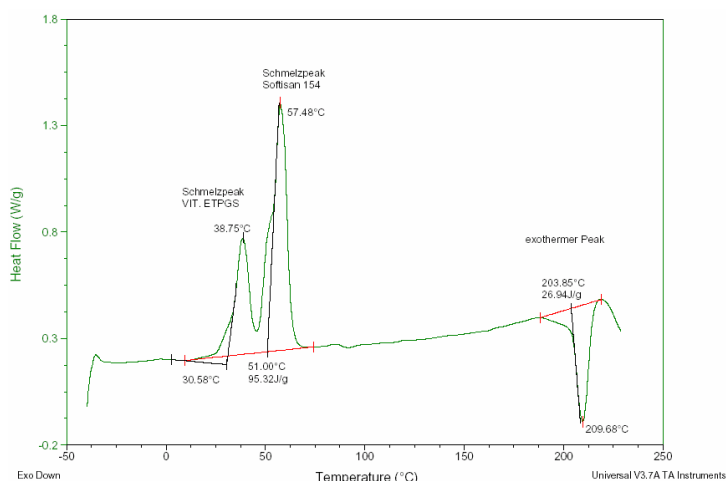


Figure IV.104 DSC curve of blended Softisan 154 and vitamin E TPGS (67.20:32.80) containing 25% spironolactone. The mixture has an endothermic melting double peak from blend Softisan 154 and vitamin E TPGS of 95.32 J/g at an onset of 30.58°C and further endothermic melting peak from spironolactone overlapped by an exothermic peak of decomposition of resulting 26.94 J/g at an onset of 203.85°C.

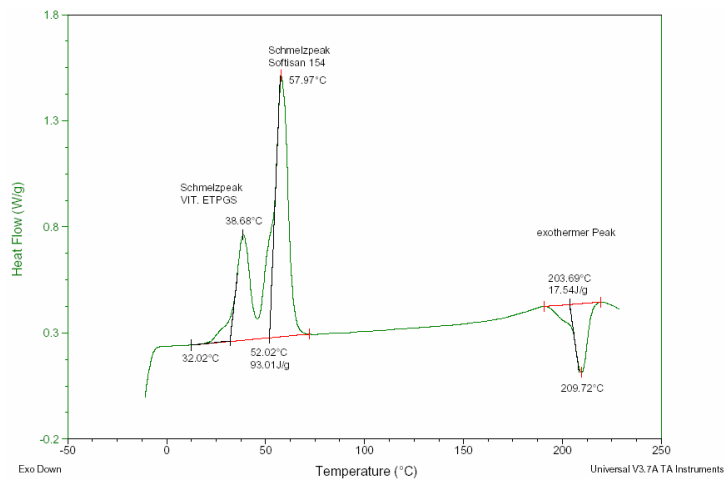


Figure IV.105 DSC curve of blended Softisan 154 and vitamin E TPGS (67.20:32.80) containing 30% spironolactone. The mixture has an endothermic melting double peak from blend Softisan 154 and vitamin E TPGS of 93.01 J/g at an onset of 32.02°C and a further endothermic melting peak from spironolactone overlapped by an exothermic peak of decomposition of resulting 17.54 J/g at an onset of 203.69°C.

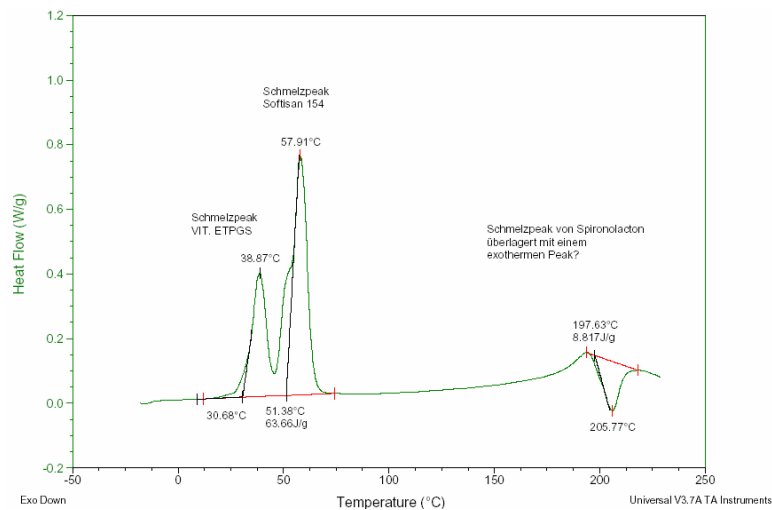


Figure IV.106 DSC curve of blended Softisan 154 and vitamin E TPGS (67.20:32.80) containing 40% spironolactone. The mixture has an endothermic melting double peak from blend Softisan 154 and vitamin E TPGS of 63.66 J/g at an onset of 30.68°C and a further endothermic melting peak from spironolactone overlapped by an exothermic peak of decomposition of resulting 8.82 J/g at an onset of 197.63°C.

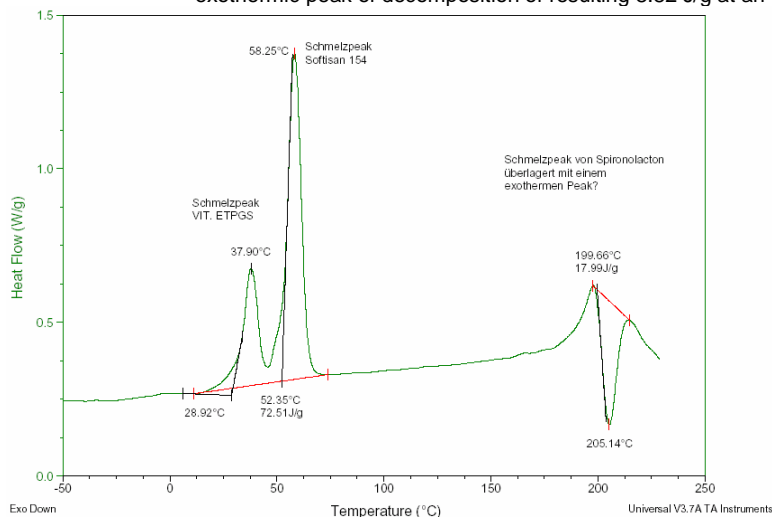


Figure IV.107 DSC curve of blended Softisan 154 and vitamin E TPGS (67.20:32.80) containing 50% spironolactone. The mixture has an endothermic melting double peak from blend Softisan 154 and vitamin E TPGS of 72.51 J/g at an onset of 28.92°C and a further endothermic melting peak from spironolactone overlapped by an exothermic peak of decomposition of resulting 17.99 J/g at an onset of 199.66°C.

The DSC curve of Softisan 154/vitamin E TPGS showed an exothermic peak at approximately 200°C, which was directly overlapping the endothermic melting peak of spironolactone. The area of the exothermic peak, which displays decomposition by pyrolysis, polymerization or hydration was not reproducible. Further, the exothermic peak exhibited in all concentrations larger than 5% endothermic shoulders, which may display an overlapped endothermic melting peak. Hence it is not possible to provide a borderline of solubility. The endothermic melting peak of the lipid matrix was a double peak hence the lipid matrix was not mixed molecular dispersely since this would lead to a mono peak.

IV.16.4.3. Explanation of the Exothermic peak at Approximately 200°C

In Figure IV.108 the DSC curves of a repeated scan of the same sample of Imwitor 312 is presented. In the first scan, the substance exhibited an exothermic peak at 197°C. In the second scan after the sample was exposed to 230°C in the first scan, the exothermic peak did not appear, whereas the endothermic melting peaks moved to lower temperatures along with an increase of the peak areas combined with a splitting into a double peak. The new maxima of the peaks were near the melting point of glycerine (18.2°C) and lauric acid (43°C) (Falbe, 1999). Based on this observation it can be concluded that at high temperatures the substances are decomposed into the fatty acid and glycerine, the lipid is destroyed and no second run is possible. Unfortunately the exothermic peak from the decomposition overlaps the melting peak of spironolactone. Hence it was not possible to show an increase of the solubility by adjusting the HLB value of the lipid matrix to the HLB value of the drug since it was not possible to determine reliable values for the solubility of the drug

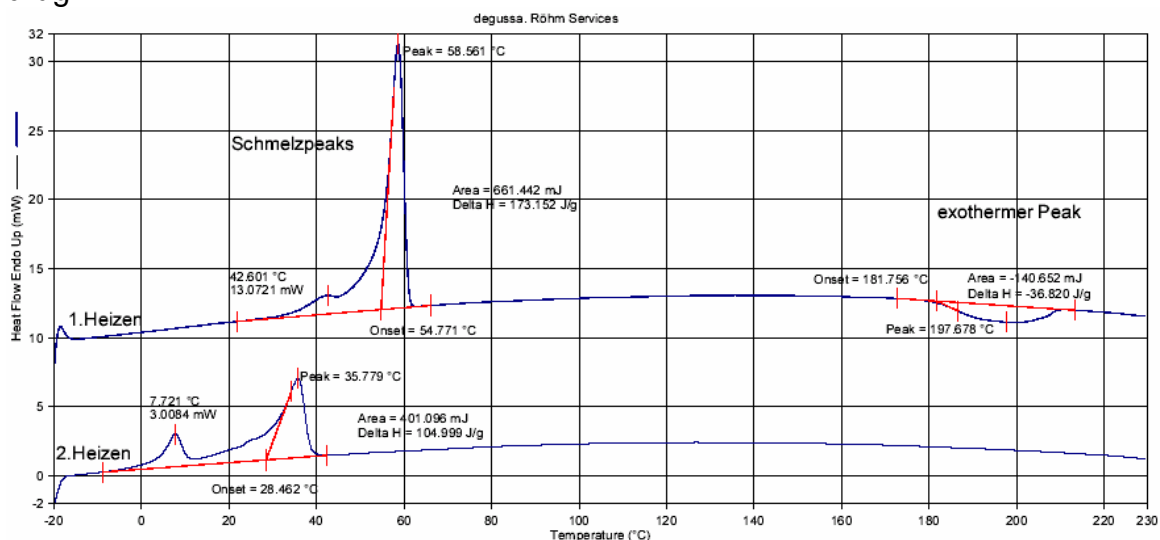


Figure IV.108 Two subsequent DSC scans of Imwitor 312. The upper line represents the first scan, the lower line the second scan.

CHAPTER V. DISCUSSION

V.1. The Granulation Process

As described in the results section, a number of parameters of the granulation process affect the product quality (see Table V.1). Particle size and friability are influenced by the spraying rate, the amount of binder, airflow, inlet air temperature, rotor speed and type of rotor disc. Except for the rotor speed and type of rotor disc these parameters are also determinants for the tapped density of the product. The span is mainly impacted by airflow and rotor speed.

Consequently in order to manufacture a product of high quality, it is necessary to apply a high spraying rate combined with a very high rotor speed in case of Na-CMC and chitosan, for Na-CMC and Na-alginate in addition a non-continuous spraying rate compared to the references in the literature with other excipients (Heng, 1996; Kristensen, 2000; Kristensen, 2002; Liew, 2002; Liew, 2000; Pisek, 2000; Qudan, 2002). All authors applied a rotor speed in a range of 480rpm to 1400rpm. The spraying rate was varied between 20 g/min to 40 g/min. However, all authors described optimized spraying rates ranging from 20 g/min to 35 g/min. Heng applied in a factorial design study a spraying rate of 59 g/min.

Table V.1 Process Parameters Affecting the Properties of Micropellets.
 An upwards directed arrow indicates that an increase of the process variables is accompanied by an increase in the micropellets response variable. On the opposite, a downwards directed arrow indicates, that an increase of the process variable leads to a decrease of the micropellet response variable. A higher number of arrows indicate a more pronounced influence of the parameter on the response variable. Process parameters marked using an "x" have been shown to be significant by ANOVA (p=0.05). "0" means that an affect was not detectable.

Process Parameters	X50	Span	Tapped Density	Friability
Average ¹ Spraying Rate	X ↑↑	0	X ↑↑	X ↓↓
Spraying Rate Cont. ²	0	↑	X ↓	X ↑
Slope Spraying Rate ³	0	0	X ↑	X ↓
Amount of Binder	X ↑↑	0	X ↑↑	X ↓↓
Airflow	↓↓	↓	X ↓↓↓	X ↑↑↑
Inlet Air Temperature	↓↓	0	↓↓	↑↑

Process Parameters	X50	Span	Tapped Density	Friability
Rotor Speed	X ↓ ↓ ↓	X ↓ ↓	0	X ↑ ↑ ↑
Plane vs. Grooves Surface	↓ ↓	↓ ↓	0	↑ ↑

¹ The "average spraying rate" is calculated from the liquid binder amount divided by the time of the spraying period.

² The "continuous spraying rate" represents the value in opposite to non continuous spraying rate.

³ The "slope spraying rate" represents the rate of the decrease of the spraying rate, which represented the line of best fit over all different spraying rates.

V.1.1. **Process Variables Influencing the Morphology and Topographical Quality of Micropellets**

Based on their morphology and topographical quality the manufactured chitosan micropellets were superior in comparison to the Na-CMC micropellets which themselves show better quality than the Na-alginate micropellets. Morphology and topographical quality may be improved by applying a higher spraying rate, a lower inlet air temperature and a higher amount of liquid binder. A non continuous spraying mode improves the morphology and topographical quality of the pellets because a higher amount of liquid binder can be applied with a moderate increase in particle size. The improvement of the morphology and topographical quality is paralleled by higher tapped density and lower friability of the micropellets.

V.1.2. **Process Variables Influencing Particle Size**

As reported previously by other authors (Holm, 1996; Liew, 2002; Wan, 1995), particle size increases with an increase in spraying rate and amount of binder in the formulation. On the other hand, particle size may be decreased and oversized particles (>2000 μ m) reduced by a higher rotor speed. The reduction of oversized particles at higher rotor speed is due to the decline of over-wetted areas and can be explained by three main factors:

- I) Higher centrifugal forces causing breakdown of the particles
- II) Short-term exposure of the particles in the spraying area which will result in less particle wetting at high rotor speed. Prior to the next wetting phase the surface water is either dried by the airflow and/or water from the surface is soaked into the pellet core due to the water retention capacity of the bioadhesive excipient. Particle growth is thus reduced due to reduction of surface water. Similarly, other factors that may lead to a decrease in particle wetting such as airflow and inlet air temperature have an influence on particle size.
- III) Particle size reduction by higher temperature

The increase in temperature at higher rotor speed is primarily the result of an increase in waste heat produced by the rotor engine. Hence the application of high rotor speed will subsequently increase the temperature in the workroom of the rotary processor. Consequently, the humidity in the outlet air is increased at higher rotor speed. As a result, the product manufactured at higher rotor speed exhibits a lower water content at the end of the spraying period.

In addition, the rotor disc surface containing grooves in a hatch pattern supplies higher shearing efficiency for more effective spheronization as compared to the surface without such structural modifications. This leads to a higher acceleration of the particles at a given rotor speed without formation of additional waste heat. Therefore, similar effects as described under I and II were observed by changing the rotor disc. The smallest particle size of the micropellets was obtained by providing their highest acceleration using the structured rotor disc at high rotor speed. Particle size reduction thus was maximized due to higher centrifugal forces, short-term exposure to the spraying liquid and production of waste heat in the workroom of the processor.

V.1.3. *Process Variables Influencing the Span*

The rotor speed, type of rotor disc and spraying rate as well as airflow influence the span of the micropellets. These findings with respect to the high rotor speed are in contrast to results of an increase of the span reported by Vertommen et al. (Vertommen, 1997b). A high rotor speed leads to a more homogenous distribution of the liquid binder in the powder and thus results in a decrease of the span. The higher shearing efficiency contributes to the narrower particle size distribution with a breakdown of oversized particles. The same phenomenon is observed by replacing the plane rotor disc with the surface-modified disc, due to its higher shearing efficiency and greater particle acceleration. A non continuous spraying rate decreases the span, since the reduced spraying rate at the end of the process favours a more homogenous particle formation.

V.1.4. *Process Variables Influencing Tapped Density*

A correlation between the water content at the end of the spraying period and the tapped density of the micropellets is shown in Figure V.1, demonstrating that an increase in the water content is accompanied by a growth in tapped density. This is due to the greater plasticity of the material such that micropellets with greater density can be formed (Schubert, 1973). Therefore, all parameters which determine the water content at the end of the spraying period also have an influence on the tapped density of the particles, i.e. amount of binder, spraying rate, airflow, and inlet air temperature. These findings of a higher density for batches with a higher moisture content are concurrent to Robinson et al. (Robinson, 1991).

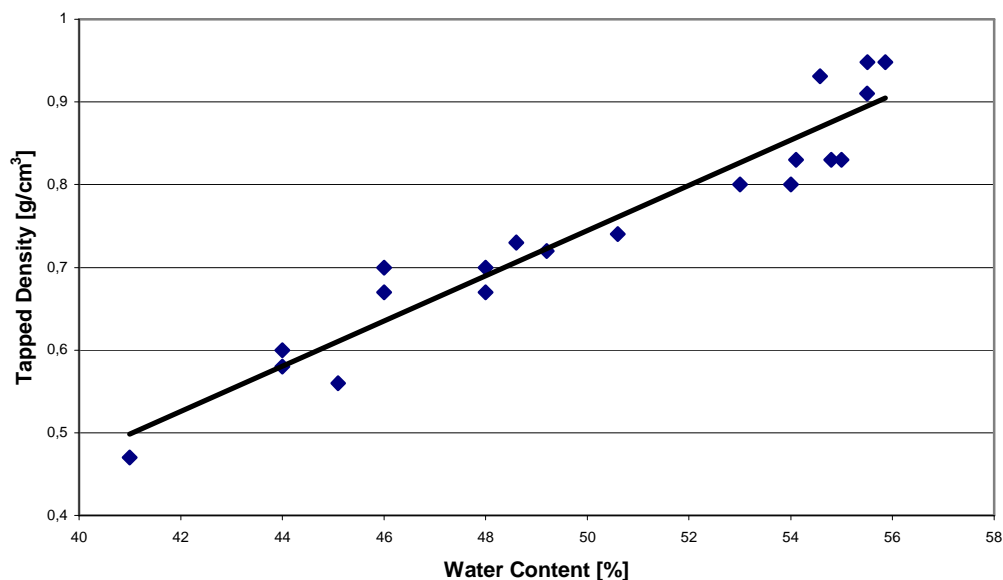


Figure V.1 Relationship between water content at the end of the spraying period and tapped density. ($y = 0.0273x - 0.022$, $R^2 = 0.918$).

V.1.5. Process Variables Influencing Friability

Two major parameters, i.e. moisture content at the end of spraying period and fast wetting rate of the particles affect the friability of bioadhesive micropellets. A reduction of the friability by applying higher amounts of liquid binder was also found by Chukwumezie et al., explained by a sufficient powder bonding and/or agglomeration from the higher amount of liquid binder (Chukwumezie, 2004). These findings are in contrast to Vertommen et al., who correlated an improved friability only with an increase in particle size. In the trials of Vertommen particles size increased and the friability was improved with an increase in MCC content, liquid binder amount, rotor speed spheronization time and spraying rate. Vertommen et al. correlated the improved friability only with the particle size because they found a strong correlation between particle size and improved hardness of the pellets in the same batch. The influence of the particle size was excluded in this work by selecting always the same particle size for inter-batch comparison. The dependence of friability on the water content of the micropellets is depicted in Figure V.2. The coefficient of determination ($R^2 = 0.4557$), however, also indicates that important factors are not included in the model. Optimum parameters for the achievement of low friability include a non continuous spraying rate with a high initial spraying rate supplemented by a low airflow, low inlet air temperature and low rotor speed or, alternatively, a plane rotor disc. This combination of influencing parameters is observed only when bioadhesive polymers are used, possibly due to the creation of a limited diffusion barrier on the surface of the particles that hinders the binder liquid from wetting the entire growing particle. Therefore, tight bonds are not being formed. This theory is also supplemented by the observation that low spraying rates are insufficient to achieve the necessary water insertion to complete the roto agglomeration, due to a collapse of the fluidized bed. In this case, fluffy agglomerates with a low density and high friability are formed. The fluidized bed collapses when no additional liquid binder can further be taken up into the dry particle core which is subsequently left unused for the agglomeration. On the contrary, when high spraying rates are applied, the

optimum amount of water can be added without an indication of collapse. At extremely high spraying rates the influence of the rotor is negligible though.

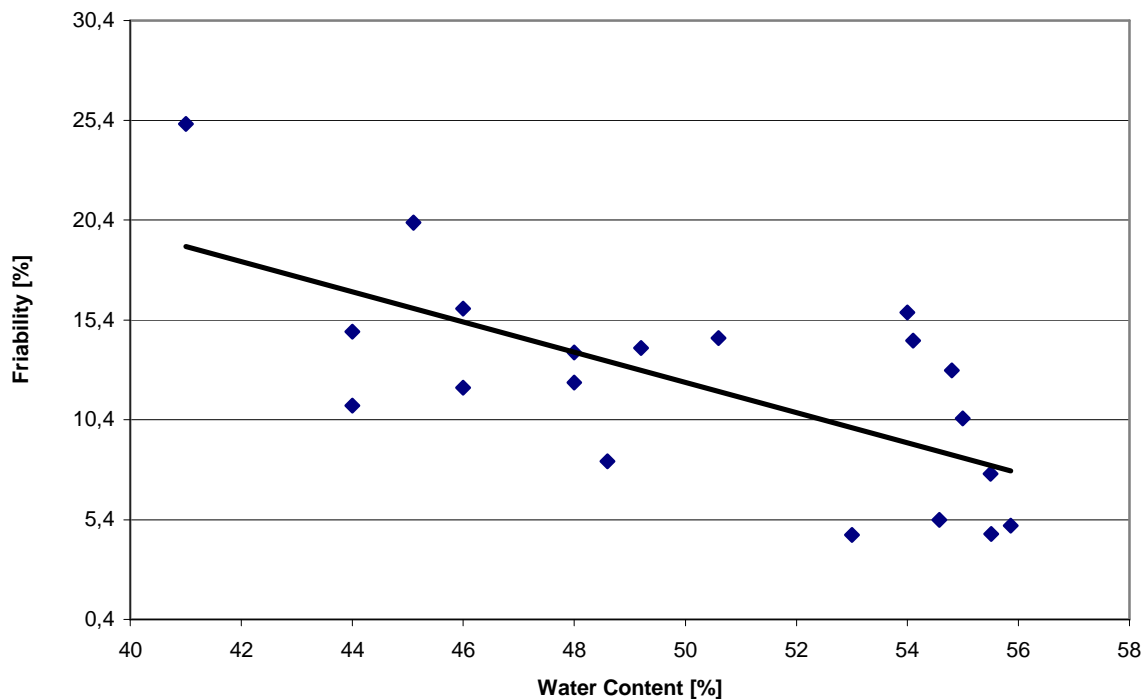


Figure V.2 Relationship between micropellet water content at the end of the spraying period and pellet friability. ($y = -0.7567x + 50.104$, $R^2 = 0.4557$).

V.1.6. **Impact of Inlet Air Conditions and Drying Conditions on the Total Yield**

In this work a relationship between the total yield at on one hand and the inlet air humidity and temperature on the other hand was found. The most visible loss of product occurs by deposition of micropellet material on the shell of the GPCG1. This deposition may reach up to 1cm in thickness. The material was mainly deposited above the product bed and occurred primarily during the drying period. This can be explained by re-condensation from the evaporated water at the colder metal shell above the product bed. During the start of the drying period a high difference between the inlet air temperature and the outlet air temperature of about 40°C exists. At the same time the relative humidity is close to 100%. Hence the decrease of product temperature in addition to a high water content leads to recondensation of the evaporated water. This phenomenon is particularly pronounced at the colder metal shell of the GPCG1 above the product. Pre-dried micropellets, ejected from the product bed reabsorb the humidity and stick directly to the metal shell or to previously deposited wet micropellets. These micropellets seem to need the longest drying times since initially they are located within the region of re-condensation at the beginning of the drying process and they are located in the region with the lowest drying capacity during the subsequent drying process. Ejected micropellets of the product bed have always the risk to stick to this wet material. An increase of the inlet humidity and temperature pronounces the phenomenon of re-condensation and increases the deposition of micropellets above the product bed while it decreases the total yield. A low initial drying temperature combined with a high air flow prevents these losses.

V.1.7. Influence of Acetic Acid Concentration on the Formation of Chitosan Micropellets

It was shown that the amount of water in combination with the amount of acetic acid is an important parameter for the successful formation of chitosan micropellets. Nevertheless, the influence of the acetic acid concentration within the liquid binder on the micropellet properties was not uniform. At a low level of liquid binder addition a high concentration of acetic acid lead to a decrease of the micropellet quality. At a high level of liquid binder addition a high acetic acid concentration lead to an increase of the micropellet quality. These observations can be explained as follows: At a low level of liquid binder combined with a high concentration of acetic acid, the amount of water is insufficient for an optimized formation of the micropellets. In contrast, at a high level of liquid binder addition combined with a high acetic acid concentration the amount of water is sufficient for the formation of the micropellets and the higher amount of acetic acid aids in the agglomeration process. Hence, for optimized micropellets a sufficient amount of water and acetic acid has to be provided.

V.1.8. Differences Between Mucoadhesive Polymers

Since, chitosan, Na-alginate and Na-CMC exhibit similar liquid binder uptake kinetics, very similar initial process parameters were selected for all polymers, i.e. high initial spraying rates, low airflow and low inlet air temperature. By applying the same process parameters as for the manufacture of Na-CMC micropellets, chitosan and Na-alginate micropellets were characterized by a smaller particle size as compared to Na-CMC. Therefore, chitosan micropellets were manufactured with an increased liquid binder proportion and a continuous maximum spraying rate. Furthermore, a 15% solution of acetic acid was used instead of water as liquid binder. The Na-alginate micropellets were manufactured with a comparatively lower rotor speed, higher amount of water as liquid binder and higher spraying rate. The density, friability and topographical quality of chitosan micropellets are superior in comparison to the Na-CMC micropellets which themselves are better than Na-alginate. Nevertheless, the friability for all three types of micropellets is lower than the friability of commercially obtained Cellets[®]. Thus the mechanical properties of bioadhesive micropellets were appropriate to be used in subsequent coating processes.

V.1.9. Statistical Analysis

In the statistical process analysis not all influencing process parameters presented in Table V.1, were shown to be significant. This is caused by the circumstances that the statistical analysis was of a retrospective type, thus the experimental design was not optimized towards a factorial design. For this case important process parameters were not shown to be significant, because the design of the experiments did not support sufficient data. Thus retrospective statistically process analysis can only be regarded as adjuvant for the analysis of the process.

V.2. Friability and Tapped Density

In contrast to the frequently used procedure reported in the literature to study the friability of a wide range of particles (Pisek, 2001; Vecchio, 1994; Vertommen, 1997b), probes with a narrower particle size range were used in the present experiments to avoid the influence of different particle size on the results. The use of

samples with a wider particle size range can lead to higher friability values. This observation may be explained as follows: The friability of particles between 400 and 500 μm (narrow population) is studied by using a 400 μm sieve defining that the friable portion is represented by all particles passing the 400 μm sieve. In case break down of the particles the resulting two fragments either large or small may probably pass the 400 μm sieve and the friability value appears great. Using a larger particle size distribution (e.g. 250-500 μm) but a smaller sieve (250 μm mesh size) for the determination of friability, the larger fragments of broken micropellets remain on top of the sieve and therefore friability values appear low. Considering this influence some authors select only a large particle population for determination of friability (e.g. larger than 600 μm) and define the friable portion as particles passing a 500 μm sieve (Pisek, 2001). With respect to this phenomenon it is also possible to calculate the friability index with the median and mode values, which represent the integrated decrease of all particle sizes during attrition (Airaksinen, 2000). Hence for this reason the reported friability values in this work are much higher compared to the literature. As reference the friability of Cellets[®] (400-500 μm), well known for their hardness, was also determined.

The mechanical stress for the pellets was found to be higher in the rotating glass cylinder as compared to the Bolatec[®] Friabimat. With higher friability of the tested material this difference is becoming smaller. The Bolatec Friabimat has the advantage of a shorter process times and standardized process conditions for an intra-laboratory comparison. In general, the tapped density of smaller particles of the same batch was higher compared to the larger particles of the same batch and the friability of the smaller particles was lower. The tapped density of the smaller particles is higher because they are able to achieve a higher packing density with smaller interparticulate spaces. The mechanical stress achieved with the small particles seems to be lower, hence their friability is lower. This is also reported by Ritschel (Ritschel, 2002).

V.3. Torque Measurements

The measurement of torque allows monitoring of the granulation process and can be used for the endpoint detection of the granulation process. Unfortunately, it was not possible to use the torque measurement as an end-point monitoring system as described by Kristensen et al. This group - in contrast to our work - was mainly interested in the total amount of water added (Kristensen, 2000). For the manufacture of mucoadhesive micropellets in our case it was further of importance to control the water addition rate, not only the total amount. A control of the water addition by adjusting the process parameters based on the torque measurement is much harder to realize based on the short period of liquid binder addition. Nevertheless, the torque measurement may be suitable for the "Process Analytical Technology" initiative of the FDA, for designing, analyzing, and controlling manufacturing through timely measurements (i.e., during processing) of critical quality and performance attributes of raw and in-process materials and processes with the goal of ensuring final product quality (FDA) (FDA, 2005) (Leuenberger, 1989).

V.4. Enteric Coating Process

V.4.1. Amount of Enteric Coating

The calculated enteric polymer coating level was not sufficient to achieve enteric resistance although the enteric film layer exhibited neither cracks nor a sponge-like structure. Considering the SEM pictures it can be seen that the layer was insufficiently thick to provide an enteric coating. The contrast between the calculated amount of 40% and the needed amount of 65% can be explained by the calibration of the Blaine method to determine the particle surface. It was calibrated with 1mm glass beads which only have a surface of $17.7\text{cm}^2/\text{g}$ compared to the micropellets ($97\text{-}192\text{ cm}^2/\text{g}$). This pronounced difference between the detected surface and the calibrated surface can lead to a loss of accuracy of the method. Especially for a conventional method in combination with a one point calibration this high discrepancy can lead to a failure in the estimation of the detected surface area. In addition the method has as a working range up to volume specific surface of $100\text{ cm}^2/\text{cm}^3$ and the detected volume specific surface of $68\text{ cm}^2/\text{cm}^3$ up to $135\text{ cm}^2/\text{cm}^3$ was even too close or above the working range of the Blaine method, respectively (Lehmann, 1999).

V.4.2. Comparison between the Mini-Glatt and the Hüttlin Mycrolab®

The process of coating mucoadhesive micropellets is complicated by the fact that the micropellets are wetted by the spraying solution and may become sticky combined with a high risk to form lumps. Hence it is important to remove the water from the process as fast as possible. Additionally, at elevated product temperatures, the EUDRAGIT® film layer might become sticky and the micropellets would form lumps. To avoid this problem it is important to balance the product temperature and water content by adjusting the inlet air temperature, spraying rate, and airflow. The Mini-Glatt® - as compared to the Hüttlin Mycrolab® - has an inherent risk to form lumps with micropellets, since its Wurster inlet provides less space for the freshly wetted product compared to the Hüttlin Mycrolab®. On the other hand, the Hüttlin Mycrolab® provides improved product movement leading to faster particle drying compared to the Mini-Glatt®.

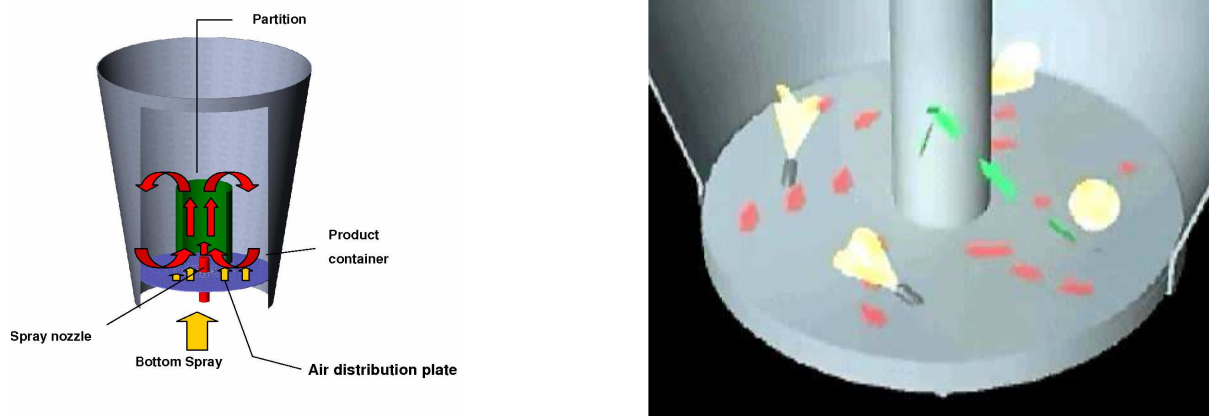


Figure V.3 Scheme of a Wurster inlet in comparison to the diskjet bottom by Hüttlin®. On the left the Wurster inlet is presented on the right the Diskjet Bottom is presented. In contrast to the presented scheme the Hüttlin Mycrolab® sprays only with one nozzle from the center.

The enteric coating process was only twice successful in the Mini-Glatt[®] and was not further reproducible. In the two successful batches the product temperature was 0.5 to 2°C lower than in the unsuccessful batches, resulting in a less stickier EUDRAGIT[®] coating. Since the applied temperatures were low in comparison to the values reported in the literature (35°C – 38°C, Lehmann, 1999), it is unlikely that these conditions lead to the formation of an unsuccessful run. A more likely explanation is, that the Mini-Glatt[®] equipment was at the border line of its skills by coating the mucoadhesive micropellets and a small change of environmental conditions resulted in a failure of the experiment.

The development of the process parameters using the Hüttlin Mycrolab[®] was very fast. The maximum spraying rate reached without particle agglomeration was 2.99g/min compared to 1.96g/min in the Mini-Glatt[®]. In summary, the Hüttlin Mycrolab[®] was superior to the Mini-Glatt[®] comparing the process alone, the process development time and the spraying rate. Last but not least, the process control and monitoring system was also superior.

V.5. Dissolution and EDX

V.5.1. Influence of the Dissolution Method

The different methods applied to the dissolution of API from the developed pellets showed great differences in terms of dissolution rates. This was also described by other authors (Langguth, 2004) (Cacace, 2004). Applying the paddle apparatus, 100% of the model drug theophyllin was liberated within 5 minutes, in contrast to the application of the basket apparatus, where 100% was liberated only within 21.75 hours. The slowing down of the dissolution profile using the basket apparatus is caused by the circumstance that all micropellets are forming one big lump thus resulting in slow diffusion-controlled dissolution. Hence, from my point of view, the basket method seems to have no *in vivo* relevance, because in the GI-tract the micropellets have a higher volume to spread and will not form one big lump. All methods except for the reciprocating cylinder show high reproducibility. As a result of the incomplete mixing of the dissolution medium the paddle apparatus with the sieve inlay does not represent an appropriate method either. The most qualified methods seem to be the unmodified paddle apparatus and the flow-through cell using the large cell with 18g glass beads and a flow rate of 20ml/min.

V.5.2. Dissolution of the Micropellets using App.2 and 4

For all coated micropellets gastric resistance was achieved during manufacture. Depending on the method, the dissolution profile changed from immediate release to slow release profiles for a given dosage form. All dissolution profiles showed an initial burst release followed by a phase of slow release due to a diffusion-control. The dissolution profile in the paddle apparatus was highly dependent on the agitation rate, where higher shearing forces broke down the micropellets and also prevented the formation of lumps. This circumstance leads to a strong correlation between dissolution rate and agitation. In general, the agitation should be selected based on appropriate discriminatory power, which will typically lead to the use of lower stirring rates (Stippler, 2004). Investigations on the effect of the agitation rate on dissolution of several solid oral dosage forms, for which the USP monograph requires a dissolution test at a paddle speed of 100 rpm, show no significant increase in dissolution rate from 75rpm to 100rpm (Shah, 1992). In contrast, the dissolution

rate of felodipine powder was highly dependent on the agitation rate in the range 50 – 150rpm (Scholz, 2003). To obtain correlations with *in vivo* situations, the hydrodynamic conditions in the paddle apparatus should mimic the gastrointestinal hydrodynamics. This requires not only an understanding of the hydrodynamics within the gastrointestinal tract but also of those in the particular dissolution apparatus. The hydrodynamics within the paddle apparatus are likely to be complex and variable at different sites in the vessel, although the paddle apparatus is composed of a relatively simple design (McCarthy, 2002). Initially the paddle apparatus was operated at 50rpm. The selection of 50rpm as stirring speed is not always justified experimentally and does not necessarily reflect the physiological conditions in the gastrointestinal tract. A successful prediction of the *in vivo* performance of felodipine micronized powder was possible by adjusting the agitation rate to 75rpm for the fasted state and 125rpm for the fed state (Scholz, 2003). In addition, coning (mounding) under the paddle which is an artefact of the test was avoided at 75rpm (Stippler, 2004).

It was not possible to convert the dissolution profile of the flow-through cell to the dissolution profile at either 50rpm or 100rpm in the paddle apparatus. In the case of Na-CMC the dissolution profile resulting from the flow-through cell was shown to be located between the curves of the paddle apparatus at 100rpm and 150rpm, in the case of Na-alginate nearly at 50rpm or slower. The dissolution profile applying the flow-through cell is highly dependent on the particle size of the formulation. Smaller particles are able to pass in greater amounts through the gaps between the glass beads resulting in coalescence of the small particles followed by a decrease in their release rate. This phenomenon also leads to a high variability between the cells, because the process of coalescence does not seem to be reproducible. In further experiments smaller glass beads should be tested to prevent coalescence of the particles.

The pronounced influence of the dissolution method is caused by a high tendency of forming lumps of mucoadhesive micropellets. This phenomenon makes it difficult to set up an *in vitro* method for predicting release rates *in vivo*, since it is not yet clear whether the micropellets are coalescing in the duodenum or not. Still a dissolution method with moderate shearing forces seems to be more reliable than others.

By comparison the fraction of the drug dissolved and the remaining EUDRAGIT[®] layer as determined by EDX combined with SEM, it was possible to show that a considerable drug portion was dissolved from all mucoadhesive micropellets without complete separation of the enteric EUDRAGIT[®] L 30D-55 film. However, the enteric coating is leaky rapidly after its exposure to a buffer at pH 6.0 and it takes much longer for the complete dissolution of the enteric coat. Regarding the poured film preparations an EUDRAGIT[®] L 30D-55 film remains at the surface even 20 minutes following the commence of dissolution. The same phenomenon is observed after 10 minutes of the dissolution test after which an EUDRAGIT[®] layer of 25 to 30µm thickness still remains on the micropellets. After 5 minutes 12% and after 15 minutes 25% of the model drug was dissolved from the coated chitosan micropellets. In this case it has to be considered that the chitosan micropellets were pre-treated for 2 hours in 0.1N HCl, which pre-wetted the film and may therefore result in a faster dissolution of the films. On the basis of these results it may be concluded that at pH 6.0 an obvious portion of theophyllin was dissolved - prior to a mucoadhesive effect *in vivo* will occur since coated mucoadhesive chitosan was not completely liberated from the EUDRAGIT[®] coating. These results have important implications for the concept of chitosan micropellet formulation because they only

exhibit mucoadhesive properties below pH 6.0. For successful mucoadhesive targeting of chitosan micropellets *in vivo* it is necessary that the complete EUDRAGIT[®] layer is dissolved before the micropellets reach the GI-tract environment where the pH is higher than 6.0. In consideration of the EDX results a considerable risk remains that the EUDRAGIT[®] layer will not dissolve completely before the micropellets reach the areas with the desired pH. In contrast to the chitosan formulation, the situation with Na-CMC and Na-alginate micropellets is different: The mucoadhesive properties are not as pH dependent as for chitosan. Since all dosage forms reach GI-tract areas as characterized by a pH higher than 6.0 relative rapidly, the dissolution of the EUDRAGIT[®] L 30D-55 coat *in vivo* will be much faster than compared to the dissolution *in vitro* at pH 6.0. Hence *in vivo*, the dissolution of the coat will be faster and cannot disturb the mucoadhesive properties of the micropellet. Only for Na-CMC and Na-alginate the mucoadhesive properties remained unchanged in an environment of relatively high pH. It can therefore be concluded that a chitosan formulation does not represent first choice formulation. The Na-CMC and Na-alginate formulations are suggested to be used for delivery to pH areas greater than pH 6.0.

The dissolution of EUDRAGIT[®] FS 30D is much faster compared to EUDRAGIT[®] L. It was completely separated from the poured film within 10 to 15 minutes, hence the problem of blocking the mucoadhesive polymer is reduced.

As can be seen from the EDX pictures the EUDRAGIT[®] layers of any formulation (chitosan, Na-CMC, Na-alginate plus coating) had a swollen appearance and were not regarded as solid as compared to the start of the test. This leads to the conclusion that a part of the dissolution of the EUDRAGIT[®] coating can be masked by the swelling process. Consequently, the thickness of the EUDRAGIT[®] coating layers have maybe no directly relationship to remaining mass of EUDRAGIT[®] layer.

V.6. Perspectives of the Mucoadhesive Micropellets

The topics of continuing activities can be split in two major fields, the improvement of the mucoadhesive micropellets and the characterization of the existing mucoadhesive micropellets. Regarding the granulation process the scope should be put on the variation of the MCC, the drug loading, a confirmation of the influencing process parameters by a factorial design experiment and in an upscaling of the process. A decrease of the MCC ratio lead to higher contents of the mucoadhesive polymer and thus maybe to an increase of the mucoadhesive capacity. A higher drug load of the mucoadhesive pellets will be important for drugs at a higher drug dosage.

Regarding the testing of the existing pellets the mucoadhesive capacity of the micropellets should be further tested *in vitro*. Furthermore, an *in vivo* test of a drug with low absorption rate or with an absorption window should be performed. Based on these *in vivo* studies an *in vivo* / *in vitro* correlation can be performed. And last but not least based on this information the most appropriate dissolution method can be selected.

V.7. Improving the Solubility of Spironolactone by Adjusting the HLB Value

The adjustment of the HLB value of a lipid matrix to the HLB of a drug to improve to solubility and dissolution is based on the theory that compounds are soluble in matrices with similar physicochemical properties. Solubility parameters are based on the same theory and have shown to predict the miscibility of two

compounds (Forster, 2001). A high correlation between the HLB value and the Moriguchi logP was found. On the basis of this correlation it was possible to calculate the HLB values of spironolactone. It was not possible within this thesis to evaluate whether an adjustment of the HLB value of the lipid matrix to the HLB value of the drug will lead to an improvement of the drug solubility. This was caused by the circumstance that all lipid matrices decomposed close to the melting temperature of spironolactone. The enthalpy of the decomposition was not reproducible and hence no reliable values for the enthalpy of fusion were calculated. Matrices with a higher solubility for the drug should have led to a decrease in enthalpy of the fusion or absence of melting peak at the same drug concentration. In contrast, Noordin et al. were able to calculate the paracetamol concentration in a lipid matrix based on the enthalpy of fusion. The onset of the melting peak of paracetamol was at 170°C and thus 30°C lower as the onset of the exothermic decomposition peak of the lipid matrix.

A blend of vitamin E TPGS and Softisan 154 exhibited two maxima as a consequence of their melting peak of the lipid matrix. The ratio between both enthalpies of fusion of the peaks was also not constant. In consideration of the incomplete molecular disperse mixture of vitamin E TPGS and Softisan 154 it is questionable how far the blend can provide improved solubility in comparison to the single excipient. The different ratio of the peaks can be explained by the different compositions of the matrix at different drug concentrations.

For an evaluation of the theory of improved solubility by adjusting the HLB values further experiments with a model drug identifiable with a lower melting point should be carried out. Further the Hansen solubility parameters should be calculated to compare the HLB value theory with existing theories of predicting solubility.

CHAPTER VI. SUMMARY

Many of the newly developed APIs in recent years exhibit poor bioavailability. To overcome this problem, new formulations such as microparticles and mucoadhesive dosage forms were developed. In this work a generally applicable method for the preparation of mucoadhesive micropellets of 250 to 600 μ m diameter is presented using rotor processing without the use of electrolytes. The mucoadhesive micropellets were developed to combine the advantages of mucoadhesion and microparticles. It was possible to produce mucoadhesive micropellets based on different mucoadhesive polymers Na-CMC, Na-alginate and chitosan. It was not possible to produce mucoadhesive micropellets consisting of two different polyacrylic acids (Carbopol[®] and Noveon AA1[®]). The resulting micropellets are characterized by a lower friability (6 to 17%) when compared to industrial produced cellulose pellets (Cellets[®]) (41.5%). They show acceptable tapped density (0.73g/ml to 0.9g/ml) and can be manufactured at high yields (>80%). The most influencing variables of the process are

- 1) the water content at the of the end spraying period, mainly characterized by
 - the liquid binder amount ,
 - the spraying rate,
 - the inlet air temperature,
 - the airflow,
 - the humidity of the inlet air,
- 2) the addition of the liquid binder, mainly characterized by
 - the spraying rate,
 - the rotor speed,
 - the type of rotor disc.

Torque measurement of the rotor disc and monitoring of the inlet and outlet air humidities have shown to be important tools for the development and production of pellets in the rotary processor.

In a subsequent step a fluidized bed coating process for the mucoadhesive micropellets was developed. It was possible to manifest a stable process in the Hüttlin Mycrolab[®] in contrast to the Mini-Glatt[®] apparatus, without agglomeration of the microparticles. To reach enteric resistance a 70% coating for Na-CMC micropellets, 85% for chitosan micropellets and 140% for Na-alginate micropellets calculated based on the amount of the starting micropellets was necessary. In consideration of the high amount of polymer needed to achieve an enteric resistance coating, long processing times were required.

Comparative dissolution experiments of the developed mucoadhesive micropellets were performed using the paddle apparatus with and without a sieve inlay, the basket apparatus, the reciprocating cylinder and flow-through cell. The paddle apparatus with a sieve inlay, the reciprocating cylinder and the basket apparatus were shown to be unqualified as dissolution apparatus. The mixing of the medium was insufficient inside the vessels of the paddle apparatus containing the sieve inlay, the cylinder of the reciprocating cylinder was blocked by the mucoadhesive micropellets and dissolution times using the basket apparatus were unusually long since the mucoadhesive micropellets formed one big lump. The paddle apparatus and the modified flow-through cell method turned out to be the successful methods for dissolution of mucoadhesive micropellets. Thus uncoated

and coated micropellets were dissolved. The flow-through cell was filled with a mixture of glass beads and micropellets to avoid coalescence. All dissolution profiles showed an initial burst release followed by a slow release due to diffusion control. Depending on the method, the dissolution profiles changed from immediate release to slow release. The dissolution rate in the paddle apparatus was mainly influenced by the agitation rate, where high rates led to fast dissolution profiles. The dissolution rate using the flow-through cell was influenced by the particle size of the micropellets since smaller particles were shown to enter the gaps between glass beads in a greater extent resulting in coalescence of the small particles followed by a decrease in their release rate. The flow-through cell and the paddle apparatus were selected because they were shown to be the most appropriate methods for dissolution.

Last but not least, the logP and the HLB value of different emulsifiers were correlated to transfer HLB values of excipients into logP values and logP values of API's into HLB values. On the basis of solubility experiments, it should be demonstrated that the adjustment of the HLB value of a lipid matrix to the HLB value of an API leads to a solubility improvement of the API within the lipid matrix. Due to the decomposition of the lipid matrix at the melting point of the tested API spironolactone, a proof of the theory of improvement of the solubility of an API by adjusting the HLB value of a lipid matrix to the HLB value of the drug was not possible. Hence the theory of solubility improvement could be not demonstrated.

The emphasis of additional research may be on one hand the further improvement of the micropellets for example first by reduction of the MCC content, second by variation of the drug load. Also a confirmation of the influencing process parameters may be important to be shown by factorial design experiments. On the other hand it would also be valuable to perform *in vitro* and *in vivo* testings of the mucoadhesive micropellets to study their effect on bioavailability.

CHAPTER VII. APPENDIX

VII.1. *Table of Contents Appendix*

VII.1.	TABLE OF CONTENTS APPENDIX.....	183
VII.2.	APPENDIX DISSOLUTION PROFILES.....	185
VII.2.1	Dissolution Profile using D1, APP.2 (100rpm)	185
VII.2.2	Dissolution Profile using D2, APP.2 (100rpm) and a Sieve Inlay of 250µm	185
VII.2.3	Dissolution Profile using D3, App.2 (100rpm), a Sieve Inlay of 250µm and Pellets between 400µm - 500µm	185
VII.2.4	Dissolution Profile using D4, App.2 (100rpm), a Sieve Inlay of 360µm and Pellets between 400µm - 500µm	186
VII.2.5	Dissolution Profile using D5, App.1 (100rpm)	186
VII.2.6	Dissolution Profile using D6, App.3 (dip rate of 25 per minute)	186
VII.2.7	Dissolution Profile using D8. App.4.....	187
VII.2.8	Dissolution Profile using D9. App.4.....	187
VII.2.9	Dissolution Profile using D10. App.4.....	187
VII.2.10	Dissolution Profile of 15658/56, App.2 D13 50rpm	187
VII.2.11	Dissolution Profile of 15658/5, App.2 D13 100rpm	188
VII.2.12	Dissolution Profile of 15658/56, App.2 D13 150rpm	188
VII.2.13	Dissolution Profile of 15658/53, App. 4 D15	188
VII.2.14	Dissolution Profile of 15658/56, App. 4 D17	189
VII.2.15	Dissolution Profile of 15658/53, App. 2 D12 150rpm	189
VII.2.16	Dissolution Profile of 15658/58, App. 2 D14 50rpm	189
VII.2.17	Dissolution Profile of 15658/58, App. 2 D14 100rpm	190
VII.2.18	Dissolution Profile of 15658/58. App. 2 D14 150rpm	190
VII.2.19	Dissolution Profile of 15658/53, App. 4 D16	190
VII.2.20	Dissolution Profile of 15658/58, App. 4 using D18	191
VII.2.21	Dissolution Profile of 15658/60, App. 2 using D11 50rpm	191
VII.2.22	Dissolution Profile of 15658/60, App. 2 using D11 100rpm	191
VII.2.23	Dissolution Profile of 15658/60, App. 2 using D11 150rpm	191
VII.2.24	Dissolution Profile of 15658/57, App. 2 using D13 50rpm	192
VII.2.25	Dissolution Profile of 15658/57, App. 2 using D13 100rpm	192
VII.2.26	Dissolution Profile of 15658/57, App. 2 using D13 150rpm	192
VII.2.27	Dissolution Profile of 15658/60, App. 4 using D15	193
VII.2.28	Dissolution Profile of 15658/57, App. 4 using D17	193
VII.2.29	Dissolution Profile of 15658/32. App. 2 using D11 50rpm	193
VII.2.30	Dissolution Profile of 15658/32, App. 2 using D11 150rpm	193
VII.2.31	Dissolution Profile of 15658/59, App. 2 using D13 50rpm	194
VII.2.32	Dissolution Profile of 15658/59, App. 2 using D13 100rpm	194
VII.2.33	Dissolution Profile of 15658/59, App. 2 using D13 150rpm	194
VII.2.34	Dissolution Profile of 15658/32 App. 4 using D15	195
VII.2.35	Dissolution Profile of 15658/59 App. 4 using D17	195
VII.3.	APPENDIX DSC FIGURES.....	196
Figure VII.3.1	DSC curve of Imwitor 308.....	196
Figure VII.3.2	DSC curve of blended Imwitor 308 and spironolactone (95:05).....	196
Figure VII.3.3	DSC curve of blended Imwitor 308 and spironolactone (90:10).....	196
Figure VII.3.4	DSC curve of blended Imwitor 308 and spironolactone (80:20).....	197
Figure VII.3.5	DSC curve of blended Imwitor 308 and spironolactone (70:30).....	197
Figure VII.3.6	DSC curve of blended Imwitor 308 and spironolactone (60:40).....	197
Figure VII.3.7	DSC curve of blended Imwitor 308 and spironolactone (50:50).....	198

Figure VII.3.8 DSC curve of Imwitor 312.....	198
Figure VII.3.9 DSC curve of blended Imwitor 312 and spironolactone (95:05).....	198
Figure VII.3.10 DSC curve of blended Imwitor 312 and spironolactone (90:10).....	199
Figure VII.3.11 DSC curve of blended Imwitor 312 and spironolactone (80:20).....	199
Figure VII.3.12 DSC curve of blended Imwitor 312 and spironolactone (70:30).....	199
Figure VII.3.13 DSC curve of blended Imwitor 312 and spironolactone (60:40).....	200
Figure VII.3.14 DSC curve of blended Imwitor 312 and spironolactone (50:50).....	200
Figure VII.3.15 DSC curve of Imwitor 742.....	200
Figure VII.3.16 DSC curve of blended Imwitor 742 and spironolactone (95:05).....	201
Figure VII.3.17 DSC curve of blended Imwitor 742 and spironolactone (90:10).....	201
Figure VII.3.18 DSC curve of blended Imwitor 742 and spironolactone (80:20).....	201
Figure VII.3.19 DSC curve of blended Imwitor 742 and spironolactone (70:30).....	202
Figure VII.3.20 DSC curve of blended Imwitor 742 and spironolactone (60:40).....	202
Figure VII.3.21 DSC curve of blended Imwitor 742 and spironolactone (50:50).....	202
Figure VII.3.22 DSC curve of Vitamin E acetate.....	203
Figure VII.3.23 DSC curve of blended Vitamin E acetate and spironolactone (95:05).....	203
Figure VII.3.24 DSC curve of blended Vitamin E acetate and spironolactone (90:10).....	203
Figure VII.3.25 DSC curve of blended Vitamin E acetate and spironolactone (80:20).....	204
Figure VII.3.26 DSC curve of blended Vitamin E acetate and spironolactone (70:30).....	204
Figure VII.3.27 DSC curve of blended Vitamin E acetate and spironolactone (60:40).....	204
Figure VII.3.28 DSC curve of blended Vitamin E acetate and spironolactone (50:50).....	205

VII.2. Appendix Dissolution Profiles

VII.2.1 Dissolution Profile using D1, APP.2 (100rpm)

Time (min)	Sample 1 [%]	Sample 2 [%]	Sample 3 [%]	Sample 4 [%]	Sample 5 [%]	Sample 6 [%]	Average [%]	SD [%]
1	42.69	61.48	63.52	57.26	47.57	37.04	51.59	9.83
2	87.02	94.11	88.73	87.65	86.34	88.17	88.67	2.55
5	91.53	95.46	95.00	96.31	94.37	98.28	95.16	2.04
10	87.12	92.38	96.83	97.49	98.20	99.46	95.25	4.25
15	90.03	95.53	96.13	97.23	94.07	94.86	94.64	2.29
20	87.08	92.45	93.06	94.00	93.17	93.96	92.29	2.39
30	89.49	93.19	94.76	95.75	94.73	98.41	94.39	2.70
45	91.04	93.66	101.14	99.13	103.33	99.21	97.92	4.25
60	93.55	100.10	97.66	97.73	97.59	98.08	97.45	1.95
90	93.42	96.72	98.79	97.98	98.41	108.78	99.02	4.72
120	87.16	93.03	94.14	99.30	96.21	97.04	94.48	3.84
150	90.51	103.56	101.84	99.39	98.64	87.78	96.95	5.80
180	90.56	99.18	102.09	100.12	97.88	99.46	98.22	3.65

VII.2.2 Dissolution Profile using D2, APP.2 (100rpm) and a Sieve Inlay of 250µm

Time (min)	Sample 1 [%]	Sample 2 [%]	Sample 3 [%]	Sample 4 [%]	Sample 5 [%]	Sample 6 [%]	Average [%]	SD [%]
1	58.85	71.25	52.83	90.14	69.47	58.39	66.82	13.42
2	92.12	96.71	88.14	106.06	108.24	109.64	100.15	9.07
3.5	97.48	102.21	84.44	103.48	102.45	106.49	99.43	7.89
5	115.13	101.75	90.69	101.41	102.11	103.81	102.48	7.78
10	107.25	102.23	94.39	100.45	100.19	100.62	100.86	4.13
15	98.81	102.96	94.01	100.85	117.65	100.49	102.46	8.03
20	97.95	101.19	95.32	101.14	99.46	100.62	99.28	2.30
30	98.96	101.42	96.81	99.72	87.85	98.46	97.20	4.83
45	98.06	100.58	97.37	100.07	99.15	99.64	99.15	1.22
60	100.03	100.94	100.81	99.64	100.29	99.93	100.27	0.51
90	99.87	102.13	102.5	98.95	100.84	99.69	100.66	1.42
120	97.90	99.29	97.79	99.16	99.33	98.99	98.74	0.71

VII.2.3 Dissolution Profile using D3, App.2 (100rpm), a Sieve Inlay of 250µm and Pellets between 400µm - 500µm

Time (min)	Sample 1 [%]	Sample 2 [%]	Sample 3 [%]	Sample 4 [%]	Sample 5 [%]	Sample 6 [%]	Average [%]	SD [%]
1	64.57	91.01	92.21	92.94	83.94	67.72	82.07	12.78
2	108.63	99.11	94.68	123.01	104.38	116.10	107.65	10.58
3.5	97.19	97.37	94.95	93.64	95.74	103.23	97.02	3.35
5	107.9	97.12	100.92	99.35	112.46	112.14	104.98	6.72
10	108.62	109.29	109.79	109.95	109.69	111.92	109.88	1.11
15	111.07	109.11	110.15	110.13	111.30	110.44	110.37	0.78
20	86.10	98.08	98.09	97.98	98.04	89.24	94.59	5.45
30	99.98	99.05	99.68	98.97	99.14	101.35	99.70	0.90
45	99.33	98.64	98.69	99.45	99.53	101.86	99.58	1.18
60	98.64	99.02	98.22	100.12	99.77	100.72	99.42	0.95
90	99.17	98.84	98.87	99.08	99.18	101.22	99.39	0.91
120	99.10	98.97	99.34	99.75	100.79	101.31	99.88	0.96

VII.2.4 *Dissolution Profile using D4, App.2 (100rpm), a Sieve Inlay of 360µm and Pellets between 400µm - 500µm*

Time (min)	Sample 1 [%]	Sample 2 [%]	Sample 3 [%]	Sample 4 [%]	Sample 5 [%]	Sample 6 [%]	Average [%]	SD [%]
1	54.15	65.96	72.16	66.43	66.82	45.32	61.81	10.01
2	97.52	100.37	99.12	95.24	100.18	96.27	98.12	2.12
3.5	100.62	99.7	98.22	96.88	98.82	101.37	99.27	1.64
5	99.79	98.55	100.78	101.67	99.08	98.89	99.79	1.21
10	100.02	98.6	97.9	96.81	96.26	98.39	98	1.35
15	100.74	98.83	97.57	98.15	97.49	98.97	98.63	1.21
20	99.84	98.85	97.84	98.97	96.35	98.03	98.31	1.2
30	88.19	97.5	98.75	95.73	95.18	86.64	93.67	5.03
45	98.83	97.53	97.21	96.93	97.67	97.9	97.68	0.66
60	101.13	99.26	98.2	99.17	98.18	101.1	99.51	1.33
90	100.64	98.72	98.9	97.46	98.84	98.45	98.84	1.03
120	100.96	105.89	100.6	100.04	98.59	98.64	100.79	2.69

VII.2.5 *Dissolution Profile using D5, App.1 (100rpm)*

Time (min)	Sample 1 [%]	Sample 2 [%]	Sample 3 [%]	Sample 4 [%]	Sample 5 [%]	Sample 6 [%]	Average [%]	SD [%]
1	3.36	5.92	3.68	5.9	4.98	4.56	4.73	0.99
2	4.46	4.98	4.4	4.72	5.2	4.81	4.76	0.28
5	5.53	6.13	5.23	6.89	6.9	6.25	6.16	0.63
10	7.53	8.12	7.06	7.56	7.92	7.9	7.68	0.35
15	8.75	9.88	8.61	9.49	9.94	9.7	9.4	0.53
20	10.74	13.28	10.58	11.12	11.76	11.28	11.46	0.9
30	12.65	13.55	13.41	13.71	13.69	13.16	13.36	0.37
45	16.34	17.88	15.79	16.7	17.26	17.14	16.85	0.67
60	19.93	21.11	18.77	21.11	20.27	19.75	20.16	0.81
90	24.95	26.45	23.91	25.96	25.49	24.89	25.28	0.82
120	29.91	32.65	28.86	31.5	30.37	29.76	30.51	1.24
150	34.69	36.94	33.24	36.52	35.4	34.44	35.21	1.26
180	38.78	40.95	37.02	39.63	39.43	38.87	39.11	1.18
240	46.9	49.83	44.48	48.38	48.57	46.13	47.38	1.76
1305	100.23	104.47	95.49	98.44	97.55	99.97	99.36	2.78

VII.2.6 *Dissolution Profile using D6, App.3 (dip rate of 25 per minute)*

Time (min)	Sample 1 [%]	Sample 2 [%]	Sample 3 [%]	Sample 4 [%]	Sample 5 [%]	Sample 6 [%]	Average [%]	SD [%]
1	2.35	3.65	4.38	5.64	2.03	1.99	3.34	1.48
2	3.16	4.58	5.24	8.61	2.83	2.71	4.52	2.25
5	4.96	5.72	8.55	14.36	5.59	3.42	7.10	3.93
10	6.92	7.11	12.62	20.23	5.85	4.85	9.60	5.87
15	8.22	8.69	15.88	14.06	7.05	6.15	10.01	3.99
20	11.22	11.02	19.34	19.19	9.29	8.12	13.03	4.96
30	13.75	14.11	23.12	24.35	11.02	9.77	16.02	6.21
45	16.84	21.65	28.82	31.02	14.13	11.71	20.70	7.90
60	21.26	26.03	33.48	38.36	16.74	13.43	24.88	9.67
90	32.97	35.45	43.79	50.90	22.66	17.46	33.87	12.54
120	49.87	42.88	51.38	57.85	26.12	21.18	41.55	14.74
150	75.72	56.79	60.03	68.32	30.80	25.18	52.81	20.40
180	81.90	61.20	68.61	74.18	34.82	27.38	58.02	22.05
240	94.07	74.04	81.31	81.93	43.71	33.45	68.09	23.96
300	100.86	82.55	90.30	86.18	50.47	37.98	74.72	24.72
1380	107.6	113.93	104.88	92.38	112.81	119.73	108.56	9.46

VII.2.7 Dissolution Profile using D8. App.4

Time (min)	Sample 1 [%]	Sample 2 [%]	Sample 3 [%]	Sample 4 [%]	Sample 5 [%]	Average [%]	SD [%]
1	6.17	6.42	7.01	8.84	5.97	6.88	1.16
2	14.15	13.63	19.34	17.42	16.72	16.25	2.37
5	27.46	26.24	38.55	35.23	34.66	32.43	5.32
10	38.57	37.12	53.47	47.72	49.05	45.19	7.05
15	45.27	43.20	61.74	55.16	56.65	52.40	7.88
30	59.54	54.64	76.15	68.19	69.31	65.57	8.49
45	69.24	62.86	84.01	75.90	77.00	73.80	8.05
60	76.90	69.82	90.32	82.95	83.26	80.65	7.70
75	83.16	75.81	95.26	88.62	88.82	86.33	7.28
90	88.40	80.86	99.12	93.44	93.39	91.04	6.84

VII.2.8 Dissolution Profile using D9. App.4

Time (min)	Sample 1 [%]	Sample 2 [%]	Sample 3 [%]	Sample 4 [%]	Sample 5 [%]	Average [%]	SD [%]
1	13.12	17.17	14.72	16.11	12.87	14.80	1.67
2	21.78	29.11	25.09	26.48	22.33	24.96	2.70
5	36.26	47.29	42.39	44.07	36.81	41.36	4.25
10	48.28	61.07	56.13	58.50	48.03	54.4	5.34
15	55.62	68.79	64.06	66.27	54.46	61.84	5.76
30	68.54	81.01	77.34	79.12	67.71	74.74	5.53
45	78.26	88.97	86.04	87.15	77.56	83.60	4.74
60	87.04	95.54	93.44	94.49	86.21	91.34	3.92
75	95.04	101.22	99.67	101.11	94.19	98.25	3.03
90	101.86	106.51	105.24	106.52	101.03	104.23	2.34

VII.2.9 Dissolution Profile using D10. App.4

Time (min)	Sample 1 [%]	Sample 2 [%]	Sample 3 [%]	Sample 4 [%]	Sample 5 [%]	Average [%]	SD [%]
1	6.51	9.32	10.75	10.53	8.85	9.19	1.7
2	14.42	20.49	20.56	20.70	18.35	18.90	2.69
5	29.13	38.63	37.59	37.13	34.53	35.40	3.82
10	41.97	53.37	51.18	50.80	47.63	48.99	4.43
15	50.00	61.89	58.90	58.54	55.51	56.97	4.50
30	65.24	77.51	76.91	73.27	68.84	72.36	5.27
45	77.41	85.39	84.35	80.52	76.52	80.84	3.99
60	83.59	90.91	89.83	86.04	82.70	86.61	3.66
75	89.09	95.99	94.83	91.22	87.85	91.80	3.53
90	93.41	99.62	98.56	94.53	91.98	95.62	3.32

VII.2.10 Dissolution Profile of 15658/56, App.2 D13 50rpm

Time (min)	Sample 1 [%]	Sample 2 [%]	Sample 3 [%]	Sample 4 [%]	Sample 5 [%]	Sample 6 [%]	Average [%]	SD [%]
0	0	0	0	0	0	0	0	0
15	0	0	0	0	0	0	0	0
30	0	0	0	0	0	0	0	0
45	0	0	0	0	0	0	0	0
60	0	0	0	0.06	0	0	0.01	0.03
90	0	0.12	0.06	0.18	0.12	0.06	0.09	0.06
120	0.36	0.54	0.48	0.60	0.54	0.42	0.49	0.09
125	14.33	13.25	12.68	13.14	12.28	11.93	12.94	0.85
135	51.21	45.43	43.69	45.87	37.21	34.96	43.06	6.00
150	61.40	62.07	67.13	61.42	58.08	59.67	61.63	3.07
180	69.57	74.65	80.23	70.89	71.50	71.37	73.04	3.90
210	74.54	80.40	85.04	75.77	77.64	77.15	78.42	3.80
240	78.03	84.15	87.02	78.96	81.16	81.13	81.74	3.34
300	84.19	88.51	87.98	84.93	86.23	85.59	86.24	1.70

VII.2.11 Dissolution Profile of 15658/5, App.2 D13 100rpm

Time (min)	Sample 1 [%]	Sample 2 [%]	Sample 3 [%]	Sample 4 [%]	Sample 5 [%]	Sample 6 [%]	Average [%]	SD [%]
0	0	0	0	0	0	0	0	0
15	0	0	0	0	0	0.07	0.01	0.03
30	0	0	0	0	0	0.07	0.01	0.03
45	0	0.07	0.07	0.07	0	0.14	0.06	0.05
60	0	0.07	0.07	0	0.07	0.14	0.06	0.05
90	0.22	0.29	0.29	0.15	0.28	0.36	0.27	0.07
120	0.74	0.88	0.79	0.73	0.84	0.79	0.80	0.06
125	9.14	9.36	6.68	7.47	12.30	5.52	8.41	2.40
135	57.85	51.44	50.83	53.95	54.25	43.83	52.03	4.72
150	68.90	60.72	62.53	64.47	62.54	59.97	63.19	3.21
180	76.93	68.39	69.63	71.28	70.98	68.51	70.95	3.17
210	81.87	73.84	74.52	76.00	76.53	73.46	76.04	3.10
240	85.63	78.04	78.39	79.70	79.97	77.26	79.83	3.02
300	91.38	84.23	84.57	85.42	85.31	83.07	85.66	2.93

VII.2.12 Dissolution Profile of 15658/56, App.2 D13 150rpm

Time (min)	Sample 1 [%]	Sample 2 [%]	Sample 3 [%]	Sample 4 [%]	Sample 5 [%]	Sample 6 [%]	Average [%]	SD [%]
0	0	0	0	0	0	0	0	0
15	0.63	0.90	0.45	0.42	0.53	0.48	0.57	0.18
30	0.59	0.60	0.62	0.77	0.67	0.84	0.68	0.10
45	0.79	0.83	0.83	0.76	0.85	1.09	0.86	0.12
60	0.73	0.83	0.95	0.99	0.88	0.74	0.85	0.11
90	1.13	1.09	1.24	1.16	1.22	1.34	1.20	0.09
120	1.78	1.88	1.80	1.96	1.82	1.83	1.85	0.07
130	88.93	83.49	86.50	89.06	89.27	93.36	88.44	3.28
140	98.27	91.36	94.71	96.42	95.43	99.99	96.03	2.99
150	97.55	92.80	95.15	96.75	96.71	99.33	96.38	2.22
180	99.16	95.85	97.74	99.23	99.79	100.21	98.67	1.61
210	99.57	98.12	99.23	99.50	99.67	99.66	99.29	0.60
240	100.34	99.35	98.72	99.57	99.71	99.72	99.57	0.53
300	99.94	99.57	98.71	99.10	99.81	99.01	99.36	0.49
360	99.58	100.32	99.69	99.59	100.15	99.69	99.84	0.32

VII.2.13 Dissolution Profile of 15658/53, App. 4 D15

Time (min)	Sample 1 [%]	Sample 2 [%]	Sample 3 [%]	Sample 4 [%]	Sample 5 [%]	Average [%]	SD [%]
0	0	0	0	0	0	0	0
5	40.31	37.80	35.42	43.75	47.93	41.08	4.93
10	53.99	48.86	49.30	61.22	61.89	55.05	6.27
20	65.55	57.36	60.00	72.88	72.36	65.63	7.03
44	78.06	66.94	71.27	83.41	82.68	76.47	7.20
68	85.61	72.58	78.05	88.92	88.37	82.71	7.13
92	90.67	77.16	82.87	93.33	92.37	87.28	7.00
116	95.25	81.59	87.22	97.11	96.40	91.51	6.82
140	98.45	85.90	90.76	100.63	99.78	95.10	6.46
164	101.43	89.42	94.01	103.06	102.88	98.16	6.14

VII.2.14 *Dissolution Profile of 15658/56, App. 4 D17*

Time (min)	Sample 1 [%]	Sample 2 [%]	Sample 3 [%]	Sample 4 [%]	Sample 5 [%]	Average [%]	SD [%]
0	0	0	0	0	0	0	0
24	0	0	0	0	0	0	0
48	1.22	1.16	1.41	1.24	1.23	1.25	0.09
72	2.45	2.60	3.08	2.45	3.09	2.73	0.33
96	3.67	3.94	4.34	3.65	4.17	3.95	0.30
120	4.96	5.34	5.58	4.86	5.36	5.22	0.30
130	28.88	26.07	26.23	25.94	26.00	26.63	1.27
140	67.59	63.85	65.26	62.52	65.80	65.00	1.93
164	85.70	82.55	84.60	80.70	84.59	83.63	2.00
188	95.18	92.81	94.46	91.72	94.45	93.72	1.42
212	99.06	97.16	98.25	96.83	98.48	97.96	0.93

VII.2.15 *Dissolution Profile of 15658/53, App. 2 D12 150rpm*

Time (min)	Sample 1 [%]	Sample 2 [%]	Sample 3 [%]	Sample 4 [%]	Sample 5 [%]	Sample 6 [%]	Average [%]	SD [%]
0	0	0	0	0	0	0	0	0
5	77.67	66.27	60.12	73.11	63.98	77.09	69.71	7.29
15	89.16	79.61	84.14	88.95	79.21	88.94	85.00	4.73
30	92.43	84.33	86.87	89.81	84.69	92.97	88.52	3.79
45	90.84	85.91	86.79	88.94	84.75	92.04	88.21	2.88
60	88.70	86.41	88.09	88.33	85.70	88.06	87.55	1.20
90	90.97	88.06	87.43	88.21	87.08	87.97	88.29	1.38
120	90.29	88.56	88.74	88.86	89.00	89.05	89.08	0.62
150	91.59	89.92	90.11	90.00	90.76	89.84	90.37	0.68
210	96.13	94.26	94.67	94.61	94.70	94.28	94.78	0.69
240	97.51	97.00	97.01	97.06	97.42	97.24	97.21	0.22

VII.2.16 *Dissolution Profile of 15658/58, App. 2 D14 50rpm*

Time (min)	Sample 1 [%]	Sample 2 [%]	Sample 3 [%]	Sample 4 [%]	Sample 5 [%]	Sample 6 [%]	Average [%]	SD [%]
0	0	0	0	0	0	0	0	0
15	0.07	0	0	0	0	0	0.01	0.03
30	0.07	0	0.06	0	0	0.08	0.04	0.04
45	0.07	0	0.06	0	0.07	0.08	0.05	0.04
60	0.07	0.07	0.06	0	0.07	0.08	0.06	0.03
90	0.07	0.07	0.06	0.07	0.07	0.08	0.07	0.01
120	0.14	0.07	0.06	0.07	0.07	0.08	0.08	0.03
125	9.60	9.40	8.17	9.99	10.04	10.64	9.64	0.84
135	10.91	11.04	9.47	10.87	10.40	12.17	10.81	0.88
150	50.55	50.27	43.34	51.14	47.22	55.78	49.72	4.16
180	52.33	57.83	50.27	62.01	57.55	64.50	57.42	5.45
210	63.44	62.33	54.29	67.23	62.82	69.55	63.28	5.23
240	67.01	65.6	57.31	70.98	66.93	73.30	66.86	5.50
300	72.29	70.44	61.63	76.12	72.85	78.65	72.00	5.86
360	83.26	74.25	64.71	79.57	76.61	82.17	76.76	6.80

VII.2.17 *Dissolution Profile of 15658/58, App. 2 D14 100rpm*

Time (min)	Sample 1 [%]	Sample 2 [%]	Sample 3 [%]	Sample 4 [%]	Sample 5 [%]	Sample 6 [%]	Average [%]	SD [%]
0	0	0	0	0	0	0	0	0
15	0	0	0	0	0	0	0	0
30	0	0	0	0	0	0	0	0
45	0	0	0	0	0	0	0	0
60	0	0	0	0.06	0	0	0.01	0.02
90	0	0.13	0.06	0.19	0.12	0.06	0.09	0.07
120	0.37	0.57	4.93	0.63	0.56	0.44	1.25	1.81
125	14.34	13.26	12.67	13.15	12.27	11.90	12.93	0.86
135	51.26	45.38	43.70	45.90	37.17	35.03	43.07	6.00
150	61.42	62.10	67.10	61.43	58.05	59.65	61.63	3.06
180	69.60	74.67	80.21	70.88	71.50	71.43	73.05	3.89
210	74.52	80.39	85.02	75.77	77.63	77.19	78.42	3.79
240	78.03	84.10	87.02	78.96	81.16	81.20	81.75	3.33
300	84.18	88.50	87.95	84.91	86.18	85.65	86.23	1.70
360	86.52	89.13	87.39	87.60	88.35	86.97	87.66	0.95

VII.2.18 *Dissolution Profile of 15658/58, App. 2 D14 150rpm*

Time (min)	Sample 1 [%]	Sample 2 [%]	Sample 3 [%]	Sample 4 [%]	Sample 5 [%]	Sample 6 [%]	Average [%]	SD [%]
0	0	0	0	0	0	0	0	0.00
15	0.2	0.47	0.32	0.17	0.04	0.71	0.32	0.24
30	0.26	0.00	0.06	0.21	0.21	0.20	0.15	0.10
45	0.02	0.11	0.17	0.23	0.17	0.12	0.14	0.07
60	-0.06	0.12	0.26	0.28	0.20	0.23	0.17	0.13
90	0.02	0.18	0.21	0.13	0.11	0.29	0.16	0.09
120	0.24	0.11	0.22	0.00	0.13	0.29	0.16	0.09
130	82.81	58.70	61.03	11.65	10.56	4.70	38.24	33.23
140	82.34	56.87	62.07	78.35	76.72	76.82	72.20	10.2
150	88.43	82.42	82.62	80.86	79.28	79.31	82.15	3.40
180	97.41	86.80	86.52	84.86	81.87	81.08	86.43	5.88
210	105.03	103.67	93.88	94.21	87.41	97.92	97.02	6.62
240	106.78	102.22	n.d.	101.21	103.87	94.70	101.76	4.47
300	105.52	103.03	101.58	101.05	101.05	101.01	102.04	1.97
360	105.48	101.61	101.68	100.50	101.29	102.43	102.16	1.74

VII.2.19 *Dissolution Profile of 15658/53, App. 4 D16*

Time (min)	Sample 1 [%]	Sample 2 [%]	Sample 3 [%]	Sample 4 [%]	Sample 5 [%]	Average [%]	SD [%]
0	0	0	0	0	0	0	0
5	37.01	38.72	36.26	36.36	42.89	38.25	2.77
10	50.52	53.64	49.25	51.80	57.08	52.46	3.05
20	61.11	63.26	59.83	62.37	67.85	62.89	3.06
40	70.65	71.22	69.66	71.34	76.93	71.96	2.86
60	76.53	75.97	75.28	76.95	81.95	77.34	2.65
80	81.09	79.84	79.56	81.41	85.60	81.56	2.55
100	85.05	83.39	83.16	85.15	89.48	85.25	2.54
120	88.60	87.54	86.36	88.40	92.56	88.69	2.34
140	91.88	90.37	89.31	91.36	95.26	91.64	2.25

VII.2.20 Dissolution Profile of 15658/58, App. 4 using D18

Time (min)	Sample 1 [%]	Sample 2 [%]	Sample 3 [%]	Sample 4 [%]	Sample 5 [%]	Average [%]	SD [%]
0	0	0	0	0	0	0	0
20	0	0	0	0	0	0	0
40	0	0	0	0	0	0	0
60	0	0	0	0	0	0	0
80	0	0	0	0	0	0	0
100	0	0	0	0	0	0	0
120	0	0	0	0	0	0	0
130	1.17	1.14	1.12	1.35	1.23	1.20	0.09
140	25.05	26.14	24.68	26.46	23.27	25.12	1.27
160	66.58	72.17	67.29	75.09	67.35	69.70	3.75
180	72.98	78.90	73.40	80.47	72.72	75.70	3.69
200	77.02	83.12	77.65	83.52	75.81	79.42	3.62
220	79.63	87.72	80.86	85.69	78.04	82.39	4.13

VII.2.21 Dissolution Profile of 15658/60, App. 2 using D11 50rpm

Time (min)	Sample 1 [%]	Sample 2 [%]	Sample 3 [%]	Sample 4 [%]	Sample 5 [%]	Sample 6 [%]	Average [%]	SD [%]
0	0	0	0	0	0	0	0.00	0.00
5	40.15	24.77	14.72	35.14	37.38	26.99	29.86	9.53
15	49.11	34.06	19.57	42.31	47.34	36.12	38.09	10.84
30	55.1	41.21	24.05	49.18	53.09	41.67	44.05	11.35
45	58.93	46.22	27.74	52.86	57.14	45.51	48.07	11.37
60	62.06	50.31	31.13	56.54	60.76	48.85	51.61	11.37
90	67.19	57.57	37.26	63.25	67.17	54.8	57.87	11.28
120	71.41	63.95	42.75	67.51	72.07	59.92	62.94	10.90
150	74.77	69.46	47.76	71.27	76.31	64.5	67.35	10.46
180	77.82	74.16	52.39	74.68	80.13	68.58	71.29	10.05
210	80.49	78.25	56.61	77.91	83.33	72.16	74.79	9.64
240	82.81	82	60.52	81.28	86.3	75.34	78.04	9.29

VII.2.22 Dissolution Profile of 15658/60, App. 2 using D11 100rpm

Time (min)	Sample 1 [%]	Sample 2 [%]	Sample 3 [%]	Sample 4 [%]	Sample 5 [%]	Sample 6 [%]	Average [%]	SD [%]
0	0	0	0	0	0	0	0	0
5	35.92	39.61	34.99	55.38	51.80	81.30	49.83	17.57
15	48.11	51.16	49.56	64.37	62.10	93.72	61.50	17.18
30	57.21	60.35	58.07	73.17	69.71	96.02	69.09	14.71
45	63.58	67.00	65.05	78.36	75.01	96.90	74.32	12.50
60	68.64	72.01	70.25	82.32	79.14	97.16	78.25	10.68
90	76.26	79.57	77.92	87.89	85.23	97.32	84.03	7.88
120	81.40	84.88	83.35	91.66	89.32	97.16	87.96	5.90
150	84.98	88.72	87.21	94.31	92.16	97.01	90.73	4.56
180	87.81	91.26	90.06	96.00	93.83	96.70	92.61	3.49
210	89.92	93.09	92.25	97.00	95.19	96.63	94.01	2.75
240	91.66	94.38	93.87	97.66	95.76	96.55	94.98	2.14

VII.2.23 Dissolution Profile of 15658/60, App. 2 using D11 150rpm

Time (min)	Sample 1 [%]	Sample 2 [%]	Sample 3 [%]	Sample 4 [%]	Sample 5 [%]	Sample 6 [%]	Average [%]	SD [%]
0	0	0	0	0	0	0	0	0
5	56.67	52.22	49.63	48.14	49.88	44.80	49.89	3.39
15	67.60	61.82	60.78	98.17	63.69	57.82	68.26	15.03
30	74.01	68.62	67.48	74.89	72.44	66.57	70.67	3.56
45	77.71	73.70	71.51	72.67	77.93	71.47	74.17	2.95
60	80.47	77.71	74.92	74.31	82.35	75.78	77.59	3.23
90	83.46	83.07	79.80	78.31	86.87	79.76	81.88	3.17
120	85.64	87.08	83.60	82.12	83.88	89.06	85.23	2.55
150	85.64	87.08	83.60	82.12	83.88	89.06	85.23	2.55
180	90.94	92.41	90.83	89.70	92.54	90.34	91.13	1.14
210	94.17	95.19	94.13	93.41	95.42	94.45	94.46	0.74
240	97.16	97.97	97.24	97.14	97.96	97.28	97.46	0.40

VII.2.24

Dissolution Profile of 15658/57, App. 2 using D13 50rpm

Time (min)	Sample 1 [%]	Sample 2 [%]	Sample 3 [%]	Sample 4 [%]	Sample 5 [%]	Sample 6 [%]	Average [%]	SD [%]
0	0	0	0	0	0	0	0	0
15	0	0	0	0	0	0	0	0
30	0	0	0	0	0	0	0	0
45	0	0	0	0	0	0	0	0
60	0	0	0	0	0	0	0	0
90	0	0	0	0	0	0	0	0
120	1.65	1.72	1.87	1.79	1.82	1.96	1.80	0.11
125	15.11	15.51	15.91	14.57	13.82	15.20	15.02	0.74
135	32.30	30.73	34.43	30.57	40.22	44.24	35.42	5.60
150	53.02	54.34	59.82	78.36	52.29	64.71	60.42	9.98
180	76.83	75.52	72.59	75.71	68.95	71.86	73.58	2.97
210	84.96	82.91	77.89	81.86	76.73	76.75	80.18	3.52
240	88.85	86.00	81.78	86.21	82.04	80.89	84.30	3.17
300	93.67	90.31	88.05	91.21	89.67	86.83	89.96	2.41
360	96.76	93.47	92.38	94.14	94.40	90.90	93.68	1.98

VII.2.25

Dissolution Profile of 15658/57, App. 2 using D13 100rpm

Time (min)	Sample 1 [%]	Sample 2 [%]	Sample 3 [%]	Sample 4 [%]	Sample 5 [%]	Sample 6 [%]	Average [%]	SD [%]
0	0	0	0	0	0	0	0	0
15	0.08	0.08	0.08	0.08	0.08	0.08	0.08	0
30	0.16	0.08	0.08	0.08	0.08	0.08	0.09	0.03
45	0.16	0.16	0.15	0.15	0.08	0.16	0.14	0.03
60	0.24	0.16	0.15	0.15	0.15	0.23	0.18	0.04
90	0.55	0.56	0.54	0.54	0.54	0.62	0.56	0.03
120	2.13	2.07	1.99	2.09	2.00	2.10	2.06	0.06
125	15.4	15.41	20.21	15.25	15.72	13.64	15.94	2.22
135	65.09	69.58	73.97	65.17	68.26	60.64	67.12	4.56
150	83.97	87.13	89.43	82.82	83.20	79.42	84.33	3.51
180	94.15	97.14	97.70	91.49	91.37	90.80	93.78	3.06
210	98.74	100.64	101.45	96.21	95.22	95.79	98.01	2.65
240	100.47	101.03	101.23	100.54	97.38	98.21	99.81	1.61
300	101.74	100.40	100.61	100.93	99.38	100.08	100.52	0.80
360	101.66	99.84	100.08	100.23	100.15	100.16	100.35	0.65

VII.2.26

Dissolution Profile of 15658/57, App. 2 using D13 150rpm

Time (min)	Sample 1 [%]	Sample 2 [%]	Sample 3 [%]	Sample 4 [%]	Sample 5 [%]	Average [%]	SD [%]
0	0	0	0	0	0	0	0
15	1.12	0.41	0.32	0.39	0.48	0.54	0.32
30	0.69	0.17	0.38	0.27	0.73	0.45	0.25
45	0.52	0.10	0.54	0.22	0.68	0.41	0.24
60	0.36	-0.96	-0.98	-1.09	-1.12	-0.76	0.63
90	1.42	1.11	1.00	0.82	1.01	1.07	0.22
120	3.14	2.83	2.99	2.61	2.79	2.87	0.20
130	54.66	71.46	87.82	81.12	84.38	75.89	13.34
140	93.23	99.26	103.97	98.84	100.27	99.11	3.86
150	94.59	99.07	102.49	99.48	99.31	98.99	2.83
180	95.09	101.30	104.33	99.16	102.57	100.49	3.56
210	95.91	101.39	104.71	104.89	103.25	102.03	3.70
240	96.41	101.37	103.47	100.47	103.23	100.99	2.85
300	96.77	101.80	102.57	103.26	104.25	101.73	2.91
360	99.37	101.63	103.66	100.52	101.94	101.42	1.61

VII.2.27 *Dissolution Profile of 15658/60, App. 4 using D15*

Time (min)	Sample 1 [%]	Sample 2 [%]	Sample 3 [%]	Sample 4 [%]	Sample 5 [%]	Average [%]	SD [%]
0	0	0	0	0	0	0	0
5	25.55	20.20	17.19	31.08	25.69	23.94	5.39
10	36.22	26.83	21.65	40.29	34.22	31.84	7.50
20	44.73	34.64	26.09	48.18	41.49	39.03	8.79
40	53.30	42.82	32.23	55.64	48.43	46.48	9.36
60	59.20	48.90	36.87	60.22	52.49	51.53	9.45
80	63.16	53.40	41.71	63.86	55.76	55.38	9.38
100	66.53	57.69	44.38	66.99	58.47	58.81	9.17
120	69.55	61.39	47.61	69.79	61.00	61.87	9.03
140	72.18	64.82	50.73	72.63	63.35	64.74	8.88

VII.2.28 *Dissolution Profile of 15658/57, App. 4 using D17*

Time (min)	Sample 1 [%]	Sample 2 [%]	Sample 3 [%]	Sample 4 [%]	Sample 5 [%]	Average [%]	SD [%]
0	0	0	0	0	0	0	0
24	0	0	0	0	0	0	0
48	0	0.36	0.15	0.09	0.09	0.14	0.14
72	0.12	0.41	0.27	0.23	0.21	0.25	0.11
96	0.48	0.75	0.59	0.60	0.50	0.58	0.11
120	1.66	1.87	1.66	1.71	1.35	1.65	0.19
130	15.16	15.62	19.47	14.47	14.73	15.89	2.05
140	40.14	41.40	50.95	40.12	43.67	43.26	4.54
164	53.64	54.83	66.51	55.64	60.29	58.17	5.30
188	58.29	59.78	72.33	59.99	66.12	63.30	5.87
212	61.76	63.43	76.38	62.84	70.13	66.91	6.23
236	64.54	66.53	79.49	65.46	73.56	69.91	6.43

VII.2.29 *Dissolution Profile of 15658/32, App. 2 using D11 50rpm*

Time (min)	Sample 1 [%]	Sample 2 [%]	Sample 3 [%]	Sample 4 [%]	Sample 5 [%]	Sample 6 [%]	Average [%]	SD [%]
0	6.65	1.50	5.71	3.04	1.71	2.58	3.53	2.15
6	57.96	64.42	70.93	71.02	67.59	81.00	68.82	7.70
15	75.32	77.28	89.54	81.82	77.73	92.16	82.31	7.00
30	85.93	79.03	94.62	88.92	83.72	95.31	87.92	6.35
45	89.52	82.88	94.83	89.23	86.70	98.27	90.24	5.55
60	92.33	85.98	95.01	91.42	89.10	98.44	92.05	4.37
90	94.13	95.68	94.52	96.13	94.47	98.79	95.62	1.73
120	97.02	94.02	100.04	97.26	96.21	98.84	97.23	2.09
150	95.36	98.81	99.17	96.35	98.31	102.02	98.34	2.34
180	97.15	99.33	101.36	96.68	96.79	102.29	98.93	2.46
210	98.42	97.65	100.24	99.26	97.26	98.83	98.61	1.09
240	98.59	98.03	99.89	98.72	97.86	99.77	98.81	0.85

VII.2.30 *Dissolution Profile of 15658/32, App. 2 using D11 150rpm*

Time (min)	Sample 1 [%]	Sample 2 [%]	Sample 3 [%]	Sample 4 [%]	Sample 5 [%]	Sample 6 [%]	Average [%]	SD [%]
0	0	0	0	0	0	0	0	0
5	88.86	92.40	91.44	89.82	88.85	91.4	90.48	1.47
15	97.74	98.79	98.65	99.01	97.79	99.32	98.55	0.65
30	98.23	99.15	99.55	99.79	99.57	99.70	99.33	0.59
45	98.23	99.15	99.55	99.79	99.57	99.70	99.33	0.59
60	98.87	99.49	99.85	99.86	99.65	99.72	99.58	0.37
90	97.99	98.70	99.16	99.51	99.03	99.56	98.99	0.58
120	98.24	99.03	99.23	99.20	99.06	99.57	99.05	0.44
150	98.19	99.11	98.97	99.09	98.91	99.05	98.89	0.35
180	98.64	99.38	99.69	99.97	99.54	99.90	99.52	0.49
210	99.25	99.84	100.42	100.06	100.14	100.17	99.98	0.40
240	99.63	100.67	100.45	100.63	100.46	100.95	100.46	0.45

VII.2.31

Dissolution Profile of 15658/59, App. 2 using D13 50rpm

Time (min)	Sample 1 [%]	Sample 2 [%]	Sample 3 [%]	Sample 4 [%]	Sample 5 [%]	Sample 6 [%]	Average [%]	SD [%]
0	0.77	0.80	0.69	0.75	0.76	0.75	0.75	0.04
15	0.77	0.80	0.69	0.75	0.76	0.75	0.75	0.04
30	0.77	0.80	0.69	0.75	0.76	0.75	0.75	0.04
45	0.77	0.80	0.69	0.75	0.76	0.75	0.75	0.04
60	0.77	0.80	0.69	0.75	0.76	0.75	0.75	0.04
90	0.77	0.80	0.69	0.75	0.76	0.75	0.75	0.04
117	0.77	0.80	0.69	0.75	0.76	0.75	0.75	0.04
125	7.98	9.62	5.69	8.82	7.93	24.44	10.75	6.84
135	24.10	23.77	20.84	26.25	25.64	28.98	24.93	2.73
150	57.99	53.83	51.00	59.25	65.45	57.30	57.47	4.95
180	76.93	77.05	75.73	84.46	86.09	76.12	79.40	4.61
210	79.99	83.25	95.28	103.84	86.13	84.19	88.78	9.00
240	90.57	98.17	96.61	106.28	90.40	91.68	95.62	6.16
300	86.01	104.58	93.22	105.16	93.71	87.28	94.99	8.25
360	96.60	103.14	87.51	105.28	90.41	90.71	95.61	7.32

VII.2.32

Dissolution Profile of 15658/59, App. 2 using D13 100rpm

Time (min)	Sample 1 [%]	Sample 2 [%]	Sample 3 [%]	Sample 4 [%]	Sample 5 [%]	Sample 6 [%]	Average [%]	SD [%]
0	0.72	0.73	0.73	0.70	0.72	0.69	0.71	0.02
15	0.72	0.73	0.73	0.70	0.72	0.69	0.71	0.02
30	0.72	0.73	0.73	0.70	0.72	0.69	0.71	0.02
45	0.72	0.73	0.73	0.70	0.72	0.69	0.71	0.02
60	0.72	0.73	0.73	0.70	0.72	0.69	0.71	0.02
90	0.72	0.73	0.73	0.70	0.72	0.69	0.71	0.02
120	0.72	0.73	0.73	0.70	0.72	0.69	0.71	0.02
125	12.89	12.56	10.18	n.d.	12.44	12.85	12.18	1.13
135	24.47	26.97	25.85	25.98	23.76	24.48	25.25	1.21
150	65.62	72.98	69.73	66.40	73.96	62.32	68.50	4.52
180	82.01	89.93	92.44	89.39	90.23	94.74	89.79	4.30
210	90.45	100.11	98.13	96.85	96.36	89.08	95.16	4.40
240	94.71	96.48	98.71	94.77	95.80	92.49	95.49	2.08
300	95.79	99.55	100.50	95.21	96.52	96.63	97.37	2.14
360	98.30	98.59	99.18	95.85	99.06	98.64	98.27	1.23

VII.2.33

Dissolution Profile of 15658/59, App. 2 using D13 150rpm

Time (min)	Sample 1 [%]	Sample 2 [%]	Sample 3 [%]	Sample 4 [%]	Sample 5 [%]	Average [%]	SD [%]
0	0	0	0	0	0	0	0
15	1.04	1.80	0.42	1.14	1.64	1.21	0.54
30	0.31	0.83	0.16	0.38	0.68	0.47	0.28
45	0.28	0.88	0.10	0.24	0.70	0.44	0.33
60	0.43	0.63	0.10	0.23	0.40	0.36	0.20
90	0.71	1.35	0.10	0.53	0.86	0.71	0.46
120	0.99	1.51	0.42	0.98	1.50	1.08	0.45
130	31.84	46.64	41.42	54.49	59.14	46.70	10.77
140	77.94	86.33	79.99	92.33	102.89	87.90	10.11
150	100.84	97.72	83.74	98.46	98.62	95.88	6.88
180	107.01	111.23	91.36	98.91	108.26	103.34	8.13
210	105.76	96.56	95.56	100.61	103.20	100.34	4.32
240	98.86	100.96	91.35	93.96	104.43	98.05	5.10
300	100.68	95.16	86.93	93.97	106.85	96.72	7.49
360	107.49	104.68	93.54	91.06	104.06	100.16	7.35

VII.2.34 *Dissolution Profile of 15658/32 App. 4 using D15*

Time (min)	Sample 1 [%]	Sample 2 [%]	Sample 3 [%]	Sample 4 [%]	Sample 5 [%]	Average [%]	SD [%]
0	0	0	0	0	0	0	0
5	57.92	51.14	69.08	57.23	72.23	61.52	8.82
10	69.00	63.69	79.10	69.21	81.88	72.58	7.62
20	76.78	71.42	85.55	77.08	87.85	79.73	6.79
40	84.35	79.36	91.19	84.67	82.89	86.49	5.52
60	90.19	86.23	95.15	89.40	96.47	91.49	4.24
80	93.93	93.25	96.90	93.14	98.95	95.23	2.58
100	97.21	95.77	98.06	94.87	99.52	97.09	1.84
120	98.97	98.02	98.96	96.95	99.85	98.53	1.09
140	99.68	99.35	99.58	97.98	100	99.32	0.78
160	100	100	100	100	100	100	0

VII.2.35 *Dissolution Profile of 15658/59 App. 4 using D17*

Time (min)	Sample 1 [%]	Sample 2 [%]	Sample 3 [%]	Sample 4 [%]	Sample 5 [%]	Average [%]	SD [%]
0	0	0	0	0	0	0	0
23	0	0	0	0	0	0	0
47	0	0	0	0	0	0	0
69	0	0	0	0	0	0	0
91	0	0	0	0	0	0	0
116	0.28	0.49	0	0.14	0	0.18	0.19
120	0.38	0.61	0.11	0.25	0.09	0.29	0.19
130	7.60	6.43	5.46	5.54	4.22	5.85	1.12
140	21.84	22.54	18.69	20.82	16.07	19.99	2.35
164	59.80	68.04	57.17	75.42	80.60	68.21	8.92
188	66.98	72.74	66.26	88.82	93.80	77.72	11.43
213	69.71	76.02	70.41	92.09	96.22	80.89	11.13

VII.3. Appendix DSC Figures

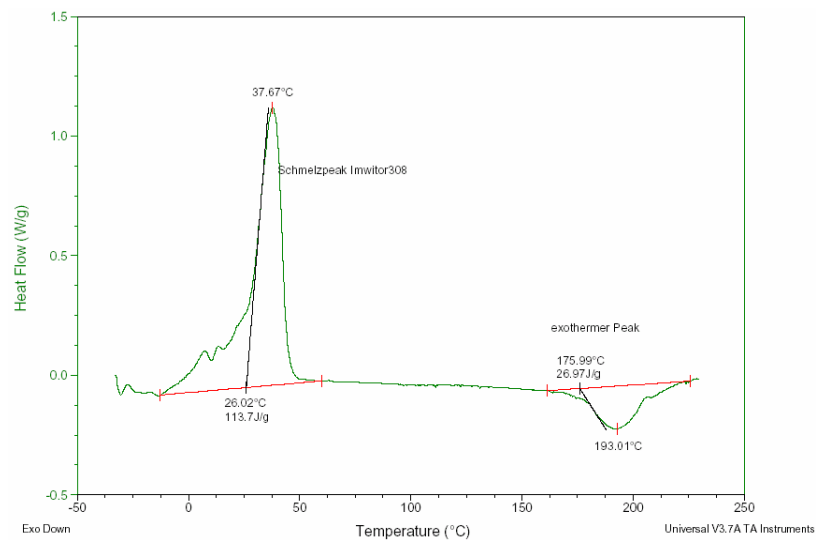


Figure VII.3.1 DSC curve of Imwitor 308.

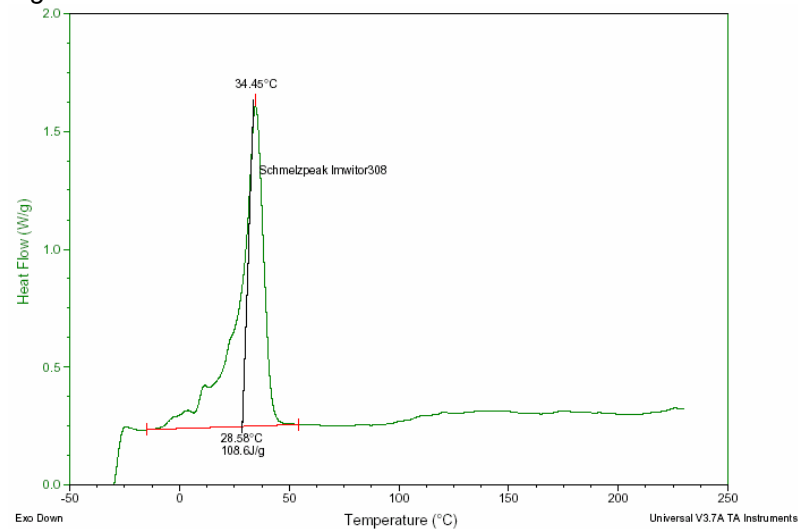


Figure VII.3.2 DSC curve of blended Imwitor 308 and spironolactone (95:05).

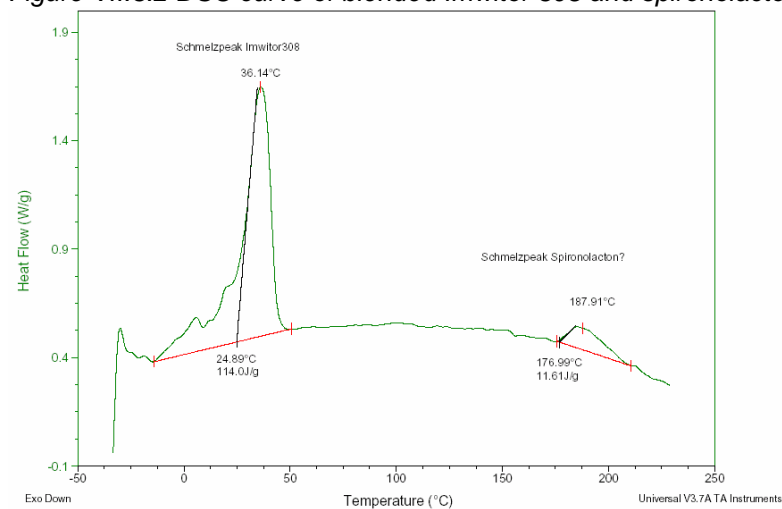


Figure VII.3.3 DSC curve of blended Imwitor 308 and spironolactone (90:10).

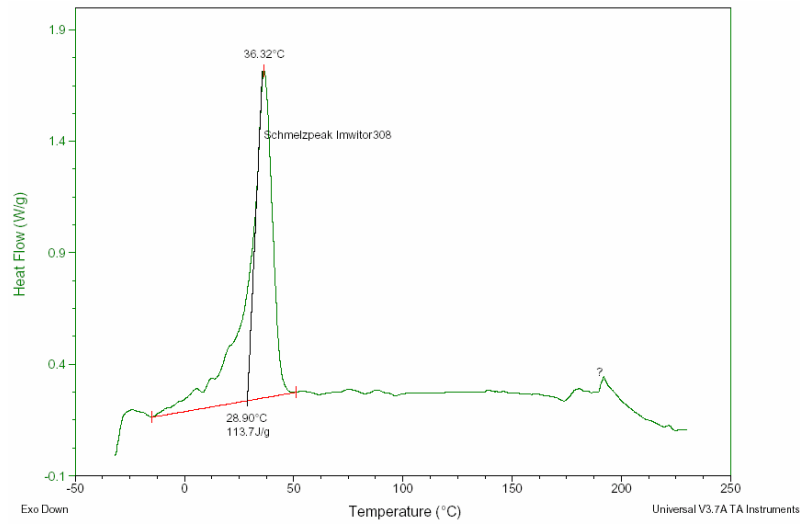


Figure VII.3.4 DSC curve of blended Imwitor 308 and spironolactone (80:20).

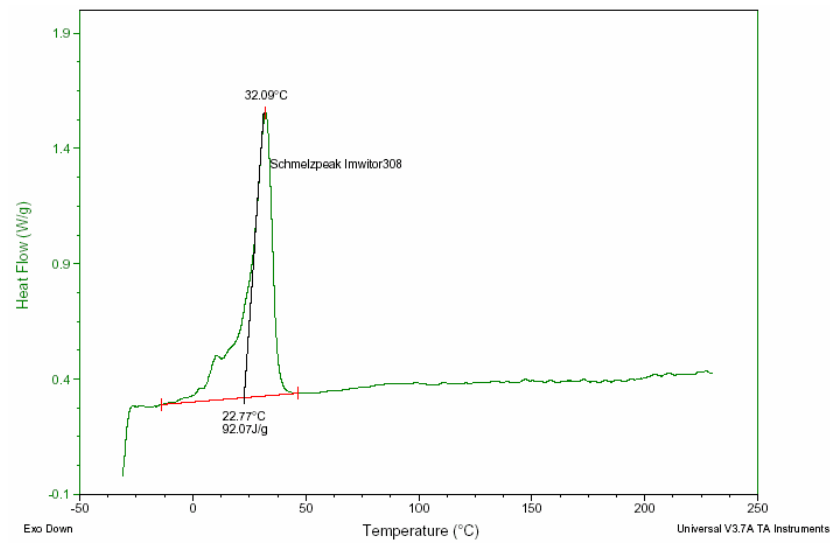


Figure VII.3.5 DSC curve of blended Imwitor 308 and spironolactone (70:30).

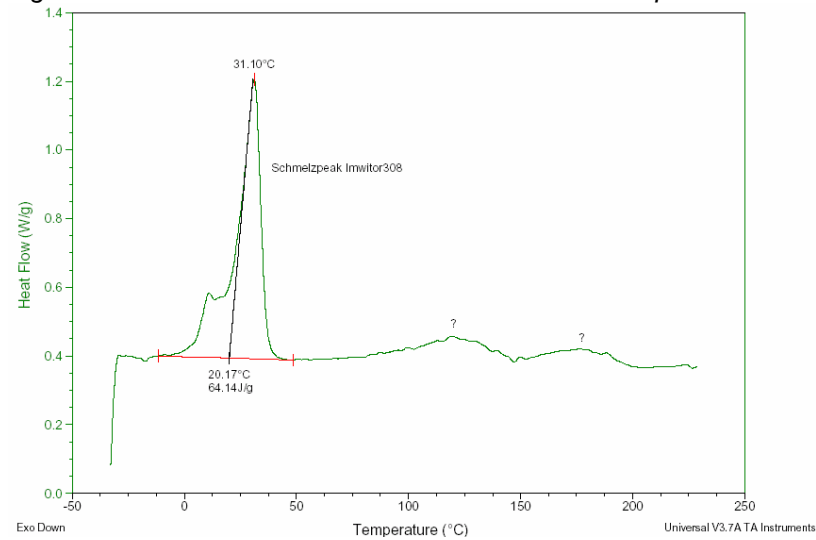


Figure VII.3.6 DSC curve of blended Imwitor 308 and spironolactone (60:40).

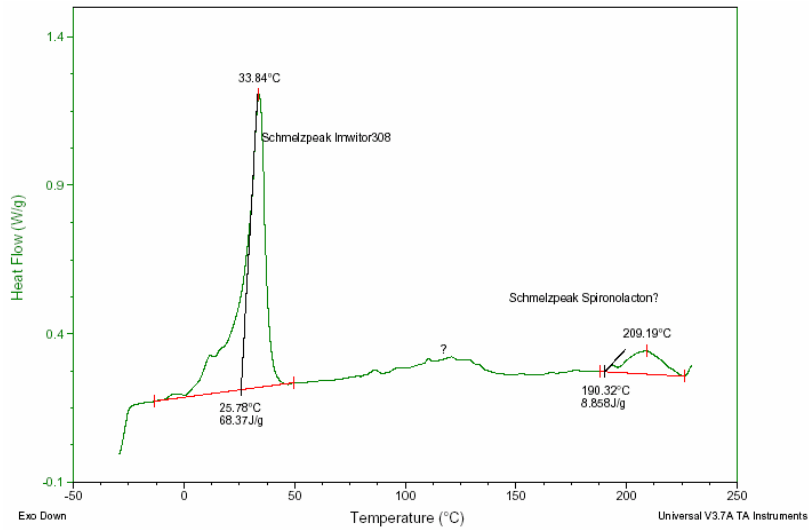


Figure VII.3.7 DSC curve of blended Imwitor 308 and spirinolactone (50:50).

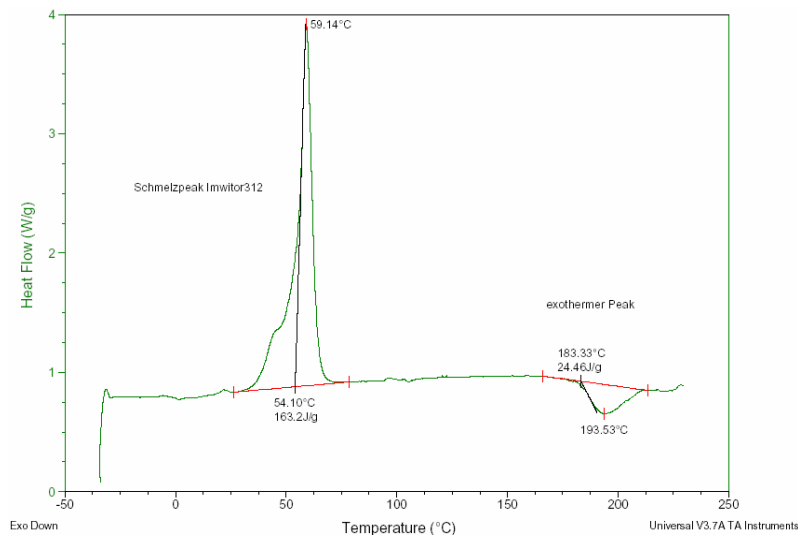


Figure VII.3.8 DSC curve of Imwitor 312.

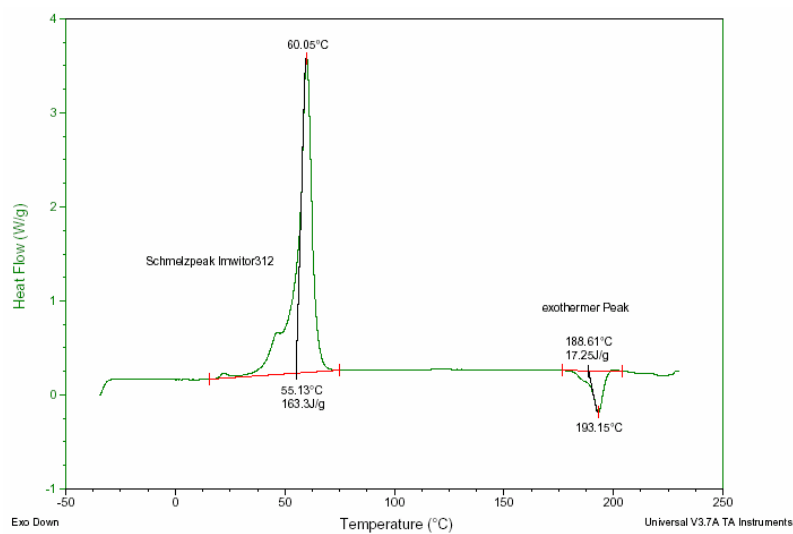


Figure VII.3.9 DSC curve of blended Imwitor 312 and spirinolactone (95:05).

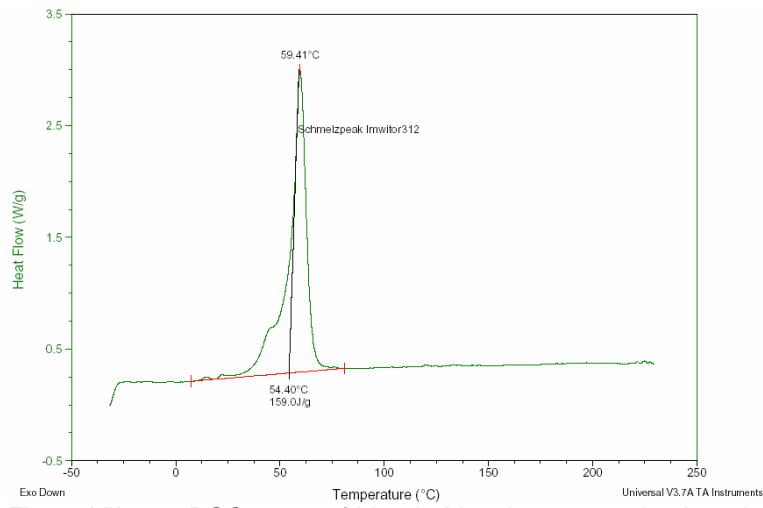


Figure VII.3.10 DSC curve of blended Imwitor 312 and spironolactone (90:10).

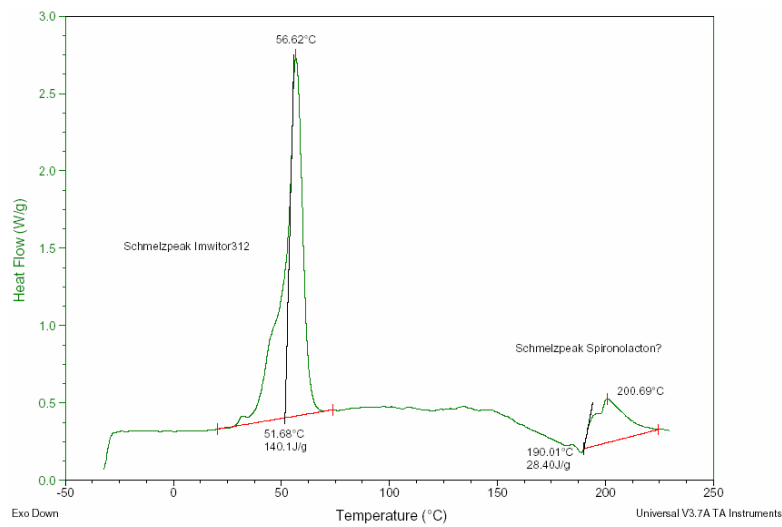


Figure VII.3.11 DSC curve of blended Imwitor 312 and spironolactone (80:20).

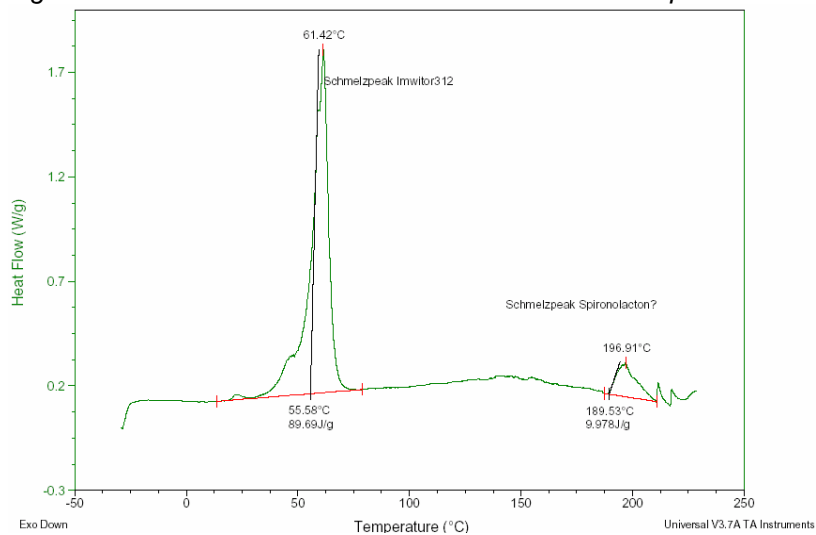


Figure VII.3.12 DSC curve of blended Imwitor 312 and spironolactone (70:30).

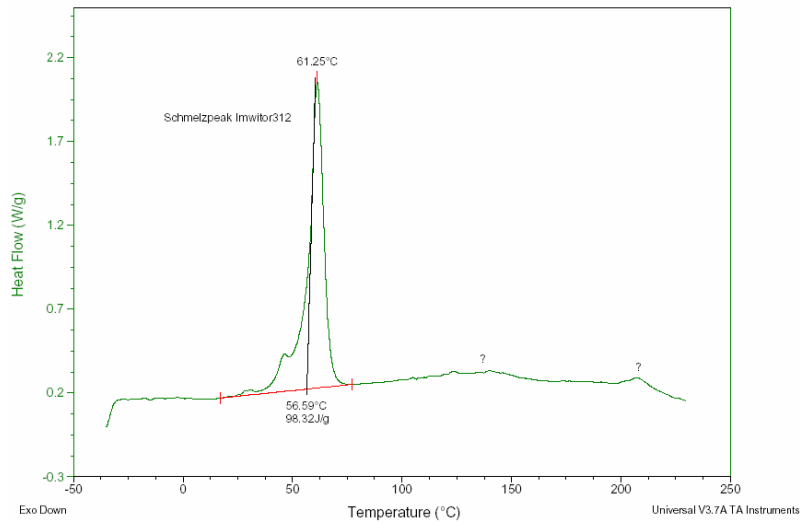


Figure VII.3.13 DSC curve of blended Imwitor 312 and spironolactone (60:40).

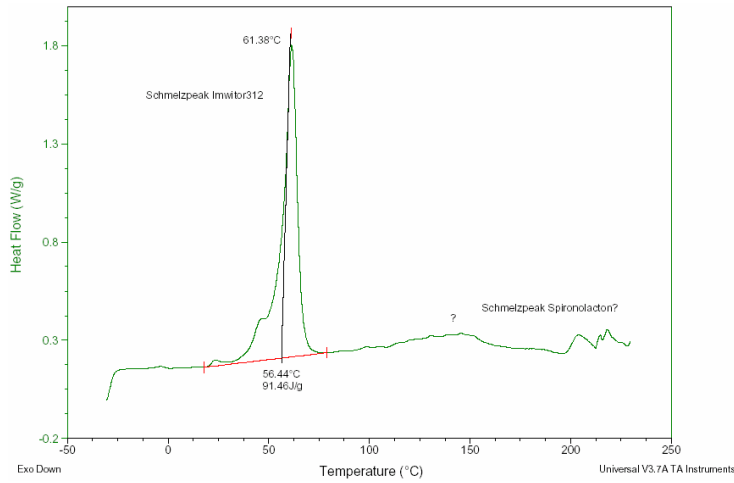


Figure VII.3.14 DSC curve of blended Imwitor 312 and spironolactone (50:50).

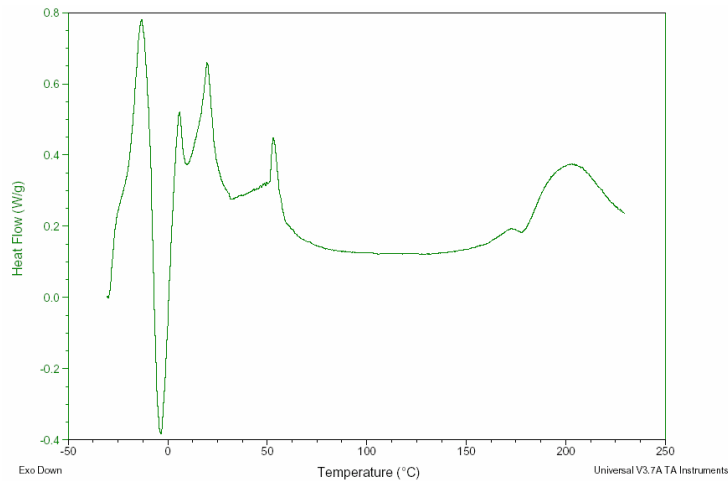


Figure VII.3.15 DSC curve of Imwitor 742.

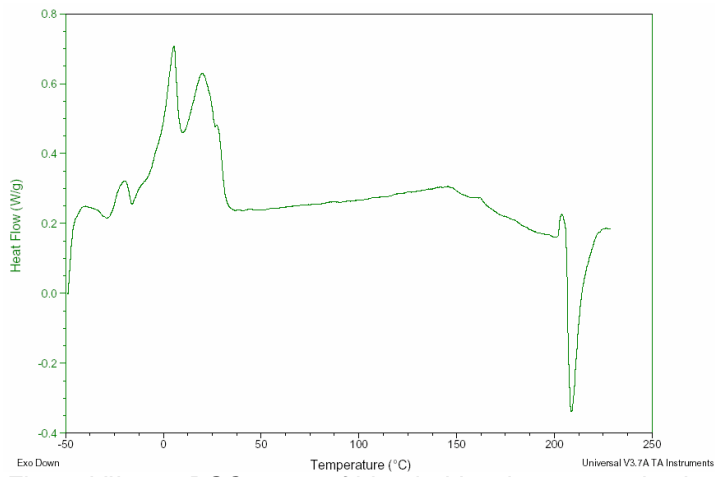


Figure VII.3.16 DSC curve of blended Imwitor 742 and spironolactone (95:05).

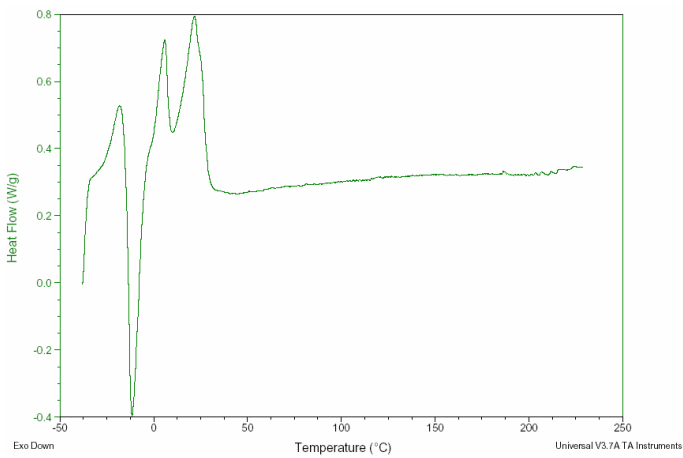


Figure VII.3.17 DSC curve of blended Imwitor 742 and spironolactone (90:10).

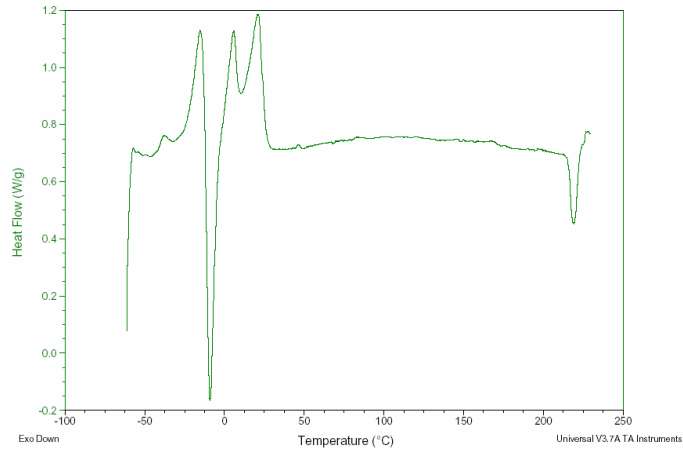


Figure VII.3.18 DSC curve of blended Imwitor 742 and spironolactone (80:20).

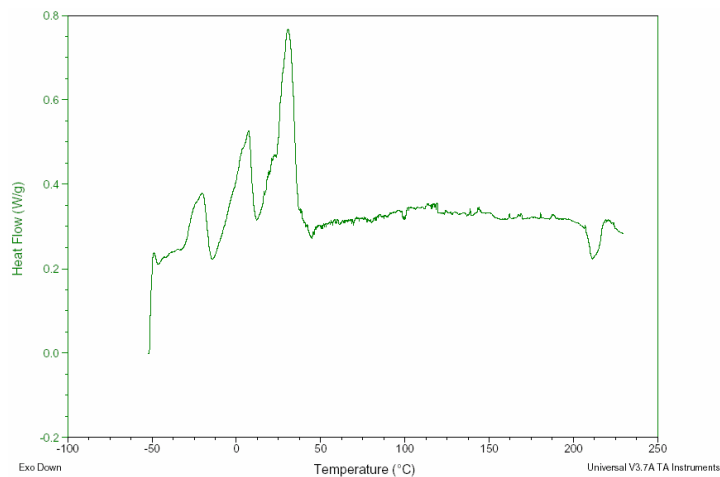


Figure VII.3.19 DSC curve of blended Imwitor 742 and spironolactone (70:30).

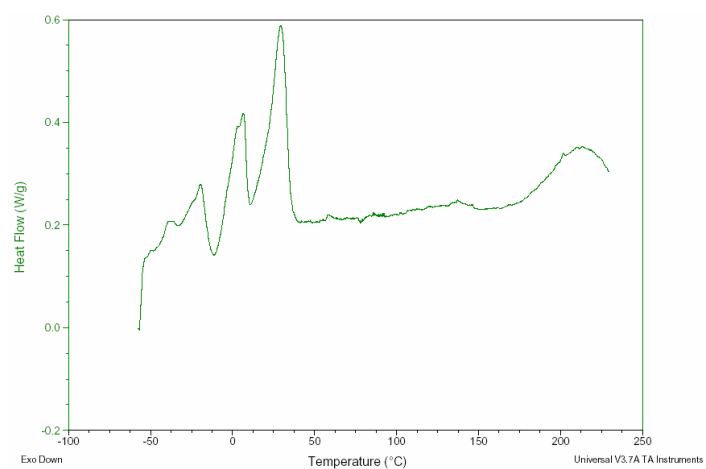


Figure VII.3.20 DSC curve of blended Imwitor 742 and spironolactone (60:40).

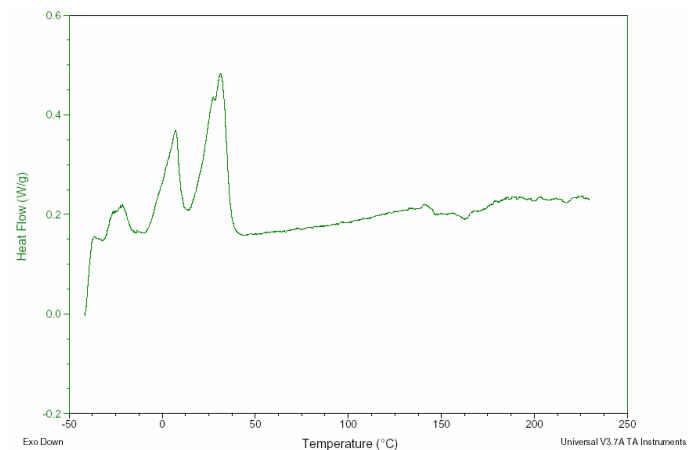


Figure VII.3.21 DSC curve of blended Imwitor 742 and spironolactone (50:50).

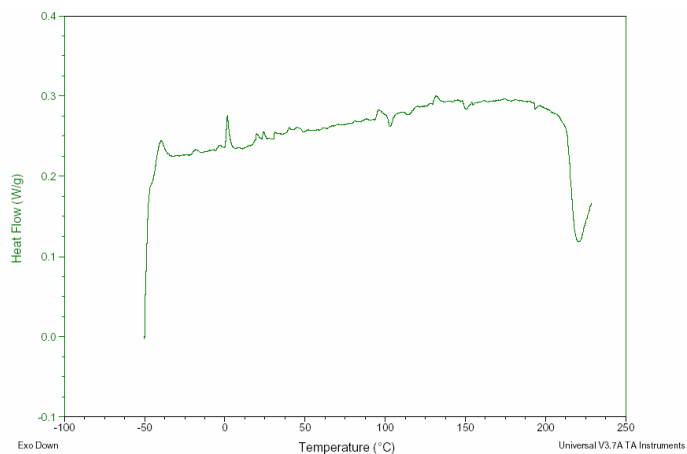


Figure VII.3.22 DSC curve of Vitamin E acetate.

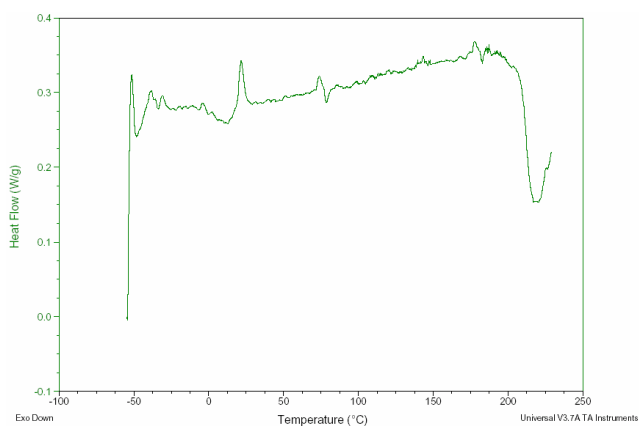


Figure VII.3.23 DSC curve of blended Vitamin E acetate and spironolactone (95:05).

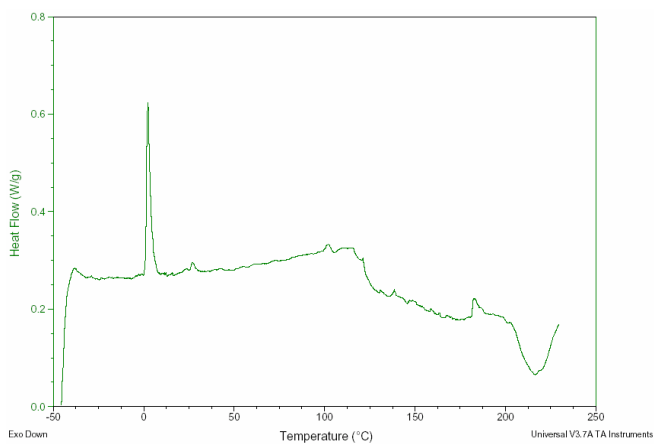


Figure VII.3.24 DSC curve of blended Vitamin E acetate and spironolactone (90:10).

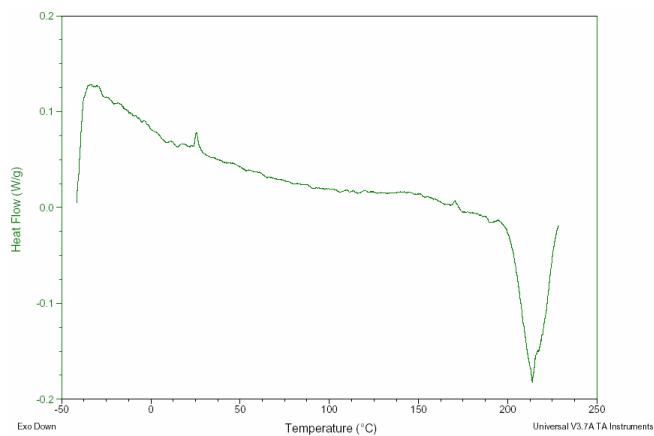


Figure VII.3.25 DSC curve of blended Vitamin E acetate and spironolactone (80:20).

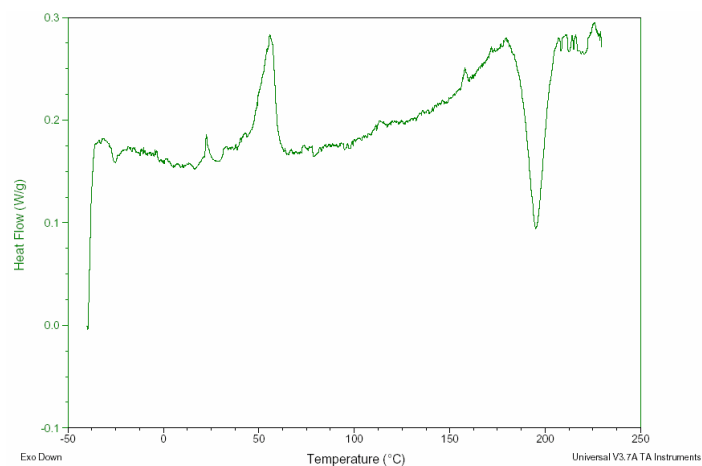


Figure VII.3.26 DSC curve of blended Vitamin E acetate and spironolactone (70:30).

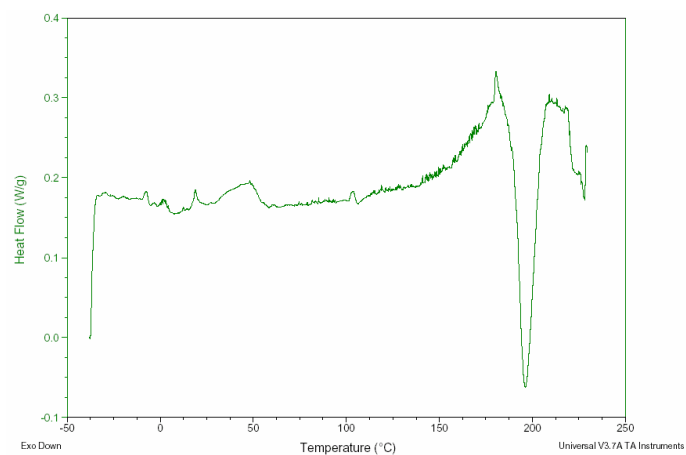


Figure VII.3.27 DSC curve of blended Vitamin E acetate and spironolactone (60:40).

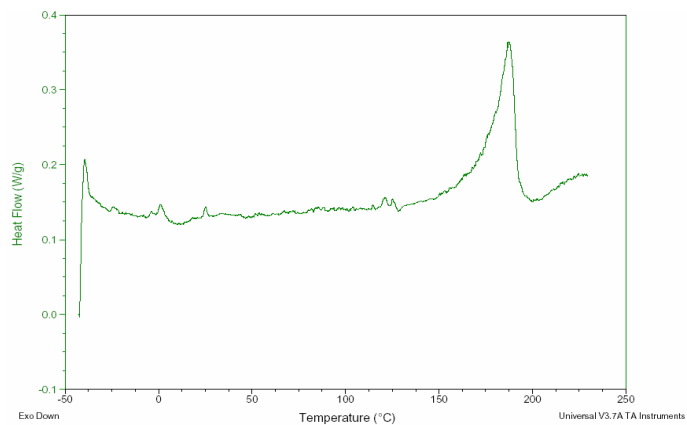


Figure VII.3.28 DSC curve of blended Vitamin E acetate and spironolactone (50:50).

CHAPTER VIII. REFERENCES

- Airaksinen, S.; Antikainen, O.; Rantanen, J.; Yliruusi, J. (2000): Advanced Testing of Granule Friability Determined from Size Distribution Data, *Pharm. Ind.* 62 (12) p. 999.
- Akiyama, Y.; Nagahara, N.; Kashihara, T.; Hirai, S.; Toguchi, H. (1995): *In vitro* and *in vivo* evaluation of mucoadhesive microspheres prepared for the gastrointestinal tract using polyglycerol esters of fatty acids and a polyacrylic acid) derivatives, *Pharm. Res.* 12 p. 397 - 405.
- Alberts, B.; Bray, D.; Lewis, J.; Raff, M.; Roberts, K.; Watson, J.D.: *Molekularbiologie der Zelle*, VCH Verlagsgesellschaft mbH: Weinheim, Germany, 1995.
- Allen, A.: Structure and function of gastrointestinal mucus In *Physiology of the Gastrointestinal Tract*, Johnson, L.R., Ed.; Raven Press: New York, 1981, p. 617 - 639.
- Allen, A.; Hutton, D.A.; Pearson, J.P.; Sellers, L.A.: Mucus glycoprotein structure, gel formation and gastrointestinal mucus function. *Ciba Found. Symp.*, 1984, p. 137-156.
- Arai, K.; Kinumaki, T.; Fujita, T. (1968): Toxicity of chitosan, *Bull Tokai Registered Fish Lab* 43 p. 89 - 94.
- Artursson, P.; Lindmark, T.; Davis, S.S.; Illum, L. (1994): Effect of chitosan on the permeability of monolayers of intestinal epithelial cells (Caco-2), *Pharm. Res.* 11 (9) p. 1358-1361.
- Bai, J.P.; Chang, L.L.; Guo, J.H. (1996): Effects of polyacrylic polymers on the degradation of insulin and peptide drugs by chymotrypsin and trypsin, *J. Pharm. Pharmacol.* 48 (1) p. 17-21.
- Bauer, K.H.; Lehmann, K.; Osterwald, H.P.; Rothgang, G.: *Coated Pharmaceutical Dosage Forms*, Medpharm: Stuttgart/Germany, 1998.
- Beermann, B.; Groschinsky-Grind, M.; Rosen, A. (1976): Absorption, metabolism, and excretion of hydrochlorothiazide, *Clin. Pharmacol. Ther.* 19 (5) p. 531-537.
- Benedetti, L.M. (1994): New Biomaterials from Hyaluronic Acid, *Med. Device Technol.* 5 (9) p. 32-37.
- Benedetti, L.M.; Topp, E.M.; Stella, V.J. (1990): Microspheres of hyaluronic acid esters-fabrication methods and *in vitro* hydrocortisone release, *J. Contr. Rel.* 13 p. 33-41.
- Beranek, J.; Rose, K.; Winterstein, G.: *Grundlagen der Wirbelschicht*, Krausskopf-Verlag: Mainz/Germany, 1975.
- Bernkop-Schnurch, A. (2000b): Chitosan and its derivatives: potential excipients for peroral peptide delivery systems, *Int. J. Pharm.* 194 (1) p. 1-13.

- Bernkop-Schnurch, A.; Aprich, A. (1997): Synthesis and evaluation of a modified mucoadhesive polymer protecting from α -chymotrypsinic degradation, *Int. J. Pharm.* p. 146-247.
- Bernkop-Schnurch, A.; Gilge, B. (2000f): Anionic mucoadhesive polymers as auxiliary agents for the peroral administration of (poly)peptide drugs: influence of the gastric juice, *Drug Dev. Ind. Pharm.* 26 (2) p. 107-113.
- Bernkop-Schnurch, A.; Kast, C.E. (2001): Chemically modified chitosans as enzyme inhibitors, *Adv. Drug Del. Rev.* 52 p.
- Bernkop-Schnurch, A.; Kast, C.E.; Richter, M.F. (2001a): Improvement in the mucoadhesive properties of alginate by the covalent attachment of cysteine, *J. Contr. Rel.* 71 (3) p. 277-285.
- Bernkop-Schnurch, A.; Krajicek, M.E. (1998a): Mucoadhesive polymers as platforms for peroral peptide delivery and absorption: synthesis and evaluation of different chitosan-EDTA conjugates, *J. Contr. Rel.* 50 (1-3) p. 215-223.
- Bernkop-Schnurch, A.; Scholler, S.; Iber, R.G. (2000d): Development of Controlled Drug Release Systems Based on Polymer - Cysteine Conjugates, *J. Contr. Rel.* 66 p. 39.
- Bernkop-Schnurch, A.; Schwarz, V.; Steininger, S. (1999b): Polymers with thiol groups: a new generation of mucoadhesive polymers?, *Pharm. Res.* 16 (6) p. 876-881.
- Bernkop-Schnurch, A.; Steininger, S. (2000c): Synthesis and characterisation of mucoadhesive thiolated polymers, *Int. J. Pharm.* 194 (2) p. 239-247.
- Bernkop-Schnurch, A.; Thaler, S.C. (2000e): Polycarbophil-cysteine conjugates as platforms for oral polypeptide delivery systems, *J. Pharm. Sci.* 89 (7) p. 901-909.
- Bernkop-Schnurch, A.; Walker, G. (2001b): Multifunctional matrices for oral peptide delivery, *Crit. Rev. Ther. Drug Carrier Syst.* 18 (5) p. 459-501.
- Borchard, G.; Luessen, H.L.; De Boer, A.G.; Verhoef, J.C.; Lehr, C.M.; Junginger, H.E. (1996): The potential of mucoadhesive polymers in enhancing intestinal peptide drug absorption. 3. Effects of chitosan-glutamate and carbomer on epithelial tight junction *in vitro*, *J. Contr. Rel.* 39 p. 131-138.
- Bouckaert, S.; Temmerman, M.; Dhont, M.; Remon, J.P.: The treatment of bacterial vaginosis with bioadhesive vaginal slow release tablet with metronidazole. In *Proceedings of International Symposium on Controlled Release of Bioactive Materials*, 1994, p. 585 - 586.
- Bugaut, M. (1987): Occurrence, absorption and metabolism of short chain fatty acids in the digestive tract of mammals, *Comp. Biochem. Physiol. B* 86 p. 439-472.
- Cacace, J.; Reilly, E.E.; Amann, A. (2004): Comparison of the dissolution of metaxalone tablets (Skelaxin) using USP Apparatus 2 and 3, *AAPS PharmSciTech* 5 (1) p. E6.
- Capes, C.A. (1967): Mechanism of Pellet Growth in Wet Pelletization, *I & EC Process Design and Development* 6 (3) p. 390-392.
- Chatchawalsaisin, J.; Podcizek, F.; Newton, J.M. (2004): The influence of chitosan and sodium alginate and formulation variables on the formation and drug

- release from pellets prepared by extrusion/spheronization, *Int. J. Pharm.* 275 p. 41-60.
- Ch'ng, H.S.; Park, H.; Kelly, P.; Robinson, J.R. (1985): Bioadhesive polymers as platforms for oral controlled drug delivery II: synthesis and evaluation of some swelling, water-insoluble bioadhesive polymers, *J. Pharm. Sci.* 74 (4) p. 399-405.
- Christiansen, P.M. (1968): The incidence of achlorhydria and hypochlorhydria in healthy subjects and patients with gastrointestinal diseases, *Scand. J. Gastroenterol.* 3 p. 497-508.
- Chukwumezie, B.N.; Wojcik, M.; Malak, P.; Adeyeye, M.C. (2002): Feasibility studies in spheronization and scale-up of ibuprofen microparticulates using the rotor disk fluid-bed technology, *AAPS PharmSciTech* 3 (1) p. E2.
- Chukwumezie, B.N.; Wojcik, M.; Malak, P.; Damico, F.; Adeyeye, M.C. (2004): Factorial design in the spheronization of ibuprofen microparticulates using the rotor disk fluid-bed technology, *Pharm Dev Technol* 9 (1) p. 49-62.
- Clausen, A.E.; Bernkop-Schnurch, A. (2000b): *In vitro* evaluation of the permeation-enhancing effect of thiolated polycarbophil, *J. Pharm. Sci.* 89 (10) p. 1253-61.
- Clausen, A.E.; Bernkop-Schnurch, A. (2001): Thiolated carboxymethylcellulose: *In vitro* evaluation of its permeation enhancing effect on peptide drugs, *Eur. J. Pharm. Biopharm.* 51 (1) p. 25-32.
- Code, C.F.; Marlett, J.A. (1975): The interdigestive myo-electric complex of the stomach and small bowel of dogs, *J. Physiol.* 246 (2) p. 289-309.
- Crane, R.K. (1975): A digestive-absorptive surface as illustrated by the intestinal cell brush border, *Trans. Am. Microsc. Soc.* 94 p. 529-544.
- Dittgen, M.; Durrani, M.; Lehmann, K. (1997): Acrylic polymers: A review of pharmaceutical applications, *S.T.P. Pharma Sci.* 7 (6) p. 403-437.
- Duchêne, D.; Touchard, F.; Peppas, N.A. (1988): Pharmaceutical and medical aspects of bioadhesive systems for drug administration, *Drug Dev. Ind. Pharm.* 14 p. 283-381.
- Eisele; Knoell, M.; Personal Communication about *Toxicity of different EUDRAGIT® types*. Darmstadt (2003).
- Faham, A.; Prinderre, P.; Piccerelle, P.; Farah, N.; Joachim, J. (2000): Hot melt coating technology: influence of Compritol 888 Ato and granule size on chloroquine release, *Pharmazie* 55 (6) p. 444-448.
- Falbe, J.; Regitz, M.: *Römpp Lexikon der Chemie*, Thieme: Stuttgart / Germany, 1999.
- Fallingborg, J.; Christensen, L.A.; Jacobsen, B.A.; Rasmussen, S.N. (1993): Very low intraluminal colonic pH in patients with active ulcerative colitis, *Dig. Dis. Sci.* 38 p. 1989-1993.
- Fassihi, A.D.; US Patent: *Method and apparatus for dissolution testing of a dosage form*. Pat. No. 5412979, 3rd May 1995.
- FDA: Homepage www.fda.gov/cder/ops/Pat.html; Process and Analytical Technology (PAT) Initiative.

- Fiebrig, L.; Harding, S.E.; Rowe, A.J.; Hyman, S.C.; Davis, S.S.: *Methods used to develop mucoadhesive drug delivery systems: bioadhesion in the gastrointestinal tract*, Nottingham University Press: Nottingham, 1996.
- Follonier, N.; Doelker, E. (1992): Biopharmaceutical comparison of oral multiple-unit and single-unit sustained release dosage forms, *S.T.P. Pharma Sci.* 2 p. 141-158.
- Forster, A.; Hempenstall, J.; Tucker, I.; Rades, T. (2001): Selection of excipients for melt extrusion with two poorly water-soluble drugs by solubility parameter calculation and thermal analysis, *Int. J. Pharm.* 226 (1-2) p. 147-161.
- Forstner, J.F. (1978): Intestinal mucins in health and disease, *Digestion* 17 p. 234-263.
- Georgarakis, M.; Gröning, M.; Henzler, P. (1987): Microencapsulation of Potassium Chloride with Mastic, *Pharmazie* 42 (7) p. 455-456.
- Ghebre-Sellassie, I.; Nesbitt, R.U.; Wang, J.: Eudragit aqueous dispersions as pharmaceutical controlled-release coatings In *Aqueous Polymeric Coatings for Pharmaceutical Dosage forms*; McGinity, J.W., Ed.; Marcel Dekker: New York, 1997, p. 267-286.
- Ghebre-Sellassie, I.: Pellets: a general view In *Pharmaceutical Pelletization Technology*; Ghebre-Sellassie, I., Ed.; Marcel Dekker: New York, 1989, p. 1-13.
- Ghebre-Sellassie, I.: *Pharmaceutical Pelletization Technology*, Marcel Decker Inc.: New York, 1989.
- Ghebre-Sellassie, I.; Knoch, A.: Pelletization Techniques In *Encyclopedia of Pharmaceutical Technology*; Swarbrick, J., Boylan, J.C., Eds.; Marcel Dekker Inc.: New York, 1995; Vol. 11, p. 369-394.
- Graeves, J.L.; Wilson, C.G. (1993): Treatment of diseases of the eye with mucoadhesive delivery systems, *Adv. Drug Del. Rev.* 11 p. 349-383.
- Gröning, R.; Heun, G. (1984): Oral dosage forms with controlled gastrointestinal transit, *Drug Dev. Ind. Pharm.* 10 p. 527-539.
- Gröning, R.; Heun, G. (1989): Dosage forms with controlled gastrointestinal passage - studies on the absorption of nitrofurantoin, *Int. J. Pharm.* 56 p. 111-116.
- Grundy, D.: *Gastrointestinal Motility*, MTP Press Ltd: Lancaster, 1985.
- Gu, J.M.; Robinson, J.R.; Leung, S.H. (1988): Binding of acrylic polymers to mucin/epithelial surfaces: structure - property relationships, *Crit. Rev. Ther. Drug Carrier Syst.* 5 (1) p. 21-67.
- Gu, L.; Liew, C.V.; Heng, P.W.S. (2004): Wet spherization by rotary processing - a multistage single-pot process for producing spheroids, *Drug Dev. Ind. Pharm.* 30 (2) p. 111-123.
- Gupte, A.R. (1976): Messung der spezifischen Oberfläche grober Granulate und der mittleren Porengrößen von Tabletten, *Acta Pharm. Tech.* 22 (3) p. 153-168.
- Hagerstrom, H.; Edsman, K. (2001): Interpretation of mucoadhesive properties of polymer gel preparations using a tensile strength method, *J. Pharm. Pharmacol.* 53 (12) p. 1589-99.

- Harris, D.; Fell, J.T.; Taylor, D.C.; Lynch, J.; Sharma, H.L. (1990a): GI transit of potential bioadhesive systems in the rat, *J. Contr. Rel.* 12 p. 55-65.
- Harris, D.; Fell, J.T.; Taylor, D.C.; Lynch, J.; Sharma, H.L. (1990b): GI transit of potential bioadhesive formulations in man: a scintigraphic study, *J. Contr. Rel.* 12 p. 45 - 53.
- Hassan, E.E.; Gallo, J.M. (1990): A simple rheological method for the *in vitro* assessment of mucin - polymer bioadhesive bond strength, *Pharm. Res.* 7 (5) p. 491-495.
- Hayton, W.L. (1980): Rate-limiting barriers to intestinal drug absorption: a review, *J. Pharmacokinet. Biopharm.* 8 (4) p. 321-334.
- Helliwell, M. (1993): The use of bioadhesives in targeted delivery within the gastrointestinal tract, *Adv. Drug Del. Rev.* 11 p. 221-251.
- Heng, P.W.; Liew, C.V.; Gu, L. (2002): Influence of teardrop studs on rotating frictional base plate on spheroid quality in rotary spheronization, *Int. J. Pharm.* 241 (1) p. 173-184.
- Heng, P.W.S.; Wan, L.S.C.; Tan, Y.T.F. (1996): Optimization of spheroid production by centrifugal rotary processing, *Int. J. Pharm.* 143 p. 107 - 112.
- Hirano, S.; Noishiki, Y. (1985): The blood compatibility of chitosan and N-acetylchitosans, *J Biomed Mater Res* 19 (4) p. 413-417.
- Holm, P. (1996b): Pelletization by Granulation in a Rotoprocessor RP-2. Part II: Effects of Process and Product Variables on Shape and Porosity of the Agglomerates, *Pharm. Tech. Europe* 8 (9) p. 38-45.
- Holm, P.; Bonde, M.; Wigmore, T. (1996): Pelletization by Granulation in a Rotoprocessor RP-2. Part I: Effects of Process and Product Variables on Granule Growth, *Pharm. Tech. Europe* 8 (8) p. 22-36.
- Illum, L. (1998): Chitosan and its use as a pharmaceutical excipient, *Pharm. Res.* 15 (9) p. 1326-1331.
- Iman, M.E.; Hornof, M.; Valenta, C.; Reznicek, G.; Bernkop-Schnurch, A. (2003): Evidence for the interpenetration of mucoadhesive polymers into the mucous gel layer, *S.T.P. Pharma Sci.* 13 (3) p. 171-176.
- Jager, V.K.F.; Bauer, K.H. (1982): Auswirkungen der Gutbewegung im Rotor-Wirbelschicht-Granulator auf die Aufbauagglomeration, *Pharm. Ind.* 44 p. 193-197.
- Junginger, H.E.; Verhoef, J.C. (1992): Perorale Applikation von Peptiden und Proteinen, *Deutsche Apotheker Zeitung* 132 (24) p. 1279-1290.
- Kast, C.E.; Bernkop-Schnurch, A. (2001): Thiolated polymers-thiomers: development and *in vitro* evaluation of chitosan-thioglycolic acid conjugates, *Biomaterials* 22 (17) p. 2345-2352.
- Kaus, L.C. (1987): The effect of density on the gastric emptying and intestinal transit of solid dosage forms: comments on the article by Davis et al, *Pharm. Res.* 4 (1) p. 78.
- Kerec, M.; Bogataj, M.; Mugerle, B.; Gasperlin, M.; Mrhar, A. (2002): Mucoadhesion on pig vesical mucosa: influence of polycarbophil/calcium interactions, *Int. J. Pharm.* 241 (1) p. 135-143.

- Kim, Y.S.; Perdomo, J.M. (1974): Membrane glycoproteins of the rat small intestine, *Biochim. Biophys. Acta* 342 p. 111-124.
- Knoell, M.; Lizio, R.; Behrisch, A.; Roth, E.; Ortlepp, B.; Petereit, H.U.; Langguth, P.: Electron Dispersive X-ray: A Method for Proving the Separation of an Enteric Coating Layer from an Additional Functional Matrix Layer. In *Proceedings: International Meeting on Pharmaceutics, Biopharmaceutics and Pharmaceutical Technology*, Nuremberg/Germany, 15 - 18 March 2004, 2004: Nuremberg/Germany, p. 685-686.
- Ko, J.A.; Park, H.J.; Hwang, S.J.; Park, J.B.; Lee, J.S. (2002): Preparation and characterization of chitosan microparticles intended for controlled drug delivery, *Int. J. Pharm.* 249 (1-2) p. 165-174.
- Korakianiti, E.S.; Rekkas, D.M.; Dallas, P.P.; Choulis, N.H. (2000): Optimization of the pelletization process in a fluid-bed rotor granulator using experimental design, *AAPS PharmSciTech* 1 (4) p. E35.
- Kotze, A.F.; Luessen, H.L.; de Leeuw, B.J.; de Boer, A.G.; Verhoef, J.C.; Junginger, H.E. (1998): Comparison of the effect of different chitosan salts and N-trimethyl chitosan chloride on the permeability of intestinal epithelial cells (Caco-2), *J. Contr. Rel.* 51 (1) p. 35-46.
- Kristensen, J.; Schaefer, T.; Kleinebudde, P. (2000): Direct Pelletization in a Rotary Processor Controlled by Torque Measurements. I. Influence of Process Variables, *Pharm. Dev. Technol.* 5 (2) p. 247-256.
- Kristensen, J.; Schaefer, T.; Kleinebudde, P. (2000b): Direct Pelletization in a Rotary Processor Controlled by Torque Measurements. II: Effects of Changes in the Content of Microcrystalline Cellulose, *AAPS PharmSci* 2 (3) p. E24.
- Kristensen, J.; Schaefer, T.; Kleinebudde, P. (2002): Development of fast-disintegrating pellets in a rotary processor, *Drug Dev. Ind. Pharm.* 28 (10) p. 1201-1212.
- Kriwet, B.; Kissel, T. (1996): Interaction between bioadhesive poly(acrylic acid) and calcium ions, *Int. J. Pharm.* 127 p. 135-145.
- Kyyrönen, K.; Hume, L.; Benedetti, L.M.; Urtti, A.; Topp, E.; Stella, V.J. (1992): Methylprednisolone esters of hyaluronic acid in ophthalmic drug delivery: *in vitro* and *in vivo* release studies, *Int. J. Pharm.* 80 p. 161-169.
- Langguth, P.: Angewandte Biopharmazie und Pharmakokinetik in der Arzneimittel Entwicklung In *Biopharmazie*; Fricker, G., Wunderli-Allenspach, H., Eds.; Wiley-VCH: Weinheim, 2004, p. 165-288.
- Lehmann, K. (1971): Programmierte Wirkstoffabgabe aus peroralen Arzneiformen, *Pharm. Ind.* p. 1-16.
- Lehmann, K.: Chemistry and application properties of polymethacrylate coating systems In *Aqueous Polymeric Coatings for Pharmaceutical Dosage Forms*; McGinity, Ed.; Marcel Dekker Inc.: New York, 1997, p. 101-176.
- Lehmann, K.; Aßmus, M.; Bössler, H.; Dreher, D.; Liddiard, C.; Petereit, H.U.; Rothgang, G.; Weisbrod, W.; Becker, T.: *Practical course in film coating of pharmaceutical dosage forms with EUDRAGIT®*, Röhm Pharma Polymers: Darmstadt, Germany, 1999.

- Lehmann, K.; Dreher, D. (1986): Mischbarkeit wässriger Polymethacrylate-Dispersion für Arzneimittelüberzüge, *Pharm. Ind.* 48 p. 1182-1183.
- Lehr, C.M. (1994b): Bioadhesion Technologies for the Delivery of Peptide and Protein Drugs to the Gastrointestinal Tract, *Crit. Rev. Ther. Drug Carrier Syst.* 11 (2-3) p. 119-160.
- Lehr, C.M.; Bouwstra, J.A.; Kok, W.; De Boer, A.G.; Tukker, J.J.; Verhoef, J.C.; Breimer, D.D.; Junginger, H.E. (1992): Effects of the mucoadhesive polymer polycarbophil on the intestinal absorption of a peptide drug in the rat, *J. Pharm. Pharmacol.* 44 (5) p. 402-407.
- Lehr, C.M.; Bouwstra, J.A.; Schacht, E.H.; Junginger, H.E. (1992a): *In vitro* evaluation of mucoadhesive properties of chitosan and some other natural polymers, *Int. J. Pharm.* 78 p. 43-48.
- Lehr, C.M.; Poelma, F.G.J.; Junginger, H.E.; Tukker, J.J. (1991): An estimate of turnover time to intestinal mucus gel layer in the rat in situ loop, *Int. J. Pharm.* 70 p. 235-240.
- Leuenberger, H.; Usteri, M.; Imanidis, G.; Winzap, S. (1989): Monitoring the granulation process: granulate growth, fractal dimensionality and precolation threshold., *Boll. Chim. Farm.* 128 (2) p. 54-60.
- Leung, S.S.; Robinson, J.R. (1988): The contribution of anionic polymer structural features to mucoadhesion, *J. Contr. Rel.* 5 p. 223-231.
- Leung, S.S.; Robinson, J.R. (1990): Polymer structure features contributing to mucoadhesion II, *J. Contr. Rel.* 12 p. 187-194.
- Liew, C.; Gu, L.; Heng, P. (2002): The influence of operational variables on mean size and size distribution of spheroids produced by rotary spheronization using teardrop studs, *Int. J. Pharm.* 242 (1-2) p. 345-348.
- Liew, C.V.; Wan, L.S.; Heng, P.W. (2000): Role of base plate rotational speed in controlling spheroid size distribution and minimizing oversize particle formation during spheroid production by rotary processing, *Drug Dev. Ind. Pharm.* 26 (9) p. 953-963.
- Linkson, P.B.; Glastonbury, J.R.; Duffy, G.J. (1973): The Mechanism of Granule Growth in Wet Pelletizing, *Instn. Chem. Engrs.* 51 p. 251-259.
- Lippold, B.C.; Günther, J. (1991): *In vivo* Prüfung einer multipartikulären Retard-Schwimmartneiform, *Eur. J. Pharm. Biopharm.* 39 p. 55.
- Lorenzo-Lamosa, M.L.; Remunan-Lopez, C.; Vila-Jato, J.L.; Alonso, M.J. (1998): Design of microencapsulated chitosan microspheres for colonic drug delivery, *J. Contr. Rel.* 52 (1-2) p. 109-118.
- Lu, R.; Kanai, N.; Bao, Y.; Schuster, V.L. (1996): Cloning, *in vitro* expression, and tissue distribution of a human prostaglandin transporter cDNA(hPGT), *J. Clin. Invest.* 98 (5) p. 1142-1149.
- Luessen, H.L.; Bohner, V.; Pérard, D.; Langguth, P.; Verhoef, J.C.; de Boer, A.G.; H.P., M.; Junginger, H.E. (1996b): Mucoadhesive polymers in peroral peptide drug delivery. V. Effect of poly(acrylates) on the enzymatic degradation of peptide drugs by intestinal brush border membrane vesicles, *Int. J. Pharm.* 141 p. 39-52.

- Luessen, H.L.; de Leeuw, B.J.; Langemeyer, M.W.; de Boer, A.B.; Verhoef, J.C.; Junginger, H.E. (1996a): Mucoadhesive polymers in peroral peptide drug delivery. VI. Carbomer and chitosan improve the intestinal absorption of the peptide drug busserelin *in vivo*, *Pharm. Res.* 13 (11) p. 1668-1672.
- Luessen, H.L.; de Leeuw, B.J.; Perard, D.; Lehr, C.M.; de Boer, A.G.; Verhoef, J.C.; Junginger, H.E. (1996d): Mucoadhesive polymers in peroral peptide drug delivery. I. Influence of mucoadhesive excipients on the proteolytic activity of intestinal enzymes, *Eur. J. Pharm. Sci.* 4 (2) p. 117-128.
- Luessen, H.L.; Lehr, C.-M.; Rentel, C.-O.; Noach, A.B.J.; de Boer, A.G.; C., V.J.; Junginger, H.E. (1991): Bioadhesive polymers for the peroral delivery of peptide drugs, *J. Contr. Rel.* 29 (1) p. 329-338.
- Luessen, H.L.; Verhoef, J.C.; Borchard, G.; Lehr, C.M.; de Boer, A.G.; Junginger, H.E. (1995a): Mucoadhesive polymers in peroral peptide drug delivery. II. Carbomer and polycarbophil are potent inhibitors of the intestinal proteolytic enzyme trypsin, *Pharm. Res.* 12 (9) p. 1293-1298.
- Luessen, H.L.; Verhoef, J.C.; Borchard, G.; Lehr, C.M.; De Boer, A.G.; Junginger, H.E. (1995b): Carbomer and Polycarbophil are Potent Inhibitors of the Intestinal Proteolytic Enzyme Trypsine, *Pharm. Res.* 12 (9) p. 1293-1298.
- Macfarlane, G.T.; Cummings, J.H.: The colonic flora, fermentation, and large bowel digestive function In *Physiology, Pathophysiology and Disease*; Philips, S.F., Pemberton, J.H., Shorter, R.G., Eds.; Raven Press: New York, 1991, p. 51-92.
- Macheras, P.; Reppas, C.; Dressman, J.B.: *Biopharmaceutics of Orally Administered Drugs*, Ellis Horwood Limited: London, 1995.
- Madara, J.L.; Trier, J.S.: Functional morphology of the mucosa of the small intestine In *Physiology of the Gastrointestinal Tract*, Johnson, L.R., Ed.; Raven Press: New York, 1987, p. 1209-1250.
- Maejima, T.; Osawa, T.; Nakajima, K.; Kobayashi, M. (1997): Preparation of spherical beads without any use of solvents by a novel tumbling melt granulation (TMG) method, *Chem. Pharm. Bull.* 45 (3) p. 518-524.
- Malagelada, J.R.; Longstreth, G.F.; Summerskill, W.H.; Go, V.L. (1976): Measurement of gastric functions during digestion of ordinary solid meals in man, *Gastroenterology* 70 p. 203-210.
- Manninen, V.; Apajalahti, A.; Melin, J.; Karesoja, M. (1973): Altered absorption of digoxin in patients given propantheline and metoclopramide, *Lancet* 1 (7800) p. 398-400.
- Marschutz, M.K.; Caliceti, P.; Bernkop-Schnurch, A. (2000): Design and *in vivo* evaluation of an oral delivery system for insulin, *Pharm. Res.* 17 (12) p. 1468-1474.
- Martin: *Physikalische Pharmazie*, Wissenschaftliche Verlagsgesellschaft: Stuttgart, 2002.
- McCarthy, L.G.; Kosiol, M.; Healy, M.; Sexton, J.C.; Corrigan, O.I. (2002): Application of computational fluid dynamics (Cfd) with high performance computing (Hpc) to simulate hydrodynamics in the paddle dissolution apparatus, *AAPS PharmSci* 4 (4 (S1)) p. M1340.

- Minami, H.; McCallum, R.W. (1984): The physiology and pathophysiology of gastric emptying in humans, *Gastroenterology* 86 (6) p. 1592-1610.
- Moes, A.J. (1993): Gastroretentive dosage forms, *Crit. Rev. Ther. Drug Carrier Syst.* 10 (2) p. 143-195.
- Mortazavi, S.A.; Smart, J.D. (1995): An investigation of some factors influencing the *in vitro* assessment of mucoadhesion, *Int. J. Pharm.* 116 p. 223-230.
- Muller-Lissner, S.A.; Blum, A.L. (1981): The effect of specific gravity and eating on gastric emptying of slow - release capsules, *N. Engl. J. Med.* 304 (22) p. 1365-1366.
- Nagai, T. (1986): Topical mucosal adhesive dosage forms, *Med. Res. Rev.* 6 (2) p. 227-242.
- Nagai, T.; Nishimoto, Y.; Nambu, U.; Suzuki, Y.; Sekine, K. (1984): Powder dosage form of insulin for nasal administration, *J. Contr. Rel.* 1 p. 15-22.
- Narisawa, S.; Nagata, M.; Danyoshi, C.; Yoshino, H.; Murata, K.; Hirakawa, Y.; Noda, K. (1994): An organic acid-induced sigmoidal release system for oral controlled-release preparations, *Pharm. Res.* 11 (1) p. 111-116.
- Neau, S.H.; Chow, M.Y.; Hileman, G.A.; Durrani, M.J.; Gheyas, F.; Evams, B.A. (2000): Formulation and process considerations for beads containing carbopol 974P, NF resin made by extrusion spheronization, *Int. J. Pharm.* 199 (2) p. 129-140.
- Neumerkel, O.; Sakr, A.; Süß, W. (1999): Studies of the production and testing of fluidized-bedrotor granules with modified release, *Pharmazie* 54 (11) p. 873-839.
- Noveon: Bulletin 2: Product and Regulatory Guide (2000)
- Noveon: Bulletin 16: Bioadhesion (2002)
- Ogata, H.; Aoyagi, N.; Kaniwa, N.; Ejima, A.; Suzuki, K.; Ishioka, T.; Morishita, M.; Ohta, M.; Takagishi, Y.; Doi, Y. (1984): Development and evaluation of a new peroral test agent GA-test for assessment of gastric acidity, *J. Pharmacobio-Dyn.* 7 p. 656-664.
- Park, H.; Amiji, M.; Park, K.: Mucoadhesive Hydrogels Effective at Neutral pH. *International Symposium on Controlled Release of Bioactive Materials*, 1989, p. 217.
- Park, H.; Robinson, J.R. (1985): Physico-chemical properties of water insoluble polymers important to mucin/epithelial adhesion, *J. Contr. Rel.* 2 p. 47-57.
- Park, K.; Park, H.: Enzyme-digestible ballon hydrogels for long term oral drug delivery; synthesis and characterization. In *Proceedings: International Symposium on Controlled Release of Bioactive Materials*, 1987, p. 41-42.
- Peppas, N.A.; Buri, P.A. (1985): Surface, interfacial and molecular aspects of polymer bioadhesion on soft tissues, *J. Contr. Rel.* 2 p. 257-275.
- Pietsch, W.; Rumpf, H. (1967): Haftkraft, Kapillardruck, Flüssigkeitsvolumen und Grenzwinkel einer Flüssigkeitsbrücke zwischen zwei Kugeln, *Chemie-Ing. Techn.* 39 (15) p. 885-893.

- Pisek, R.; Planinsek, O.; Tus, M.; Srcic, S. (2000): Influence of rotational speed and surface of rotating disc on pellets produced by direct rotor pelletization, *Pharm. Ind.* 62 (4) p. 312-319.
- Pisek, R.; Sirca, J.; Svanjak, G.; Srcic, S. (2001): Comparison of rotor direct pelletization (fluid bed) and extrusion/spheronization method for pellet production, *Pharm. Ind.* 63 (11) p. 1202-1209.
- Poelma, F.G.; Tukker, J.J. (1987): Evaluation of a chronically isolated internal loop in the rat for the study of drug absorption kinetics, *J. Pharm. Sci.* 76 (6) p. 433-436.
- Pritchard, K.; Lansley, A.B.; Martin, G.P.; Helliwell, M.; Marriott, C.; Benedetti, L.M. (1996): Evaluation of the bioadhesive properties of hyaluronan derivatives: detachment weight and mucociliary transport rate studies, *Int. J. Pharm.* 129 p. 137-145.
- Prudat-Christiaens, C.; Arnaud, P.; Allain, P.; Chaumeil, J.C. (1996): Aminophylline bioadhesive tablets attempted by wet granulation, *Int. J. Pharm.* 141 (1-2) p. 109-116.
- Qudan, A.: *Untersuchungen zur Pelletisierung von hydrophilen Polymeren durch Fluid-bed-Rotorgranulierung*, Ph.D. Thesis, Fakultät für Biowissenschaften, Pharmazie und Psychologie, Universität Leipzig, Germany, 2002.
- Rastrelli, A.; Beccaro, M.; Biviano, F.; Calderini, G.; Pastorello, A.: Hyaluronic acid esters, a new class of semisynthetic biopolymers: chemical and physico-chemical properties In *Clinical Implant Materials*; Heimke, G., Soltesz, U., Lee, A.J.C., Eds.; Elsevier: Amsterdam, 1990, p. 199-200.
- Ritschel, W.A.: Herstellung verpressbarer Tablettiermassen - Mechanische Widerstandskraft, Abrieb In *Die Tablette*; Ritschel, W.A., A., B.-B., Eds.; ECV-Editio-Cantor-Verlag: Aulendorf, 2002, p. 363-364.
- Robinson, K.; Chamberlain, L.M.; Schofield, K.M.; Wells, J.M.; Le Page, R.W. (1997): Oral vaccination of mice against tetanus with recombinant *Lactococcus lactis*, *Nat. Biotechnol.* 15 (7) p. 653-657.
- Robinson, R.L.; Hollenbeck, R.G. (1991): Manufacture of spherical acetaminophen pellets: comparison of rotary processing with multiple-step extrusion and spheronization, *Pharmaceutical Technology* 15 (5) p. 50-54.
- Rubinstein, A.; Tirosh, B. (1994): Mucus gel thickness and turnover in the gastrointestinal tract of the rat: response to cholinergic stimulus and implication for mucoadhesion, *Pharm. Res.* 11 (6) p. 794-799.
- Rumpf, H. (1958): Grundlagen und Methoden des Granulierens. 1. Teil. Begriffe, Anwendungen und Eigenschaften der Granulate, *Chemie-Ing. Techn.* 30 (3) p. 144-158.
- Rumpf, H. (1958b): Grundlagen und Methoden des Granulierens. 3. Teil. Überblick über die technischen Granulierverfahren, *Chemie-Ing. Techn.* 30 (5) p. 329-336.
- Rumpf, H. (1972): Haftung und Festigkeit von Agglomeraten - Vergleich zwischen Modellrechnung und Experiment, *Pharm. Ind.* 34 (4) p. 270-281.
- Rumpf, H. (1974): Die Wissenschaft des Agglomerierens, *Chemie-Ing. Techn.* 46 (1) p. 1-11.

- Sakkinen, M.; Linna, A.; Ojala, S.; Jurjenson, H.; Veski, P.; Marvola, M. (2003b): *In vivo* evaluation of matrix granules containing microcrystalline chitosan as a gel-forming excipient, *Int. J. Pharm.* 250 (1) p. 227-237.
- Sakkinen, M.; Tuononen, T.; Jurjenson, H.; Veski, P.; Marvola, M. (2003): Evaluation of microcrystalline chitosans for gastro-retentive drug delivery, *Eur. J. Pharm. Sci.* 19 (5) p. 345-53.
- Sangekar, S.; Vadino, W.A.; Chaudry, I.; Parr, A.; Beihn, G.; Digenis, G. (1987): Evaluation of the effect of food and specific gravity of tablets on gastric retention time, *Int. J. Pharm.* 35 p. 187-191.
- Santos, H.; Veiga, F.; Pina, M.; Podczek, F.; Sousa, J. (2002): Physical properties of chitosan pellets produced by extrusion-spheronization; influence of formulation variables, *Int. J. Pharm.* 246 p. 153-169.
- Sastry, K.V.S.; Fuerstenau, D.W. (1970): Size Distribution of Agglomerates in Coalescing Dispersed Phase System, *Ind. Eng. Chem. Fundam.* 9 (1) p. 145-149.
- Sastry, K.V.S.; Fuerstenau, D.W. (1971): A Laboratory Method for Determining the Balling Behaviour of Taconite Concentrates, *Transaction* 250 p. 64-67.
- Sastry, K.V.S.; Fuerstenau, D.W. (1972): Ballability Index to Quantify Agglomerate Growth by Green Pelletization, *Transaction* (252) p. 252-258.
- Sastry, K.V.S.; Fuerstenau, D.W. (1973): Mechanism of Agglomerate Growth in Green Pelletization, *Powder Technology* 7 p. 97-105.
- Schipper, N.G.; Olsson, S.; Hoogstraate, J.A.; de Boer, A.G.; Varum, K.M.; Artursson, P. (1997): Chitosans as absorption enhancers for poorly absorbable drugs 2: mechanism of absorption enhancement, *Pharm. Res.* 14 (7) p. 923-929.
- Schipper, N.G.; Varum, K.M.; Artursson, P. (1996): Chitosans as absorption enhancers for poorly absorbable drugs. 1: Influence of molecular weight and degree of acetylation on drug transport across human intestinal epithelial (Caco-2) cells, *Pharm. Res.* 13 (11) p. 1686-1692.
- Scholz, A.; Kostewicz, E.; Abrahamsson, B.; Dressman, J.B. (2003): Can the USP paddle method be used to represent *in-vivo* hydrodynamics?, *J. Pharm. Pharmacol.* 55 (4) p. 443-451.
- Schor, J.M.; Davis, S.S.; Nigalye, A.; Bolton, S. (1983): Susadrin transmucosal tablets (nitroglycerin in synchrom controlled release base), *Drug Dev. Ind. Pharm.* 9 p. 1359 -1377.
- Schubert, H. (1973): Kapillardruck und Zugfestigkeit von feuchten Haufwerken aus körnigen Stoffen, *Chemie-Ing. Techn.* 45 (6) p. 396-401.
- Schubert, H. (1979): Grundlagen des Agglomerierens, *Chemie-Ing. Techn.* 51 (4) p. 266-277.
- Sekigawa, F.; Onda, Y.; US Patent. Pat. No. 5217720, 1993.
- Shah, V.P.; Gurbarg, M.; Noory, A.; Dighe, S.; Skelly, J.P. (1992): Influence of higher rates of agitation on release patterns of immediate-release drug products, *J. Pharm. Sci.* 81 (6) p. 500-503.

- Shek, E. (1978): Buffer capacity, not buffer catalysis, affects the dissolution rate of cellulose acetate phthalate, *Pharm. Ind.* 40 p. 981.
- Shilpa, A.; Agrawal, S.S.; Ray, A.R. (2003): Controlled Delivery of Drugs from Alginate Matrix, *Journal of Macromolecular Science C43* (2) p. 187-221.
- Sienkiewicz, G.; Pereira, R.; Rudnic, E.M.; Lausier, J.M.; Rhodes, C.T. (1997): Spheronization of Theophylline-Avicel Combinations Using a Fluidized-Bed Rotogranulation Technique, *Drug Dev. Ind. Pharm.* 23 (2) p. 173-182.
- Sieval, A.B.; Thanou, A.F.; Kotzé, A.F.; de Boer, A.G.; Verhoef, J.C.; Junginger, H.E. (1998): Preparation and NMR characterization of highly substituted N-trimethyl chitosan chloride, *Carboh.Polymers.* 36 p. 157-165.
- Singla, A.K.; Chawla, M.; Singh, A. (2000): Potential applications of carbomer in oral mucoadhesive controlled drug delivery system: a review, *Drug Dev. Ind. Pharm.* 26 (9) p. 913-924.
- Smart, J.D. (1993): Drug delivery using buccal-adhesive systems, *Adv. Drug Del. Rev.* 11 (3) p. 253-270.
- Smart, J.D.; Kellaway, I.W. (1982): *In vitro* techniques for measuring mucoadhesion, *J. Pharm. Pharmacol.* 34 p. 70.
- Smart, J.D.; Kellaway, I.W.; Worthington, H.E. (1984): An *in-vitro* investigation of mucosa-adhesive materials for use in controlled drug delivery, *J. Pharm. Pharmacol.* 36 (5) p. 295-299.
- Staib, A.H.; Woodcock, B.G.; Loew, D.: Remote control of gastrointestinal drug delivery in man In *Novel Drug Delivery and Its Therapeutic Application*; Prescott, L.F., Nimmo, W.S., Eds.; Wiley: London, 1989, p. 77-88.
- Steckel, H.; Mindermann-Nogly, F. (2004): Production of chitosan pellets by extrusion/spheronization, *Eur. J. Pharm. Biopharm.* 57 (1) p. 107-114.
- Steward, P.A.; Hearn, I.; Wilkonson, M.C. (1995): Studies on permeation through polymer latex films I : Films containing no or only low levels of additives, *Polymer International* 38 (1) p. 1-12.
- Stippler, E.: *Biorelevant dissolution test methods to assess bioequivalence of drug prodrugs*, Shaker Verlag: Aachen, 2004.
- Takeuchi, H.; Matsui, Y.; Yamamoto, H.; Kawashima, Y.: Mucoadhesive liposomes coated with chitosan or carbopol for oral administration of peptide drugs. In *Proceedings: Int Symp Control Release Bioactive Mater*, 1999, p. 988.
- Takeuchi, H.; Yamamoto, H.; Niwa, T.; Hino, T.; Kawashima, Y. (1996): Enteral absorption of insulin in rats from mucoadhesive chitosan-coated liposomes, *Pharm. Res.* 13 (6) p. 896-901.
- Tetko, I.V.; Tanchuk, V.Y.: <http://www.vcclab.org>; ALOGPS 2.1 program.
- Thanou, M.; Florea, B.I.; Langemeyer, M.W.; Verhoef, J.C.; Junginger, H.E. (2000a): N-trimethylated chitosan chloride (TMC) improves the intestinal permeation of the peptide drug buserelin *in vitro* (Caco-2 cells) and *in vivo* (rats), *Pharm. Res.* 17 (1) p. 27-31.
- Thanou, M.; Verhoef, J.C.; Marbach, P.; Junginger, H.E. (2000b): Intestinal absorption of octreotide: N-trimethyl chitosan chloride (TMC) ameliorates the

- permeability and absorption properties of the somatostatin analogue *in vitro* and *in vivo*, *J. Pharm. Sci.* 89 (7) p. 951-957.
- Timmermanns, J.: *Floating Hydrophilic Matrix Dosage forms for Oral Use: Factors Controlling Their Buoyancy and Gastric Residence Capabilities*, Ph.D. Thesis, Libre de Bruxells, Brussels, 1991.
- Timmermanns, J.; Moes, A.J. (1990): How well do floating dosage forms float, *Int. J. Pharm.* 62 p. 207-216.
- Tobyn, M.J.; Johnson, J.R.; Dettmar, P.W. (1996): Factors affecting *in vitro* gastric mucoadhesion II: Physical properties of polymers, *Eur. J. Pharm. Biopharm.* 42 p. 56.
- Tomita, M.; Hayashi, M.; Awazu, S. (1994): Comparison of absorption-enhancing effects between sodium caprate and disodium ethylenediaminetetraacetate in Caco-2 cells, *Biol. Pharm. Bull.* 17 (5) p. 753-755.
- Tozaki, H.; Komoike, J.; Tada, C.; Maruyama, T.; Terabe, A.; Suzuki, T.; Yamamoto, A.; Muranishi, S. (1997): Chitosan capsules for colon-specific drug delivery: improvement of insulin absorption from the rat colon, *J. Pharm. Sci.* 86 (9) p. 1016-1021.
- Tsai, G.-J.; Hwang, S.-P. (2004): *In vitro* and *in vivo* antibacterial activity of shrimp chitosan against some intestinal bacteria, *Fisheries Science* 70 (4) p. 675-681.
- Uch, A.S.: *Intestinal Uptake of Azole Antifungals In Rats*, Ph.D. Thesis, Dept. of Biochemistry, Pharmaceutics and Food Chemistry, Johann Wolfgang Goethe-University, Frankfurt am Main/Germany, 1999.
- Uch, A.S.; Dressmann, J.B.: Improving bioavailability by colonic administration In *Formulation of poorly-available drugs for oral administration*; Couvreur, P., Duchêne, D., Eds.; Editions de Santé: Paris, 1996, p. 152-161.
- Vasir, J.K.; Tambwekar, K.; Garg, S. (2003): Bioadhesive microspheres as a controlled drug delivery system, *Int. J. Pharm.* 255 (1-2) p. 13-32.
- Vecchio, C.; Bruni, G.; Gazzaniga, A. (1994): Preparation of Indobufen Pellets By using Centrifugal Rotary Fluidized Bed Equipment Without Starting Seeds, *Drug Dev. Ind. Pharm.* 20 (12) p. 1943-1956.
- Vecchio, C.; Fabiani, F.; Sangalli, M.E.; Zema, L.; Gazzaniga, A. (1998): Rotary tangential spray technique for aqueous film coating of indobufen pellets, *Drug Dev. Ind. Pharm.* 24 (3) p. 269-274.
- Vertommen, J.; Kinget, R. (1996): The influence of five selected processing and formulation variables on the release of riboflavin from pellets produced in a rotary processor, *S.T.P. Pharma Sci.* 6 (5) p. 335-340.
- Vertommen, J.; Kinget, R. (1997b): The Influence of Five Selected Processing and Formulation Variables on the Particle Size, Particle Size Distribution, and Friability of Pellets Produced in a Rotary Processor, *Drug Dev. Ind. Pharm.* 23 (1) p. 39-46.
- Vertommen, J.; Rombaut, P.; Kinget, R. (1997): Shape and Surface Smoothness of Pellets made in a Rotary Processor, *Int. J. Pharm.* 146 p. 21-29.
- Vertommen, J.; Rombaut, P.; Kinget, R. (1998): Internal and External Structure of Pellets made in a Rotary Processor, *Int. J. Pharm.* 161 p. 225-236.

- Vertommen, J.; Rombaut, P.; Michoel, A.; Kinget, R. (1998b): Estimation of the Amount of Water Removed by Gap and Atomization Air Streams during Pelletization in a Rotary Processor, *Pharm. Dev. Technol.* 3 (1) p. 63-72.
- Voigt, R.: *Pharmazeutische Technologie*, Deutscher Apotheker Verlag: Stuttgart, Germany, 2000.
- Walker, G.F.; Ledger, R.; Tucker, I.G. (1999): Carbomer inhibits tryptic proteolysis of luteinizing hormone-releasing hormone and N-alpha-benzoyl-L-arginine ethyl ester by binding the enzyme, *Pharm. Res.* 16 (7) p. 1074-1080.
- Wan, L.S.; Heng, P.W.; Liew, C.V. (1994): The Role of Moisture and Air Gap Pressure in the Formation of Spherical Granules by Rotary Processing, *Drug Dev. Ind. Pharm.* 20 p. 2551-2561.
- Wan, L.S.; Heng, P.W.; Liew, C.V. (1995): The role of moisture and gap air pressure in the formation of spherical granules by rotary processing, *Int. J. Pharm.* 118 p. 213-219.
- Wang, M.T.; Tsai, F.H.; Wang, D.P. (2000): Formulation optimization of controlled-release pellets of metoclopramide hydrochloride using dissolution fit factor approach, *Drug Dev. Ind. Pharm.* 26 (5) p. 577-581.
- Wearley, L.L. (1991): Recent progress in protein and peptide delivery by non-invasive routes, *Crit. Rev. Ther. Drug Carrier Syst.* 8 (4) p. 331-394.

CURRICULUM VITAE

Name: Marcus Hans Knöll
Born: 06.02.1976 in Frankfurt
Residency: Raiffeisenstrasse 3
79539 Lörrach, Germany
Family status: Married with Dr. Antje Sabine Knöll, former Uch
1 daughter Catina-Sophie
1 son Mika Dominic

Education

June 1995 General qualification for University entrance (Abitur) from the Immanuel-Kant-School, Kelkheim, Germany

Civilian service

09/1995 – 09/1996 Oncological Laboratory of the Gynaecological hospital, JWG University hospital Frankfurt / Main, Germany

Studies

10/1996 – 2000 Pharmacy at the Philipps-University Marburg, Germany
10/2000 2nd State exam

Professional Life

03/2005 – today Hüttlin GmbH: Head of Pharma Services
04/2002 – 03/2005 Different pharmacies: Pharmacist on duty during Emergency Service and Saturday shifts
02/2002 – 03/2005 Conferral of a doctorate at the Johannes – Gutenberg – University Mainz/ Germany, Institute of Biopharmacy, Pharmaceutical Technology and Geological Sciences as external Ph.D. student (at Degussa Röhm Pharma Polymers, Darmstadt)
11/2001–12/2003 Pharmacist, Rundschau Apotheke Frankfurt/Main, Germany
11/2001 Approbation as Pharmacist
11/2001 3rd. State exam
05/2001 – 11/ 2001 Practical training in the Pharmacy
11/2000 – 04/2001 Practical training at the University of Florida, College of Pharmacy, Dept. of Pharmaceutics
06/1999 – 05/2000 Representative of the company ratiopharm (fairs)
02/1997 –11/2001 Member of pharmaceutical personal, Rundschau Apotheke Frankfurt

Additional Business

1994 Exam as trainer for the Hessian Handicapped and Rehabilitation Association
1994-1996 Therapeutically training of mentally (multiple-) handicapped, young persons
1995- 2000 Trainer of Walking-Groups

Experiences abroad

11/2000-04/2001 Work in Gainesville, Florida, USA
08/1998 Language school in Besancons /France
08/1997 – 09/1997 California and New York, USA

Languages

German (Native language)
English (fluent)
French (basics)

Publications

- Knöll, M., Lizio, R., Behrisch, A., Roth, E., Ortlepp, B., Petereit, H.U. and Langguth, P. (2004), Electron-Dispersive X-Ray – A Method for Proving the Separation of an Enteric Coating Layer from an Additional Functional Matrix Layer, Int. meeting of Pharmaceutics and Biopharmaceutics, Nuremberg.
- Lizio, R., Petereit, H.-U., Langguth, P. and Knöll, M. (2004), Patent DE 10 2004 036 437 A1, Multipartikuläre Arzneiform für wenig lösliche Wirkstoffe, sowie ein Verfahren zur Herstellung der Arzneiform .
- Knoell, M., Lizio, R., Petereit, H.U. and Langguth, P., (2005), Rotary Agglomeration – A Process for Wet Spheronization of Bioadhesive Micropellets. Drug Dev. Ind. Pharm. (Submitted).